Synthesis, characterization and photochemical properties of 3d transition metal supported by aroyl-hydrazone ligands

Khaled Cheaib

UNIVERSITÉ DE STRASBOURG

ÉCOLE DOCTORALE DES SCIENSES CHIMIQUES

Institut de chimie – UMR 7177

THÈSE

présentée par :

Khaled CHEAIB

soutenue le : **5 septembre 2013**

Pour obtenir le grade de : **Docteur de l'université de Strasbourg**

Discipline/ Spécialité : CHIMIE

Synthèse, caractérisation et propriétés photochimiques de complexes de métaux de transition 3d supportés par des ligands de type aroyle-hydrazone

THÈSE dirigée par :
M. WELTER Richard Professeur, Université de Strasbourg

RAPPORTEURS :
M. BELEY Marc Professeur, Université de Lorraine
M. GROS Claude Professeur, Université de Bourgogne

AUTRE MEMBRE DU JURY :
M. MATT Dominique Docteur, Université de Strasbourg

INVITEE :
Mme CHOUA Sylvie Docteur, Université de Strasbourg

REMERCIEMENTS

Un très grand merci à Prof. Richard Welter pour m'avoir accueilli dans son laboratoire, pour son humanité et sa bienveillance envers moi, et pour la confiance qu'il m'a accordé dès le début de cette thèse.

Je tiens aussi à remercier Prof. Marc Bely, Pr. Claude Gros, Dr. Dominique MATT pour m'avoir fait l'honneur de juger ce travail en tant que membre de la commission d'examen.

Ce travail n'aurait pas pu aboutir sans une collaboration et un échange des idées. Mes vifs remerciements vont, à Madame Sylvie CHOUA, Dr. à l'université de Strasbourg et membre du Laboratoire POMAM, pour la partie RPE, pour ses conseils, sa disponibilité au quotidien ainsi que les échanges scientifiques que nous avons pu avoir ensemble. J'adresse également mes remerciements à M. Mohamedally KURMOO qui m'a fait la grande faveur de partager son expérience scientifique, pour nos discussions enrichissantes et pour les mesures magnétiques. Merci également à M. David MARTEL, pour les mesures d'électrochimie et pour les échanges scientifiques qui m'ont été très utiles.

J'ai pu travailler dans un cadre particulièrement agréable, grâce à l'ensemble des membres de l'équipe DECOMET. Je pense particulièrement à Christophe et David, toujours souriants et toujours disponible .Merci à Fred et Gille (les knaackes), à Samuel, à Weiwei. Merci à tous pour votre bonne humeur, pour toutes ces séances de rires et de sourires, et pour toutes ces discussions autour d'un verre.

Mes sincères remerciements à la France pour m'avoir accueilli et permis de continuer mes études et de réaliser cette thèse.

Merci Irene pour l'amour qui m'a envahi lorsque tu es arrivée dans ma vie

J'ai une pensée très tendre pour ma mère, mon père, mon frère et ma sœur pour leur apport quotidien, même à distance, à la réalisation de ce travail. Ils m'ont toujours donné l'espoir et le courage.

Abreviations

Ac	acetate
Acac	acetylacetonato
CV	Cyclic voltammetry
NMR	nuclear magnetic resonance
EPR	electron paramagnetic resonance
LMCT	ligand to metal charge transfer
IL	intraligand
ORTEP	Oak ridge thermal-ellipsoid plot Program
THF	tetrahyudrofuran
EtOH	ethanol
MeOH	methanol
DMF	dimethylformamide
$CHCl_3$	Chloroform
NEt_3	triethylamine
Et_2O	diethyl ether
$TBA(PF_6)$	tetrabutylammonium hexafluorophosphate
UV	ultraviolet
EWG	electron withdrawing group
eq	equivalent
app.	appendix
Ch.	chapter
DMSO	dimethylsulfoxide
ic	internal conversion
isc	intersystem crossing
IR	infrared
TEA	triethylamine
DCM	dichloromethane

Table of Contents

Preface

Coordination complexes show diversity in structures depending on the metal ions, its coordination number and the denticity of the ligands used, and therefore, the selection of ligand is crucial in determining the properties and structures of coordination compounds. Hence the coordination chemistry of nitrogen-oxygen donor ligands is an interesting area of research. In this aspect, a great deal of attention has been focused on the complexes formed by transition metal ions with aroyl-hydrazones. Hydrazones are promising ligands in coordination chemistry with interesting binding modes and applications.

Our laboratory explores the chemistry of these ligands for many years. The present work deals with the synthesis and the characterization of first row transition metal complexes of some bidentate ant tridentate aroyl-hydrazones.

This work was financed by the Alsace Region in order to valorise an international patent published by Professor WELTER in 2008 witch deals with the producing and storing of solar energy via photo reduction of ferric complexes. Thus, some results related to the Start-Up IS2 (Start-Up company who valorize the patent) will not be carried on this manuscript.

The primary aim of these investigations was focused on the photo chemistry of Iron complexes supported by N,O- bidentate ligands, in particularly to elucidate the mechanism of their photoreduction process. Other fields are also being explored, such as molecular magnetism and homogeneous catalysis.

This thesis is presented in 5 chapters and chapter 1 provides an introduction on aroyl-hydrazones. Chapter 2 and 3 concerned the photochemical properties of ferric complexes and precisely their photoreduction process. In chapter 4, we will present the magnetic properties of some manganese and iron complexes supported by N,O- bidentate ligands. In chapter 5, the coordination mode of a N,S,O-tridentate aroyl-hydrazone ligand was been investigated with different Nickel precursor. One of the isolated Ni complexes had shown an activity for ethylene oilgomerization. A brief summary and conclusion is also included on the last part of the manuscript.

General Introduction

Our laboratory explores the chemistry of aroyl-hydrazones for many years. The present work deals with the synthesis and the characterization of first row transition metal complexes supported by some bidentate and tridentate aroyl-hydrazones.

When exploring the coordination chemistry of 2-salicyl-hydrazono-1,3-dithiolane ligand, we have observed spontaneous reduction of Fe(III) complex to his corresponding Fe(II) complex after exposure to sun light. Interestingly, this photo reduction appears to be reversible, as Fe(II) may be rapidly converted back to Fe(III) by electrochemical procedure or by simple exposure to air. The fact that the absorption of the light induces a change in the oxidation state of the metal to another stable oxidation state; this can be used for the transfer of electrons through an appropriate system. Iron is the most abundant metal on earth, and the starting materials for the synthesis of ligands are so cheap. Hence the obvious advantage of this system in the production of energy from sunlight. This photo-induced redox reaction opens up new research opportunities, as recently pointed by Wernsdorfer et al and demonstrated by a patent published in 2008 by Professor WELTER which deals with the producing and storing of solar energy (Method and Device for Producing and Storing energy, WO 2009/130562 A1). The present work was mainly concerned by the synthesis, characterization and photochemical properties of ferric ion supported by N,O-bidentate ligands in order to understand the mechanism of the photoredox process and further to use the system for solar cell application. Other fields are also being explored, such as molecular magnetism and homogeneous catalysis.

This thesis is divided into five chapters:

Chapter 1: provides an introduction on aroyl-hydrazones and their metal complexes with an extensive literature survey revealing their binding modes, applications and recent developments

In chapter 2: the photochemical properties of mononuclear iron III supported by bidentate ligands was fully investigated and a mechanism was proposed for the photoredox process.

In chapter 3: some work was carried with a ditopic, tetraprotic ligand. Bis aroyl hydrazine is able to coordinate two iron (III) atom instead of one. Upon irradiation by sun light the FeIII complex will photoreduce to iron (II) complex. The dinuclear Iron (III) complex was isolated

and characterized using single-crystal diffraction, infrared and UV-vis spectroscopies, and its magnetic properties studied. The photoredox process was studied and the corresponding Fe(II) complex was isolated as single crystal.

In chapter 4: The coordination chemistry of 2-salicyloylhydrazono-1,3-dithiane (N,O-bidentate ligand) was studied with manganese and iron ions. Different complexes have been isolated as crystalline materials, and their crystal structures have been determined by single crystal X-Ray crystallography. Magnetic properties of new iron dinuclear μ-methoxo complex was studied, which is in agreement with the theoretical study proposed previously for its manganese analogue.

In chapter 5: The coordination chemistry of Ni(II) with a S,N,O-tridenate ligand is reported and discussed. The crystal structure of the ligand has been determined as well as those of three new Ni(II) complexes. One of the isolated Ni complexes was evaluated as catalyst for the oligomerization of ethylene and found to provide ethylene dimers and trimers as primary products with a turnover frequency (TOF) of 31200 mol. of C_2H_4 per mol. of Ni and per hour.

A brief summary and conclusion is included on the last part of the manuscript.

Chapter 1:

Acyl-/Aroyl-hydrazones

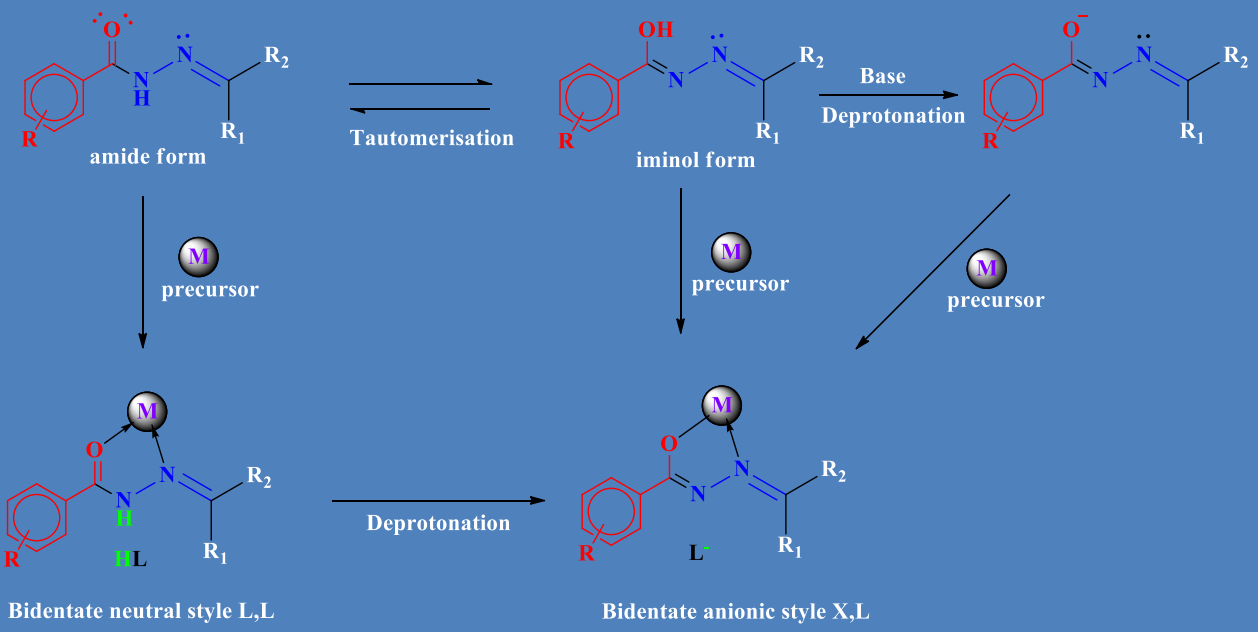

1.1 Introduction

Coordination complexes were known although not understood in any sense since the beginning of chemistry, e.g. prussian blue and copper vitriol. Coordination chemistry was pioneered by Nobel Prize winner Alfred Werner. He received the Nobel Prize in 1913 for his coordination theory of transition metal-amine complexes.[1] At the start of 20th century, inorganic chemistry was not a prominent field until Werner studied metal amine complexes such as $[Co(NH_3)_6Cl]$. When coordination theory was enunciated in 1893, the electron had not been discovered till 1897. Electron later became the basic of all theories of chemical bonding. The elucidation of geometry and bonding which were based mainly on preparative procedures received a theoretical foundation from electronic theory of valence. This was followed in 1940 by the concept of valence bond (VB) theory and valence shell electron pair repulsion (VSEPR) given by Nevil Vincent Sidgwick and Herbert Powell,[2] which are still used extensively, though the ideas have undergone a significant change. Since then the field of coordination chemistry has been widely explored. The number, variety and complexity of coordination compounds still continue to grow. A survey of literature in inorganic chemistry reveals that at least 70% of the published articles deal with coordination compounds.

Coordination complexes show diversity in structures depending on the metal ions, its coordination number and the denticity of the ligands used, and therefore, the selection of ligand is crucial in determining the properties and structures of coordination compounds. The presence of electronegative atoms such nitrogen and oxygen on the ligand is established to enhance the coordinating possibilities. Hence the coordination chemistry of nitrogen-oxygen donor ligands is an interesting area of research. In this aspect, a great deal of attention has been focused on the complexes formed by transition metal ions with acyl-hydrazones. In view of their applicability on various fields, acyl-hydrazones, with the structure **R─CO─NH─N═R_1R_2**, where the N-donor atoms can become partially charged (anionically) take the forefront position in the development of coordination chemistry.[3]

1.2 Acyl-/Aroyl-hydrazones

Hydrazones are a class of azomethines with the structure $R_1R_2C=N-NH_2$. They are characterized by the presence of two interlinked nitrogen and are generally prepared by the condensation of appropriate hydrazine on an aldehyde or ketone.

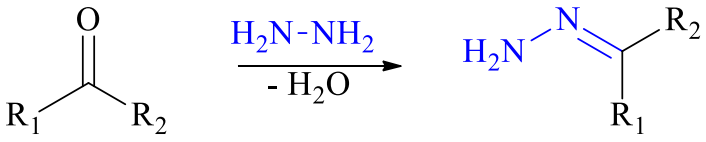

Hydrazone

Introduction of a -C=O group in the hydrazine part increase the electron delocalization and the denticity of the hydrazone and the resulting compound is known as an acyl-/ aroyl- hydrazone.[4,5]

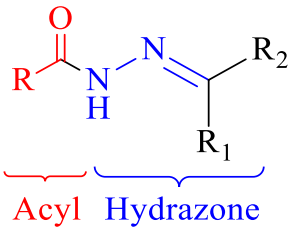

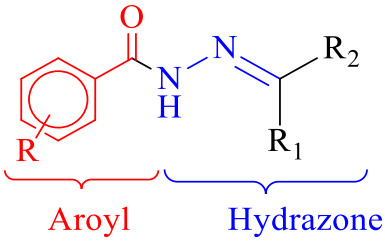

The acyl-/aroyl-hydrazone can be seen as resulting from the reaction of an aldehyde or a ketone with an acyl-/aroyl- hydrazine that has a free NH_2 group.

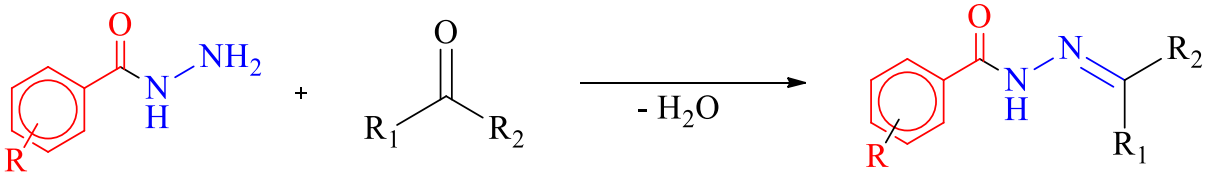

Aroyl hydrazine

1.3 Bonding and coordination mode

Bidentate and tautomerization

Schiff bases, the compounds containing imines C=N group have gained special attention owing to their easy synthesis and wide variety of applications. A large number of Schiff bases are often used as ligands in coordination chemistry because of their excellent metal binding capability.[6-10] Hydrazones, a subdivision of azomethine family, in which, the nitrogen in C=N group is attached to another nitrogen atom instead of carbon in simple Schiff bases, acts as very promising ligands in coordination chemistry.

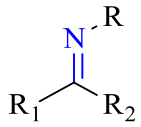

Azomethine

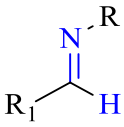

Schiff base

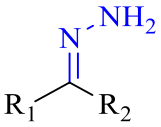

Hydrazone

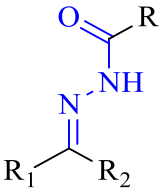

acyl/aroyl Hydrazone

The carbonyl oxygen and trigonal azomethine nitrogen are the available donor sites present in the aroyl-hydrazone compounds. One important face of aroyl-hydrazones is their ability to exist in tautomeric equilibrium forms known by keto-enol or amido-iminol tautomerism[11] (**Fig. 1**). Depending on the reaction conditions, such as the pH of the medium, the nature and the oxidation state of the metal ion, and its concentration, these ligands coordinate to the metal, either in the neutral amide form (Ia) or in the monoanionic iminolate form (Ib), as N,O-bidentate ligands forming five-membered chelate ring with the metal.[12-18] If the medium of the reaction is acidic, then the deprotonation will not be easy and therefore, in such cases, coordination with neutral amido form style L,L is expected. Deprotonating of the ‑NH‑ group by adding a base or which is readily occurred during the complexation proceed via the anionic iminolate form style X,L (**Fig. 1**).

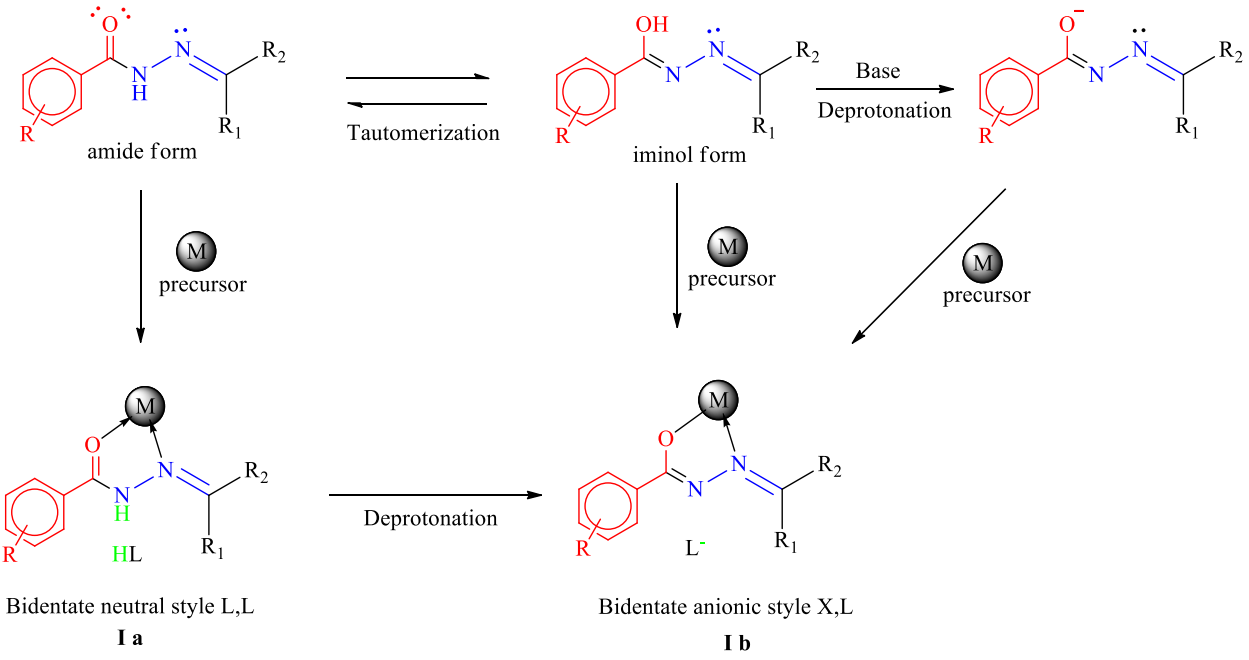

Figure 1: Aroyl-hydrazones tautomerization and coordination forms

The stability of the acyl-/aroyl-hydrazones (-CONHN=CR_1R_2) chelates is higher than that of the corresponding acyl-/aroyl-hydrazine (-$CONHNH_2$) with a free NH_2 compounds and depends on the different substituents.

With first row transition metal, planar square and octahedral geometric, are the often structures forms adapted by the complexes. Neutral mononuclear complexes, surrounded by two or three ligands, are usually expected. Ligands often bound to the metal via there anionic iminolate form[19-25] (see structure I, II, III and IV in figure 2) and some other time via the protonated neutral amide form[26-28] in case of low oxidation state of the metal precursor (Structure V in figure 2). Coligands such as anions, halides or solvent molecule, may be present to complete the first coordination sphere (Structure II, III and V in figure 2).[29-32] In some cases cationic complexes[33-35], where the presence of counter anion (Cl^-, NO_3^-, Br^-, ClO_4^-, SO_4^{2-}, $CuCl_2^-$ and $FeCl_4^-$) to neutralize the charge of the ionic metal, were been reported on the literature as shown in figure 3. In other cases an atom or group (MeO^-, H_2O or O^{2-}) may act as bridging ligand and the resulting complex will be a dimer (Fig. 4).[25,36,37]

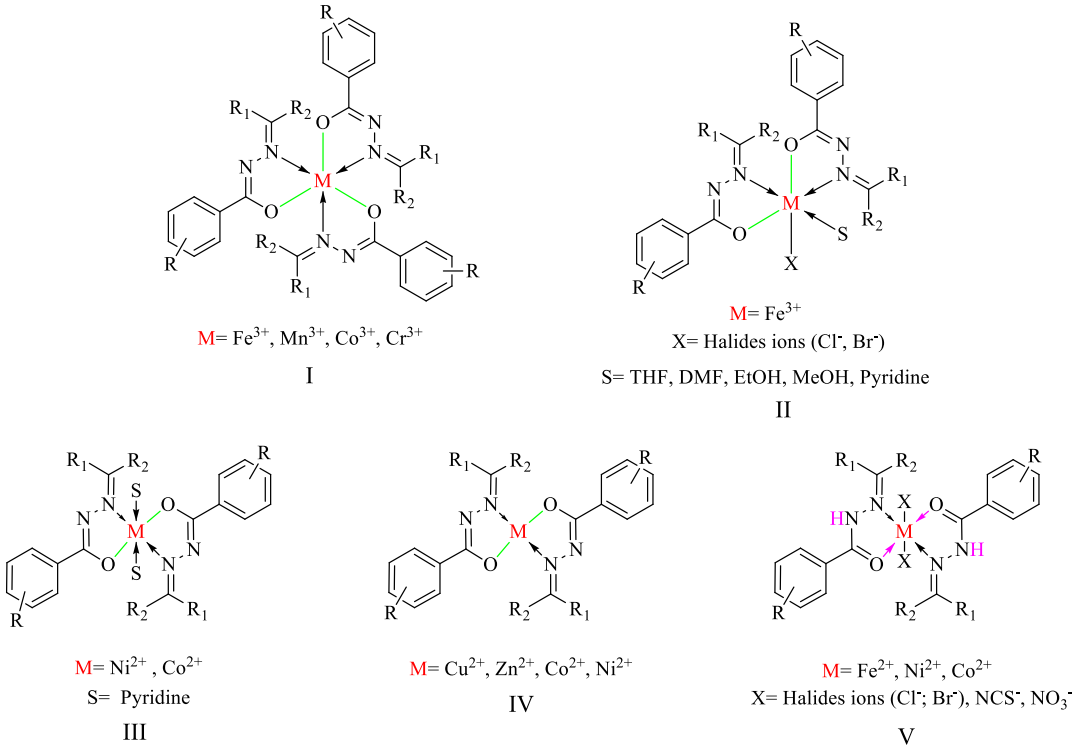

Figure 2: N,O-bidentate neutral complexes reported on the literature

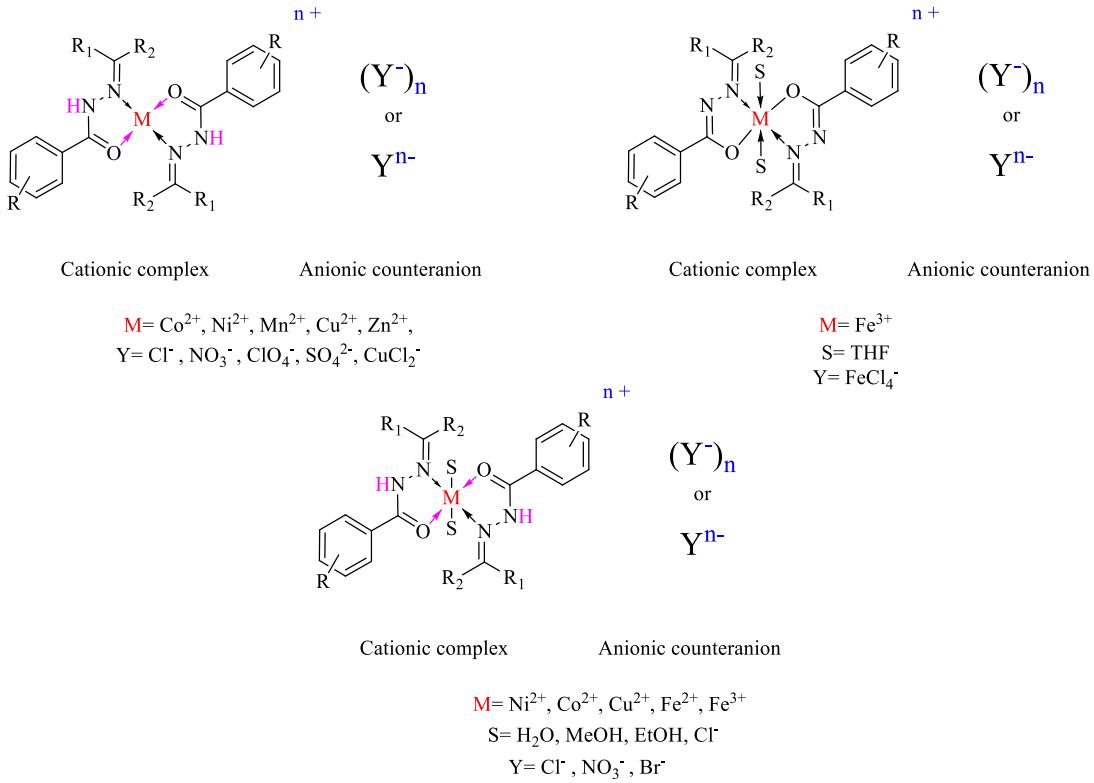

Figure 3: N,O-bidentate cationic complexes reported on the literature

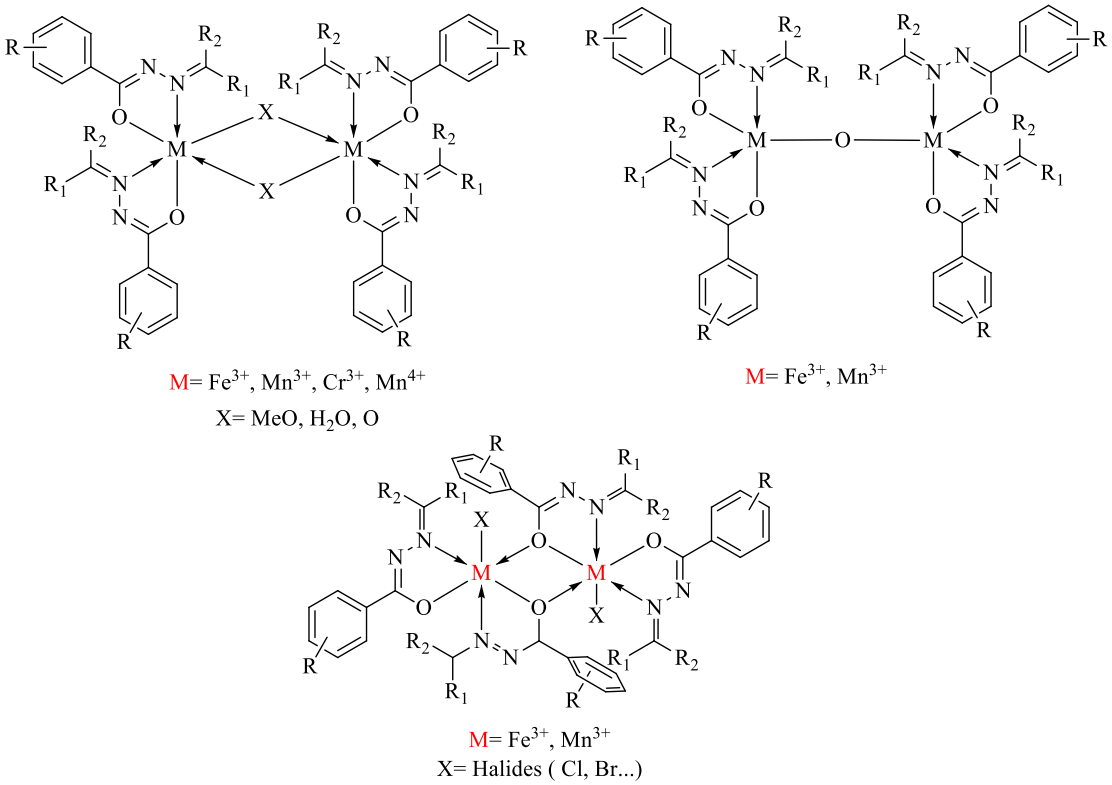

Figure 4: N,O-bidentate dinuclear complexes reported on the literature

Tridentate and isomerization forms

Tridentate

Coordination sites can be further improved by suitable substitution on the hydrazone part as well on the carbonyl part.

Introduction of an heterocycle (thiophene, pyridine) or an heteroatom coordination site, such O, N and S by appropriate substitution (ortho position in case of phenyl), on the hydrazone moiety, increases the chelating effect, and the resulting molecule acts like tridentate potential chelating ligand upon complexation with a metal ion. In figure 5 you will find different tridentate aroyl-hydrazones ligands reported on the literature.[16,38-40]

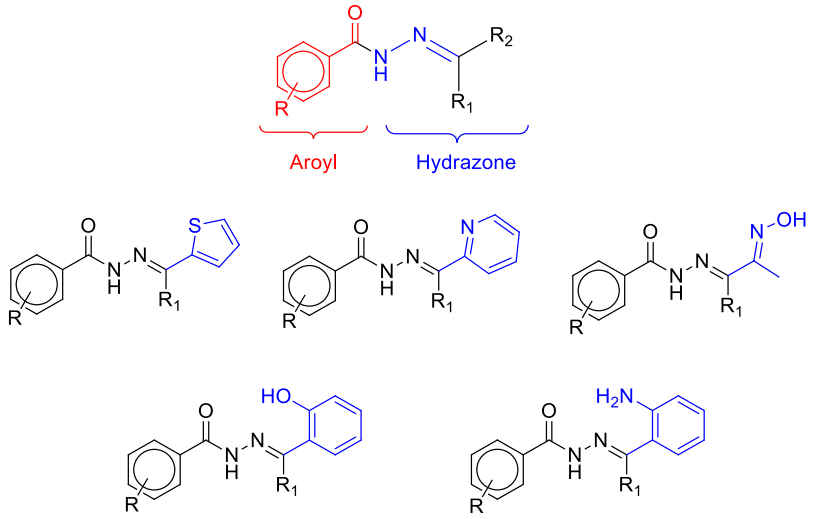

Figure 5: Tridentate aroyl-hydrazones reported on the literature

The ligands from this series are potential N,N,O- ; S,N,O- and O,N,O- tridentate ligands. For example if we take an aroyl-hydrazone having a pyridine group on the hydrazone skeleton, it can coordinate to the central metal, either through neutral amido form (B figure 6) or through the deprotonated iminolate form (A Fig.6) and offer different various structures (Fig. 5). The metal ion could be chelated by one ligand where the presence of coligands and solvent molecules to complete the first coordination sphere (I and II Fig.6).[41,42] Another possibility is the formation of a six coordinated metal complex with two deprotonated ligands (III Fig. 6).[43-46] Anions present in the metal salt or ions like azide and thiocyanate can act as a bridging ligand results the formation of a dimeric structure.[44] (IV Fig.6)

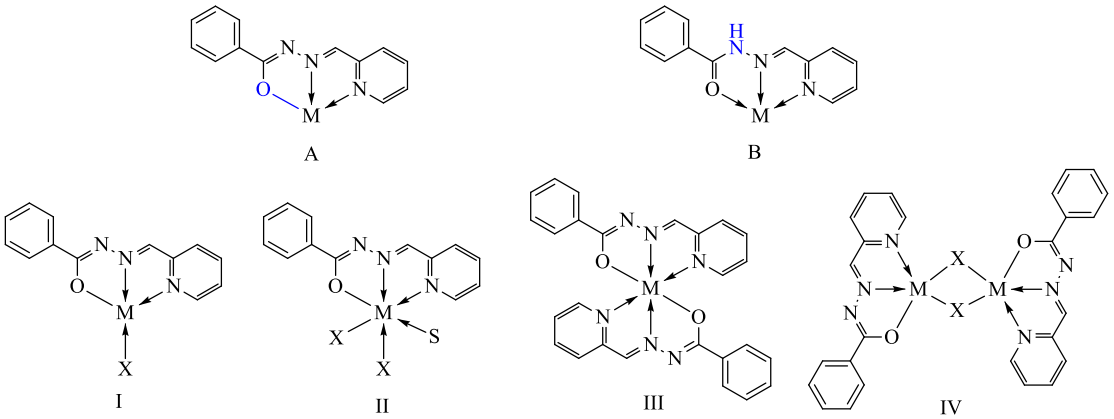

Figure 6: Different structures for tridentate aroyl-hydrazone complexes in the literature

For the hydrazone possessing a phenolic group in the aldehyde/ketone part which is in suitable position for O,N,O- coordination mode, it was reported the formation of dimeric complexes with phenolate oxygen bridges (Figure 7).[41]

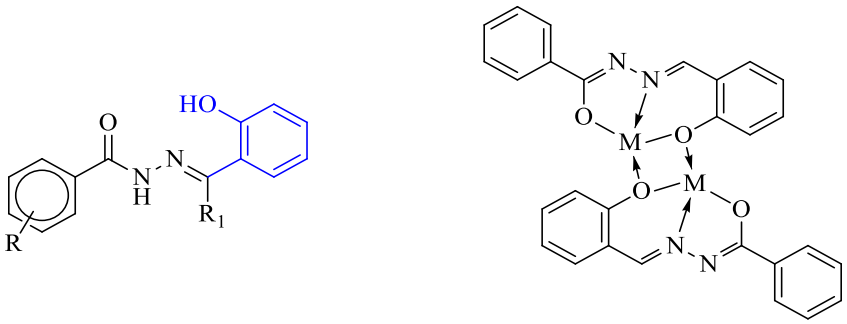

Figure 7: Tridentate aroyl-hydrazone reported on the literature

Isomerization

The amide form itself exists in different stereoisomers forms depending on the substituents and resulting in a more stable structure (see figure 8). The form I (E configuration) leads to II (Z configuration) by rotation about the C=N bond, but to III (E configuration) by a rotation about the N-N bond. Stereochemistry of the hydrazone is much decided by the pH medium of the solution, presence of water in the organic solvents, the steric effects of the various substituents and also favored by additional interactions such as intra molecular hydrogen bonding.[47] Existence of the free acyl/ aroyl-hydrazones in these geometrical forms in solution and in the solid state is well established by NMR, IR, UV-Visible, Raman, crystallographic studies and theoretical investigation.[48,49] In absence of a third coordination site (e.g. Fig. 8), the aroyl-hydrazone transforms to a suitable geometry and acts as bidentate (form I or II) upon complexation to a transition metal. Form III was not been observed upon complexation with a metal ion. This phenomenon is assumed to be due to chelate effect, which results in an increased stability due to better electron delocalization in chelated ring system consisting of metal ions.

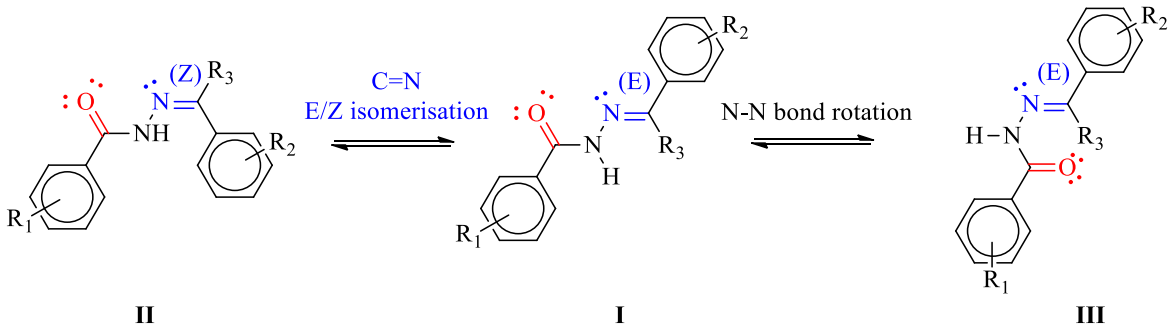

Figure 8: Geometrical isomers for the amide form

Or the case of tridentate ligand, with the existing of a third coordination site like pyridine on the hydrazone skeleton, is more sophisticated. The enol form of the ligand could exist in four possible forms (Fig. 9).

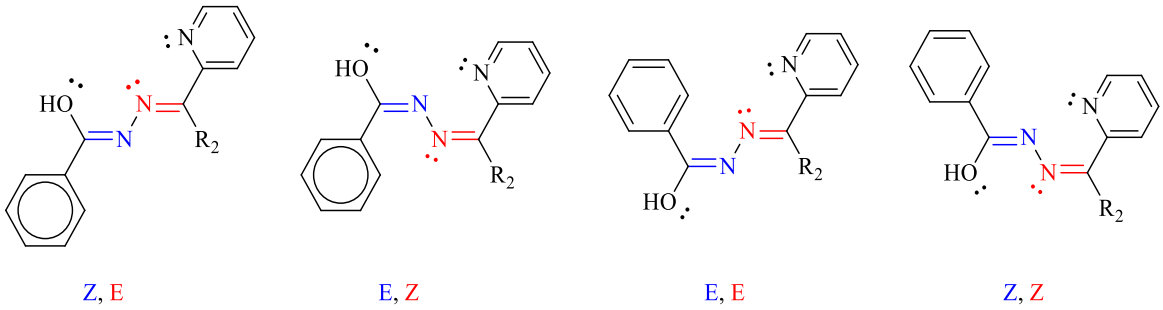

Figure 9: Possible Configurations of the iminolic form

The presence of the C=N bond that presents a very attractive feature of being double dynamic entities capable of undergoing cis trans isomerization[50,51] , as well as the presence of N-N which can freely rotate [52] according to the demand of coordination and the presence of the third coordination site can switch on the coordination from tridentate to bidentate with keeping the traditional coordination site or by the generation of a new bidentate chelate [53] and that depending on the substituents (Fig. 10). The same case for thiophene, phenol ring and other tridentate ligands reported in the literature.[54-56]

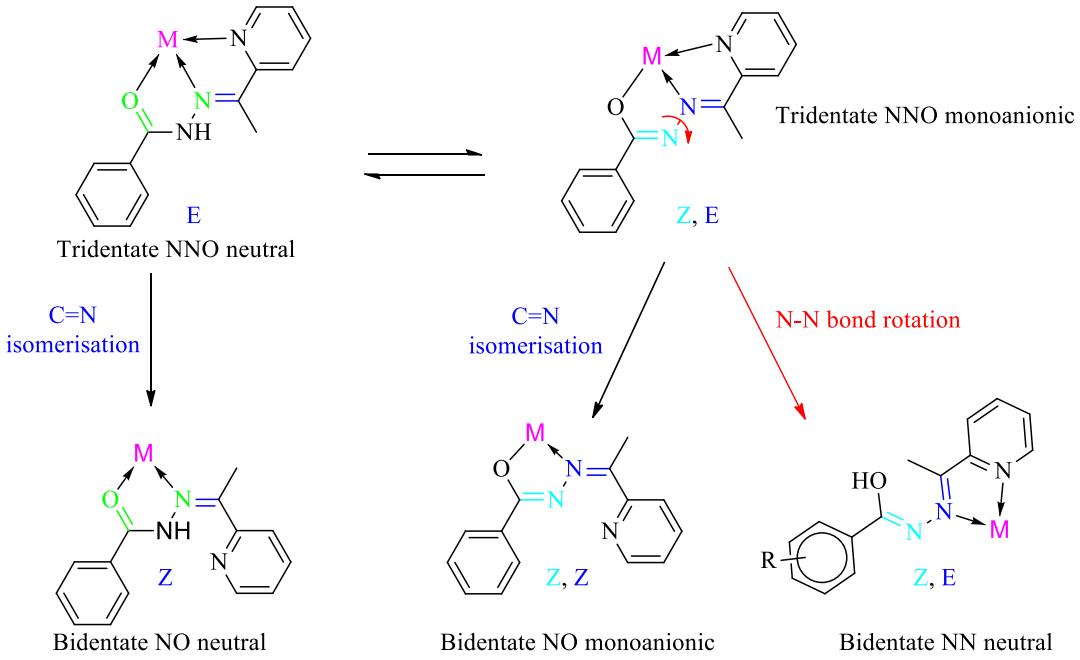

Figure 10: Tridentate Switching to bidentate upon C=N isomerization or N-N bond rotation

Polymers and supramolecular structures

If the acyl-/aroyl-hydrazone possesses additional electron donating groups such N and O in suitable position. In this case it can act as multidentate ligand that will coordinate to two or three metals centers and allowed the construction of polymers with defined geometry and special properties (Fig. 11). The presence of methoxy group in the extremity part of the extended hydrazone moiety[57] (structure I), or if the hydrazide part of the ligand contains a heteroatom such a nicotinoyl derivate (structure II) or NO_2 on the para position of the the ring[53] (structure III), that will provide an additional coordination site on a terminal position. Usually this donor atom does not involve in coordination to the metal in the same molecule, but it can coordinate to the adjacent metal centre giving a polymeric compound. With aroyl-hydrazone ligand possessing a hydroxyl group on the ortho position inspected polymers structures was been obtained.[21,58] Different polymers structures reported on the literature are depicted in figure 11.

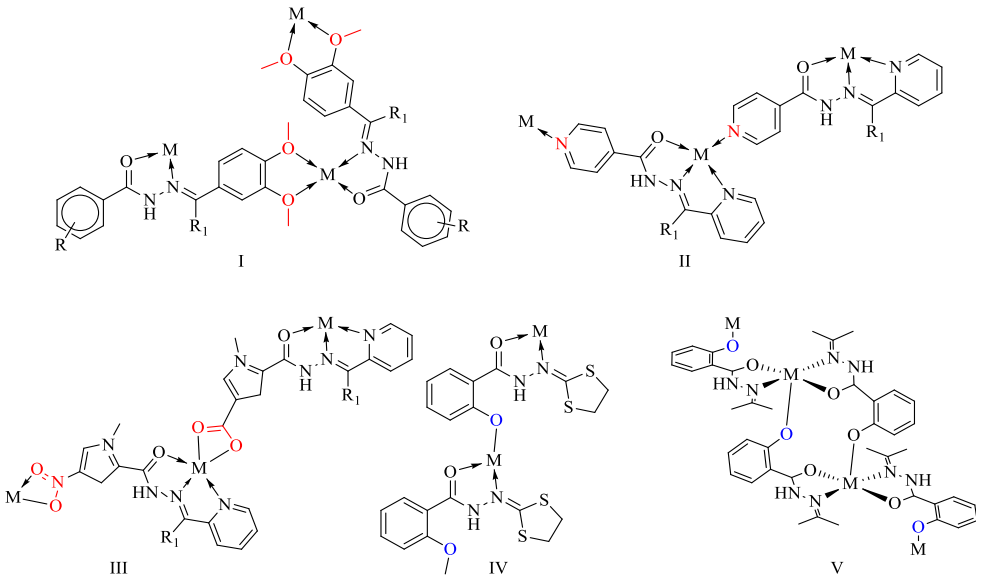

Figure 11: Polymer structures reported on the literature

Lehn and co-workers have demonstrated that suitably substituted hydrazones are capable of coordination metal to give multimetallic square grid complexes whose optical and magnetic properties can be modulated by the degree of protonation of the ligands. Shown be useful to build up controllable supramolecular and polymer structures.[59-61] Their use of diprotic, ditopic ligands known by bis acyl-/aroyl-hydrazone in which the two hydrazones parts are linked by a central unit, increases the topicity of the molecule. The ligands will act as multidentate and offer different polymer and supramolecular structures upon complexation to a metal.[3,62,63]

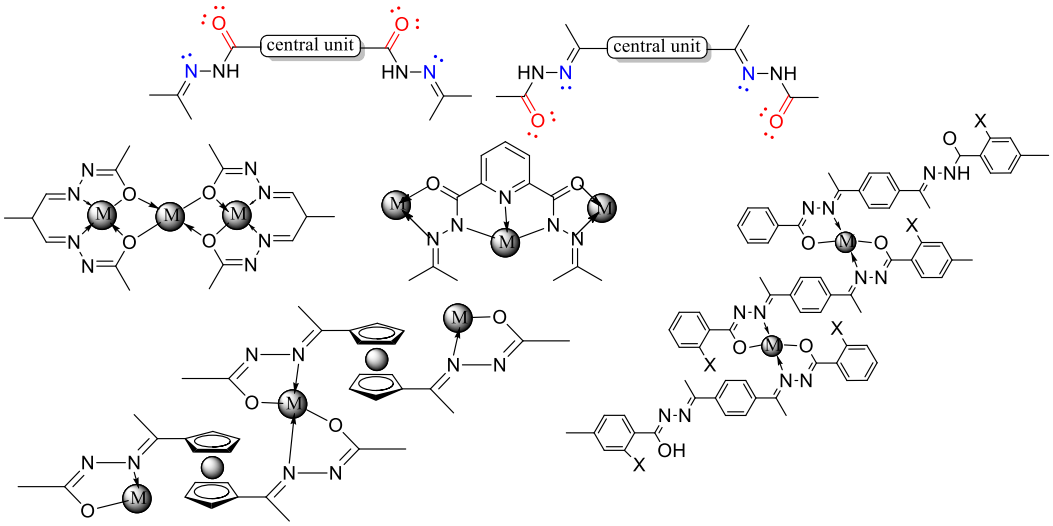

Figure 12: Some examples of bis aroyl-hydrazone polymers and multimetallic grid

1.4 Applications

The interest in the design, syntheses and characterization of hydrazones and their metal complexes has come from their applications in various fields. Their ease of syntheses, easily tunable steric and electronic properties and good solubility in common solvents enhances research interest in this area. They have wide applications in biology, medicine, optics, catalysis and analytical chemistry.

Biological and medicinal applications

Metal complexes of hydrazones have been found to have biological and therapeutic activity and this is the most important practical reason for the continuing interest in these materials. Biological activity can be influenced by linking the hydrazide function with pharmacologically active carbonyl compounds by condensation reactions. Many of the aryl / hydrazone complexes of transition metal ions are known to be effective models for elucidation of the mechanisms of enzyme inhibition.[64,65] Antitubercular activities shown by some hydrazones are comparable to that of the drugs available for the treatment of tuberculosis.[66] Many hydrazone derivates have been found to possess antimicrobial[67,68] and anti-inflammatory activities.[69] Salicylaldehyde benzoylhydrazone was a potent inhibitor of DNA syntheses and cell growth in a variety of human and rodent cell lines. Further studies revealed that the copper (II) complexes of salicylaldehyde benzoylhydrazone exhibits appreciably greater inhibitor activity than the free ligand itself, and suggests that the metal complexes are more biologically active than the free ligands.[70-72] Epilepsy is a common neurological disorder and a collective term given to a group of syndromes that involve spontaneous, irregular, abnormal electrical activity in the brain. The biological results revealed that some of the hydrazones have prominent anti-convulsant activity.[73,74] sulfonamidoindole, nitrobenzylidene-hydrazide showed antidepressant activity.[73] Iron is an essential element and it involved in various biological processes, though in excess it is highly toxic. This condition is referred to iron overload and leads to many diseases like E thalassemia. Nowadays chelation therapy is one of the most useful therapeutic methods for the treatment of iron overload. Some hydrazone analogues are found to be potential oral iron chelating drugs for the treatment of thalassemia and have also been suggested as possible metalchelating agents for treating neurodegenerative disorders such as Alzheimer disease. HPCIH and HPKIH, two different derivate of isonicotinoyl hydrazone, are two iron chelators with contrasting biological behavior. HPCIH is a well-tolerated iron chelator with limited

antiproliferative activity that has potential applications in the treatment of iron overload diseases while HPKIH has significant antiproliferative activity against cancer cells.[75-77]

Analytical applications

According to the review of Singh et al. hydrazones can act as selective metal extracting agents as well as in spectroscopic determination of specific transition metals.[78] Sasaki studied the spectroscopic determination of iron and vanadium using 2,6-diacetylpyridine bis benzoyl hydrazone and the bis 2-hydroxy benzoyl hydrazone. Nickel (II) ions present in edible oils, plant materials and in alloy samples can be analysed using cinnamaldehyde-4-hydroxy benzoyl hydrazones. Gravimetric determinations of metal ions can be effectively done with the help of different hydrazones. Salicylaldehyde phenylhydrazone was found to be the best gravimetric reagent for the determination of copper. Metal complexes of pyridine-2-carbaldehyde-2-pyridylhydrazone have been used as acid-base indicators. Due to the high stability and readily observable colour changes some of the p-nitrophenylhydrazones were proved to be better acid-base indicators. Some of the hydrazones can also be used as spot test reagents for the determination of transition metals.[78] Metal complexes of hydrazones have been used as luminescent probes as well as molecular sensors.[79,80]

Hydrazones in nonlinear optics

Recently studies on the nonlinear optical properties of materials gathered considerable attention because they provide valuable information regarding the structural analysis of these materials and for their practical use in various optoelectronic devices. Compounds which are non centrosymmetric, planar and properly functionalized with strong electron donating and electron withdrawing groups at the terminal position could exhibit large molecular non linearity. Serbutoviez et al. established the relevance of push-pull hydrazones for quadratic nonlinear optics by the measurement of the molecular hyper polarizabilities of some phenyl hydrazone derivatives.[81] Hydrazones possess the ability to exhibit amido-iminol tautomerism, so upon coordination to metal centre through the iminol form improves the conjugation and thus enhances the non-linearity. Second-order nonlinear optical properties of copper and palladium complexes of N-salicylidene-N'-aroylhydrazines were studied by Cariati et al. and the results showed that the complexes have considerable nonlinearity.[82] Optical power limiting, a nonlinear optical effect, is interesting due to its application to the protection of eyes and

sensitive optical devices from high power laser pulses. Naseema et al. investigated the third-order nonlinear optical properties of some hydrazones derived from p-tolyloxy acetohydrazide, and found that the compounds show optical limiting behaviour at a particular wavelength.[83]

Catalytic applications

In metal complexes of hydrazones, the environment at the coordination center can be modified by attaching different substituents to the hydrazone moiety and a useful range of steric and electronic properties essential for the fine-tuning of structure and reactivity can thus be provided. Many of the hydrazone complexes show remarkable catalytic activity in various organic reactions. Monfared et al. studied the catalytic abilities of some oxo- and dioxovanadium(V) complexes of tridentate hydrazones towards the oxidation of various hydrocarbons and found that the complexes are effective catalysts .[84] Coordination complexes of VO with tridentate naphthohydrazone derivatives are found to be a new class of VO catalysts for the oxidation of olefins.[85] One of the cis-dioxomolybdenum(VI) complexes based on amino acid functionalized N-salicylidene hydrazide is an efficient catalyst for the peroxidic oxidation of sulfides.[86] According to Mahmudov et al., a copper (II) dimer with 3-(2-hydroxy-4-nitrophenylhydrazo) pentane-2,4-dione exhibits a good catalytic activity in the peroxidative oxidation of cyclohexane by aqueous H_2O_2, under mild conditions, to afford cyclohexanol, cyclohexanone and cyclohexyl hydroperoxide.[87] Pouralimardan et al. demonstrated that some of the dissymmetric hydrazone manganese (II) complexes are highly selective catalysts for oxidation of cyclohexene under mild conditions.[88]

Other applications

Some of the aroyl-hydrazones can act as herbicides, insecticides, nematocides, rodenticides and plant-growth regulators. Hydramethylnon is an amidinohydrazone insecticide has the trade name Amdro for control of the red fire ant and for use against cockroaches .[89] Hydrazones of 2-methylphthalazone are effective sterilants for houseflies.[78] Many hydrazones are found to be effective corrosion inhibitors of metals. Fouda et al. studied the effect of 2-hydroxyacetophenone-aroyl hydrazone derivatives on the inhibition of copper and found that the corrosion is significantly decreased in presence of the investigated compounds.[90]

1.5 Physical measurements

Single crystal X-ray structure determination

Single crystals of the different ligands, and different complexes were mounted independently on glass fibers for intensity data collections on a Nonius Kappa-CCD area detector diffractometer (Mo Kα = 0.71073 Å). The details of data collection (DENZO software) and structure refinements of each compound are given in the appendix. The cell parameters were determined from reflections taken from one set of 10 frames (1.0° steps in phi angle), each exposure during 20 seconds. The structures were solved using direct methods and refined against F2 using SHELXL97. No absorption correction was applied. All non-hydrogen atoms were refined anisotropically and hydrogen atoms were introduced as fixed contributors (SHELXL97).

Electronic spectroscopy

The UV-Visible spectra were recorded by transmission through N,N-dimethylformamide (DMF) (Sigma Aldrich; <0.1% H_2O) solutions of the compounds using a 8453 Agilent spectrophotometer and a standard 1 cm path length cell. The acid (commercial HCl) and base (distilled triethylamine) solutions were employed for the titration experiments.

Magnetic measurements

Magnetic measurements were performed at the Institut de Physique et Chimie des matériaux de Strasbourg (UMR CNRS ULP 7504) using a Quantum Design MPMS-XL SQUID magnetometer. The susceptibility measurement was performed in the 300–1.8 K temperature range and an applied field of 5 kOe. Isothermal field dependent magnetization measurement at room temperature confirms the absence of ferromagnetic impurities. Data were corrected for the sample holder and diamagnetism of the content estimated from Pascal constants.

Electrochemistry

Electrochemical measurements were performed in pure dimethylformamide (DMF) (Sigma Aldrich; <0.1 % H_2O) which was used as received. Tetrabutylammonium

hexafluorophosphate $TBAPF_6$ (Fluka, electrochemical grade) was used as supporting electrolyte. All electrochemical measurements were carried out at ambient temperature (20 ± 2 °C) in a conventional one compartment, three-electrode cell. The working electrodes were platinum (2 mm diameter), glassy carbon (3.5 mm diameter) or a microelectrode (10 μm diameter), while the counter electrode was a platinum wire and a second platinum wire was used as pseudo-reference. The cell was connected to a PGSTAT 302 potentiostat (Eco Chemie, Holland). Prior to measurements, all the solutions were deoxygenated with argon. When it was necessary, ferrocene was used as internal potential reference.

EPR Measurements

The EPR spectra were recorded at X-band (ca. 9.8 GHz) with an ESP-300E spectrometer (Bruker) equipped with a rectangular TE 102 cavity and an ESR 900 continuous flo cryostat for liquid He circulation (Oxford). The static field was controlled with a Hall probe, whereas the microwave frequency was simultaneously recorded with a frequency counter (HP-5350 B). Solutions were degassed with argon before recording the spectra.

Partial elements analysis

Elemental analysis was performed by the ‘‘Service de microanalyses’’, University of Strasbourg.

Infrared spectroscopy

IR spectra were recorded in the region 4000-400 cm^{-1} on a Nicolet 6700 FT-IR spectrometer (ATR mode, ZnSe Crystal).

NMR spectroscopy

^{1}H and ^{13}C NMR spectra were recorded at RT, on Bruker AVANCE 300, 400, 500, or 600 spectrometers and referenced to the residual solvent resonance. Assignments are based on ^{1}H, ^{1}H COSY, and ^{13}C NMR experiments. Chemical shifts are given in ppm and coupling constants are in Hz.

Solar simulator

Samples were illuminated with solar simulator generating approximately 1.3 sun output. The solar simulator uses a 150 W ozone free xenon lamp, and produces a 1.3-inch (33 mm) diameter collimated beam. Optional air mass and bandpass filters can be added to re-shape the spectral output. It generates more than 1 sun power with an AM1.5G filter installed.

Laser

Samples were illuminated with an Argon-Krypton laser (model stabilite 2018-RM from Spectra Physic) using the multiline mode (superposition of visible lines from the blue (457 nm) up to the green (574 nm)) directly *in situ* in the EPR cavity

1.6 References

(1) Werner, A. *Alfred Werner,... Sur la constitution et la configuration des combinaisons d'ordre élevé, conférence faite à l'occasion de la réception du prix Nobel, le 11 décembre 1913*; Éditions de la "Revue politique et littéraire" (Revue bleue) et de la "Revue scientifique": Paris, 1914.

(2) Sidgwick, N. V. *The electronic theory of valency*; The Clarendon Press: Oxford, 1953.

(3) Stadler, A.-M.; Harrowfield, J. *Inorg Chim Acta* **2009**, *362*, 4298-4314.

(4) Angelusiu, M. V.; Almajan, G. L.; Rosu, T.; Negoiu, M.; Almajan, E. R.; Roy, J. *Eur J Med Chem* **2009**, *44*, 3323-3329.

(5) Angelusiu, M. V.; Barbuceanu, S. F.; Draghici, C.; Almajan, G. L. *Eur J Med Chem* **2010**, *45*, 2055-2062.

(6) Huang, Z.; Tian, J. L.; Bu, X. H. *Inorg Chem Commun* **2005**, *8*, 194-198.

(7) Li, B. Y.; Yao, Y. M.; Wang, Y. R.; Zhang, Y.; Shen, Q. *Polyhedron* **2008**, *27*, 709-716.

(8) Patel, R. N.; Gundla, V. L. N.; Patel, D. K. *Polyhedron* **2008**, *27*, 1054-1060.

(9) Sakiyan, I.; Logoglu, E.; Arslan, S.; Sari, N.; Sakiyan, N. *Biometals* **2004**, *17*, 115-120.

(10) Tumer, M.; Koksal, H.; Sener, M. K.; Serin, S. *Transit Metal Chem* **1999**, *24*, 414-420.

(11) Jamadar, A.; Duhme-Klair, A. K.; Vemuri, K.; Sritharan, M.; Dandawate, P.; Padhye, S. *Dalton T* **2012**, *41*, 9192-9201.

(12) Desousa, G. F.; Filgueiras, C. A. L.; Abras, A.; Aljuaid, S. S.; Hitchcock, P. B.; Nixon, J. F. *Inorg Chim Acta* **1994**, *218*, 139-142.

(13) Dinda, R.; Sengupta, P.; Ghosh, S.; Mayer-Figge, H.; Sheldrick, W. S. *Journal of the Chemical Society-Dalton Transactions* **2002**, 4434-4439.

(14) Galic, N.; Rubcic, M.; Magdic, K.; Cindric, M.; Tomisic, V. *Inorg Chim Acta* **2011**, *366*, 98-104.

(15) Hou, J. X.; Sun, W. H.; Zhang, D. H.; Chen, L. Y.; Li, W.; Zhao, D. F.; Song, H. B. *Journal of Molecular Catalysis a-Chemical* **2005**, *231*, 221-233.

(16) Mishra, D.; Naskar, S.; Blake, A. J.; Chattopadhyay, S. K. *Inorg Chim Acta* **2007**, *360*, 2291-2297.
(17) Prabhu, R. N.; Ramesh, R. *Rsc Adv* **2012**, *2*, 4515-4524.
(18) Seth, S.; Chakraborty, S. *Acta Crystallogr C* **1984**, *40*, 1530-1533.
(19) Clément, N.; Toussaint, C.; Rogez, G.; Loose, C.; Kortus, J.; Brelot, L.; Choua, S.; Dagorne, S.; Turek, P.; Welter, R. *Dalton T* **2010**, *39*, 4579.
(20) Matoga, D.; Szklarzewicz, J.; Grybos, R.; Kurpiewska, K.; Nitek, W. *Inorg Chem* **2011**, *50*, 3501-3510.
(21) Matoga, D.; Szklarzewicz, J.; Gryboś, R.; Kurpiewska, K.; Nitek, W. *Inorg Chem* **2011**, *50*, 3501-3510.
(22) Matoga, D.; Szklarzewicz, J.; Nitek, W. *Polyhedron* **2012**, *36*, 120-126.
(23) Patel, R. N.; Singh, A.; Shukla, K. K.; Patel, D. K.; Sondhiya, V. P. *Journal of Coordination Chemistry* **2011**, *64*, 902-919.
(24) Toussaint, C.; Beghidja, C.; Welter, R. *Comptes Rendus Chimie* **2010**, *13*, 343-352.
(25) Zuo, W. W.; Rosa, V.; Tourbillon, C.; Specklin, D.; Khaled, C.; Kurmoo, M.; Welter, R. *Rsc Adv* **2012**, *2*, 2517-2526.
(26) Bouslimani, N.; Clement, N.; Toussaint, C.; Hameury, S.; Turek, P.; Choua, S.; Dagorne, S.; Martel, D.; Welter, R. *Eur J Inorg Chem* **2009**, 3734-3741.
(27) Singh, B.; Narang, K. K.; Srivastava, R. *Synthesis and Reactivity in Inorganic and Metal-Organic Chemistry* **2001**, *31*, 1375-1386.
(28) Singh, B.; Srivastava, R.; Narang, K. K. *Synthesis and Reactivity in Inorganic and Metal-Organic Chemistry* **2000**, *30*, 1175-1192.
(29) Bouslimani, N.; Clement, N.; Toussaint, C.; Hameury, S.; Turek, P.; Choua, S.; Dagorne, S.; Martel, D.; Welter, R. *Eur J Inorg Chem* **2009**, 3734-3741.
(30) Beghidja, C.; Wesolek, M.; Welter, R. *Inorg Chim Acta* **2005**, *358*, 3881-3888.
(31) Bouslimani, N.; Clement, N.; Rogez, G.; Turek, P.; Bernard, M.; Dagorne, S.; Martel, D.; Cong, H. N.; Welter, R. *Inorg Chem* **2008**, *47*, 7623-7630.
(32) Xiao, W.; Lu, Z. L.; Wang, X. J.; Su, C. Y.; Yu, K. B.; Liu, H. Q.; Kang, B. S. *Polyhedron* **2000**, *19*, 1295-1304.
(33) Naskar, S.; Naskar, S.; Mondal, S.; Majhi, P. K.; Drew, M. G. B.; Chattopadhyay, S. K. *Inorg Chim Acta* **2011**, *371*, 100-106
(34) Galal, S. A.; Hegab, K. H.; Kassab, A. S.; Rodriguez, M. L.; Kerwin, S. M.; El-Khamry, A. M. A.; El Diwani, H. I. *Eur J Med Chem* **2009**, *44*, 1500-1508.
(35) Singh, V. P. *Spectrochim Acta A* **2008**, *71*, 17-22.
(36) Beghidja, C.; Rogez, G.; Kortus, J.; Wesolek, M.; Welter, R. *J Am Chem Soc* **2006**, *128*, 3140-3141.
(37) Specklin, D.; Tourbillon, C.; Rosa, V.; Kurmoo, M.; Welter, R. *Inorg Chem Commun* **2012**, *20*, 172-176.
(38) Datta, A.; Chuang, N.-T.; Huang, J.-H. *Journal of Chemical Crystallography* **2011**, *41*, 1780-1784.
(39) Naskar, S.; Naskar, S.; Mondal, S.; Majhi, P. K.; Drew, M. G. B.; Chattopadhyay, S. K. *Inorg Chim Acta* **2011**, *371*, 100-106.
(40) Saadeh, S. M. *Arabian Journal of Chemistry* **2013**, *6*, 191-196.
(41) Bessy Raj, B. N.; Prathapachandra Kurup, M. R.; Suresh, E. *Spectrochimica Acta Part A: Molecular and Biomolecular Spectroscopy* **2008**, *71*, 1253-1260.
(42) Pouralimardan, O.; Chamayou, A.-C.; Janiak, C.; Hosseini-Monfared, H. *Inorg Chim Acta* **2007**, *360*, 1599-1608.
(43) Ray, A.; Banerjee, S.; Sen, S.; Butcher, R. J.; Rosair G. M.; Maria T. G.; Mitra, S. *Inorg Chim Acta* **2006**, *350*, 1590-1600.
(44) Mondal, S.; Naskar, S.; Dey, A. K.; Sinn, E.; Eribal, C.; Herron, S. R.; Chattopadhyay, S. K. *Inorg Chim Acta* **2013**, *398*, 98-105.

(45) Naskar, S.; Biswas, S.; Mishra, D.; Adhikary, B.; Falvello, L. R.; Soler, T.; Schwalbe, C. H.; Chattopadhyay, S. K. *Inorg Chim Acta* **2004**, *357*, 4257-4264.
(46) Naskar, S.; Mishra, D.; Butcher, R. J.; Chattopadhyay, S. K. *Polyhedron* **2007**, *26*, 3703-3714.
(47) Blanco, F.; Egan, B.; Caboni, L.; Elguero, J.; O'Brien, J.; McCabe, T.; Fayne, D.; Meegan, M. J.; Lloyd, D. G. *Journal of Chemical Information and Modeling* **2012**, *52*, 2387-2397.
(48) Cordier, C.; Vauthier, E.; Adenier, A.; Lu, Y. H.; Massat, A.; Cosse-Barbi, A. *Struct Chem* **2004**, *15*, 295-307.
(49) Galić, N.; Dijanošić, A.; Kontrec, D.; Miljanić, S. *Spectrochimica Acta Part A: Molecular and Biomolecular Spectroscopy* **2012**, *95*, 347-353.
(50) Chaur, M. N.; Collado, D.; Lehn, J.-M. *Chemistry - A European Journal* **2011**, *17*, 248-258.
(51) Zhao, N.; Wu, Y.-H.; Luo, J.; Shi, L.-X.; Chen, Z.-N. *The Analyst* **2013**, *138*, 894.
(52) Bermejo, A.; Ros, A.; Fernandez, R.; Lassaletta, J. M. *J Am Chem Soc* **2008**, *130*, 1 5798.
(53) Jing-lin, W.; Bin, L.; Bin-sheng, Y. *CrystEngComm* **2011**, *13*, 7086.
(54) Agarwal, C.; Prasad, E. *New Journal of Chemistry* **2012**, *36*, 1859.
(55) Jamadar, A.; Duhme-Klair, A.-K.; Vemuri, K.; Sritharan, M.; Dandawate, P.; Padhye, S. *Dalton T* **2012**, *41*, 9192.
(56) Zuo, W. W.; Tourbillon, C.; Rosa, V.; Cheaib, K.; Andrade, M. M.; Dagorne, S.; Welter, R. *Inorg Chim Acta* **2012**, *383*, 213-219.
(57) Li, S. H.; Gao, S. K.; Liu, S. X.; Guo, Y. N. *Cryst Growth Des* **2010**, *10*, 495-503.
(58) Bouchameni, C.; Beghidja, C.; Beghidja, A.; Rabu, P.; Welter, R. *Polyhedron* **2011**, *30*, 1774-1778.
(59) Ruben, M.; Lehn, J. M.; Vaughanc, G. *Chem Commun* **2003**, 1338-1339.
(60) Uppadine, L. H.; Gisselbrecht, J. P.; Lehn, J. M. *Chem Commun* **2004**, 718-719.
(61) Uppadine, L. H.; Lehn, J. M. *Angew Chem Int Ed* **2004**, *43*, 240-243.
(62) Naskar, S.; Corbella, M.; Blake, A. J.; Chattopadhyay, S. K. *Dalton T* **2007**, 1150.
(63) Yu, G.-M.; Zhao, L.; Guo, Y.-N.; Xu, G.-F.; Zou, L.-F.; Tang, J.; Li, Y.-H. *Journal of Molecular Structure* **2010**, *982*, 139-144.
(64) Siemann, S.; Evanoff, D. P.; Marrone, L.; Clarke, A. J.; Viswanatha, T.; Dmitrienko, G. I. *Antimicrob Agents Ch* **2002**, *46*, 2450-2457.
(65) Tamasi, G.; Chiasserini, L.; Savini, L.; Sega, A.; Cini, R. *J Inorg Biochem* **2005**, *99*, 1347-1359.
(66) Patole, J.; Sandbhor, U.; Padhye, S.; Deobagkar, D. N.; Anson, C. E.; Powell, A. *Bioorg Med Chem Lett* **2003**, *13*, 51-55.
(67) El-Sherif, A. A. *Inorg Chim Acta* **2009**, *362*, 4991-5000.
(68) Filipovic, N.; Borrmann, H.; Todorovic, T.; Borna, M.; Spasojevic, V.; Sladic, D.; Novakovic, I.; Andjelkovic, K. *Inorg Chim Acta* **2009**, *362*, 1996-2000.
(69) Todeschini, A. R.; de Miranda, A. L. P.; da Silva, K. C. M.; Parrini, S. C.; Barreiro, E. J. *Eur J Med Chem* **1998**, *33*, 189-199.
(70) Ainscough, E. W.; Brodie, A. M.; Dobbs, A. J.; Ranford, J. D.; Waters, J. M. *Inorg Chim Acta* **1998**, *267*, 27-38.
(71) Johnson, D. K.; Murphy, T. B.; Rose, N. J.; Goodwin, W. H.; Pickart, L. *Inorg Chim a-Bioinor* **1982**, *67*, 159-165.
(72) Pickart, L.; Goodwin, W. H.; Burgua, W.; Murphy, T. B.; Johnson, D. K. *Biochem Pharmacol* **1983**, *32*, 3868-3871.
(73) Rollas, S.; Kucukguzel, S. G. *Molecules* **2007**, *12*, 1910-1939.
(74) Sridhar, S. K.; Pandeya, S. N.; Stables, J. P.; Ramesh, A. *Eur J Pharm Sci* **2002**, *16*, 129-132.
(75) Becker, E.; Richardson, D. R. *J Lab Clin Med* **1999**, *134*, 510-521.

(76) Bernhardt, P. V. *Dalton T* **2007**, 3214-3220.
(77) Bernhardt, P. V.; Wilson, G. J.; Sharpe, P. C.; Kalinowski, D. S.; Richardson, D. R. *J Biol Inorg Chem* **2008**, *13*, 107-119.
(78) Singh, R. B.; Jain, P.; Singh, R. P. *Talanta* **1982**, *29*, 77-84.
(79) Basu, C.; Chowdhury, S.; Banerjee, R.; Evans, H. S.; Mukherjee, S. *Polyhedron* **2007**, *26*, 3617-3624.
(80) Ganjali, M. R.; Rezapour, M.; Rasoolipour, S.; Norouzi, P.; Adib, M. *J Brazil Chem Soc* **2007**, *18*, 352-358.
(81) Serbutoviez, C.; Bosshard, C.; Knopfle, G.; Wyss, P.; Pretre, P.; Gunter, P.; Schenk, K.; Solari, E.; Chapuis, G. *Chem Mater* **1995**, *7*, 1198-1206.
(82) Cariati, F.; Caruso, U.; Centore, R.; Marcolli, W.; De Maria, A.; Panunzi, B.; Roviello, A.; Tuzi, A. *Inorg Chem* **2002**, *41*, 6597-6603.
(83) Naseema, K.; Sujith, K. V.; Manjunatha, K. B.; Kalluraya, B.; Umesh, G.; Rao, V. *Opt Laser Technol* **2010**, *42*, 741-748.
(84) Monfared, H. H.; Kheirabadi, S.; Lalami, N. A.; Mayer, P. *Polyhedron* **2011**, *30*, 1375-1384.
(85) Monfared, H. H.; Bikas, R.; Mayer, P. *Inorg Chim Acta* **2010**, *363*, 2574-2583.
(86) Mancka, M.; Plass, W. *Inorg Chem Commun* **2007**, *10*, 677-680.
(87) Mahmudov, K. T.; Kopylovich, M. N.; da Silva, M. F. C. G.; Figiel, P. J.; Karabach, Y. Y.; Pombeiro, A. J. L. *Journal of Molecular Catalysis a-Chemical* **2010**, *318*, 44-50.
(88) Pouralimardan, O.; Chamayou, A. C.; Janiak, C.; Hosseini-Monfared, H. *Inorg Chim Acta* **2007**, *360*, 1599-1608.
(89) Hollingshaus, J. G. *Pestic Biochem Phys* **1987**, *27*, 61-70.
(90) Fouda, A. S.; Gouda, M. M.; Abd El-Rahman, S. I. *B Kor Chem Soc* **2000**, *21*, 1085-1089.

Chapter 2:

Iron(III) high spin photoreduction

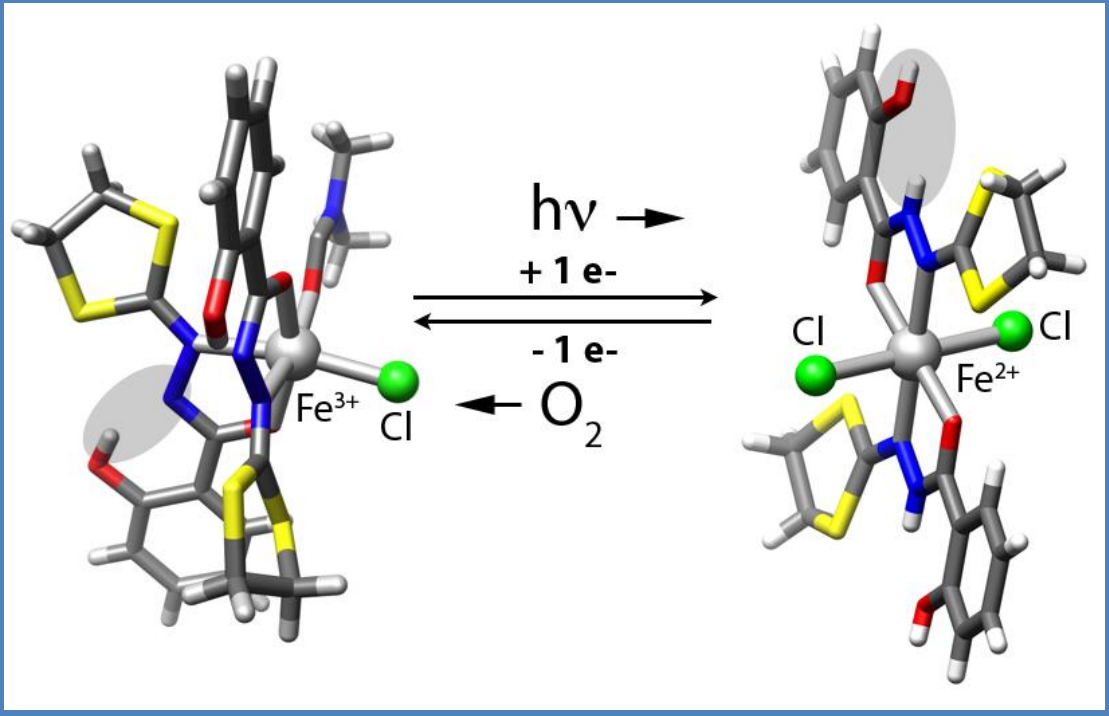

Foreword:

There are increasing public awareness that the earth's oil reserves will run out during this century and there would be a major shortage of energy supply unless new energy sources especially the renewable ones are discovered or developed.

Because solar energy is the most abundant renewable energy resource, the clear connection between human activity and global warming has strengthened the interest in photovoltaic science.

Dye sensitized solar cells (DSSCs) (**Fig. I**) provide a promising low-cost technology for harnessing this energy source. Until recently, much of the research surrounding DSSCs had been focused on the sensitization of n-type semiconductors, such as titanium dioxide (Graetzel cells). In an n-type dye sensitized solar cell (n-DSSC), an electron is injected into the conduction band of an n-type semiconductor (n-SC) from the excited state of the sensitizer. The first step on this photo conversion system is the **photo oxidation** of the **Ruthenium** complexes dye. However, there is still a drawback in such photon current conversion system: the non-abundant distribution of ruthenium metal in the earth, whose relative high price would contribute to the main cost of the whole device.

Comparatively few studies have examined the sensitization of wide band gap p-type semiconductors (**Fig. II**). In a p-type DSSC (p-DSSC), the photo excited sensitizer is **reductively** quenched by hole injection into the valence band of a p-type semiconductor (p-SC). p-DSSCs are the mirror images of conventional n-DSSCs, they share some structural similarities, but they use **different materials** and have different charge transfer kinetics. In this technology, nickel oxide is the predominant p-SC material used, but much higher photo conversion efficiencies could be achieved with new p-SCs materials with deeper valence band potential. The first step on this photo conversion system is the **photo reduction** of the dye sensitizer.

Iron is the most abundant metal on earth, and it is so cheap comparing to Ruthenium. From here comes our motivation to investigate on the photo reduction of ferric complexes in order to understand the mechanism of the photochemical process and further to use ferric complexes as Dyes for p-type DSSC as well as photo rechargeable batteries

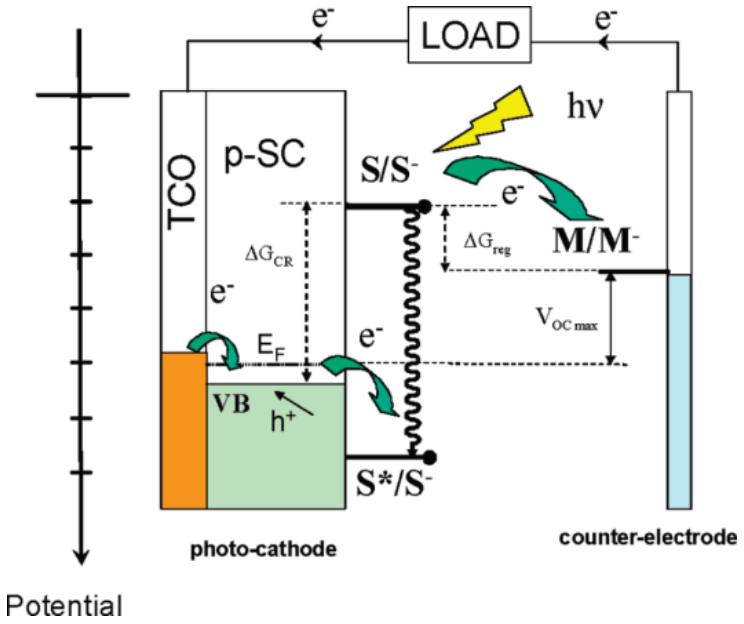

Figure I: p-type DSSC

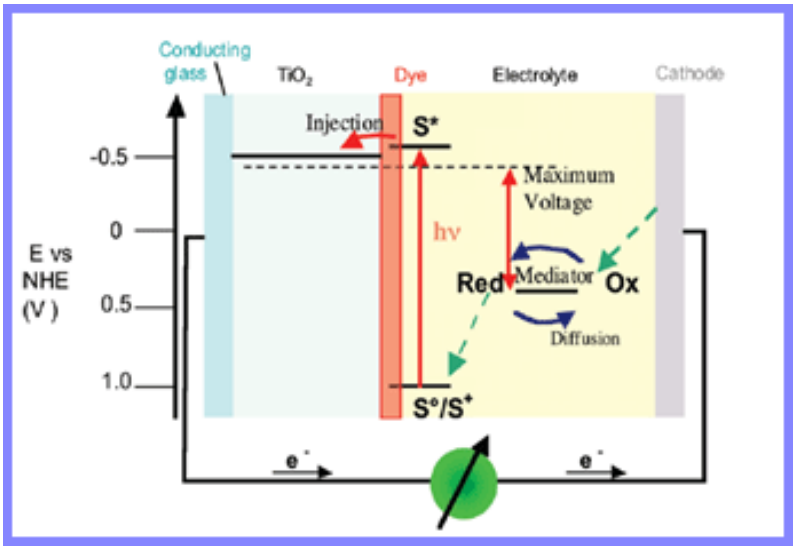

Figure II: n-type DSSC

Chapter 2 :

Photo reduction of Iron(III) high spin supported by N,O-bidentate ligands.

Photoreduction of Iron(III) high spin supported by N,O-bidentate ligands.

KEYWORDS: Photoreduction, LMCT, aroyl-hydrazone, bidentate ligand, high spin iron, EPR, DMF radical, EtOH radical, spin adduct, withdrawing group.

Abstract: Photo-redox reaction occurring in irradiated DMF solutions of $Fe^{III}(HL)_2(DMF)(Br)$ complex, where HL is an anionic N,O-bidentate ligand, has been investigated and a mechanism has been proposed. The complex is redox stable in the dark. Upon irradiation with UV-Visible light the $Fe^{III}(HL)_2(DMF)(Br)$ complex was photo reduced to the $Fe^{II}(H_2L)_2(Br)_2$ complex where H_2L is a neutral N,O-bidentate ligand. Both Fe^{III} and Fe^{II} complexes have been isolated and characterized by single crystal diffraction. The photoreduction occurs in polar solvents such as MeOH and EtOH but it doesn't take place in non-polar solvent. The photochemical process has been followed by UV-Visible spectroscopy and the photochemical properties was attributed to LMCT excited state. The presence of the halide atom on the ferric coordination sphere seems to be crucial for the reduction. The photo-redox process takes place in frozen solution. As intermediate, $\dot{C}H_2(CH)_3NCHO$ radical was identified in the irradiated frozen DMF solution. Using spin trapping EPR technique, the formation of $CH_3\dot{C}HOH$ radical was identified in the irradiated EtOH solution. Modification on the ligand aromatic moiety with different substituents was performed, and the photoreduction of the Fe(III) complex doesn't take place for the ligand bearing a strong electron withdrawing group such as $-NO_2$.

1.1 Introduction

Iron is one of the most abundant elements in the earth's crust, where is present as both Fe(II) and Fe(III) oxidation states.[1] It has been proved that redox properties of iron and certainly photoreduction of Fe(III) to Fe(II) plays an essential role in different natural processes such as atmosphere, sea, ocean and biological. For example, once in the atmosphere, iron (as Fe (II) and Fe (III)) plays an important role in the multiphase atmospheric chemistry of S(IV).[2-7] When iron (III) containing aerosols, particulate Fe participates in electron transfer reactions within the cloud droplet. Graedel and coworkers have stressed the importance of iron speciation as a major factor controlling the reactivity of Fe (III) as a catalyst, as an oxidant, and as photolytic source of $OH^{\cdot}$ Radical in fog, cloud and rain.[8] Fe(III) and Fe(II) have been also found to coexist in oxic surface waters.[9-11] Bencala et al. pointed out the importance of the photoreduction of Fe(III) in acidic mountain stream.[12] The photoreduction of Fe(III) porphyrins complexes as catalysts for mono-oxygenation reactions has been also extensively investigated, these process mimicking the behavior in vivo of cytochrome P- 450.[13-18] In the Photo-Fenton reaction, the most additional oxidant process (AOP) used like practical industrial applications for the treatment of waste polluted waters and the degradation of pollutants and toxic organic compounds, the photo reduction of Fe(III) to Fe(II) plays an important role in accelerating the rate of the process and regenerating Fe(II) which are essentials in the degradation process.[19,20] Major potential realized applications of the photochemistry of Fe (III) complexes can be grouped in four main categories: photo catalysis, photo initiators, photo destructors in polymer chemistry and on a smaller scale as photoconductors, active substance of conventional photographic materials.[21] The photochemical properties of iron(III) complexes have been attributed to the presence of ligand to metal charge transfer absorption band as reported by balzani.[22] Scrutiny of the vast coordination chemistry of iron reveals that certain ligands provide significant stabilization to the +3 oxidation state while others ligands prefer to bind iron in the +2 state. It is now established that ligands with carboxamide,[23-28] oxime and carboxylate[29,30] group exhibit preference toward Fe (III) centers. Ligands with pyridine and imidazole nitrogens and thioether on the other hand afford stable Fe (II) complexes.[31-34] Therefore, a varying number of these donor ligands can be assembled in a designed complex to tune the redox, optical and magnetic properties of the iron center. Within the complete range of N,O-bidentate ligands,

there are groups where the N,O-donor atoms can become charged anionically and an important group of this type is those based on –CONHN= acyl-/aroyl-hydrazones and their derivatives. These ligands coordinate to the metal ion, either in the monoanionic iminolate form (Ia in scheme 1) or the neutral amide form (Ib in scheme 1) forming five-membered chelate rings with the metal. The present work is based on the photoreduction of Fe(III) aroyl- hydrazone complex stabilized by the deprotonated iminolate form of the ligand to his corresponding Fe(II) complex stabilized by the neutral amide form of the ligand.

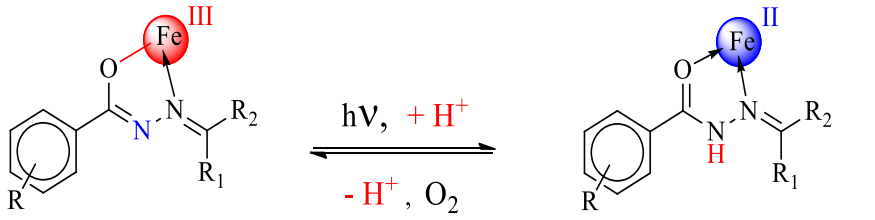

Bidentate anionic style X,L
I a

Bidentate neutral style L,L
I b

Scheme 1: Photoreduction and coordination mode of aroyl-hydrazone ligands

1.2 Results and discussion

Synthesis and crystal structures

The reaction of 2 eq of 2-salicyloylhydrazono-1,3-dithiolane (H_2L) with 1 eq of $FeBr_3$ in DMF results in a green solution where upon diffusion of diethyl ether it affords single crystals of the ferric complex **C1** (Fe^{III}(**HL**)$_2$(DMF)(Br) **scheme 2**) in a good yield. An important procedure to be respected in this synthesis is the absent of natural light. This is because exposure of the green solution to a natural light induces a gradual color change to yellow. Slow diffusion of diethyl ether into the yellow solution leads the formation of the ferrous complex **C2** (Fe^{II}(**H_2L**)$_2$(Br)$_2$), as single crystals suitable for X-Ray diffraction. Upon air exposure, the latter yellow solution turns back to its original green color within a few seconds. Noteworthy, the photochemical process doesn't take place in non-polar solvent; it just occurs in polar solvents such as EtOH, MeOH, DMF and DMSO. The complexes of Fe(III) in MeOH (**C3**) and EtOH (**C4**) were isolated as single crystals suitable for X-Ray diffraction.

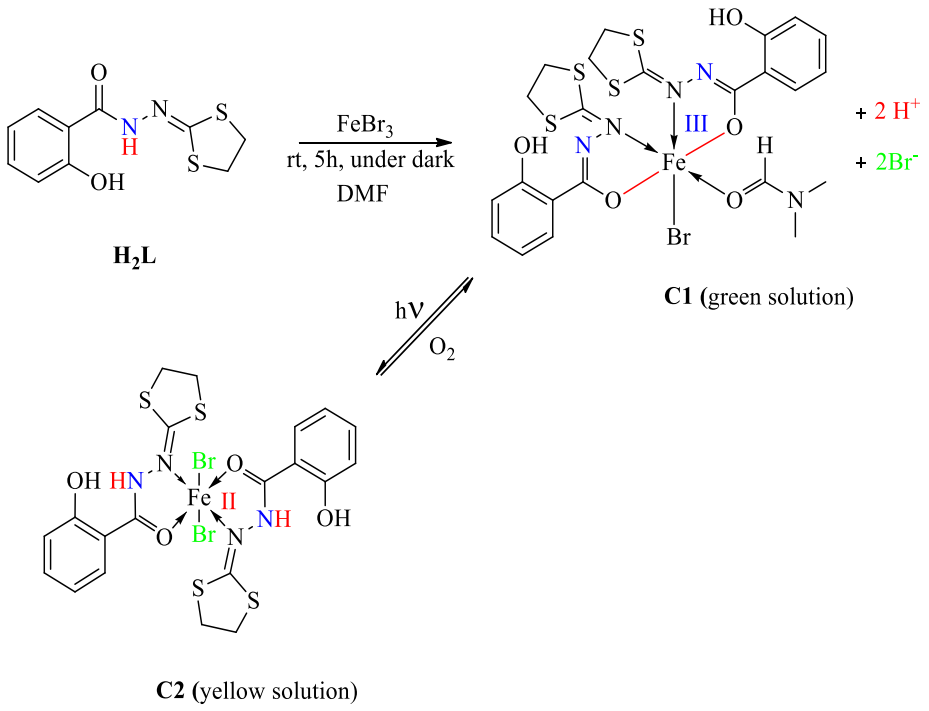

Scheme 2: Synthetic pathways for **C1** and **C2**

Crystal structure of C1

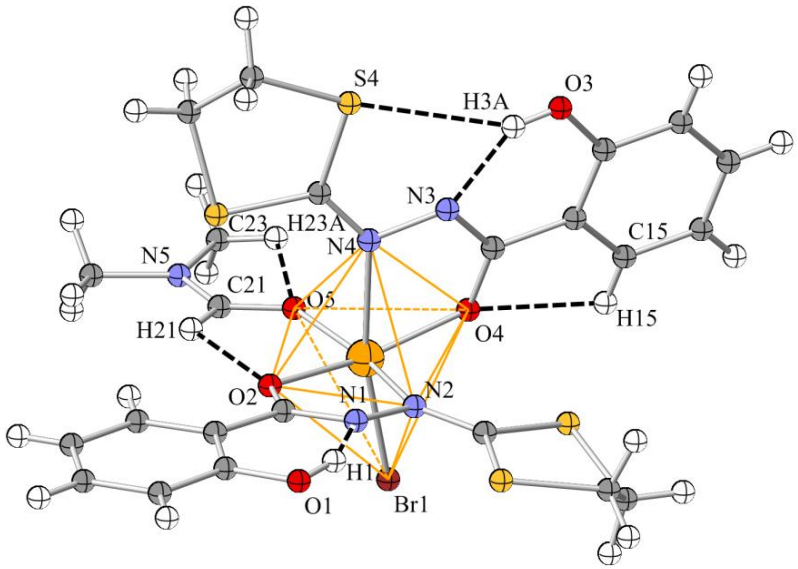

Figure 1*:* Ball and stick view of **C1** with parttial labeling scheme (dashed black lines show the intramolecular H-Bond)

Fe(**HL**)$_2$(DMF)(Br) or **C1** crystallizes in the monoclinic space group ***P*2$_1$/c** as a mononuclear **Fe^{III}** species. The ferric atom is in a distorted octahedral geometry. As clearly shown in

Figure 1, both **HL**$^-$ are anionic bidentate ligands (absence of hydrogen atom on N_1 and N_3) forming 5 member chelating ring with the metal. Iminolate oxygen (O_2 and O_4) and trigonal azomethine nitrogen (N_2 and N_4) are the available coordination sites for the ligands. One HL^- is in the equatorial position of the octahedral and the other adopts a *cis* configuration. The octahedral coordination environment of the Fe^{III} ion is completed by an axial bromide atom and one DMF molecule (figure 1). The large Fe-N (average distance = 2.2164(15) Å), and Fe-Br (2.4160(3) Å) bond distances deduced from the diffraction data (table I appendix Ch. 2) are in accordance with a high-spin electronic configuration **(S=5/2)** for this complex. This is confirmed by solid state EPR as well as by magnetometric.[35,36] Six classical intramolecular hydrogen bonds has been detected (PLATON software) and located, 2 medium strength between O1 and N1 via H1 (d=1.85 Å), O3 and N3 via H3A (1.84 Å). Four other weak bonds located between C23 and O5 via H23A; C21 and O2 via H21; C15 and O4 via H15; O3 and S4 via H3A with the distances 2.36 Å, 2.44 Å 2.48 Å and 2.88 Å respectively. As non-classical hydrogen bonds, only one intermolecular C–H···π interaction has been pointed out (PLATON software): C10–H10A···(C1–C6)′ (′is related to the symmetry code -x, 1/2 - y, 1/2 - z); 2.66 Å between the hydrogen atom and the centre of the benzene ring (C1–C6) of an adjacent molecule, with an angle of 146°. The corresponding packing diagram is represented in figure 2.

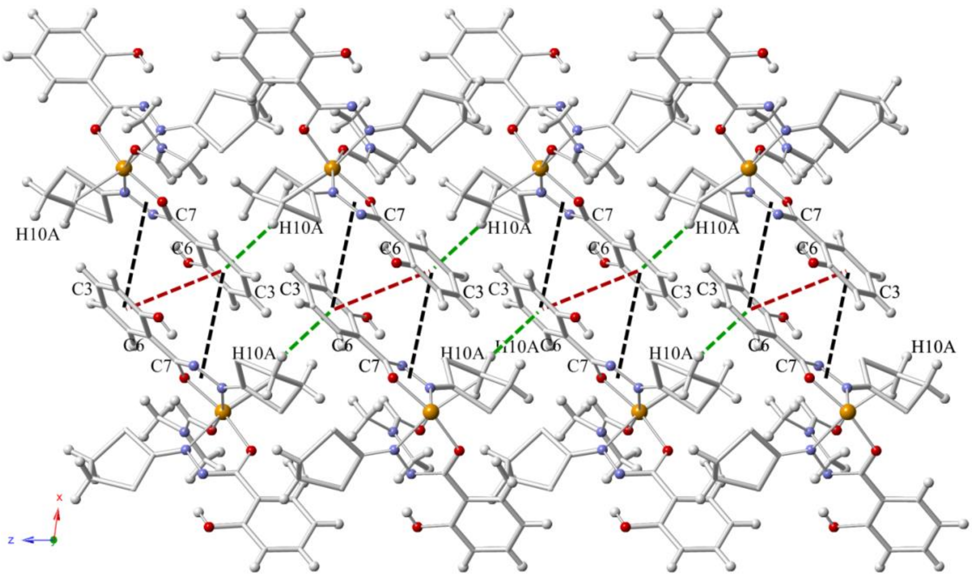

Figure 2: Packing view of **C1** (projection in the lattice plane x, 0, z).Green dashed lines show the C-H···π interaction between C10-H10A and the centre of the benzene ring (C1-C6)' of an adjacent molecule (' is the symmetry code: -x, ½-y, ½-z). Black dash lines indicate the interaction between the centre of (C1-C6)' and Cg(1) (Cg(1) is the five member ring Fe, N1, N2, O2 and C7). Red dash line show the interaction between (C1-C6) and (C1-C6)'

Crystal structure of C2

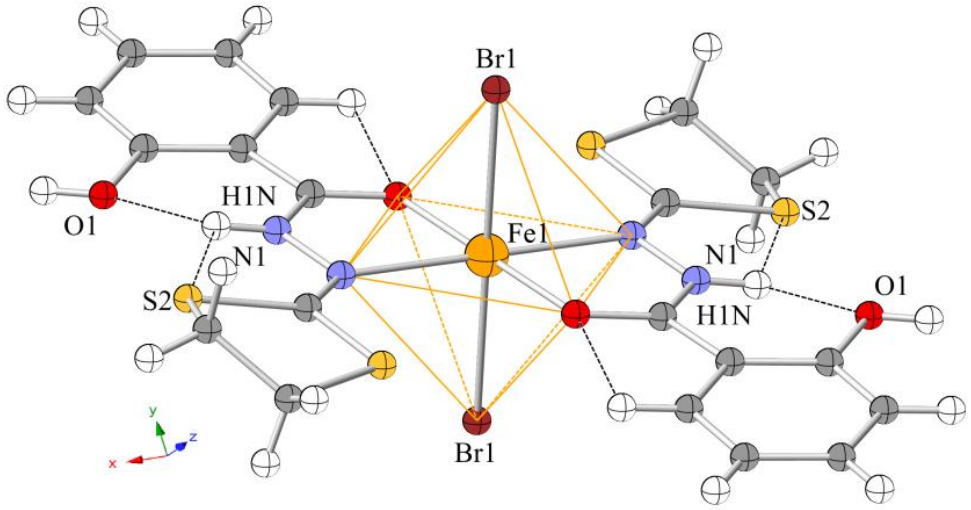

Figure 3: Ball and stick view of of **C2** with parttial labeling scheme (dashed lines show the intramolecular H-Bond)

5 ml of the green solution of **C1** was degassed with nitrogen for 20 minutes to remove dissolved oxygen. Under an atmosphere of nitrogen, the 5 ml was transferred to the lower part of a 20 ml closed glass test tube with a septum cap. The solution was exposed to light by a solar simulator and when it had changed from green to yellow, the tube was carefully filled with Et_2O under inert atmosphere. Yellow crystals (suitable for X-ray diffraction) of **C2** were obtained. The quick surface coloration indicates the air sensitivity of the $\mathbf{Fe^{II}}$ species. This compound crystallizes in the monoclinic space group $\boldsymbol{P2_1/c}$ as a mononuclear $\mathbf{Fe^{II}}$ species. A structural representation view of the molecular is depicted in figure 3. The asymmetric unit contains one half of the molecule of **C2**, and the complete molecule $Fe(\mathbf{H_2L})_2(Br)_2$ is generated by the inversion symmetry centered on the Fe atom. The unit cell contains two molecules and the coordination of the ferrous ion is octahedral. As clearly shown in figure 2 both $\mathbf{H_2L}$ are bidentate neutral ligands (presence of hydrogen atom H1N on the N1 nitrogen atom clearly pointed out by Fourier differences), which chelate the metal ion by the amide oxygen and the trigonal azomethine nitrogen. Both H_2L are in the equatorial position of the octahedral and adopt a *trans* configuration. The coordination sphere around the Fe(II) cation being completed by two axial bromide (-I). The large Fe-N (average distance = 2.209(2) Å) and Fe-Br (2.6547(12) Å) bond distances deduced from the diffraction data (table II app. Ch. 2) are in accordance with a high spin electronic configuration (S=2) for octahedral Fe(II) complex.[36-38] Three intramolecular hydrogen bonds have been detected (PLATON software)

and located between N1 and S2 via H1N; N1 and O1 via H1N; C5 and O2 via H5 with distances 2.48 Å, 1.99 Å and 2.40 Å respectively (see figure 3). No classical hydrogen bond has been detected in this crystal structure. One intermolecular hydrogen bond between O1 and Br1' via H1A (' is related to the symmetry code 2-x, -y, 1-z) with a distance of 2.43 Å. The corresponding packing diagram is represented in figure 4.

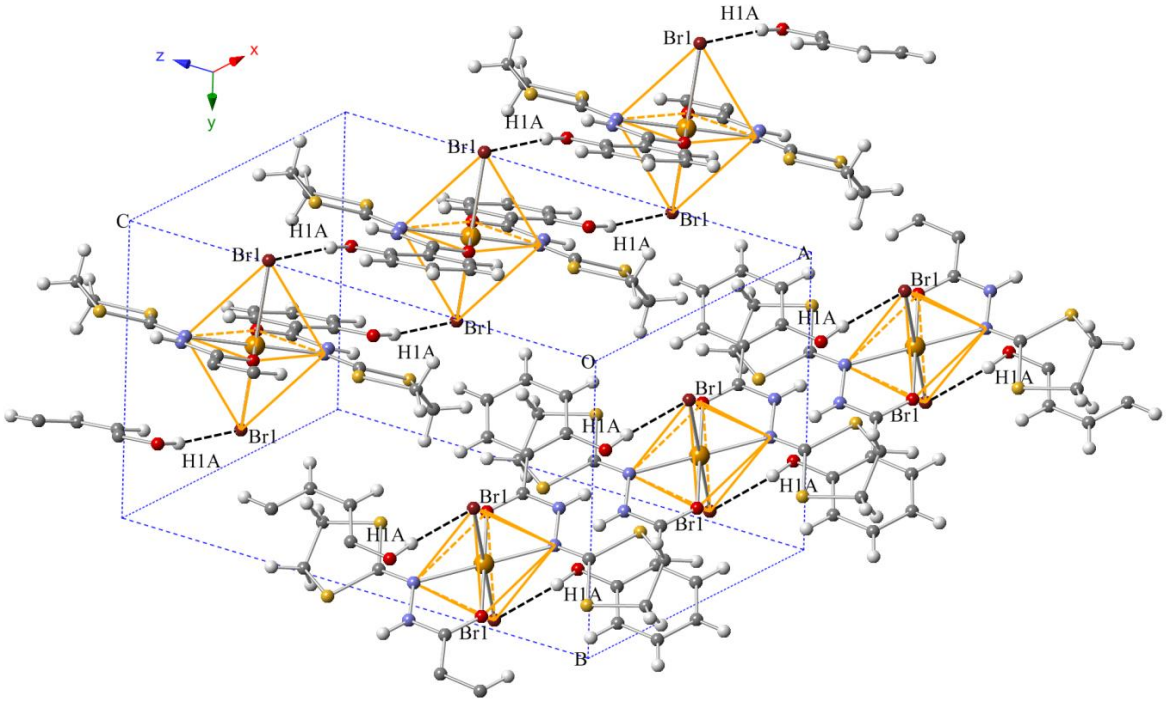

Figure 4: Packing view of **C2**. Black dashed line: intermolecular hydrogen bonds between Br1 and H1A' (' is related to thesymmetry code 2-x, -y, 1-z).

Crystal structure of C3 (Fe^{III} in MeOH) **and C4** (Fe^{III} in EtOH)

Following the same procedure described for **C1** in scheme 2, the reaction of 2 eq of **H_2L** with 1 eq of $FeBr_3$ in MeOH and EtOH yields the formation of green solutions. The corresponding Fe(III) complexes **C3** (in **MeOH**) and **C4** (in **EtOH**) were isolated as single crystals suitable for X-Ray diffraction after diffusion of diethyl ether into the green solutions mixtures, in the dark. Light exposure of this green solutions of the investigated Fe(III) complexes, leads to a gradual color change (from green to yellow). No suitable single crystals of the yellow solutions could be grown thus far despite numerous attempts; nevertheless the color changing from green to yellow upon light exposure, which switch back to green after air exposure (or O_2 bubbling) could be an strong indicative to the presence of iron(II) species. As same as **C3**, complex **C4** crystallizes in the space group ***P*2$_1$/c**, and the overall structure is almost the same. Structural representation of **C4** and a comparison table of structural parameters between **C3**

and **C4** (bond distances and angles degrees), showing the similarity are depicted on the appendix(fig. A3, A4, A5 and table III, IV app. Ch. 2). In the following we will describe the crystal structure of **C3**. Complex **C3** crystallizes in space group ***P*2₁/c**. Unit cell of **C3** comprises of four molecules. The asymmetric unit contains two independent unit of Fe^{III}. Here it is interesting to note that in «unit A», ferric iron is hexacoordinated while in «unit B»; it is penta coordinated (figure 5). The Fe atoms in the two units (A and B) are separated by a distance of 9.645 Å. The two iron atoms in the same asymmetric unit face the same donor environment with the exception of one extra coordinated methanol moiety in «unit A» which is absent in «unit B». The methanol moiety accounts for the different coordination geometry around the two Ferric iron atoms.

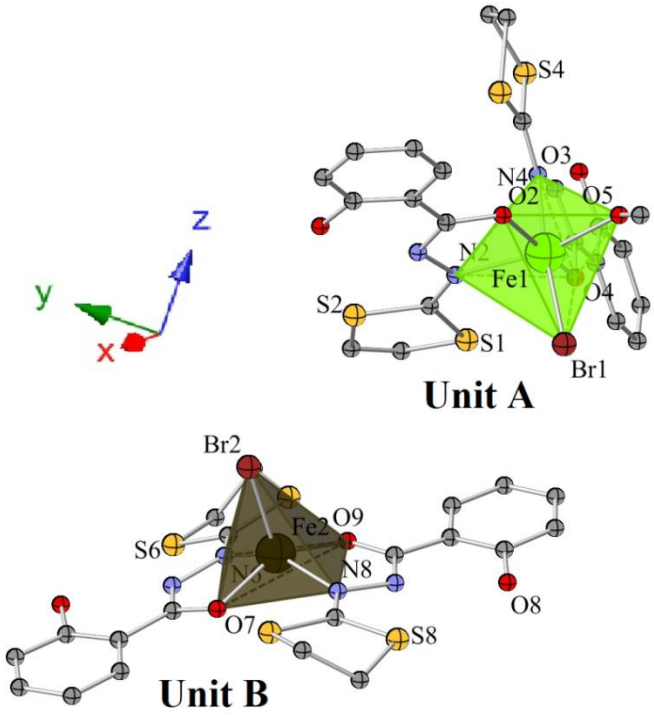

Figure 5: The two different units of **C3** (Fe^{III} in MeOH)

For unit A, the iron atom is in distorted octahedral geometry (see figure 6), where four equatorial positions are coordinated by three oxygen atoms (deprotonated iminolate oxygens O2, O4 and protonated methyl oxygen O5) and one azomethine nitrogen (N2) atom, while the free axial position is occupied by one bromide atom and one azomethine N4 atom. Both ligands are deprotonated in a *cis* configuration. Three classical intramolecular hydrogen bonds have been detected (PLATON software) and located, 2 medium strength between O1 and N1 via H1 (d=1.85 Å), O3 and N3 via H3A (d=1.84 Å). One other weak bond located between C5 and O2 via H5.

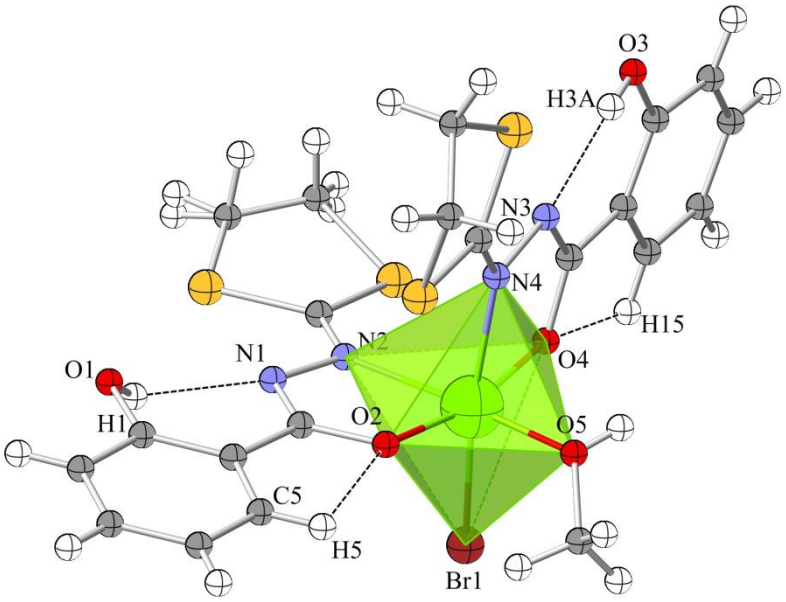

Figure 6: Ball and stick view of **unit A** (dashed lines show the intramolecular H-Bond).

In unit B, the Ferric atom is in distorted square pyramidal geometry (figure 5). Here four equatorial positions are occupied by two HL^- ligands in a *trans* configuration (deprotonated iminolate oxygen O7 and O9, and two azomethine nitrogens N6 and N8) and the axial coordination site is completed by one bromide atom. Four classical intramolecular hydrogen bonds have been detected (PLATON software) and presented with dashed black lines in fig. 5. The large Fe-N(average distance 2.09 Å) and Fe-Br (d= 2.34 Å) bond distances deduced from the diffraction data (table IV and V app. Ch. 2) are in accordance with a high-spin electronic configuration (S=5/2) for this complex.[39]

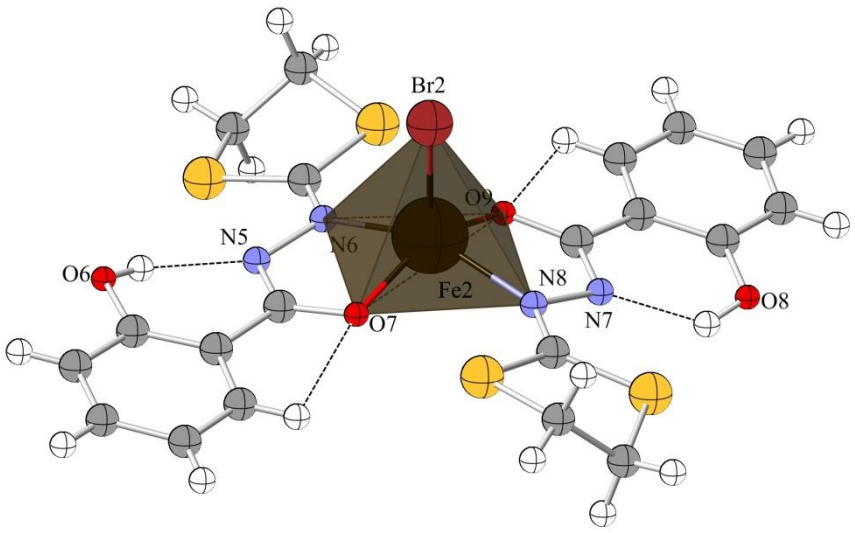

Figure 7: Ball and stick view of **unit B** (dashed lines show the intermolecular H-Bond).

1.3 Electronic spectroscopy

The photoredox process was monitored by UV-Visible spectroscopy. A solution mixture (Concentration 5.10^{-5} M) of two eq of **H_2L** and one eq of $FeBr_3$ in DMF which yields the formation of **C1** as already proved by X-Ray was prepared. The solution was added in a special designed quartz cuvette (figure A6 app. Ch. 2).The O_2 was totally removed by freeze pump procedure by the use of primary and secondary vacuum. Typically, the electronic absorption spectrum of the complex **C1** consists of several distinct bands and shoulders (spectrum of **C1** in fig. 8). As already observed for similar iron (III) complexes with high spin state and hexacoordinated geometry, the absorption of a photon in the visible region (550 nm) can be attributed to a LMCT transition (ε= 2060 $M^{-1}.cm^{-1}$),[21,40-43] and the ultraviolet bands centered at 298, 305 and 320 nm to the intraligand transitions IL($\pi\rightarrow\pi^*$) localized predominantly on the phenol ring, the azomethine C═N double bond and the iminolate C═N fragments of the deprotonated ligands (iminolate form HL^-). Owing to their spin-forbidden nature, d-d transitions bands were not observed. Control experiments confirmed that **C1** do not undergo spontaneous redox changes in DMF solution in the dark. First the light source was a solar simulator generating approximately 1.3 sun output (UV and visible radiations, the IR was totally blocked).The cuvette was located 10 cm away from the light source. Continuous irradiation of the stirred free oxygen DMF solution of the investigated complex leads the complete disappearing of the LMCT at 550 nm (figure 8 and 9). After three hours, the absorption spectrum didn't evolve, even with extending the time of irradiation, the photoreduction was completed and the investigated Fe(III) was totally transformed. Over the time, bands on the UV region shifted to lower energy (298 nm *vs* 302 nm and 320 nm *vs* 325 nm) with hypochromic effects (figure 9 and 10). Formation of isosbestic points (figure 8) and the disappearing of the LMCT which is spin forbidden for Fe(II) high spin is a prove for the formation of **C2**. Introducing oxygen into the system after switching off the irradiation lead to a slow reappearance of the initial Fe(III) complex spectra.

We also changed the source of irradiation with an Argon-Krypton laser using the multiline mode (superposition of visible lines from the blue (457 nm) up to the green (574 nm)). The photoreduction occurred with the same spectral features on the UV-visible spectra. It follows from the above interpretation that the photochemical properties of **C1** could be attributed to LMCT exited state and the primary step on the photo-redox process is to populate the LMCT exited state.

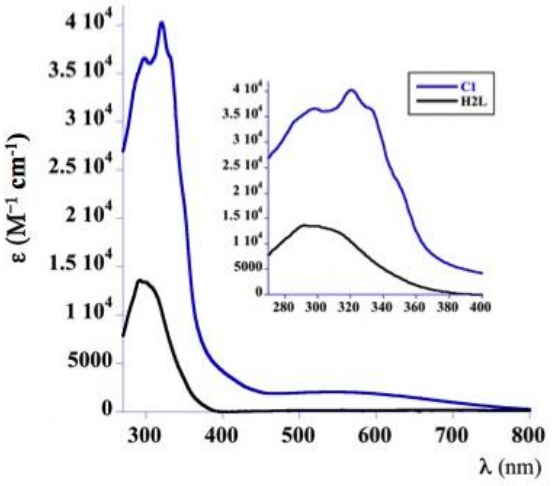

Figure 8: Electronic spectrum for **C1** (blue line), and the ligand (black line)

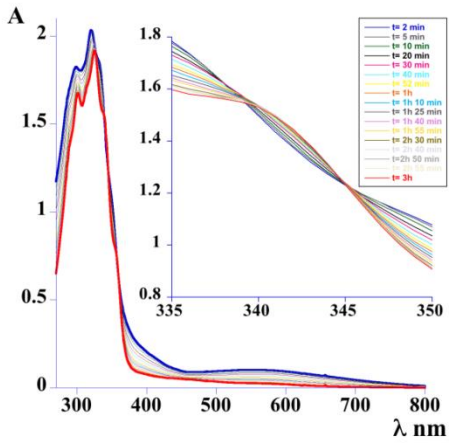

Figure 9: evolution of **C1** spectra upon light irradiation

Table 1: maximum absorption and corresponding molar absorptivity of **H_2L** and **C1**

Compound	wavelength (max)	ε (M^{-1} cm^{-1})
H_2L	292 299	13600 13400
C1	298 305 320 550	36600 36100 40300 2060
After 3hours of irradiation	302 325	33500 38300

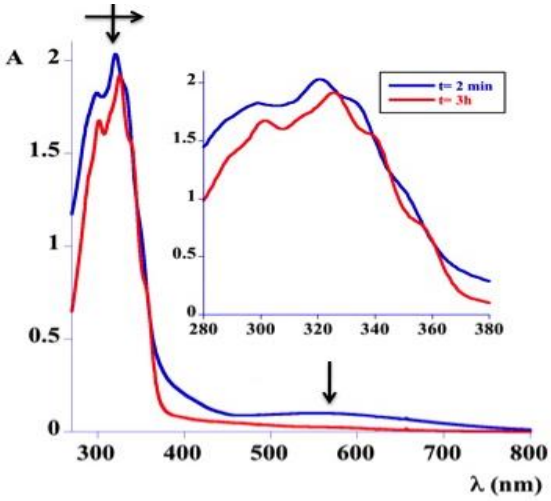

Figure 10: Beginning (blue line) and the end (red line) of the photoredox process

1.4 Presence of halides on the axial position

The Fe─X bond (X= halide) seems to be crucial on the photoreduction reaction. The photochemical process takes place even if we replace the bromide by a chloride (**C1** and **C5** **scheme 3**). The Fe^{III} complex (**C5**) and his corresponding Fe^{II} (**C6**) have been also isolated as single crystals and were reported.[36] Light exposure of **C7** where the complex is supported by three bidentate ligands (absence of halide atom), didn't lead any change on the blue color of the solution mixture and the UV-Visible spectrum didn't change with irradiation. No photo

redox process in case of **C7** recently published.[35] In order to understand the role of halide and to have more information about the mechanism, the photochemical process has been followed by electronic paramagnetic resonance (EPR) spectroscopy.

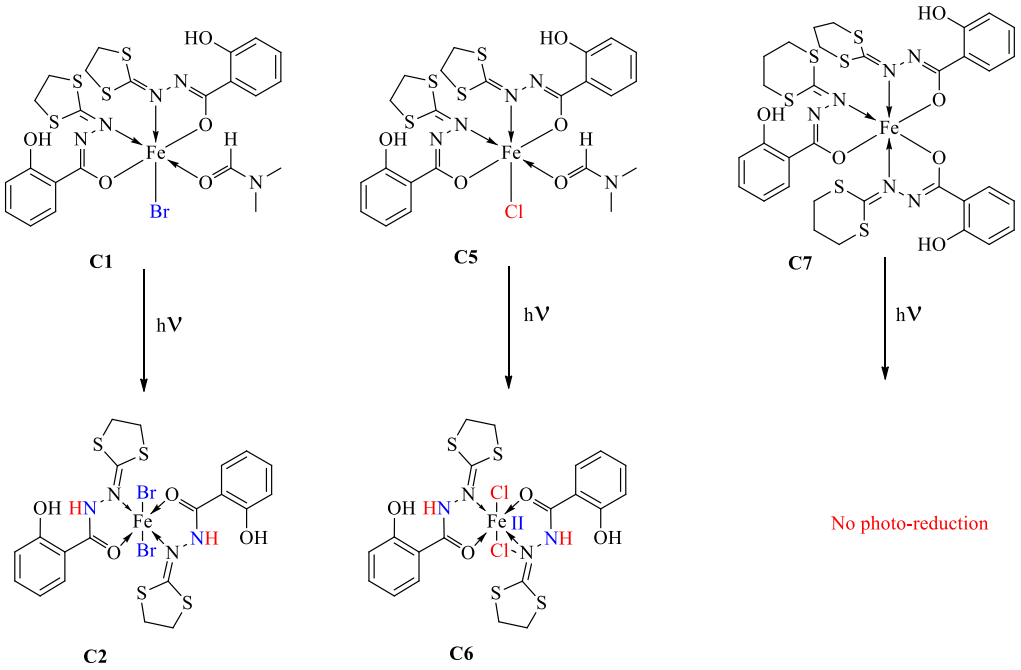

Scheme 3: Effect of light on **C1**, **C5** and **C7**

1.5 EPR spectroscopy and intermediate

Solvent effect

Ethanol

Irradiation in visible region was investigated in CH_3CH_2OH solvent. In order to explore the mechanism of the photoreduction, we used EPR (electron paramagnetic resonance) spin trapping technique to identify intermediate such as $CH_3\dot{C}HOH$ radical. Nitroso and nitrone compounds are well known for their radical trapping and their ability to form stable spin adduct detectable by EPR spectroscopy (Free radicals in Biology, Vol. IV, Ed. By William A. Pryor). One of the most commonly used nitrone spin trap is PBN (α-phenyl-N-*tert*-butyl nitrone) which can react with carbon centered radicals (see scheme 4).

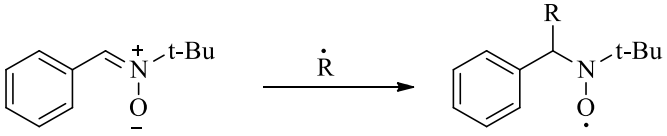

Scheme 4: Reaction of PBN with organic radical

The resultant spin adduct from the reaction with PBN and the radical ethanol can be readily distinguished from other spin adduct with characteristic EPR parameters. Irradiation with visible light (λ> 450 nm) of an argon-saturated solution containing 10^{-2} M of a mixture of one equivalent of $FeCl_3$, two equivalent of H_2L and three equivalent of PBN in ethanol gave the EPR signal in figure 11. The signal intensity increased upon irradiation and reached a maximal level at 5 minutes. The hyperfine coupling constants extracted from the signal (a^N= 16 G and a^H=3.7 G) correspond to those PBN- $CH_3\dot{C}HOH$ adduct (figure 11 b).[44]

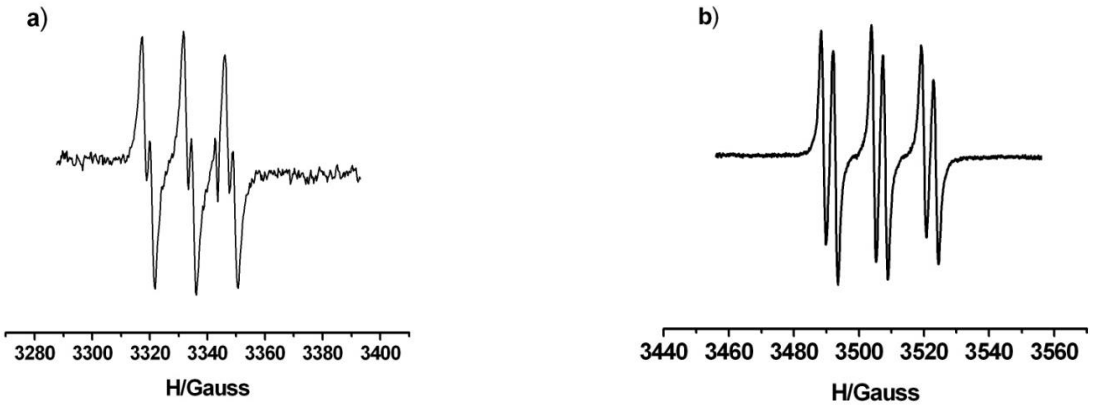

Figure 11: EPR spectrum showing the spin adduct obtained after irradiation in the visible at room temperature in the presence of 3×10^{-2} mol/L of PBN with 10^{-2} M of a mixture of a) one equivalent of $FeBr_3$, two equivalent of H_2L b) one equivalent of $FeCl_3$, two equivalent of H_2L.

The same result is observed with one equivalent of $FeBr_3$ in the same experimental conditions but with a less intense EPR signal. The maximum of the EPR intensity is observed after 30 minutes of irradiation and we accumulated the spectrum (see figure 11 a).

DMF

Before irradiation of different samples, we have characterized the complexes in DMF solution by EPR spectroscopy. Both spectra **C1** (Fe(**HL**)$_2$(DMF)(Br)) and **C5** (Fe(**HL**)$_2$(DMF)(Cl)) were recorded at low temperature due to the fast relaxation time which induces broad lines at high temperature. The spectra recorded in frozen DMF solution exhibit for **C1** and **C5** an intense signal at g_{eff}= 4.2 with a tiny signal at g=6.7; 5.32; and a very broad feature around g=2.0. These signals are attributed to a high spin (S=5/2) hexacoordinated Fe(III) ions.[37,45]

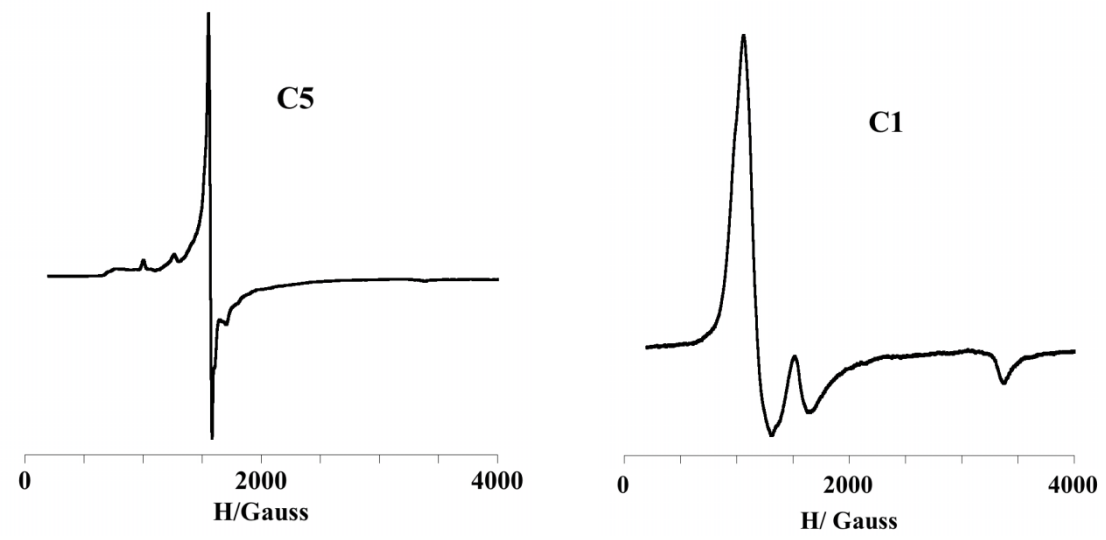

Figure 12: EPR spectra recorded in frozen DMF solution at low temperature (6K). right for C1(10^{-2} M) and left for C5 (10^{-2} M)

We started the irradiation in the visible region *in situ* in the EPR cavity with **C5** and **C1** complexes at low temperature. At 5 K the photoreduction didn't started and to accelerate the initial reaction we increase the temperature up to 120 K and 80 K for **C1** and **C5** respectively. The time course of the signal at g_{eff}=4.2 was examined for the both compounds. The signal intensity decreases with time after 30 minutes of irradiation and subsequently a new signal formed by a poor resolved triplet appeared in the g=2.002 region (see figure 13a and b). The EPR spectra observed are consistent with $HCON(CH_3)\dot{C}H_2$ radical with an hyperfine coupling constant of 19 G.[46] As the temperature increased the signal disappeared.

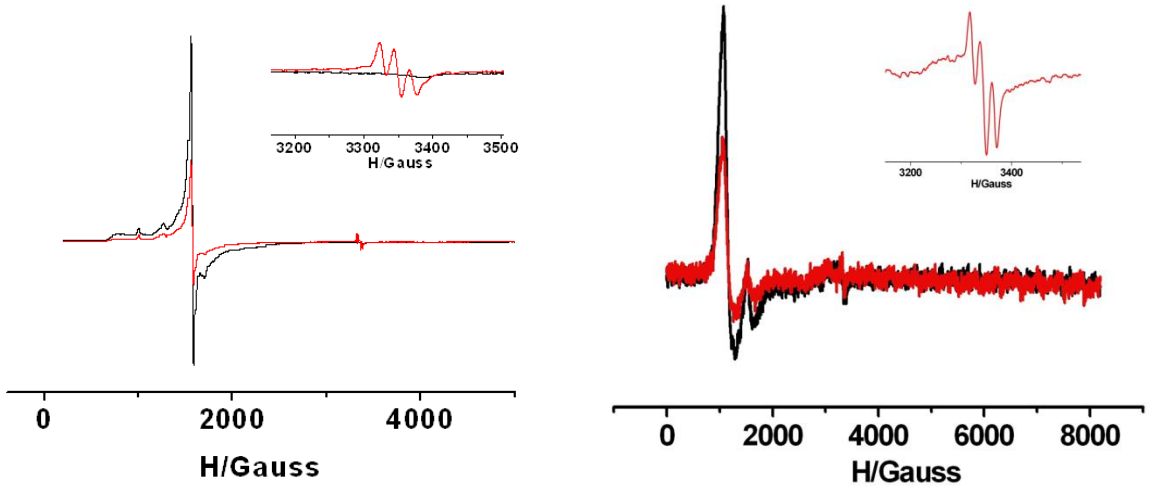

Figure 13: On the left EPR spectra of Fe(**HL**)$_2$ (DMF)(Cl) 10^{-2} M in DMF at 80 K: black line before irradiation, red line after 3 hours of irradiation. On the left EPR spectra of Fe(**HL**)$_2$(DMF)(Br) 10^{-3} M in DMF at 120K: black line before irradiation, red line after 3 hours of irradiation.

Based in the above spectra, EPR spectroscopy allowed to identify radicals intermediate to propose mechanism of the processes occurring in irradiated systems of Fe(III) complexes.

1.6 Electronic effect of different substituents on the ligand peripheral

In order to understand the electronic effect of the ligands on the photochemical process, three bidentate ligands (**H_2L**, **HL'** and **HL''** scheme 5) bearing different substituents on the aroyl skeleton were synthesized. **HL'** with a naked phenyl, **H_2L** bearing a hydroxyl donor group on the ortho position of the phenyl ring, and **HL''** with a strong electron withdrawing group (EWG) -NO_2 located at the para position of the phenyl ring. **HL''** was isolated as crystals and characterized using single-crystal diffraction.

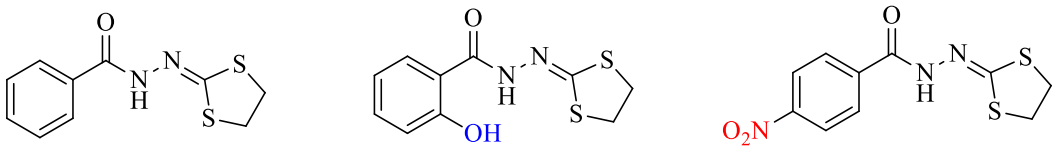

HL' **H_2L** **HL''**

Scheme 5: different aroyl hydrazono-1,3-dithiolane ligands

Crystal structure of HL''

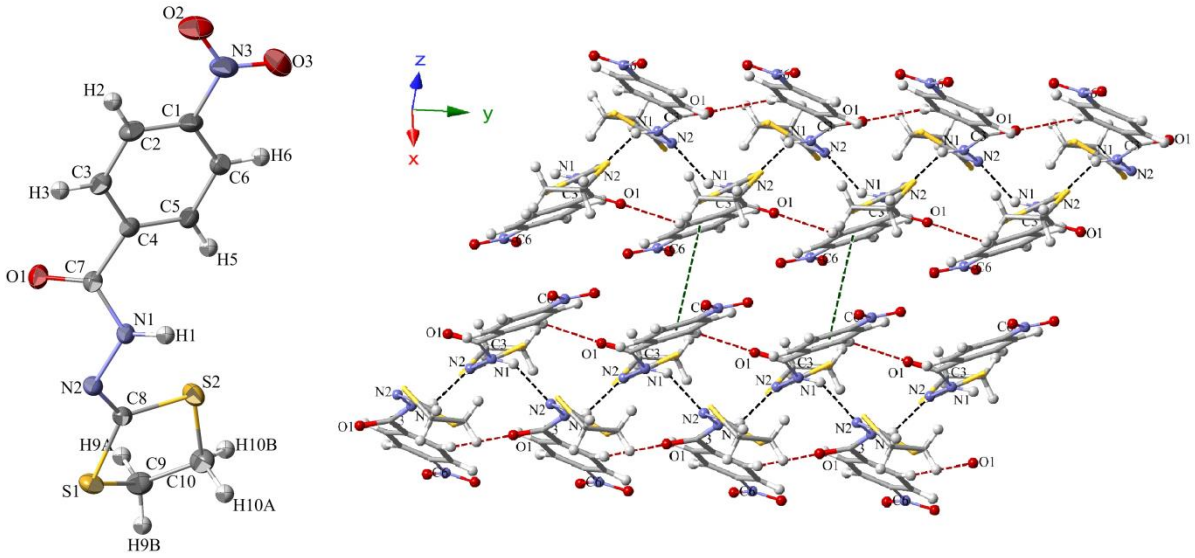

Figure 14 : On the left ORTEP View for **HL''**. On the right stacking view belon the lattice (X, 0, Z) (dashed Green line interaction between centre of the benzene ring (C1 – C6) and (C1-C6)'''; dashed red line interaction between O1 and C5' via H5'; dashed black line interaction between N2 and N1" via H1")/ ' is the symmetry code x, -1+y, z ; " is the symettry code -x,-1/2+y, 1/2-z and ''' is the symmetry code -x,-y,-z.

The prism crystals suitable for analysis were grown by slow diffusion of Et_2O into a DMF solution of **HL''**. The molecule crystalises in a monoclinic system with a space group ***P*2$_1$/c**. A perspective view of the compound showing the crystallographic numbering scheme is shown in figure 14; selected geometric parameters are collected in table 2 (Comparison of structural parameters for **HL'** and **H_2L** published earlier by our laboratory[47,48] and **HL''** is also shown in table 2). The azomethine nitrogen N2 is *syn* to O1 with respect to the C7─N1 bond. The molecule exists in the keto form in the solid-state, this could be confirmed by the C7–O1 bond distance of 1.223(2)Å wich is so close to the standard C═O bond length 1.21 Å.[49,50] The N2–C8 (azomethine) bond length is 1.284(2) Å, with significant double-bond character, is comparable to those previously reported in analogous hydrazone structures.[51,52] The central part of the molecule adopts a completely extended double bonded conformation. The C7–O1 is close to that expected for a carbon–oxygen double bond, the C7–N1 and N1–N2 distances of 1.359(2) and 1.4153(18) Å are significantly shorter than the expected single bond values of 1.47 and 1.45 Å, respectively.[49,50,53] Similar observation was reported in the case of early published crystal structures of hydrazone molecules. Two intermolecular hydrogen bonds have been detected (PLATON software) and located between O1 and C5**'** via H5**'** (**'** is related to the symmetry code x, -1+y, z); between N2 and N1**''** via H1**"** (**"**is related to the symmetry code -x,-1/2+y, 1/2-z), with distances of 2.53 and 2.26 Å. The corresponding packing diagram is represented in figure 14.

Table 2: Selected atomic distances (Å) and bond angles (°) of **H_2L**, **HL'** and **HL''**

	HL"	**H_2L**	**HL'**
C8─N2(azomethine)	1.284(2)	1.281(4)	1.278(4)
N2─N1	1.4153(18)	1.385(3)	1.406(4)
C7─N1(amide)	1.359(2)	1.342(3)	1.346(5)
C7─O1(amide)	1.223(2)	1.230(3)	1.241(4)
C7─C4	1.498(2)	1.494(4)	1.491(5)
N2 C8 S1	120.02(12)	125.9(2)	126.8(3)
N2 C8 S2	124.86(13)	118.8(2)	118.6(3)
C8 N2 N1	112.07(13)	115.1(2)	113.1(3)
C7 N1 N2	116.51(13)	119.3(2)	118.5(3)
O1 C7 N1	123.98(15)	122.3(2)	122.0(3)
N1 C7 C4	114.74(14)	116.4(2)	115.8(3)
O1 C7 C4	121.13(14)	121.2(2)	122.0(3)

Complexation and photo redox process

$FeCl_3$ was used in the present studies as our primary Fe(III) source. In dark, the reaction of two eq of aroyl-hydrazono-1,3-dithiolane ligands (**H_2L, HL' and HL''** in scheme 6) with one eq of $FeCl_3$ yields the formation of different Fe(III) complexes **C5, C8** and **C10** respectively, surrounded by two bidentate ligands, one chloride atom and one DMF molecule. The solution mixture is blue for **C5** and **C8**, and green for **C10**. The ferric complexes **C5**, **C8** and **C10** were isolated as single crystals after diffusion of Et_2O into the DMF solutions. C8 and C10 were characterized by EPR spectroscopy. The spectra have the same features than the corresponding high spin C5 complex (see figure A7 app. Ch. 2).

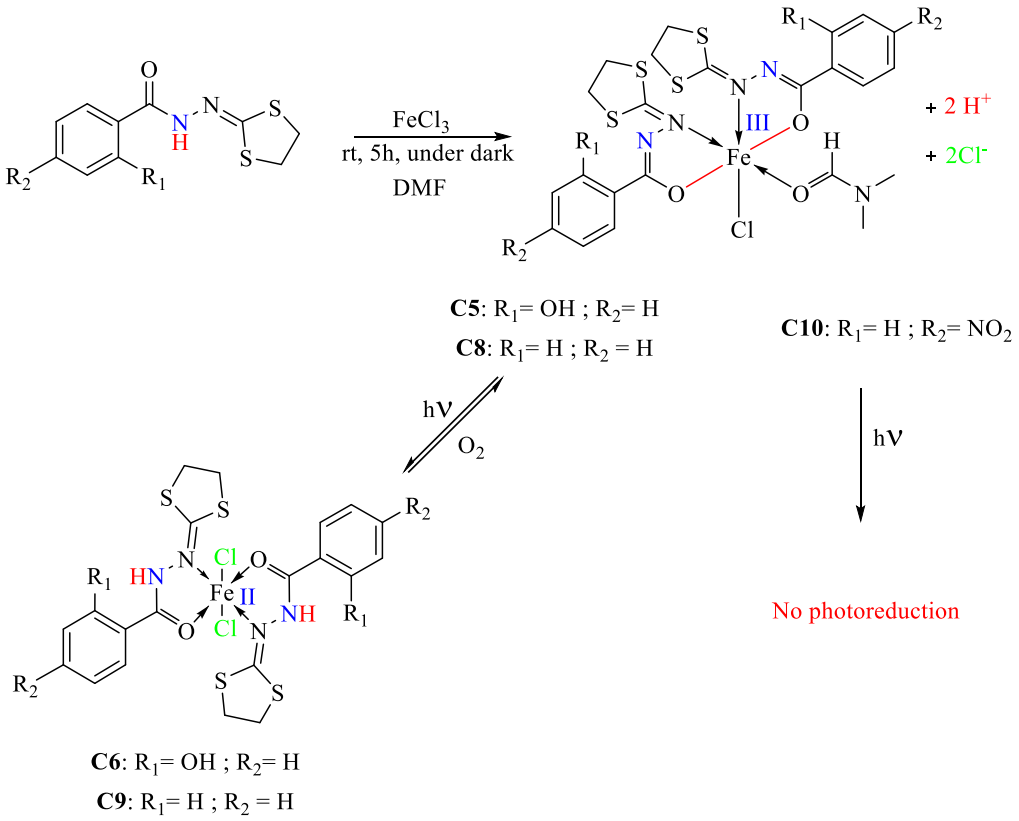

Scheme 6: Synthetic pathway for **C5**, **C6**, **C8**, **C9**, **C10** and their photo redox process

Light absorption by the blue solutions induces a color transformation to a yellow whereas no change was observed for **C10.** The color switching and the following of the photo redox process by UV-Visible spectroscopy pointed that the photoreduction takes place in case of **C5** and **C8**. Fe(III) was completely transformed to Fe(II) and the corresponding ferrous iron complexes (**C6** and **C9**) were isolated as single crystals. In the other hand the green mixture (**C10** presence of withdrawing group on the ligand) didn't change upon light irradiation. Light

exposure didn't lead any change on the nature of the investigated compound, and the UV-Visible spectrum didn't show any variation with the progressing for the time of irradiation.

Crystal structure of C10

Complex C**10**, isolated as suitable single crystals for X-Ray analysis, crystallizes in the space group ***P*2₁/c** as a mononuclear Fe(III) species, in which the central Fe atom adopts an octahedral geometry (see figure 14). Both deprotonated (**L"**) ligands (the absence of hydrogen atom on N1 and N3 is unambiguously observed by X-ray diffraction) are in a *cis* configuration and the deformed octahedral environment is completed by one chloride atom and one DMF solvent molecule. The overall structure of **C10** appears to be very similar to **C5** and **C8** recently published by our group.[36,54] The average distance of the bonds Fe─N_{imine} (2.184 Å) is consistent with the high-spin state of iron(III) in a pseudo octahedral geometry. Typically, octahedral HS distances of Fe─N_{imine} are in the ranges 2.09 – 2.22 Å, whereas the corresponding distances for LS iron(III) are in the ranges 1.92- 1.96 Å.[55-60] The average Fe─O bond length is known to be insensitive to the spin state of the Fe(III).[55-66]

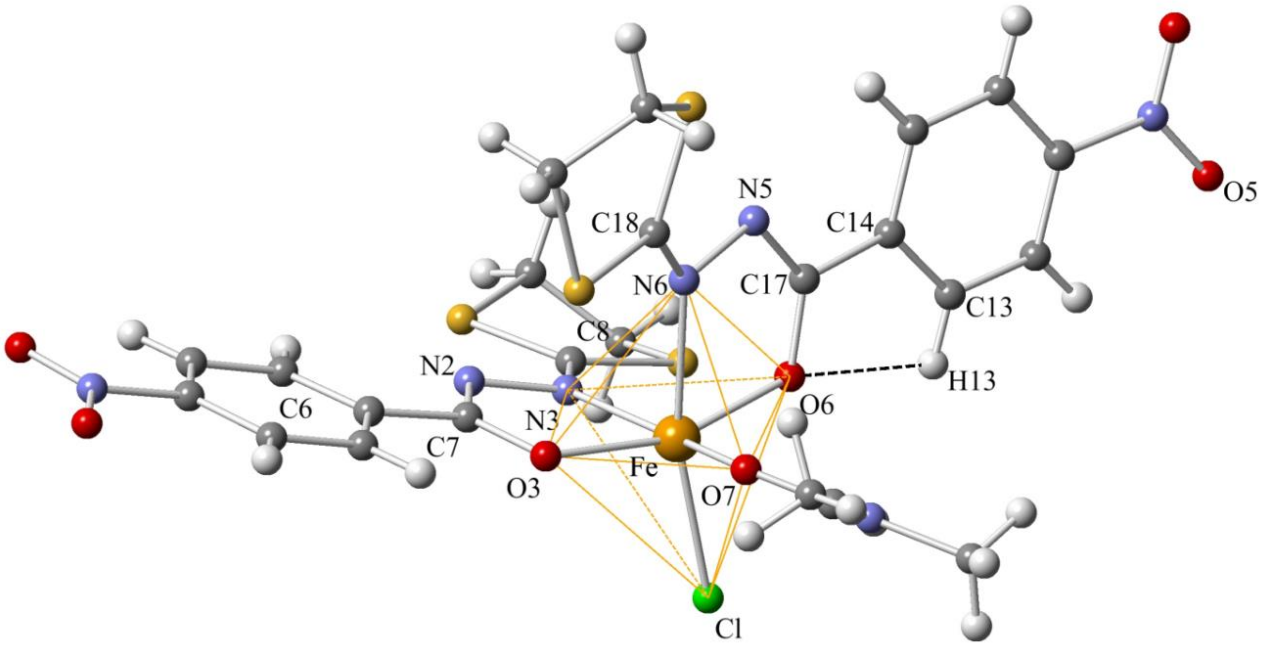

Figure 15: Ball and stick view of **C10 (**dashed black line show the non classical intramolecular H bond between O6 and C13 via H13)

No significant changing on the average distance of the bonds Fe─N_{imine} for the different Ferric complexes (Comparison of structural parameters for **C5**, **C8** and **C10** is shown in table 3). For **C10,** the Fe─$O_{iminolate}$ bonds (avarage distance= 1.961 Å) are slightly shorter than Fe─$O_{iminolate}$ bonds in **C5** and **C8** (average distance = 1.975 Å). In another hand the Fe─Cl bond in C10 (distance= 2.3011(8) Å) is shorter than Fe─Cl bond in C5 (Fe─Cl bond length 2.3318(14) Å) and larger than Fe─Cl bond in C8 (Fe─Cl bond length 2.2699(9) Å).

Table 3 : Selected atomic distances (Å) and bond angles (°) of **C5**, **C8** and **C10**

	C5	**C8**	**C10**
Fe─O3	1.977(4)	1.9823(19)	1.9684(17)
Fe─O6	1.973(4)	1.9676(18)	1.9535(18)
Fe─O7	2.035(4	2.0566(18)	2.0074(18)
Fe─N3	2.145(5)	2.135(2)	2.156(2)
Fe─N6	2.213(5)	2.217(2)	2.212(2)
Fe─Cl	2.3318(14)	2.2699(9)	2.3011(8)
C8─N 3	1.295(7)	1.292(3)	1.299(3)
N3─N2	1.412(6)	1.410(3)	1.404(3)
N2─C7	1.309(7)	1.310(4)	1.298(3)
C7─O3	1.292(7)	1.300(3)	1.307(3)
C18─N6	1.308(7)	1.291(3)	1.290(3)
N6─N5	1.408(7)	1.403(3)	1.415(3)
N5─C17	1.316(7)	1.305(4)	1.304(3)
C17─O6	1.302(7)	1.298(3)	1.308(3)
O6 Fe O3	159.84(17)	161.23(8)	161.54(8)
O6 Fe O7	98.14(16)	97.71(8)	100.16(8)
O3 Fe O7	91.33(16)	91.04(7)	88.33(7)
O6 Fe N3	92.17(17)	93.03(8)	92.67(8)
O3 Fe N3	76.27(17)	76.25(8)	76.13(7)
O7 Fe N3	166.56(17)	166.24(9)	162.57(8)
O6 Fe N6	74.22(17)	74.09(8)	74.98(8)
O3 Fe N6	88.52(17)	89.69(8)	89.88(7)
O7 Fe N6	87.61(18)	88.36(8)	83.65(8)
N3 Fe N6	86.93(18)	86.34(8)	88.40(8)
O6 Fe Cl	94.07(12)	93.45(6)	93.41(6)
O3 Fe Cl	103.04(12)	102.72(6)	102.52(6)
O7 Fe Cl	93.93(13)	92.71(6)	93.16(6)
N3 Fe Cl	93.91(13)	95.20(7)	97.82(6)
N6 Fe Cl	168.29(13)	167.52(6)	167.13(6)

Crystal structure of C9

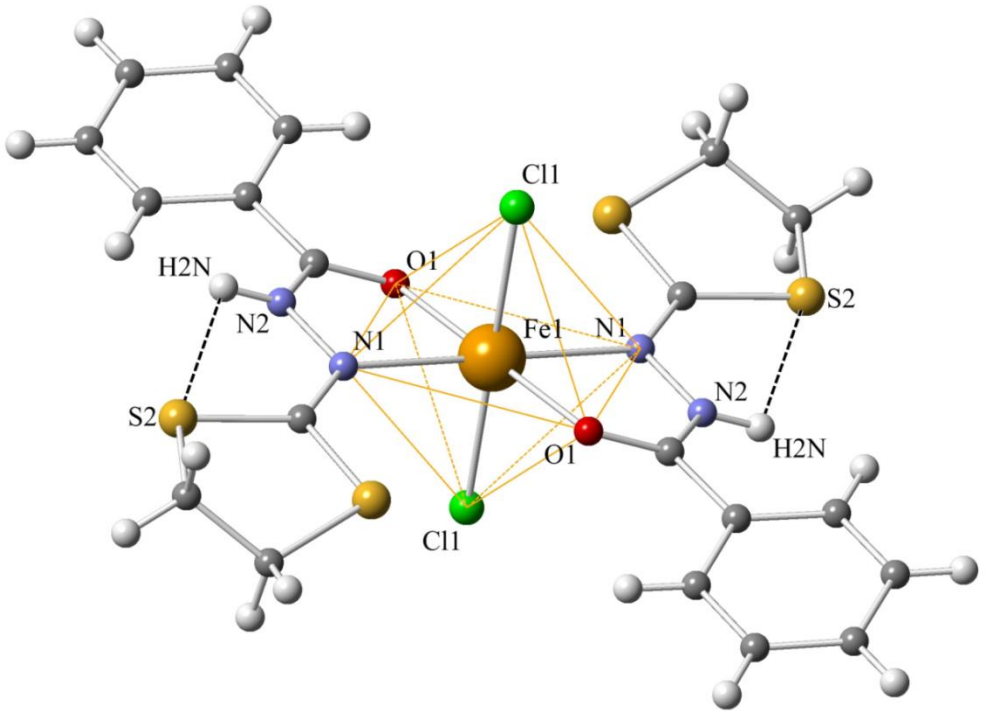

Figure 16: Ball and stick view of **C9** with potential labeling scheme **(**dashed black line show the classical intramolecular H bond between S2 and N2 via H2N)

5 ml of the blue solution of **C8** was degassed with nitrogen for 20 minutes to remove dissolved oxygen. Under an atmosphere of nitrogen, the 5 ml was transferred to the lower part of a 20 ml closed glass test tube with a septum cap. The solution was exposed to light by a solar simulator and when it had changed from blue to yellow, the tube was carefully filled with Et_2O under inert atmosphere. Yellow crystals (suitable for X-ray diffraction) of **C9** were obtained. The solid-state molecular structure of compound **C9** (Figure 16) was thus established by X-ray crystallographic studies, identifying **C9** as a Fe(II) mononuclear species. In the latter complex, the metal center Fe(II) located on the crystallographic inversion center) is surrounded by two neutral **HL'** ligands and two chloride atoms in a *trans* position to one other (Figure16). The overall structure of **C9** appears to be very similar to **C2** (see figure 2) and to **C6** that is recently published by our group.[54] One classical intramolecular hydrogen bond has been detected (PLATON software) and located between S2 and N2 via H2N with a S2···N2 distance of 2.886(2) Å. One π····π interaction between the centre of the aromatic ring (C5-C10) and (C5-C10)' of an adjacent molecule was been located and the corresponding

packing diagram is represented in figure A9 appendix chapter 2 (' is the symmetry code 1-x, 1-y, 1-z).

Electronic spectroscopy

The UV-Visible of all the ligands and the Fe(III) complexes were taken in DMF solutions and the spectral data are summarized in table 3 (for the ligands) and table 4 (for the complexes). The electronic spectra of **HL'** (naked phenyl) shows two bands at 282 nm (ε= 9040 M^{-1}. cm^{-1}) and 292 nm (ε=9000 M^{-1}. cm^{-1}) (see red line figure 17). These two bands are attributed to $\pi \rightarrow \pi^*$ transition, of the phenyl ring and the azomethine (C═N) bond.[67-69] On incorporating the electron-donating groups OH (case of **H_2L**) on the ortho position with respect to the C═O double bond, the bands of 282 and 287 nm on the electronic spectra of **HL'** shifted to higher energy 292 nm (ε=13598 M^{-1}. cm^{-1}) and 298 nm (ε=13413 M^{-1}. cm^{-1}) respectively with a hyperchromic effect (see blue line figure 17) . This is attributed to the increased electron drift from electron-donating group (OH) to the central part of the molecule (─CONHN═) through π-bond of phenyl ring. In another hand the electronic spectra of **HL''** (presence of -NO_2) shows one band at 265 nm attributed to $\pi \rightarrow \pi^*$ transition on the phenyl ring and a shoulder around 320 nm due to the presence of the chromophore -NO_2 group. The conjugation effect of the EWG with π-electrons of the aromatic ring is observed (see green line figure 17), the absorption band is strongly expanded to the near visible region.

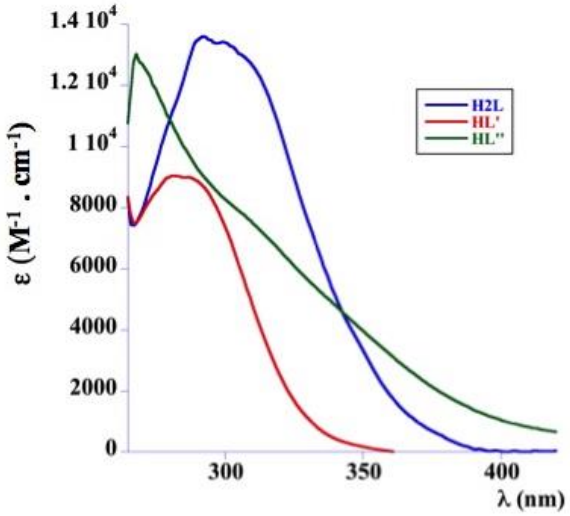

Figure 17: Electronic absorption spectra of **H_2L**, **HL'** and **HL''**

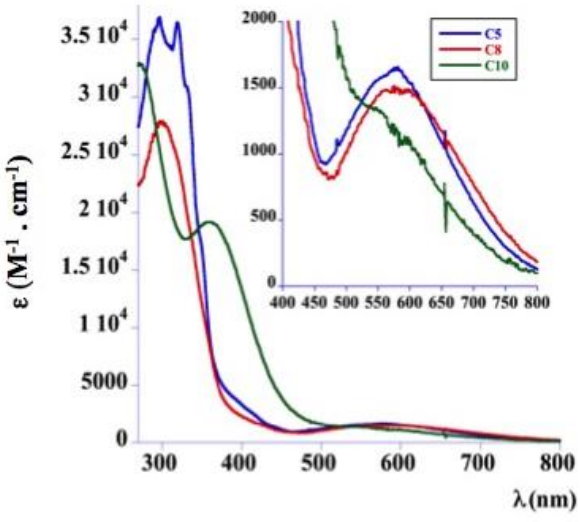

Figure 18: Electronic absorption spectra of **C5**,**C8** and **C10**

;

Table 3: maximum absorption and corresponding molar absorptivity of **H_2L**, **HL'** and **HL"**

Compound	λ max	ε (M^{-1} cm^{-1})
H_2L	292 299	13600 13400
HL'	282 287	9040 9000
HL"	268	13000

Table 4: maximum absorption and corresponding molar absorptivity of **C5, C8** and **C10**

Compound	λ max	ε (M^{-1} cm^{-1})
C5	297 311 581	36900 34400 1650
C8	301 555	27900 1420
C10	273 359	32800 19100

The electronic absorption spectra of the complexes **C5** (blue line figure 18) and **C8** (red line figure 18) display intense bands in the 280-330 nm region which is assigned to IL ($\pi \rightarrow \pi^*$) transitions localized on the phenyl ring, the azomethine C═N double bond and the iminolate C═N fragments of the deprotonated ligands. On the other hand the lowest energy band observed in the 550-590 nm range is assigned to LMCT transition.

On incorporating the EWG group (─NO_2) on the aromatic moiety the lowest energy band (LMCT band) totally disappeared. On the UV region, a new transition band appear on 359 nm and attributed as π to NO_2 intraligand charge transfer (C10 green line figure 18) which is also observed as a shoulder in the spectrum of the uncoordinated ligand (L" green line figure 17).

It follows from the above interpretation that the populated LMCT exited states seem to have the electron distribution suitable for the observed photoreduction of Fe(III) to Fe(II). On incorporating the EWG (─NO_2) the photo-redox process didn't take place, the LMCT transition band disappeared and the electron drift is increasing form the central part (─CONHN═) to the ─NO_2 group which is observed by the appearance of the new band on the 359 nm.

1.7 Conclusion and mechanism of the photo redox process

In this chapter we reported that the reaction of 2 eq. of different aroyl hydrazono-1,3-dithiolane ligands with one eq. of iron precursor FeX_3 (X= Cl or Br) yields the formation of Fe^{III} complexes supported by two deprotonated ligands and one halide (equation I). Light exposure of the solution mixture containing the ferric complexes, two equivalents of H^+ and

two equivalents of X^- induces a photoreduction to the corresponding ferrous complexes supported by two protonated ligands and two halides atoms.

$$2\ \text{eq}\ H_2L + 1\ \text{eq}\ FeX_3 \xrightarrow[\text{X= Cl or Br}]{\text{S= DMF, EtOH}} Fe^{III}(HL)_2(X)(S) + 2H^+ + 2X^- \quad (I)$$

Based on the experimental results obtained as well as the redox stability of the investigated iron(III) in the dark the following mechanism of the process occurring in the irradiated systems can be proposed.

The first step is to populate a spin-allowed excited IL(intraligand charge transfer) state by UV light or the LMCT (ligand to metal charge) excited state by visible light. Irradiation with solar simulator (superposition of UV and visible light, IR was totally blocked) results on the population of the IL and/or the LMCT exited states. Irradiation with the laser on the visible region results only on the population of the LMCT exited state. (eq. 1 and 2)

$$Fe^{III}(HL)_2(X)(S) + 2H^+ + 2X^- \xrightarrow[\text{S= DMF, EtOH}]{h\nu\ \text{(UV and visible)}} \text{IL}\ [Fe^{III}(HL)_2(X)(S)]^* \text{ and/or LMCT}\ [Fe^{III}(HL)_2(X)(S)]^* + 2H^+ + 2X^- \quad (1)$$

$$Fe^{III}(HL)_2(X)(S) + 2H^+ + 2X^- \xrightarrow[\text{S= DMF, EtOH}]{h\nu\ \text{(visible)}} \text{LMCT}\ [Fe^{III}(HL)_2(X)(S)]^* + 2H^+ + 2X^- \quad (2)$$

Owing to their electronic density distribution, the IL states are not considered, in general, responsible for the observed Fe(III) photoreduction since they do not involve any electron density transfer to the central atom.[22,70] It is obvious that the populated IL states (in eq. 1) cannot be responsible for the observed redox process as the corresponding change in orbitals occupation is localized far from the central atom. Of all the accessible excited states, LMCT states have the electron distribution suitable for the observed photoreduction of Fe(III) to Fe(II) (see part 1.3 and 1.6 electronic spectroscopy).[21,22] Such manifold of states can be populated directly with visible light or via internal conversion (*ic*) and/or intersystem crossing (*isc*) from the primary populated states which are higher in energy. The excited states of iron(III) complexes are non-luminescent due to their extremely short lifetimes. Until now, evidently no data on the kinetics of transient decay processes have been available in the literature. The missing possibility to scan any phosphorescence or fluorescence spectra strongly precludes a more detailed characterization of the actual photophysical deactivation steps.

$$\text{IL } [Fe^{III}(HL)_2(X)(S)]^* + 2H^+ + 2X^- \xrightarrow[S= DMF, EtOH]{ic / isc} \text{LMCT } [Fe^{III}(HL)_2(X)(S)]^* + 2H^+ + 2X^- \quad (3)$$

LMCT exited states can be deactivated either by a non-redox process (photophysical deactivation, substitution, etc.), either by an outer-sphere electron transfer process giving rise to Fe(II) and the solvent radical or by an inner-sphere redox decomposition by the splitting of the Fe─X bond forming the halide radical (**Ẋ)** such **Ċl (**chlorine radical) or **Ḃr** (bromine radical). The inner-sphere redox decomposition is more probable for this system certainly because in the absent of the halide for **C7** (Fe^{III} supported by three bidentate ligand) where there is no photoreduction reaction (see part 1.4 presence of halide).

$$\text{LMCT } [Fe^{III}(HL)_2(S)]^* + 2H^+ + 2X^- \xrightarrow[S= DMF, EtOH]{} Fe^{II}(\mathbf{H_2L})_2(X)_2 + \dot{X} \quad (4)$$

Halide radicals (chlorine or bromine radicals) subsequently react with solvent by hydrogen abstraction, forming the solvated cations radical which have been detected by the EPR investigation. (See part 1.5 EPR spectroscopy).

If S=EtOH: $\dot{X}$ + H_3C–CH(H)–OH → H_3C–C(H)(·)–OH + HX (5)

Or

If S=DMF: $\dot{X}$ + H_3C–N(CH=O)–CH_3 → $H_2\dot{C}$–N(CH=O)–CH_3 + HX (6)

Due to their negative redox potential value,[71] $HCON(CH_3)\dot{C}H_2$ (DMF radical) and $CH_3\dot{C}HOH$ (EtOH radical) radicals behaves as a strong reducing agent able to reduce further Fe(III). In equation 7 the Fe^{III} complex is reduced to his corresponding Fe^{II}, and in the other hand the EtOH radical is oxidizes to acetaldehyde, its corresponding oxidation well known form.

$$Fe^{III}(HL)_2(X)(S) + H_3C\text{–}C(H)(\cdot)\text{–}OH \rightarrow H_3C\text{–}C(=O)\text{–}H + Fe^{II}(\mathbf{H_2L})_2(X)_2 \quad (7)$$

$+ 2H^+ + 2X^-$ $\qquad$ $+ H^+ + X^-$

1.8 Experimental

General procedures.

All manipulations were performed under aerobic conditions, using reagents and solvents as received. The NMR spectra were recorded using a Bruker AC 400MHz NMR spectrometer at ambient temperature. $^{13}C\{^{1}H\}$ NMR spectra were recorded on a Bruker AVANCE 300 instrument at ambient temperature. ^{1}H-NMR chemical shifts are referenced to $SiMe_4$ and were determined by reference to the residual ^{1}H solvent peaks. Elemental analyses were performed by the ¨Service de microanalyses¨, Université de Strasbourg. Ligands were prepared according to the reported procedure

Ligand 2-salicyloylhydrazono-1,3-dithiolane (H_2L): The ligand H2L was synthesized as previously described. To a well stirred solution of salicylhydrazide (2.525 g, 16.6 mmol) and NaOH (1.32 g, 33.2 mmol) in absolute ethanol (30 ml) at ambient temperature, CS2 (1 ml, 16.6 mmol) and CH_3I (2 ml,33.2 mmol) are successively added dropwise. The time, between additions is 30 min. Stirring is continued for 8 h, the mixture is poured into cooled water (25 ml), and the resulting white precipitate was filtered and rinsed with water. Recrystallization from DMF/water affords compounds H_2L (2.98 g, 70.5% yield). ^{1}H NMR (DMSO-d6): δ 11.81, 10.99 (br s, 2H, at amide and phenolic OH), 7.95–7.93 (m, 1H, H at phenyl), 7.44–7.38 (m, 1H, H at phenyl), 7.01–6.94 (m, 2H, Hs at phenyl), 3.77–3.73, 3.62–3.58 (m, m, 4H, Hs at SCH_2CH_sS). ^{13}C NMR (DMSO-d6): d = 36.1, 39 (2 CH_2); 117.3, 120.1, 130.8, 133.9, 157 (C_{arom}); 161.51 (CO); 163.50 (S–C–S). Anal. Calc. for $C_{10}H_{10}N_2O_2$: C, 47.24; H, 3.96; N, 11.02. Found: C, 47.4; H, 4.1; N, 11.2%.

Ligand 4-Nitrobenzoic acid 2-(1,3-dithiolan-2-ylidene)hydrazide (HL"): 4-Nitrobenzohydrazide (2.5 mmol) was suspended in 5 cm^3 methanol and 0.87 cm^3 TEA (6.25 mmol) and 0.23 cm^3 CS_2 (3.75 mmol) were added. The mixture was stirred for 1 h at room temperature. Then 3.75 mmol 1,2-dibromoethane was added and the mixture was stirred for another 2 h. Ice (20 g) was then added. The precipitate was isolated by filtration, dried, and recrystallized from dioxane–water (1:1). The crude products were treated with dry diethyl ether, isolated by filtration, dried, and recrystallized from methanol. This compound was obtained as pale yellow crystals in 84% yield (0.59 g). ^{1}H NMR (200 MHz, $CDCl_3$): δ = 3.50–3.56 (m, 2H, SCH_2), 3.67–3.73 (m, 2H, SCH_2), 8.00 (d, 2H, Ph, J = 8.8 Hz), 8.31 (d, 2H, Ph, J = 8.1 Hz), 9.15 (s, 1H, NH) ppm; 13C NMR (50 MHz, DMSO-d6): d = 35.91 (SCH2), 123.81

(Ph), 129.37 (Ph), 139.35 (Ph-CO), 149.37 (Ph-NO2), 161.33 (C=N), 173.05 (C=O) ppm.

Synthesis of $Fe(HL)_2(DMF)(Br)$ (C1): To a well-stirred solution of $FeBr_3$ (58.1 mg, 0.196 mmol) in DMF (10 ml) was added 2 eq. of H_2L (100 mg, 0.393 mmol). The green solution was left stirring for 5 hours in the dark at room temperature and 80 ml of diethyl ether was added to the solution. The dark green powder precipitated was filtered and washed with Et_2O. Crystals of **C1** that are suitable for X-Ray diffraction were grown by diffusing diethyl ether into a DMF solution of **C1** in the dark (112.18 mg; 80% yield). Anal. Calc. (%) For $C_{23}H_{25}BrFeN_5O_5S_4$: C 38.61; H 3.52; N 9.79. Found (%): C 39.02; H 3.73; N 9.62.

Synthesis of $Fe(H_2L)_2(Br)_2$ (C2): To a well-stirred solution of $FeBr_3$ (58.1 mg, 0.196 mmol) in DMF (10 ml) was added 2 eq. of H_2L (100 mg, 0.393 mmol). The solution was left stirring for 5 hours at room temperature. The resulting green solution was degassed with nitrogen for 20 minutes to remove dissolved oxygen. Under an atmosphere of nitrogen, 5 ml of the solution was transferred to the lower part of a 20 ml closed glass test tube with a septum cap. The solution was exposed to natural light and when it had changed from green to yellow, the tube was filled with Et_2O. Yellow crystals (suitable for X-Ray diffraction) of **C2** were obtained. The quick surface coloration indicates the air sensitivity of the Fe^{II} species. The lack of chemical stability of complex **C2** has hampered its chemical analyses.

Synthesis of $[(Fe(HL)_2(MeOH)(Br)].[Fe(HL)_2(Br)]$ (C3): To a well-stirred solution of H_2L in MeOH (100 mg, 0.393 mmol in 20 mL) was added FeBr3 (58.1 mg, 0.196 mmol), after 5 h of stirring at room temperature in absence of light, diethyl ether were added carefully on the surface of the solution mixture which was then left undisturbed for slow precipitation (5 to 7 days). The resulting crystals of the titled complex were collected by filtration and washed with diethyl ether. (Yield: 310 mg, 59%). Anal. Calcd for $C_{41}H_{39}Br_2Fe_2N_8O_9S_8$: C, 37.42; H, 2.99; N, 8.52. Found: C, 38.12; H, 3.23; N, 8.44.

Synthesis of $[(Fe(HL)_2(EtOH)(Br)].[Fe(HL)_2(Br)]$ (C4): To a well-stirred solution of $FeBr_3$ (58.1 mg, 0.196 mmol) in EtOH (20 ml) was added 2 eq. of H_2L (100 mg, 0.393 mmol). The red solution was left stirring for 5 hours in the dark at room temperature and 100 ml of diethyl ether was added to the solution. The dark powder precipitated was filtered and washed with Et_2O. Dark crystals of **C4** that are suitable for X-Ray diffraction were grown by diffusing diethyl ether into **EtOH** solution of **C4** in the dark (441 mg, 84% yield). Anal. Calc. (%) For

$C_{42}H_{41}Br_2Fe_2N_8O_9S_8$: C 37.93; H 3.11; N 8.43. Found (%): C 37.82; H 3.25; N 9.13

Synthesis of Fe(L")$_2$(DMF)(Cl) (C10): To a well-stirred solution of HL" in DMF (100 mg, 0.353 mmol in 3 ml) was added $FeCl_3$ (28.62 mg, 0.176 mmol), after 5 h of stirring at room temperature, 8 mL of diethyl ether were added carefully on the surface of the green solution which was then left undisturbed for slow precipitation (2 to 3 days). The resulting crystals of the titled complex were collected by filtration and washed with diethyl ether. (Yield: 80 mg, 62%). Anal. Calcd for $C_{23}H_{23}ClFeN_7O_7S_4$: C, 37.89; H, 3.18; N, 13.65. Found: C, 37.2; H, 3,01; N, 13.1.

1.9 References

(1) Taylor, S. R. *Nature* **1985**, *316*, 112-112.
(2) Jacob, D. J.; Hoffmann, M. R. *Journal of Geophysical Research-Oceans and Atmospheres* **1983**, *88*, 6611-6621.
(3) Graedel, T. E.; Mandich, M. L.; Weschler, C. J. *Journal of Geophysical Research-Atmospheres* **1986**, *91*, 5205-5221.
(4) Weschler, C. J.; Mandich, M. L.; Graedel, T. E. *Journal of Geophysical Research-Atmospheres* **1986**, *91*, 5189-5204.
(5) Martin, L. R.; Hill, M. W. *Atmospheric Environment* **1987**, *21*, 1487-1490.
(6) Jacob, D. J.; Gottlieb, E. W.; Prather, M. J. *Journal of Geophysical Research-Atmospheres* **1989**, *94*, 12975-13002.
(7) Martin, L. R.; Hill, M. W.; Tai, A. F.; Good, T. W. *Journal of Geophysical Research-Atmospheres* **1991**, *96*, 3085-3097.
(8) Faust, B. C.; Hoigne, J. *Atmospheric Environment Part a-General Topics* **1990**, *24*, 79-89.
(9) Hong, H. S.; Kester, D. R. *Limnology and Oceanography* **1986**, *31*, 512-524.
(10) Landing, W. M.; Westerlund, S. *Marine Chemistry* **1988**, *23*, 329-343.
(11) Sulzberger, B.; Schnoor, J. L.; Giovanoli, R.; Hering, J. G.; Zobrist, J. *Aquatic Sciences* **1990**, *52*, 56-74.
(12) McKnight, D. M.; Kimball, B. A.; Bencala, K. E. *Science* **1988**, *240*, 637-640.
(13) Chaudhury, N. K.; Saini, G. S. S.; Verma, A. L. *Inorg Chem* **1995**, *34*, 346-349.
(14) Dhanasekaran, T.; Grodkowski, J.; Neta, P.; Hambright, P.; Fujita, E. *J Phys Chem A* **1999**, *103*, 7742-7748.
(15) Maldotti, A.; Andreotti, L.; Molinari, A.; Varani, G.; Cerichelli, G.; Chiarini, M. *Green Chem* **2001**, *3*, 42-46.
(16) Ozaki, Y.; Iriyama, K.; Ogoshi, H.; Kitagawa, T. *J Am Chem Soc* **1987**, *109*, 5583-5586.
(17) Sakai, H.; Onuma, H.; Umeyama, M.; Takeoka, S.; Tsuchida, E. *Biochemistry-Us* **2000**, *39*, 14595-14602.
(18) Sato, S.; Kamogawa, K.; Aoyagi, K.; Kitagawa, T. *Journal of Physical Chemistry* **1992**, *96*, 10676-10681.
(19) Homem, V.; Santos, L. *Journal of Environmental Management* **2011**, *92*, 2304-2347.
(20) Sun, C.; Chen, C.; Ma, W.; Zhao, J. *Physical Chemistry Chemical Physics* **2011**, *13*, 1957.
(21) Sima, J.; Makanova, J. *Coord Chem Rev* **1997**, *160*, 161-189.
(22) Balzani, V.; Carassiti, V. *Photochemistry of coordination compounds*; Academic Press: London ; New York, 1970.
(23) Marlin, D. S.; Mascharak, P. K. *Chem Soc Rev* **2000**, *29*, 69-74.
(24) Marlin, D. S.; Olmstead, M. M.; Mascharak, P. K. *Inorg Chem* **1999**, *38*, 3258.
(25) Nguyen, C.; Guajardo, R. J.; Mascharak, P. K. *Inorg Chem* **1996**, *35*, 6273-6281.
(26) Noveron, J. C.; Olmstead, M. M.; Mascharak, P. K. *Inorg Chem* **1998**, *37*, 1138.
(27) Noveron, J. C.; Olmstead, M. M.; Mascharak, P. K. *J Am Chem Soc* **2001**, *123*, 3247-3259.
(28) Rowland, J. M.; Olmstead, M.; Mascharak, P. K. *Inorg Chem* **2001**, *40*, 2810-2817.
(29) Du Bois, J.; Mizoguchi, T. J.; Lippard, S. J. *Coordin Chem Rev* **2000**, *200*, 443-485.
(30) Mizoguchi, T. J.; Kuzelka, J.; Spingler, B.; DuBois, J. L.; Davydov, R. M.; Hedman, B.; Hodgson, K. O.; Lippard, S. J. *Inorg Chem* **2001**, *40*, 4662-4673.
(31) Nordlander, E.; Whalen, A. M. *Coord Chem Rev* **1995**, *142*, 43-99.

(32) Nordlander, E.; Whalen, A. M.; Prestopino, F. *Coord Chem Rev* **1995**, *146*, A225-A306.
(33) Patra, A. K.; Olmstead, M. M.; Mascharak, P. K. *Inorg Chem* **2002**, *41*, 5403-5409.
(34) Powell, A. K. *Coordin Chem Rev* **1994**, *134*, 91-169.
(35) Zuo, W. W.; Rosa, V.; Tourbillon, C.; Specklin, D.; Khaled, C.; Kurmoo, M.; Welter, R. *Rsc Adv* **2012**, *2*, 2517-2526.
(36) Bouslimani, N.; Clement, N.; Rogez, G.; Turek, P.; Bernard, M.; Dagorne, S.; Martel, D.; Cong, H. N.; Welter, R. *Inorg Chem* **2008**, *47*, 7623-7630.
(37) Bouslimani, N.; Clement, N.; Toussaint, C.; Hameury, S.; Turek, P.; Choua, S.; Dagorne, S.; Martel, D.; Welter, R. *Eur J Inorg Chem* **2009**, 3734-3741.
(38) Cheaib, K.; Martel, D.; Clement, N.; Eckes, F.; Kouaho, S.; Rogez, G.; Dagorne, S.; Kurmoo, M.; Choua, S.; Welter, R. *Dalton Trans* **2013**, *42*, 1406-1416.
(39) Scherlis, D. A.; Estrin, D. A. *Int J Quantum Chem* **2002**, *87*, 158-166.
(40) Shongwe, M. S.; Al-Rahbi, S. H.; Al-Azani, M. A.; Al-Muharbi, A. A.; Al-Mjeni, F.; Matoga, D.; Gismelseed, A.; Al-Omari, I. A.; Yousif, A.; Adams, H.; Morris, M. J.; Mikuriya, M. *Dalton T* **2012**, *41*, 2500-2514.
(41) Shongwe, M. S.; Al-Zaabi, U. A.; Al-Mjeni, F.; Eribal, C. S.; Sinn, E.; Al-Omari, I. A.; Hamdeh, H. H.; Matoga, D.; Adams, H.; Morris, M. J.; Rheingold, A. L.; Bill, E.; Sellmyer, D. J. *Inorg Chem* **2012**, *51*, 8241-8253.
(42) Sima, J. *Coord Chem Rev* **1997**, *159*, 195-204.
(43) Sima, J.; Makanova, J.; Kotocova, A.; Bradiakova, A. *J Photoch Photobio A* **1997**, *103*, 197-200.
(44) Bartocci, C.; Maldotti, A.; Varani, G.; Battioni, P.; Carassiti, V.; Mansuy, D. *Inorg Chem* **1991**, *30*, 1255-1259.
(45) Walker, F. A. *Chem Rev* **2004**, *104*, 589-615.
(46) Melnikov, M. Y.; Belevskii, V. N.; Belopushkin, S. I.; Melnikova, O. L. *Russ Chem B+* **1997**, *46*, 1245-1247.
(47) Bouslimani, N.; Clément, N.; Rogez, G.; Turek, P.; Choua, S.; Dagorne, S.; Welter, R. *Inorg Chim Acta* **2010**, *363*, 213-220.
(48) Toussaint, C.; Beghidja, C.; Welter, R. *Comptes Rendus Chimie* **2010**, *13*, 343-352.
(49) Bessy Raj, B. N.; Prathapachandra Kurup, M. R.; Suresh, E. *Spectrochimica Acta Part A: Molecular and Biomolecular Spectroscopy* **2008**, *71*, 1253-1260.
(50) Mangalam, N. A.; Sivakumar, S.; Sheeja, S. R.; Prathapachandra Kurup, M. R.; Tiekink, E. R. T. *Inorg Chim Acta* **2009**, *362*, 4191-4197.
(51) Raj, B. N. B.; Kurup, M. R. P. *Spectrochim Acta A* **2007**, *66*, 898-903.
(52) Xiao, W.; Lu, Z. L.; Wang, X. J.; Su, C. Y.; Yu, K. B.; Liu, H. Q.; Kang, B. S. *Polyhedron* **2000**, *19*, 1295-1304.
(53) Naskar, S.; Naskar, S.; Mondal, S.; Majhi, P. K.; Drew, M. G. B.; Chattopadhyay, S. K. *Inorg Chim Acta* **2011**, *371*, 100-106.
(54) Bouslimani, N.; Clément, N.; Toussaint, C.; Hameury, S.; Turek, P.; Choua, S.; Dagorne, S.; Martel, D.; Welter, R. *Eur J Inorg Chem* **2009**, *2009*, 3734-3741.
(55) Gandolfi, C.; Moitzi, C.; Schurtenberger, P.; Morgan, G. G.; Albrecht, M. *J Am Chem Soc* **2008**, *130*, 14434.
(56) Griffin, M.; Shakespeare, S.; Shepherd, H. J.; Harding, C. J.; Letard, J.-F.; Desplanches, C.; Goeta, A. E.; Howard, J. A. K.; Powell, A. K.; Mereacre, V.; Garcia, Y.; Naik, A. D.; Mueller-Bunz, H.; Morgan, G. G. *Angew Chem Int Ed* **2011**, *50*, 896-900.
(57) Hayami, S.; Gu, Z. Z.; Yoshiki, H.; Fujishima, A.; Sato, O. *J Am Chem Soc* **2001**, *123*, 11644-11650.
(58) Nihei, M.; Shiga, T.; Maeda, Y.; Oshio, H. *Coord Chem Rev* **2007**, *251*, 2606-2621.

(59) Shongwe, M. S.; Al-Rashdi, B. A.; Adams, H.; Morris, M. J.; Mikuriya, M.; Hearne, G. R. *Inorg Chem* **2007**, *46*, 9558-9568.
(60) Tweedle, M. F.; Wilson, L. J. *J Am Chem Soc* **1976**, *98*, 4824-4834.
(61) Bhadbhade, M. M.; Srinivas, D. *Polyhedron* **1998**, *17*, 2699-2711.
(62) Boca, R.; Fukuda, Y.; Gembicky, M.; Herchel, R.; Jarosciak, R.; Linert, W.; Renz, F.; Yuzurihara, J. *Chem Phys Lett* **2000**, *325*, 411-419.
(63) Brewer, C. T.; Brewer, G.; Jameson, G. B.; Kamaras, P.; May, L.; Rapta, M. *Journal of the Chemical Society-Dalton Transactions* **1995**, 37-43.
(64) Brewer, C. T.; Brewer, G.; May, L.; Sitar, J.; Wang, R. *Journal of the Chemical Society-Dalton Transactions* **1993**, 151-155.
(65) Hayami, S.; Inoue, K.; Maeda, Y. *Mol Cryst Liq Crys A* **1999**, *335*, 1285-1294.
(66) Maeda, Y.; Miyamoto, M.; Takashima, Y.; Oshio, H. *Inorg Chim Acta* **1993**, *204*, 231-237.
(67) Bessy Raj, B. N.; Kurup, M. R. P. *Spectrochimica Acta Part A: Molecular and Biomolecular Spectroscopy* **2007**, *66*, 898-903.
(68) Galić, N.; Dijanošić, A.; Kontrec, D.; Miljanić, S. *Spectrochimica Acta Part A: Molecular and Biomolecular Spectroscopy* **2012**, *95*, 347-353.
(69) Lu, Y. H.; Lu, Y. W.; Wu, C. L.; Shao, Q.; Chen, X. L.; Bimbong, R. N. B. *Spectrochim Acta A* **2006**, *65*, 695-701.
(70) Horvath, O.; Stevenson, K. L. *Charge transfer photochemistry of coordination compounds*; VCH: New York ; Cambridge, 1993.
(71) Schwarz, H. A.; Dodson, R. W. *Journal of Physical Chemistry* **1989**, *93*, 409-414.

Chapter 3:

Magnetic and photo-electro chemical properties of Fe(III) dimer complex

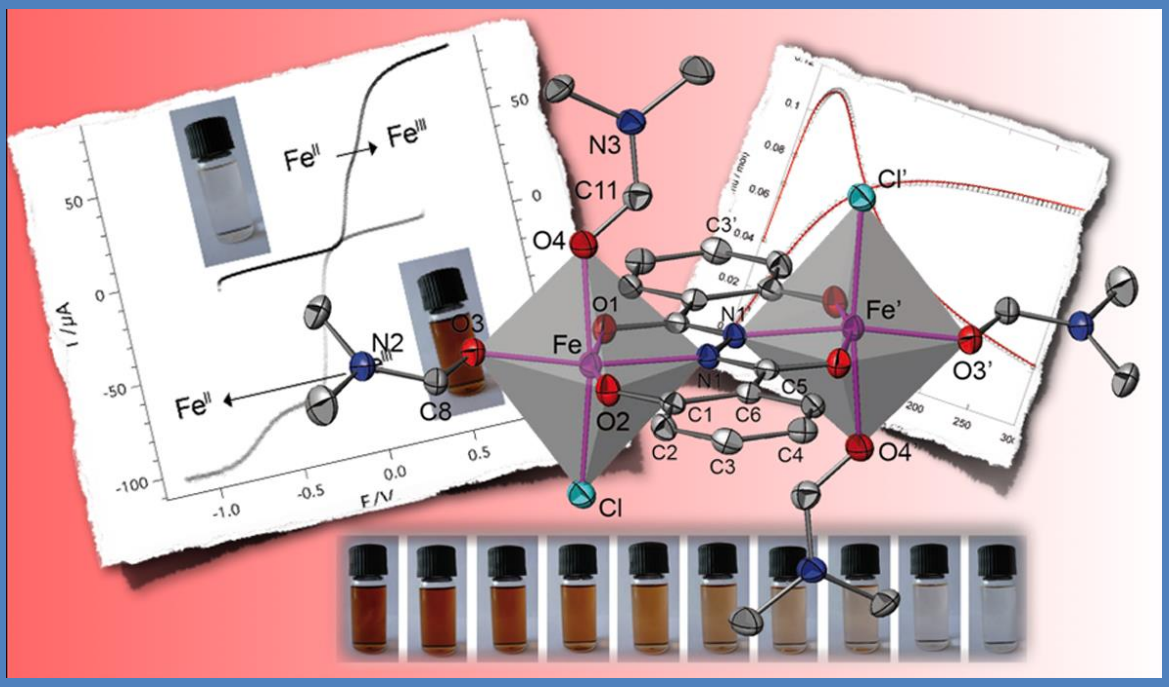

Chapter 3:

Structural, Magnetic and Optical Properties of a Fe^{III} Dimer Bridged by the Meridional Planar Divergent *N,N'-bis(*salicyl)hydrazide and its Photo- and Electro-Chemistry in Solution

Structural, Magnetic and Optical Properties of a Fe^{III} Dimer Bridged by the Meridional Planar Divergent *N,N'-bis(*salicyl)hydrazide and its Photo- and Electro-Chemistry in Solution

Abstract

$\{Fe^{III}Cl(DMF)_2\}_2(L)$ where L is N,N'-bis(salicyl)hydrazide has been synthesized as red crystals and characterized using single-crystal diffraction, infrared and UV-vis spectroscopies, and its magnetic properties studied. The dimeric unit in the structure is formed through the two meridional sets of divergent O, N, O coordinating atoms of the hexacoordinated and quadruply charged ligand. With the presence of the inversion symmetry the Fe atoms are strictly planar with the ligand. The magnetic exchange interaction is found to be antiferromagnetic with a $J = -5.98(3)$ cm^{-1} through the rare Fe-N-N-Fe pathway. Irradiation of the $FeCl_3/H_4L$ red DMF solution in the visible region of the spectrum resulted in its complete discoloration and from which the unknown colorless salt $[Fe^{II}(DMF)_6][Fe^{II}Cl_4]$ and the neutral ligand have been identified by single crystal diffraction. The UV-visible spectra of $FeCl_3$, H_4L and their mixture in DMF solution indicate that the iron complex is the absorbing species and the presence of the free ligand in the irradiated solution suggests that the ligand is potentially acting as a catalyst to the photoreduction of Fe^{III} to Fe^{II}, while electrochemistry points to a mixed-valent (Fe^{II}-Fe^{III}) intermediate in the process.

Keywords : N,N'-bis(salicyl)hydrazide, Iron, Crystal structure, Magnetism, Photo-reduction.

1.1 Introduction

Considerable efforts have been made over the past thirty years in understanding the magnetic exchange interaction between moment carriers in the solid-state.[1] In doing so a whole gamut of ligands has been employed to generate the chemical connection between near neighbours. A simple way of classification has been the number of non-magnetic atoms between neighbouring moment carriers.[2] From natural sources the ligand is usually oxide, that is one-atom bridge, and the long-range magnetic ordering temperature is rather high (up to 800 K),[3] thus indicating strong exchange interaction. However, similar connection using hydroxide reduces the dimensionality to two and the highest transition temperature is 60 K.[4] Azide and sometimes carboxylate can provide one-atom bridges but transition temperatures are still low (<100 K). However, two-atom bridge such as cyanide favours linear connectivity and has produced several homo- and hetero-metallic Prussian-Blue analogues where transition temperature can exceed 300 K.[5] Other two-atom bridges that have been considered are pyrazole, triazole, and tetrazole for providing N-N connectivity between carriers and to a lesser extent dithione (S-S).[6] Extending to three-atom bridges there are dicyanamide,[7] azide,[8] carbonate,[9] oxalate,[10] carboxylate,[11] amongst others. These simple commercially available ligands have been very popular for they have provided many solids displaying long-range magnetic ordering at measurable temperatures.

In the last twenty years, there have been major interests in the development of organic ligands for accommodating high paramagnetic metal density and favourable and desired magnetic exchange pathways. For example Kahn *et al*. have developed the chemistry of oxamato derivatives,[12] which importantly provided divergent coordinating sites to generate infinite networks. This divergent nature of connecting ligands in molecular magnetism has since exploded to what we are now seeing in the metal-organic-framework field. The use of organic ligands with divergent coordinating sites have been useful to program the organization of paramagnetic centres within molecules; for example, Ruben *et al*.[13] have produced square grids while Peng *et al*.[14] made linear chains of up to nine metal centres. However, to date the simplest divergent ligand remains the oxalate anion and a whole family of magnetic networks made use of it. It is also interesting to note that nature has provided oxalate as well as inorganic non-magnetic ligands, such as sulfate, phosphate, molybdate, which are known to generate magnetic networks.[15]

One of the present waves of development of organic ligand is to use 2-salicyl-hydrazine moieties, where the O, N, O atoms can provide chelating sites.[16-20] This has been our motive for the last few years and it followed the observation of the strongest ferromagnetic exchange between two Mn^{III}.[21] The following works on Fe^{III} have found antiferromagnetic exchange but the compounds proved to be more interesting in solar energy conversion.[22, 23] However, the ligands used in these studies were asymmetric and not with divergent coordination sites, which consequently ended as peripheral chelates. Others have shown that related ligands can produce ring clusters of up to six metal centres.[24] To extend this work, we have made use of the existing symmetric and potentially bis-meridional chelate ligand, N,N'-bis(salicyl)hydrazine (H_4**L**) (scheme 1), that has been shown to form dimers with transition metals such as cobalt, nickel and zinc.[25-28] However, the magnetic properties have not been explored. Here, we present its coordination with Fe^{III} and the structural, optical and magnetic characterizations of a dimer, $(Fe^{III}Cl(DMF)_2)_2L$. Furthermore, we explore the photochemistry and the electrochemistry of the $Fe^{III}Cl_3$ / H_4L couple in DMF solution in view of understanding the accompanied discoloration upon exposure to natural sunlight. The unknown $[Fe^{II}(DMF)_6][Fe^{II}Cl_4]$ and the free ligand, H_4L, resulted as colourless crystals from the decolorized solution have consequently been structurally characterized by diffraction. Electrochemistry and optical spectroscopy of H_4L and in the presence of Fe^{III} in DMF provide additional arguments for a proposed mechanism of the photo-reduction process.[29,30]

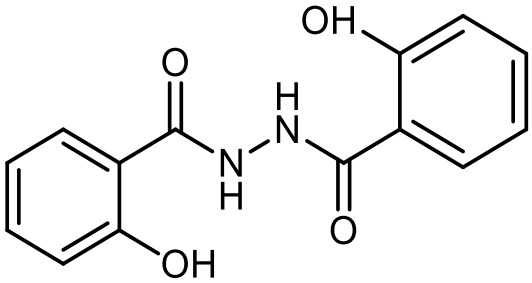

Scheme 1: Representation of N, N'-bis(salicyl)hydrazine (H_4**L**)

1.2 Results and discussion

H_4L is among a rare collection of ligand that can potentially carry charges from zero to four due to the easy deprotonation of both the phenol and the hydrazine moieties.[25] Furthermore, for the neutral and the quadruply charged anion, one expects the geometry to be

planar. Important with respect to the present work is this planarity and the divergent nature of the coordinating atoms to give two potentially symmetric meridional coordination sites. This aspect of the ligand has been demonstrated previously through its coordination with transition metals. Although, the ligand is potentially able to coordinate metals into linear or even cyclic coordination networks, as known for a related ligand, none has been found so far. Our present study has confirmed the previously determined crystal structure of the ligand at a lower temperature.[25] This is consistent to the molecular structure determined by NMR spectroscopy in solution. Interestingly, these functional groups are involved in double intermolecular hydrogen bonding of ketone-alcohol pairs, O…H-O of 2.616 Å, between nearest neighbours leading to a two-dimensional supramolecular network. In addition, two equivalent intramolecular hydrogen bonds of amine-ketone pairs (N-H…O of 2.579 Å) exist. In this work, the synthesis and X-Ray crystal structure of the first trivalent iron coordination complex – supported by N, N'-bis(salicyl)hydrazine ligand - is performed.

The reaction of one equivalent of the ligand H_4**L** with 2 equivalents of $FeCl_3$ in DMF results in a dense red solution where upon diffusion of ether it affords red crystals of **1** (scheme 2) in good yield. An important procedure to be respected in this synthesis is the absence of natural light. This is because exposure of the red solution to natural light results in a fast discoloration to colourless (Figure 1). The process can take as little as ten minutes for a solution of millimolar concentration. In the absence of light, dark red crystals suitable for single crystal X-Ray analyses and other characterizations have been obtained by slow diffusion of diethyl ether into the DMF solution of **1** in air. The red crystals are stable in air and are soluble in H_2O, $CHCl_3$ and DMF but are insoluble in methanol, ethanol and diethyl ether.

Figure 1: Discoloration of a DMF solution of **1** (10^{-3} M) under exposure to natural sunlight over a period of 10 minutes.

The curiosity of the nature of the product(s) of this discoloration led us to the following. Crystallization tests were performed on the colourless solution obtained after exposure to natural light of **1** in DMF in sealed glass tubes. After few hours of slow diffusion of diethyl ether into the irradiated DMF solution of **1**, colourless crystals start to form.

Analyses of the X-Ray data from different single crystals found the presence of two compounds, H_4**L** and **2**. With the help of a microscope, the two types of crystal were separated because the colourless crystalline blocks of **2** tarnished rapidly at the surfaces in air, indicating the sensitivity of the Fe^{II} species. In contrast, the crystals of H_4**L** do not change their colour.

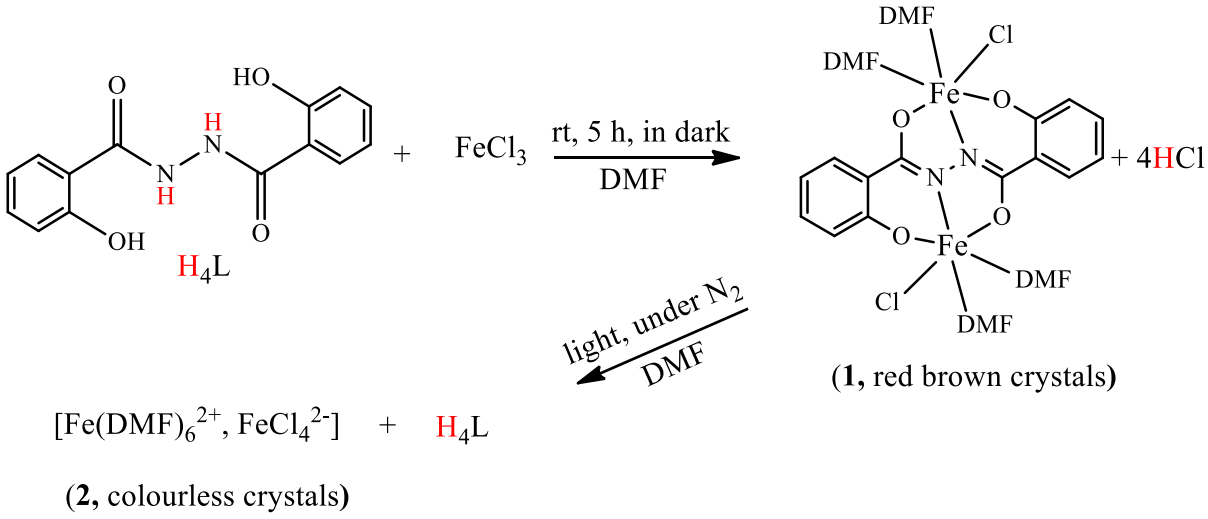

Scheme 2: Synthetic pathways for **1** and **2**

1.3 Crystal structure of 1.

1 crystallizes in the orthorhombic centro-symmetric space group *Pbca*. An ORTEP view of the molecular structure is depicted in figure 2. The asymmetric unit contains one half of the molecule of **1**, and the complete molecule $(FeCl(DMF)_2)_2L$ is generated by the inversion symmetry centred on the N-N bond. The unit cell has four molecules. **1** consists of a dinuclear Fe^{III} compound bridged symmetrically by one anionic ligand L^{4-}. The coordination of the ferric ion is pseudo-octahedral with two oxygen atoms (O1 and O2) and one nitrogen atom (N1) from the ligand in a meridional plane (Figure 2), and the coordination sphere being completed by one chloride atom and 2 DMF molecules (O3 and O4). The iron atoms are in trans position with respect to the N-N bond and are symmetry restricted to be in the plane of the ligand. The Fe-Fe' distance is 4.832(1) Å. This core of the molecular structure of the present Fe^{III} compound is similar to those found previously containing Ni, Co and Zn ions.[26-28] For the latter the secondary ligands were neutral amine (pyridine or ethylenediamine) to balance the charge so that in all cases the molecules are neutral within the crystal structures.

In the present case a chloride atom bonded to each Fe^{III} satisfies the charge balance. By comparing the observed bond lengths of **1** to those of the free ligands (Table 1), we can note the following. First the ketone C=O distance is lengthened while the phenol C–O is shortened upon coordination, implying a transformation from a localised C=O and C–O picture in the pure ligand to a delocalisation of electron densities via resonance effect upon deprotonation. While these distances are consistent for all the metal complexes reported, there are noticeable differences arising from the different valences and the ionic size of the cations as well as the nature of the other peripheral ligands. In all the compounds the geometry of the metals is pseudo-octahedral, and the M–O and M–N distances are normal except for those of cobalt, which are unexpectedly quite short. The M–O (ketone) is consistently longer that the M–O (alcohol). Surprisingly, the M–O (alcohol) bond length of the two compounds of nickel are very different, although they only crystallise with different solvates. No classical hydrogen bond has been detected. As a non-classical hydrogen bonds, only one intermolecular C-H…π interaction has been pointed out (PLATON software[35]): C10-H10…(C1-C6)'' ('' is related to the symmetry code –x, ½+y, ½-z); 2.866(1) Å between the hydrogen atom and the centre of the benzene ring (C1-C6) of an adjacent molecule, with an angle of 158(1)°. The corresponding packing diagram is represented on figure 3 and the main observation is the zigzag chains formed by the complexes along the ***a*** crystallographic axis, the ***(a,c)*** lattice plane. Although an infinite network is potentially expected, none have been characterized so far.

Table 1: Selected bond distances (Å) of known compounds and of the free ligand.

Compound	H_4L	H_4L in $(Ni^{II}_2Lpy_6).H_4L$[26]	$Fe^{III}_2LCl_2(DMF)_4$	$(Co^{II}_2Lpy_6).(Co^{III}Cl_3py)_2$[27]	$(Ni^{II}_2Lpy_6).H_4L$[26a]	$(Ni^{II}_2Lpy_6).2py$[26]	$(Zn_2Len_2).2DMF.2H_2O$[28]
M-M			4.832	4.409	4.687	4.674	4.783
C=O (O1)	1.242	1.235	1.301	1.275	1.284	1.283	1.285
C-OH (O2)	1.362	1.356	1.339	1.325	1.339	1.302	1.325
N-N	1.379	1.378	1.401	1.368	1.409	1.408	1.396
M-O1			2.027	1.914	2.055	2.060	2.121
M-O2			1.898	1.852	2.049	1.989	2.049
M-N			2.037	1.849	1.974	1.955	2.003

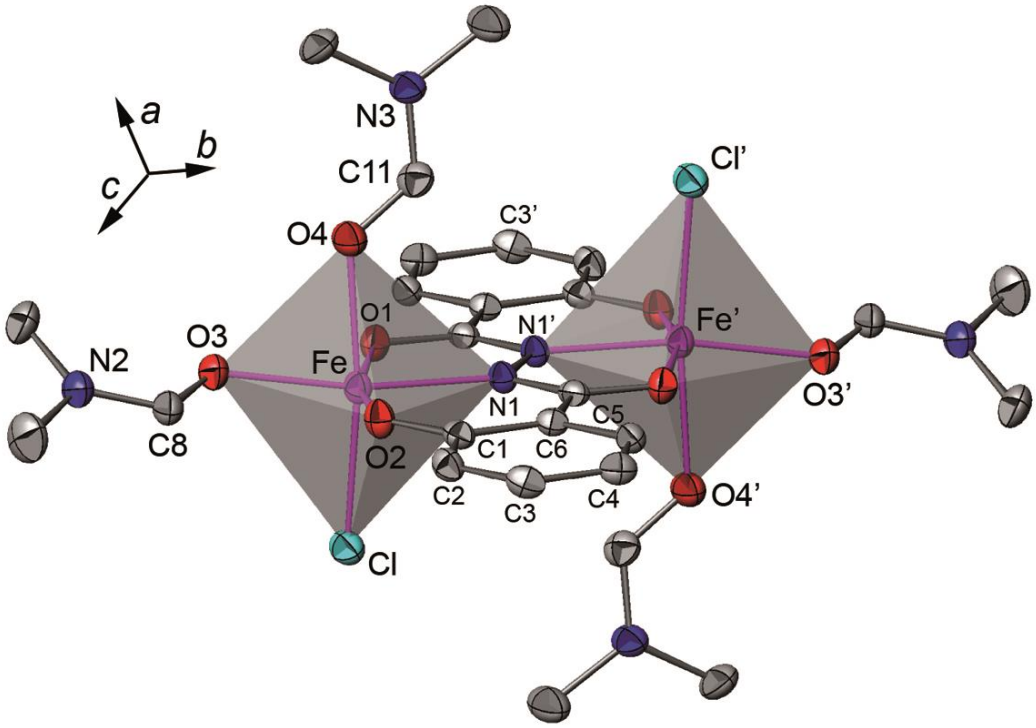

Figure 2: ORTEP view of **1** with partial labelling. The polyhedra around Fe^{III} are represented in grey. The ellipsoids enclose 50% of the electronic density. Symmetry codes for equivalent positions ’are: -x, -y+1, -z+1.

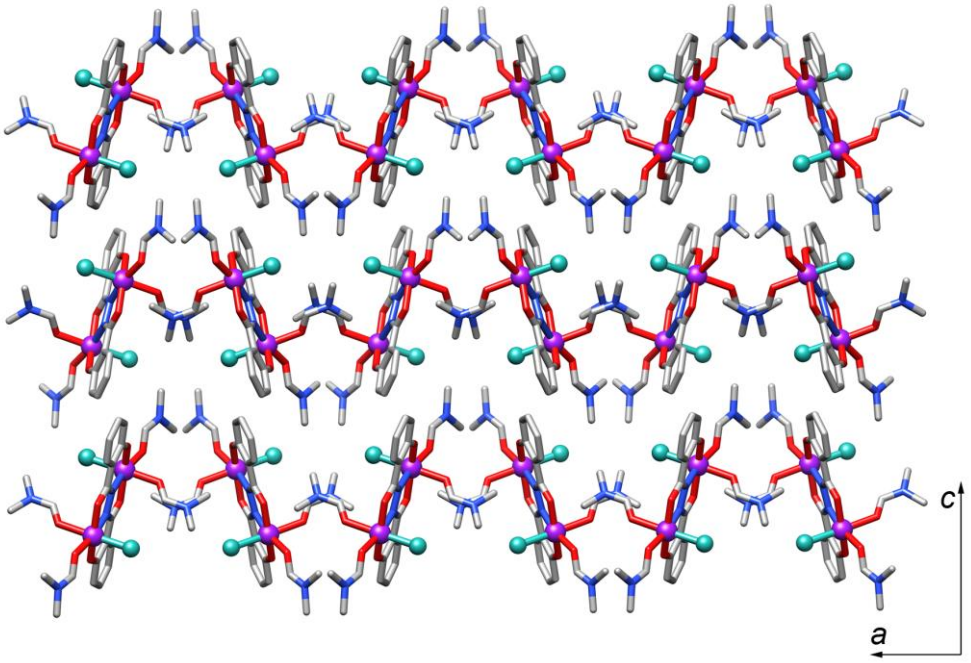

Figure 3: Packing view of **1** (projection in the lattice plane x, 0, z). Iron atoms are represented as purple spheres and chloride atoms as blue green spheres.

1.4 Magnetic properties of 1.

With the two Fe^{3+} (S = 5/2) of the complex bridged by the short N–N entity and the lack of an extended network in the present complex should potentially behave like a paramagnet with measurable intramolecular magnetic exchange. The magnetic measurements were undertaken on a sample of selected crystals of **1**, specifically to estimate the magnetic coupling between the two paramagnetic centres.

The magnetic moment represented as χT at room temperature of 7.95 emu K mol^{-1} (figure 4) is lower than that expected for two uncoupled Fe^{III} ions (8.75 emu K mol^{-1} assuming g = 2.0). Upon cooling to 1.8 K, the χT product decreases gradually to near zero indicating the occurrence of intramolecular antiferromagnetic interaction (see figure 4). The temperature dependence of the magnetic susceptibility (χ) shows a gradual increase upon lowering the temperature to a maximum at 25 K. The data were fit using the following spin Hamiltonian where all parameters have their usual meaning and the spin operator $\hat{S}$ is defined as $\hat{S} = \hat{S}_{Fe1} + \hat{S}_{Fe2}$: $\hat{H} = -J\,\hat{S}_{Fe1}.\hat{S}_{Fe2} + g\,H\,\hat{S}$.[36]

Although reasonable fits were obtained, the low temperature data deviate from the theoretical curve. To improve the fits a certain amount ρ of paramagnetic impurity ($S_{impurity}$ = 5/2) has been considered. The best fit leads to the following values: J = –5.98(3) cm^{-1}, g = 2.02(1) and ρ = 1 % with an agreement factor R = = 2×10^{-4}. The strength of the antiferromagnetic interaction (J = –5.98(3) cm^{-1}) between the ferric ions in **1** is comparable to those available in the literature for complexes having similar Fe^{III}-N-N-Fe^{III} exchange pathway, for example, ferric 24-Azametallacrown-8 complex[24a] (J = –3.93 cm^{-1}) and ferric 18-azametallacrown-6 compound[24b] (J = –3.38 cm^{-1}).

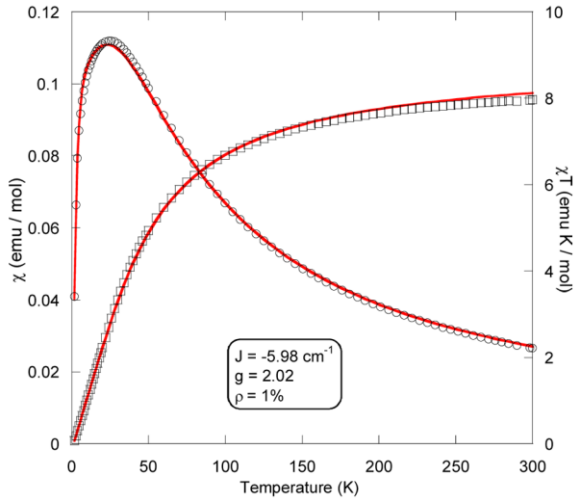

Figure 4: Temperature dependence of χ (circles) and χT (squares) of **1**. The lines correspond to the best fit for a S=5/2 dimer model.

1.5 Crystal structure of 2.

Single crystals of **2** have been picked quickly -under a microscope- from a collection of colourless single crystals, and mounted for intensity data collection. The crystalline blocks of **2** (stable in air for only few minutes) have been selected taking into account the surface coloration, indicating the air sensitivity of these Fe^{II} species (confirmed by the crystal structure obtained and described hereafter). The other crystalline blocks were also analyzed and the data analyses of the X-Ray diffraction indicate that they correspond to that H_4**L** (see also scheme 2).

2 crystallises in the triclinic centro-symmetric space group *P*-1. The asymmetric unit contains five independent iron atoms, two of anion, $FeCl_4^{2-}$, and three of the cation, $Fe(DMF)_6^{2+}$ (Figure 5 and 7). The anion has 100% occupancy and with their symmetry related counter parts there are four per unit cell. For the three cations (Figure 5 and 7), two of them are on special crystallographic positions [Fe1: (0, ½ ,0), 25% occupancy; Fe2: (0, 0, 0), 12.5% occupancy] and one Fe3 (100% occupancy). While Fe1 and Fe2 have inversion centre and are ordered, Fe3 has no symmetry and the four equatorial DMF are disordered. Consequently, the cell contains one Fe1, one Fe2 and two Fe3 giving a total of four. Thus, the only possible charge balance is that the cation and the anion are double charged; that is all iron atoms are in the divalent state. This confirms the reduction of the Fe^{III} to Fe^{II} in solution. Furthermore, the decomplexation of the ligand has taken place in the process, which may be associated to weakening of the metal ligand coulombic forces in relation to those with DMF. It is important to note that the cationic complex has not been reported.[37] The DMF is coordinated through the oxygen atoms and the relative orientation of the $N(CH_3)_2$ units define the overall geometry of the octahedral. However, there is no example of the cation in the literature for comparison but the Fe-O distances are all normal (2.090 – 2.162 Å) for the distorted octahedral geometry for each of the three cations observed. Concerning the anion, $FeCl_4^{2-}$, there are several examples in the literature and the geometries are invariably distorted tetrahedral, with all Fe–Cl distances and angle being normal (2.296 – 2.329 Å and 105.5 – 114.8° in the present case). No classical hydrogen bond has been detected in this crystal structure.

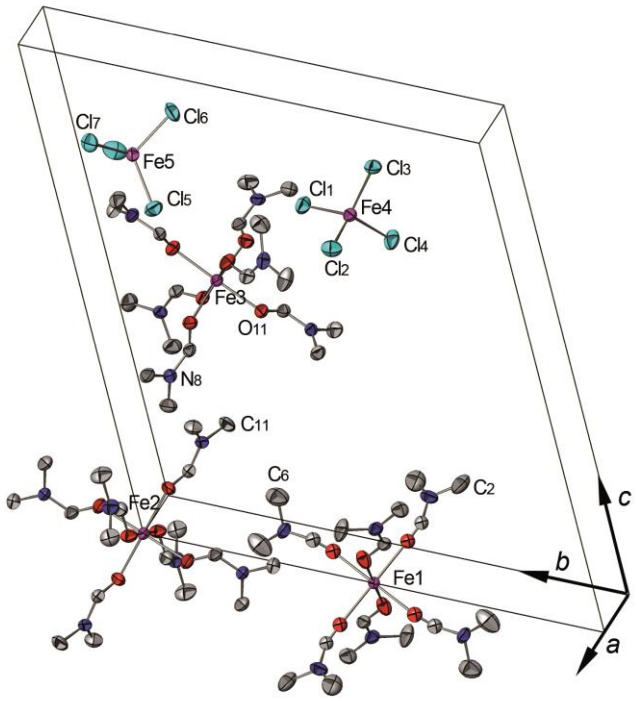

Figure 5: ORTEP view of the asymmetric unit of **2** with partial labelling scheme. The ellipsoids enclose 50% of the electronic density.

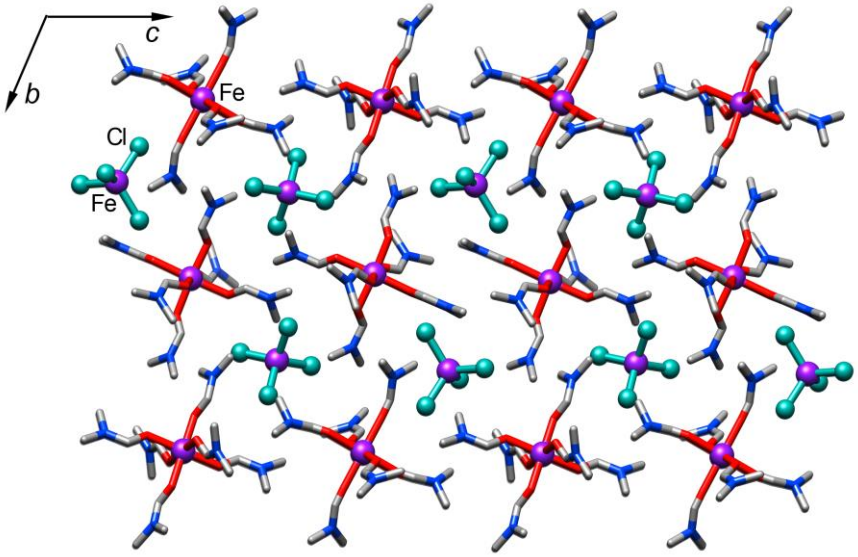

Figure 6: Packing view (projection in the lattice plane 0,y,z). Iron and chlorine atoms are represented as spheres.

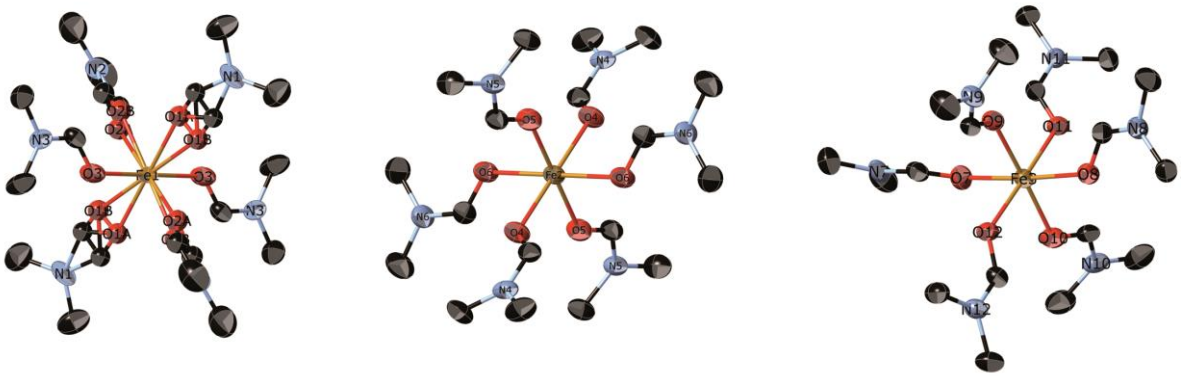

Figure 7: Geometries of the three independent Fe cations in the crystal structure of **2**.

1.6 Electrochemical and Spectroscopic Characterizations.

In order to collect data helping to understand the processes involved in the photoreduction of the Fe^{III} to Fe^{II} a series of additional experiments were undertaken. First we explored the properties of the ligand on its own by using photometric investigation.

Figure 8 shows the concentration dependence of the spectrum of the ligand H_4L in DMF. Two overlapping absorption bands, centred at ca. 305 nm and 345 nm, were observed. The molar absorptivity of the 345 nm band increases with the concentration at the expense of the one at 305 nm. The observation of one isosbestic point is an indication of at least one equilibrium between two (or more) species. This can be due to agglomeration[38] of the molecules in solution at high concentration giving rise to the band at 345 nm that disappears upon lowering the concentration. The second possibility is the formation of the deprotonated species in solution that is favoured by the presence of water acting as base.

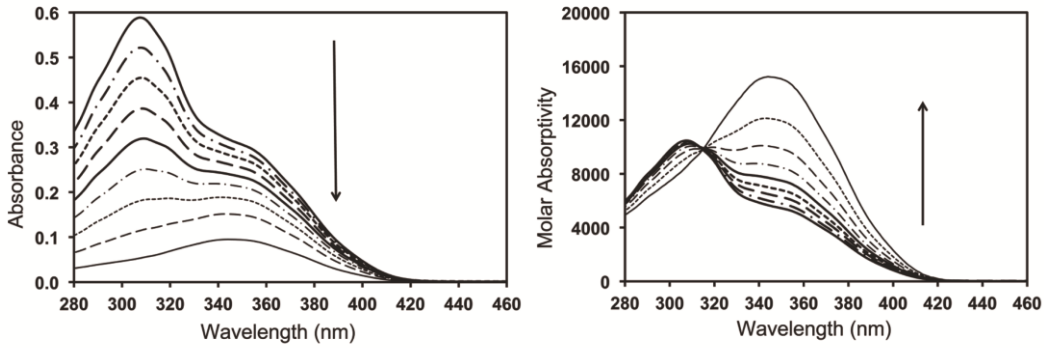

Figure 8: Absorption spectra and its relative molar absorptivity of H_4L for different concentrations in DMF: 5.6, 5.0, 4.4, 3.7, 3.1, 2.5, 1.9, 1.3 10^{-5} M and 6.3 10^{-6} M
(The arrow indicates the sense of the absorbance changes with decrease of the concentration)

DOSY NMR (see Figure A4 of appendix chapter 2) measurement provided an estimate of the hydrodynamic volume of the molecule in solution. The estimation of 285 $Å^3$ per molecule (based on Stock-Einstein relation) is close to 308 $Å^3$ obtained from crystallography and therefore we can exclude any aggregation under the conditions employed. It is important to note that the DOSY measurement was made with a concentration of H_4L of 1 mM, which is, at least, twenty times more concentrated than the solution used in the case of the spectroscopic studies. Supplementary measurements involving addition of base (Figure 9) and acid (Figure 10) to the solutions of the compounds were performed. Spectral changes associated with the addition of base or acid are in agreement with acid-base properties of the ligand (similar behaviour is observed for asymmetric ligand: see Figure A1, A2 and A3 of appendix chapter 2).

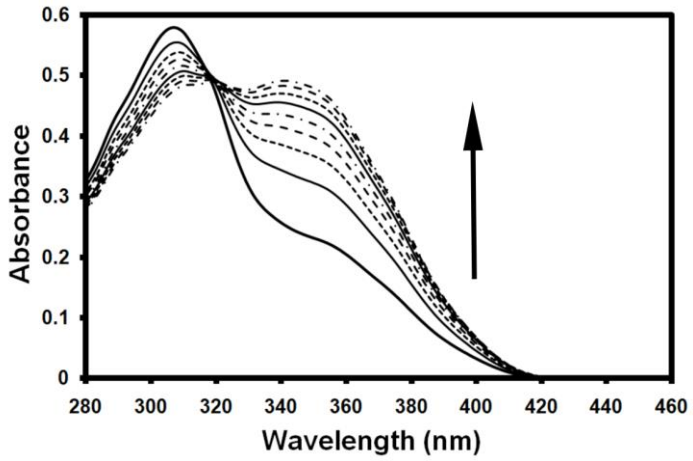

Figure 9: Changes in the spectrum of H_4L (5.10^{-5} M) upon addition of triethylamine [0, 1, 2, 3, 4, 5, 6, 7 and 8.10^{-4} M]

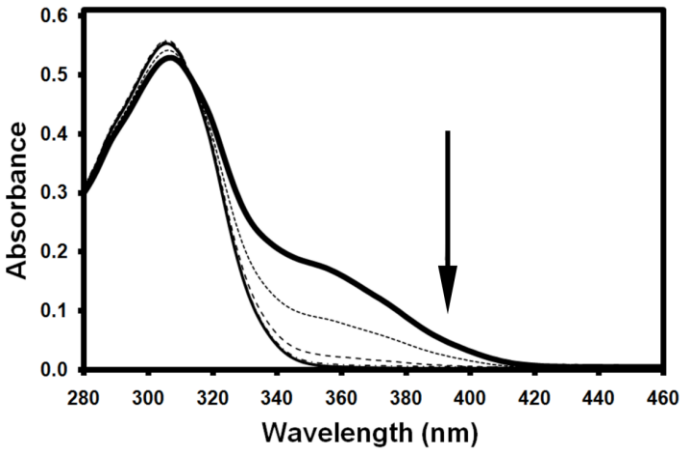

Figure 10: Changes in absorption spectrum H_4L (5.10^{-5} M) upon addition of HCl [0, 1.25, 2.5, 3.75 and 5.10^{-5} M]

The second experiment performed to elucidate the process of photoreduction was the electrochemistry of the Fe^{III}/H_4L solutions. First quasi-steady-state technique (Figure 11) and secondly cyclic voltammetry were employed.

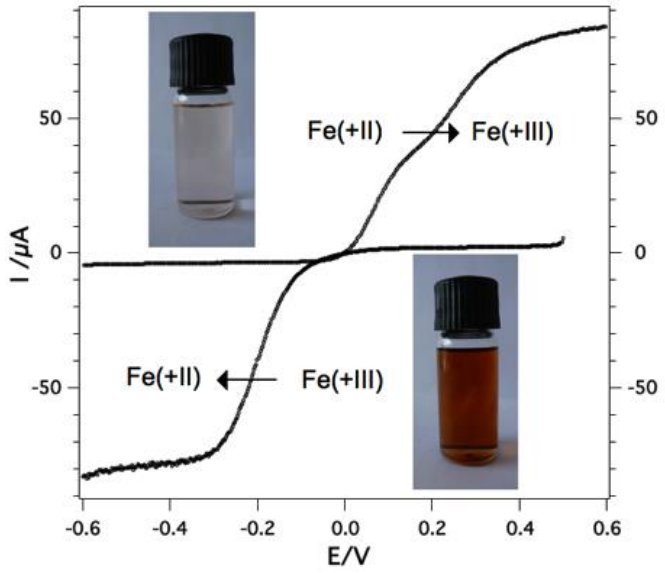

Figure 11: Quasi-steady-state current-potential curves measured for the virgin Fe^{III} and the photoreduced Fe^{II} species at 1.25 mM in DMF (nBu_4NPF_6 0.15 M). Working electrode: glassy carbon. $\nu = 2$ mV.s^{-1} and rotation rate is 1000 rpm.

Figure 11 shows the quasi-steady-state current-potential curves for the iron species in solution before and after light absorption. That of the starting red brown solution of Fe^{III} presents two reduction signals corresponding to probably the mononuclear species at -0.2 V and the dinuclear species at - 0.6 V. After visible light irradiation no reduction wave was observed indicating the absence of ferric ions in this colourless solution. However, two near oxidation processes are observed (Figure 11). These two waves can be attributed to the oxidation of the iron in the cation DMF-Fe^{II} and the anion Cl-Fe^{II} with possible Cl^-/DMF exchange during the Fe^{II} complexation/oxidation process, as demonstrated in the case of porphyrinic iron complexes[39]. The first wave most likely corresponds to Cl^--Fe^{II} oxidation, being the easier to be oxidized, and the second wave (kinetic contribution) corresponds to the DMF-Fe^{II} oxidation. These two oxidation processes possibly lead finally to the stable Cl^--Fe^{III}/ligand compound giving rise, subsequently, to only one reduction step.

Concerning the reduction processes, one has to consider the Fe-L species present in the solution. In addition to the starting $FeCl_3$, both monomeric and dimeric complexes are also

present. For the latter we can assume the complex found in the solid-state structure (see figure 2), with one ligand coordinating two iron atoms, is present. The first reduction step is that of the monomers. The irreversible second reduction step (B on figure 12), which is not related to the ligand (see Figure A7 of appendix chapter 2), may be assigned to the reduction of the second Fe^{III} of the dimers resulting in Fe^{II} complexes. As found by the crystallographic study of **2**, the cation $[Fe(DMF)_6]^{2+}$ and anion $[FeCl_4]^{2-}$ must be present. Thus, this observation suggests that at least for the second Fe^{III} complex, a chemical equilibrium exists between the ligand and solvated Fe^{III} and may be dependent on the first reduction step.

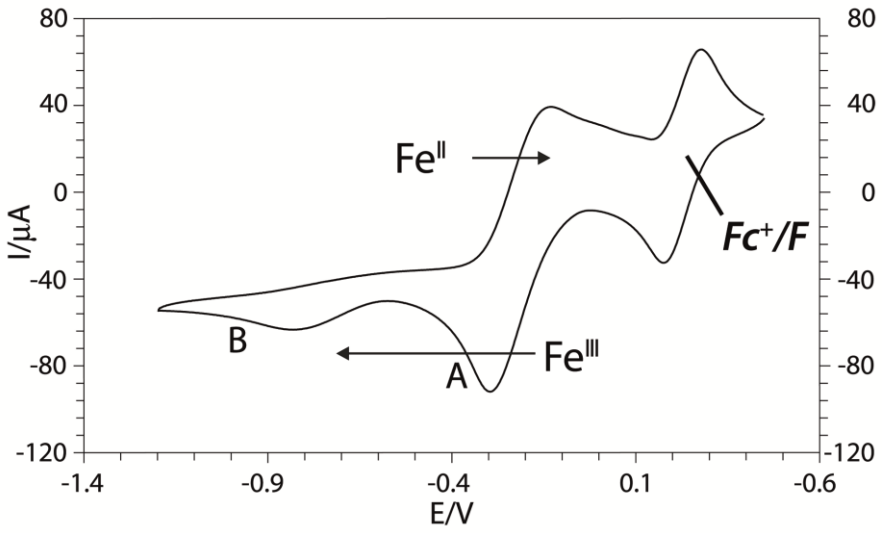

Figure 12: Cyclic voltammogram of 2 $FeCl_3$ and H_4L 10 mM in DMF ($TBA(PF_6)$ = 0.15 M). Working electrode glassy carbon; v = 0.1 V s^{-1}.

A further observation was the dependence of the intensity of the second reduction on the scan rate (figure 13). Without further speculation about the mechanistic reaction model, one can suppose that time (kinetic) is a pertinent parameter. While the current peak of reduction at A is independent of the scan rate, current peak of reduction at B shows a noticeable dependence. This is an indication of a kinetic process associated with the first reduction step. It seems to confirm that the formation of dimers is a slow process; thus more of the mixed-valent compound is produce at low scan rate.

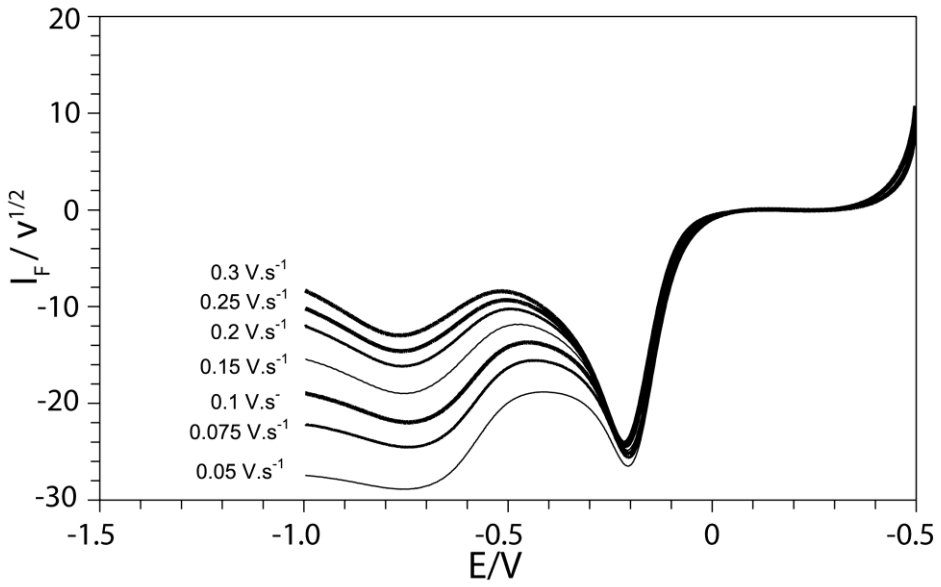

Figure 13: Half cyclic voltammograms of $2FeCl_3$ and H_4L 1 mM at different scan rates in DMF ($TBA(PF_6)$ = 0.15 M). Working electrode: glassy carbon. I_F is the Faradic current obtained after subtracting the capacitive current.

The UV-visible absorption spectra of DMF solutions of H_4L, $FeCl_3$ and their mixture have been recorded to shed some light of the photoreduction (Figure 14). For H_4L and $FeCl_3$ the optical transitions are at energies higher than 450 nm. In contrast, that of a mixture of H_4L and $FeCl_3$ has an additional band centred at 500 nm, which gives the solution its characteristic red coloration. Given the matching of energy of the absorption band with that used for the photoreduction, it is highly conceivable that this band is the one absorbing the visible light and drives the reduction of the Fe^{III}, possibly via a transient mixed-valent state. Preliminary study indicates the photo reduction also takes place in both THF and EtOH solvents.

After exposure of the ferric solution to natural light, the spectrum (B in figure 14) shows that the band at 500 nm disappears and the high-energy bands are at different energies to those of $FeCl_3$ but instead correspond to those of the ligand. This observation and the crystallographic study of **2** are consistent with the decomplexation of the dimeric Fe^{III} unit to Fe^{II} and the free H_4L ligand. A preliminary study of the EPR spectroscopy using a frozen DMF solution shows the formation of an organic radical (Figure A13 of appendix chapter 2) upon irradiation with a laser delivering all the visible light (457 - 574 nm). The multiplicity of three, the g-values of 2.003, close to the free electron resonance, and the hyperfine constant A= 20 G are consistent with those of a free radical of DMF.[40] Thus a mechanism of photoreduction involving this radical is strongly possible.

To sum up the discussion of the pertinent results presented above and to explain the

process of photoreduction in DMF solution, it is necessary to invoke also the crystallographic studies of the pure ligand and its salts with other transition metals. First it is important to comment on the formation of the crystals of the pure ligand after the irradiation of the Fe^{III}-H_4L solution. The observed results point out that the ligand is potentially acting as a catalyst promoting the formation of the dimer which is subsequently photoreduced to produce the Fe^{II} in the solution while being liberated. Thus, it is conceivable that the reaction can be carried out to completion with much less that the equivalent quantities; an experiment which is in progress. Secondly, the results force us to conclude that the ability of the ligand to coordinate to transition metals of different ionic size and charge is quite subtle and variable. The works of Chen *et al.*[25-28] on Co, Ni and Zn suggest that the presence of pyridine and ethylenediamine stabilises the dimer formation by occupying the peripheral coordination. In their absence the dimeric Fe^{II} has not been observed. In our case, there is a subtle competition for coordination between the ligand and the other potential coordinating units in the solution; here, we note in the absence of other ligands it is the DMF and chloride ion that are coordinated to the Fe^{II}. In contrast for Fe^{III}, the ligand, chlorine and DMF are all favoured.

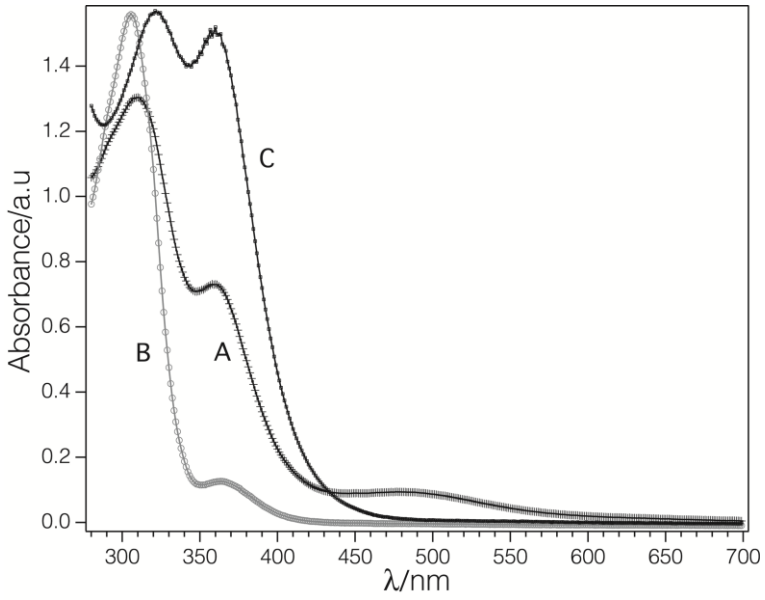

Figure 14: Absorption spectra of A) Fe_2^{III}**L**, B) Fe^{II}/H_4**L** obtained after light exposure of Fe_2^{III}**L**, and C) $FeCl_3$. All solutions are about 1 mM in DMF.

1.7 Conclusion

In this work, we have explored further the chemistry of the *N,N'*-bis(salicyl)hydrazide ligand (H_4L) with $FeCl_3$ in DMF which has produced the dinuclear $(Fe^{III}Cl(DMF)_2)_2L$ complex. Its structure from single crystal X-ray diffraction provided an interesting comparison to the free ligand and other transition metal complexes, revealing the strength of the ligand towards different charged cations and their ionic radii in view of its quadruply charged state with bis-meridional coordination sites. Fitting of the magnetic susceptibility gave an antiferromagnetic coupling of J = –6 cm^{-1} for the rare Fe–N-N–Fe pathway. Interestingly, the $Fe^{III}Cl_3/H_4L$ solution in DMF is very sensitive to visible light and loses its red coloration in very short times in the absence of oxygen to form $[Fe^{II}(DMF)_6][Fe^{II}Cl_4]$. Crystallography of the products of this reaction and those known in the literature in conjunction with UV-vis spectroscopy and electrochemistry point to the fact that the photoreduction is promoted by the ligand and the active light receptor is the iron dimer in the solution. Furthermore, electrochemistry suggests the process involves a mixed-valent Fe^{II}-Fe^{III} intermediate.

1.8 Experimental

General procedures.

All manipulations were performed under aerobic conditions, using reagents and solvents as received. The NMR spectra were recorded using a Bruker AC 400MHz NMR spectrometer at ambient temperature. $^{13}C\{^1H\}$ NMR spectra were recorded on a Bruker AVANCE 300 instrument at ambient temperature. ^1H-NMR chemical shifts are referenced to $SiMe_4$ and were determined by reference to the residual ^1H solvent peaks. IR spectra were recorded using a Nicolet 6700 FT-IR spectrometer in the region 4000-400 cm^{-1} and employing an ATR mode through a ZnSe crystal. Elemental analyses were performed by the ¨Service de microanalyses¨, Université de Strasbourg.

Synthesis of H_4L.

The ligand was prepared using a modified procedure to those in the literature. [31] To a clear well-stirred solution of salicylic acid (2.72 g, 19.7 mmol) and salicylhydrazide (3 g; 19.7 mmol) in DMF (25 ml) was added drop-wise to a solution of dicyclohexylcarbodiimide (4.7 g, 19.7 mmol) in DMF (15 ml). Butyl alcohol was added to catalyse the reaction. The

resulting exothermic reaction caused the solution to become yellow and a white precipitate is formed. After four hours, the stirring was stopped and the white precipitate of dicyclohexylurea was removed by filtration. The filtrate was concentrated and then briefly heated under reflux to dissolve the precipitated material. On cooling to room temperature, a white precipitate of the desired product was deposited, which was collected by filtration and washed with diethyl ether (3.32 g, 62 % yield). ^{1}H-NMR (300 MHZ, DMSO-d_6) δ (ppm): 11.70 (br s, 1H, NH); 11.11 (br s, 1H, NH); 7.94-7.90 (dd, 2H, J=8 Hz, J= 1.6 Hz); 7.94 (dd, 2H, J = 1.76; 7.98 Hz); 7.46 (ddd, 2H, J = 1.71; 7.25; 8.35 Hz); 7.01- 6.94 (m, 4H). ^{13}C-NMR (DMSO-d_6) δ (ppm): 165.80 (C-OH phenol); 158.56 (C=O amide); 134.08; 128.81; 119.23; 117.27 (C_{arom}); 114.96 (-C-CONH-). IR, ν (cm^{-1}): 3288, 3070, 2705, 1600, 1549, 1503, 1472, 1444, 1361, 1303, 1231, 1163, 1138, 1097, 1035, 955, 857, 780, 752, 688, 661. Anal. Calc. (%) for $C_{14}H_{12}N_2O_4$: C 61.76; H 4.44; N 10.29. Found (%): C 61.30; H 4.58; N 10.41. Single crystals (colourless) suitable for X-Ray structure determination were obtained by slow diffusion of diethyl ether into a DMF solution of H_4**L**.

Synthesis of $(Fe^{III}Cl(DMF)_2)_2$L (1).

To a well-stirred solution of $FeCl_3.9H_2O$ (595.7 mg, 3.64 mmol) in DMF (10 ml) was added 0.5 eq. of H_4L (500 mg, 1.82 mmol). The red solution was left stirring for 5 hours in the dark at room temperature and 40 ml of diethyl ether was added to the solution. The dark red powder precipitated was filtered and washed with Et_2O. Red crystals of **1** that are suitable for X-Ray diffraction were grown by diffusing diethyl ether into a DMF solution of **1** in the dark (0.94 g, 70% yield). Anal. Calc. (%) For $C_{26}H_{36}Cl_2Fe_2N_6O_8$: C 42.02; H 4.88; N 11.31. Found (%): C 41.88; H 5.01; N 11.45.

Synthesis of $[Fe^{II}(DMF)_6][Fe^{II}Cl_4]$ (2).

To a well-stirred solution of $FeCl_3$ (595.7 mg, 3.64 mmol) in DMF (10 ml) was added 0.5 eq. of H_4L (500 mg, 1.82 mmol). The solution was left stirring for 5 hours at room temperature. The resulting red solution was degassed with nitrogen for 20 minutes to remove dissolved oxygen. Under an atmosphere of nitrogen, 5 ml of the solution was transferred to the lower part of a 20 ml closed glass test tube with a septum cap. The solution was exposed to natural light and when it had changed from red to colourless, the tube was filled with Et_2O.

Colourless crystals (suitable for X-Ray diffraction) of **2** and the free ligand H_4L were thus obtained and they have been separated with the help of a microscope for further studies. The crystalline blocks (stable in air for only few minutes) of compound **2** have been selected by its slight tarnished coloration upon exposure to air compared to the free ligand. The quick surface coloration indicates the air sensitivity of the Fe^{II} species. The lack of chemical stability of complex **2** and its contamination with H_4L has hampered its chemical analyses.

Single crystal X-ray structure determination.

Single crystals of the ligand H_4**L**, and the iron complexes **1** and **2** were mounted independently on glass fibers for intensity data collections on a Nonius Kappa-CCD area detector diffractometer (Mo Kα = 0.71073 Å). The details of data collection (DENZO)[32] and structure refinements are given in Table 2. The cell parameters were determined from reflections taken from one set of 10 frames (1.0° steps in phi angle), exposed for 20 seconds each. The structures were solved using direct methods and refined against F^2 using SHELXL97.[33, 34] No absorption correction was applied. All non-hydrogen atoms were refined anisotropically and hydrogen atoms were introduced as fixed contributors (SHELXL97).

Crystallographic data (excluding structure factors) have been deposited at the Cambridge Crystallographic Data Centre under the deposition numbers CCDC 855119 (H_4L), 893268 & 893269 (iron complexes). Copies can be obtained free of charge on application to the CCDC, 12 Union Road, Cambridge CB2 1EZ, UK.

Electrochemistry.

Electrochemical measurements were performed in N,N-dimethylformamide (DMF) (Sigma Aldrich; <0.1% H_2O) which was used as received. Electrochemical grade tetrabutylammonium hexafluorophosphate TBA(PF_6) (Fluka) was used as supporting electrolyte. All electrochemical measurements were carried out at ambient temperature (20 ± 2°C) in a conventional one compartment, three-electrodes cell. The working electrodes were platinum (2 mm diameter), glassy carbon (3.5 mm diameter) or a microelectrode of platinum (10 µm diameter). The counter electrode was a platinum wire and a second platinum wire was used as pseudo-reference. The cell was connected to a PGSTAT 302 potentiostat (Eco Chemie, Holland). Prior to measurements, all the solutions were deoxygenated with argon.

For complex **1**, the DMF solution was kept in the dark before measurements. When necessary ferrocene was used as internal potential reference.

UV-visible spectroscopy.

The UV-Visible spectra were recorded by transmission through N,N-dimethylformamide (DMF) (Sigma Aldrich; <0.1% H_2O) solutions of the compounds using a 8453 Agilent spectrophotometer and a standard 1 cm path length cell. The acid (commercial HCl) and base (distilled triethylamine) solutions were employed for the titration experiments.

Table 1: Crystal data and refinement details for **1**, **2**, and H_4L.

Compound	**$Fe^{III}_2(L)Cl_2DMF_4$**	**$[Fe^{II}DMF_6][Fe^{II}Cl_4]$**	**H_4L**
Formula	$C_{26}H_{36}Cl_2Fe_2N_6O_8$	$4[Fe_2C_{18}H_{42}N_6O_6Cl_4]$	$C_{14}H_{12}N_2O_4$
Colour	Red	Colourless	Colourless
Formula weight ($g.mol^{-1}$)	743.21	2768.3	272.26
Crystal system	Orthorhombic	Triclinic	Monoclinic
Space group	*P b c a*	*P* -1	*P* 2_1/n
a [Å]	16.1661(10)	9.223(7)	8.3000(10)
b [Å]	9.4408(10)	18.6840(10)	6.2890(10)
c [Å]	21.396(4)	20.178(2)	12.1960(10)
α [°]	90.00	114.76(5)	90.00(5)
β [°]	90.00	92.29(5)	104.58(5)
γ [°]	90.00	91.81(5)	90.00(5)
V [$Å^3$]	3265.4(7)	3150(2)	616.11(19)
Z	4	1	2
Density (calc) [$g.cm^{-3}$]	1.512	1.459	1.468
μ(Mo Kα) [mm^{-1}]	1.107	1.300	0.110
F(000)	1536	1440	284
Crystal Size [mm]	0.14 × 0.09 × 0.09	0.12 × 0.10 × 0.08	0.15 × 0.08 × 0.08
Data Collection			
θ Min-Max [°]	1.90 - 27.49	1.25 - 25.68	2.68 - 27.48
Data set [h, k, l]	-20/18, -7/12, -25/27	-11/10, -22/21, -23/24	-10/10, -8/7, -15/15
Total, Unique data R(int)	20823, 3749 0.0837	13910, 10078 0.0258	2456, 1416 0.0270
Observed data [I > 2σ(I)]	2386	6838	953
Refinement			
Reflections, Parameters	3749, 200	10078, 644	1416, 100
R2, R1 wR2, wR1 GooF	0.1031, 0.0552, 0.1629, 0.1280, 1.071	0.0868, 0.0480, 0.1230, 0.1053, 1.015	0.0738, 0.0429 0.1215, 0.1050 1.030
Maximum and Average Shift/Error	0.000, 0.000	0.002, 0.000	0.000, 0.000
Min., Max. Residual Density [$e/Å^3$]	-0.747, 0.994	-0.730, 0.770	-0.256, 0.206

1.9 References

1. (a) D. Gatteschi, *Adv. Mat*. **1994**, *6*, 635. (b) A. Caneschi, D. Gatteschi, *Prog. Inorg. Chem.* **1991**, ***37***, 331. (c) O. Kahn, *Molecular Magnetism*, VCH Publishers, New York, **1993**. (d) *Metal–Organic and Organic Molecular Magnets*, Spec. Publ. - R. Soc. Chem., Eds. P. Day and A. E. Underhill, Cambridge, UK, 2000, volume 252. (e) *Molecular Magnetism, New Magnetic Materials*, Eds. K. Itoh and M. Kinoshita, Gordon Breach-Kodansha, Tokyo, **2000**. (f) *Magnetism: A Supramolecular Function*, Ed. O. Kahn, Kluwer Academic Publishers, **1996**.
2. M. Kurmoo, *Chem. Soc. Rev.*, **2009**, *38*, 1353.
3. (a) R. M.Cornell, U. Schwertmann, *The Iron Oxides, Structure, Properties, Reactions, Occurrence and Uses*, VCH Publishers: Weinheim, Germany, **1996**. (b) S. J. Blundell, Magnetism in Condensed Matter, Oxford University Press, **2001**.
4. M. Kurmoo, H. Kumagai, S. M. Hughes, C. J. Kepert, *Inorg. Chem.*, **2003**, *42*, 6709.
5. M. Verdaguer, G. Girolami, *Magnetism: Molecules to Materials V* (WILEY-VCH Verlag GmbH&KGaA, Weinheim, 2004.
6. J.-P. Zhang and X.-M. Chen, *Chem. Commun*., **2006**, 1689.
7. (a) M. Kurmoo, C. J. Kepert, *New J. Chem.*, **1998**, 1515. (b) S. R. Batten and K. S. Murray, *Coord. Chem. Rev.*, **2003**, *246*, 103
8. J. Ribas, A. Escuer, M. Monfort, R. Vicente, R. Cortes, L. Lezapma, T. Rojo, *Coord. Chem. Rev.*, **1999**, *193*, 1027. (b) Y. F. Zeng, X. Hu, F.-C. Liu, X.-H. Bu, *Chem. Soc. Rev*., **2009**, *38*, 469.
9. (a) M. Kurmoo, *Mol. Cryst. Liq. Cryst.*, **2002**, *379*, 271. (b) T. Lancaster, S. J. Blundell, F. L. Pratt, M. Kurmoo, *Physica*, **2003**, *B326*, 522.
10. (a) H. Tamaki, Z. J. Zhong, N. Matsumoto, S. Kida, M. Koikawa, N. Achiwa, Y. Hashimoto and H. Okawa, *J. Am. Chem. Soc*., ***1992***, *114*, 6974. (b) S. Decurtins, *Philos. Trans. R. Soc. London*, Ser. A, **1999**, *357*, 3025. (c) C. Mathoniere, C. J. Nuttall, S. G. Carling and P. Day, *Inorg. Chem*., **1996**, *35*, 1201
11. (a) C. N. R. Rao, A. K. Cheetham, A. Thirumurugan, *J. Phys.: Condens. Matter*, **2008**, *20*, 083202. (b) G. Ferey, *Chem. Soc. Rev*., 2008, 37, 191.
12. O. Kahn, *Adv. Inorg. Chem*., 1995, 43, 179.
13. M. Ruben, J. Rojo, F. J. Romero-Salguero, L. H. Uppadine, J-M. Lehn, *Angew. Chem. Int. Ed.* 2004, *43*, 3644.
14. S-M. Peng, C-C. Wang, Y-L. Jang, Y-H. Chen, F-Y. Li, C-Y. Mou, M-K. Leung, *J. Mag. Mag. Mater.*, **2000**, *209*, 80.
15. S. Vilminot, G. André, F. Bourée-Vigneron, P. J. Baker, S. J. Blundell, M. Kurmoo, *J. Am. Chem. Soc.*, **2008**, *130*, 13490.
16. K Mogilaiah, E Anitha , K.S. Kumar, R.S. Prasad, *Ind. J. Chem. B*, **2011**, 50B, 126-128.
17. L. Saíz-Urra, M.P. González, Y. Fall, G. Gómez, *Eur. J. Med. Chem.*, **2007**, 42, 64-70
18. K. Mogilaiah, M. Prashanthi, G.R. Reddy, *Synth. Comm.*, **2003**, 33, 3741-3745
19. V.F. Shul'gin, E.A. Sarnit, O.V. Konnik, E.B. Rusanov, A.S. Bogomyakov, V. I. Ovcharenko, V.V. Minin, *Russ. J. Coord. Chem*, **2012**, 38, 44-49.
20. G. I. Mustata, A. Brigo, J. M. Briggs, *Bioorganic & Medicinal Chemistry Letters*, **2004**, 14, 6, 22, 1447-1454
21. C. Beghidja, G. Rogez, J. Kortus, M. Wesolek, R. Welter, *J. Am. Chem. Soc*. **2006**, 128, 3140.
22. (a) N. Bouslimani, N. Clément, G. Rogez, P. Turek, M. Bernard, S. Dagorne, D. Martel, H. N. Cong, R. Welter, *Inorg. Chem*. **2008**, 47, 7623. (b) N. Clément, C. Toussaint, G. Rogez, C. Loose, J. Kortus, L. Brelot, S. Choua, S. Dagorne, P. Turek,

R. Welter, *Dalton Trans.* **2010,** *39*, 4579.
23. R. Welter, *Patent*, **2009**, WO 2009/130562 A1; "Method and device for producing and storing energy".
24. (a) S. Lin, S-X. Liu, Z. Chen, B-Z. Lin, S. Gao, *Inorg. Chem*., **2004**, 43, 2222. (b) S. Lin, S-X. Liu, B-Z. Lin, *Inorg. Chim. Acta*, **2002**, *328*, 69.
25. Y. T. Chen, D. C. Li, D. Q. Wang, Y. H. Zhu, *Acta Cryst. E.* **2008**, 64, o120.
26. Z. Y. Wang, S. X. Liu, *Acta Cryst. E*, **2007**, 63, m2503.
27. Y. T. Chen, J. M. Dou, D. C. Li, D. Q. Wang, Y. H. Zhu, *Acta Cryst.* E. **2007**, 63, m3129.
28. Z. Y. Wang, S-X. Lin, *Acta Cryst.* E. **2007**, *63*, m3105.
29. V. Bazani and V. Carassiti, *Photochemistry of Coordination compounds, Academic Press London and New-York*, **1970**.
30. J. Sima and J. Makanova, *Coord. Chem. Rev.*, **1997**, *160*, 161.
31. Ligand synthesis: (a) H. Zhao, T. R. Burke Jr., *Tetrahedron*. **1997**, *53*, 4219. (b) P. V. Bernhardt, P. Chin, P. C. Sharpe, J. C. Wang, D. R. Richardson, *Biol. Inorg. Chem*., **2005**, *10*, 761.
32. *Kappa CCD Operation Manual*, Nonius B. V., Delft, The Netherlands, **1997**.
33. G. M. Sheldrick, *SHELXL97, Program for the refinement of crystal structures*. University of Gottingen. Germany, **1997**.
34. R. Welter, the Crystalbuilder Project, *Acta Cryst.,* **2006**, *A62*, s252.
35. A. L. Spek, PLATON software, *J. Appl. Cryst*., **2003**, *36*, 7
36. C. J. O'Connor, *Magnetic susceptibility measurements*. *Prog. Inorg. Chem*., S. J. Lippard, Ed., **1982**, *29*, 203.
37. A. L. Rheingold, B. S. Hammes, *Private Communication*, **2002**, (CCDC 187571), Contribution from Department of Chemistry and Biochemistry, University of Delaware, DE 19716, USA.
38. L. Antonov, G. Gergov, V. Petrov, M. Kubista, J. Nygren, *Talanta* 1999, **49**, 99–106.
39. D. Lexa, M. Momenteau, P. Rentien, G. Rytz, J. M. Savéant, F. Xu, *J. Am. Chem. Soc*., **1984**, *106*, 4755.
40. I. A. Shkrob, T. W. Marin, *J. Phys. Chem.*, **2012**, *116*, 1746–1757.

Chapter 4:

Crystal structures and magnetic properties of Mn(III) and Iron(III) supported by 2-salicyloylhydrazono-1,3-dithiane

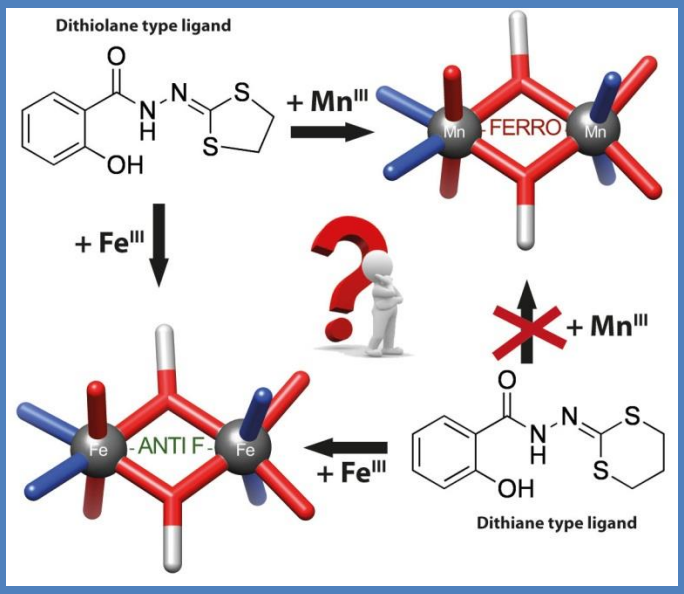

Chapter 4:

Mononuclear and Dinuclear Complexes of Manganese(III) and Iron(III) Supported by 2-Salicyloylhydrazono-1,3-dithiane Ligand: Synthesis, Characterization and Magnetic Properties

Mononuclear and Dinuclear Complexes of Manganese(III) and Iron(III) Supported by 2-Salicyloylhydrazono-1,3-dithiane Ligand: Synthesis, Characterization and Magnetic Properties

Abstract

The coordination chemistry of 2-salicyloylhydrazono-1,3-dithiane (H_2**L**) was studied with manganese and iron ions. The following complexes have been isolated as crystalline materials, and their crystal structures have been determined by single crystal X-Ray crystallography: Mn^{III}(acac)(H**L**)$_2$ (**1**) (acac = acetylacetonate), Mn^{III}(H**L**)$_3$·CH_2Cl_2 (**2**), Fe^{III}(H**L**)$_3$·2$CHCl_3$ (**3**), Fe^{II}(H_2**L**)$_2Cl_2$·2CH_3OH (**4**), Fe^{III}_2(μ-OMe)$_2$(H**L**)$_4$·0.5CH_3OH (**5**), Fe^{III}_2(μ-O) (H**L**)$_4$·3CH_2Cl_2 (**6**). All attempts to synthesize the dinuclear μ–methoxo complex [Mn^{III}_2(μ-OMe)$_2$(H**L**)$_4$] have so far failed, even when the procedure used in the case of 2-salicyloylhydrazono-1,3-dithiolane (H_2**L**') ligand, which worked very efficiently, was employed. The new iron dinuclear μ–methoxo complex (**5)** presented in this study shows antiferromagnetic intramolecular coupling (J = –21.1 K), which is in agreement with the theoretical study proposed previously for its manganese analogue.

Keywords: Iron, Manganese, 2-Salicyloylhydrazono-1,3-dithiane, Molecular magnetism

1.1 Introduction

The control of magnetic coupling in addition to the possibility of inducing a spin-state modification at the molecular scale is among the most challenging themes in the field of molecular magnetism. Considering a variety of magnetically interesting molecules,[1] special attention has been paid to exchange coupled multinuclear paramagnetic complexes.[2,3] Systems presenting lower nuclearity are of interest as, among others, versatile building blocks for cooperatively associated magnetic systems.[4] For instance they can be incorporated in crystal lattices along with conducting molecules, which may lead to the formation of innovative magnetic/conducting bifunctional materials.[5] Due to the dependence of coupling pathways on the structure and symmetry of the organic ligands, dinuclear molecular systems offer interesting possibilities to tune metal-to-metal interactions by subtle structural changes within the organic periphery. We have reported an interesting dinuclear Mn^{III} complex $Mn^{III}_2(\mu\text{-OMe})_2(H\mathbf{L}')_4$, which was found to exhibit the largest J value (J = +19.7 cm^{-1}) reported so far for a Mn^{III}–Mn^{III} interaction. The peculiarity of the $Mn^{III}_2(\mu\text{-OMe})_2(H\mathbf{L}')_4$ solid-state structure arises from an unsymmetrical arrangement of the ligands leading to orthogonality of the magnetic orbital's and consequently the ferromagnetic exchange coupling. This situation is certainly related to intramolecular non-classical H-bonds occurring between hydrogen atoms of the dithiolane rings and the centroids of the phenol groups.[6] In addition to the Mn^{III} chemistry, we have also studied the coordination chemistry of the 2-salicyloylhydrazono-1,3-dithiolane ligand to other metal ions such as iron,[7,8] cobalt[9] and chromium[10] to form a series of mononuclear and dinuclear complexes (scheme 1). These complexes have shown interesting chemical and physical properties. For example, an unusual spontaneous reduction from Fe^{III} to Fe^{II} of the mononuclear complexes was observed.[7] This redox reaction was subsequently fully investigated by electrochemistry, EPR studies, magnetic measurements and solid-state molecular structure determination. Such a phenomenon opens up new research opportunities, as recently been pointed out by Wernsdorfer *et al.*[11] and forms the basis of a patent.[12]

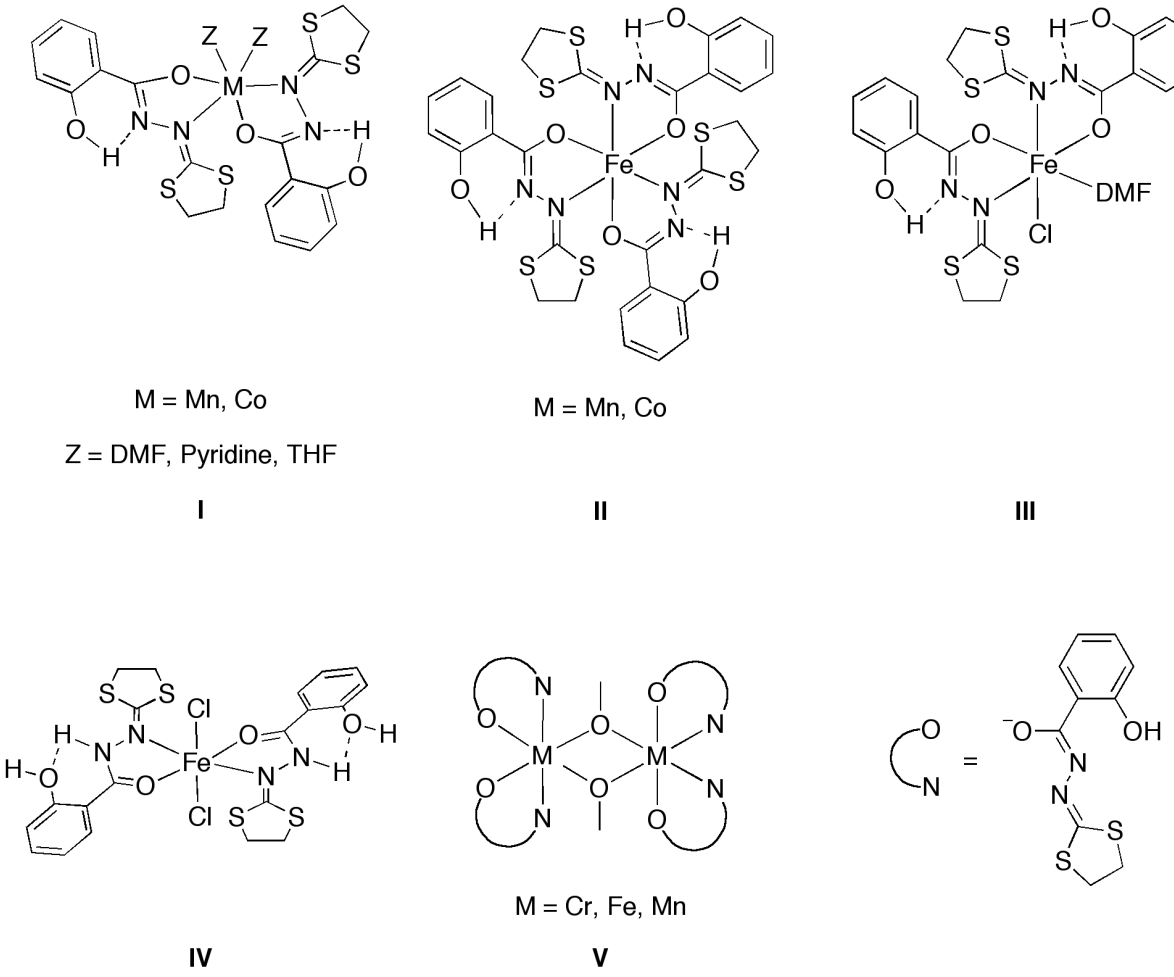

Scheme 1: Transition metal complexes of 2-salicyloylhydrazono-1,3-dithiolane ligand.

The asymmetric $Fe^{III}_2(\mu\text{-}OMe)_2(H\mathbf{L}')_4$ complex has also been synthesized and characterized.[7] This dinuclear Fe^{III} compound shows antiferromagnetic intramolecular coupling, which is in agreement with the previously proposed theoretical model for the related Mn^{III} complex.[6] As predicted by DFT calculations, Cr^{III} μ-methoxo dinuclear complex featuring the same ligand also exhibited a strong antiferromagnetic coupling.[10]

Via minor modifications of the chelating ligand, it is expected to control the structural geometry of the complexes obtained, as well as their physical properties. We have thus started to explore the coordination chemistry of 2-salicyloylhydrazono-1,3-dithiane ($H_2\mathbf{L}$), which is closely related to $H_2\mathbf{L}'$ where it has a 1,3-dithiane group in place of the 1,3-dithiolane moiety.[9,10] A dinuclear μ-methoxo $Cr^{III}_2(\mu\text{-}OMe)_2(H\mathbf{L})_4$ complex chelated by H**L** exhibiting a

strong antiferromagnetic coupling, was successfully synthesized by the reaction of $CrCl_3$ with this ligand in the presence of zinc.[10] In addition, one novel Co^{II} mononuclear complex and one diamagnetic μ-hydroxo dinuclear Co^{III} complex $[Co^{III}_2(\mu\text{-}OH)_2(H\mathbf{L})_4]$ supported by the ligand H**L** were also stabilized and characterized.[9]

The hypothesis that the similarity between the structures of $H_2\mathbf{L}$ and $H_2\mathbf{L}$' would allow H**L** to be a suitable ligand to stabilize a dinuclear μ-methoxo Mn^{III} complex, which is expected to exhibit very strong intramolecular ferromagnetic interaction, prompted us to extend the coordination chemistry of ligand $H_2\mathbf{L}$ to Mn^{III}. In this article, we report our attempts to synthesize the desired dinuclear μ-methoxo Mn^{III} complex stabilized by 2-salicyloylhydrazono-1,3-dithiane. In addition, following a systematic approach and due to their similar coordination behaviour, we also describe the synthesis and characterization of four iron mononuclear and dinuclear complexes supported by H**L** and $H_2\mathbf{L}$, and the synthesis and magnetic property measurement of μ-methoxo dinuclear iron complex.

1.2 Results and discussion

Synthesis and characterization of manganese complexes $Mn^{III}(acac)(HL)_2$ (1) and $Mn^{III}(HL)_3$ (2)

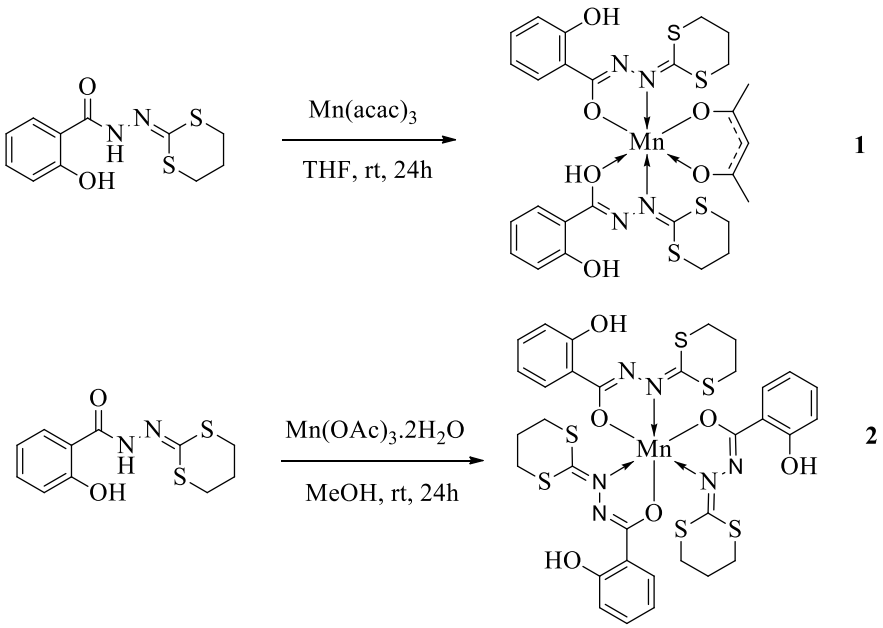

Scheme 2: Synthesis of complexes $Mn^{III}(acac)(H\mathbf{L})_2$(**1**) and $Mn^{III}(H\mathbf{L})_3$ (**2**).

In an attempt to synthesize the dinuclear complex, the first trials were those applying the conditions used previously in our laboratory.[6,13] This procedure resulted in two new mononuclear complexes described here after. The complex $Mn^{III}(acac)(H\mathbf{L})_2$ (**1**) obtained in a 67% yield by reacting 2-salicyloylhydrazono-1,3-dithiane ($H_2\mathbf{L}$) with manganese acetylacetonate in THF. Good quality crystals were obtained by slow diffusion of methanol to the complex solution in chloroform. An ORTEP view with selected distances and angles is given in figure 1. The dark red complex **1** crystallizes in the monoclinic space group $P\ 2_1/c$ and consists in a mononuclear Mn^{III} species chelated by two ligands in their basic forms $H\mathbf{L}^-$, and the coordination sphere of the Mn^{III} atom being completed by one acetylacetonate molecule.

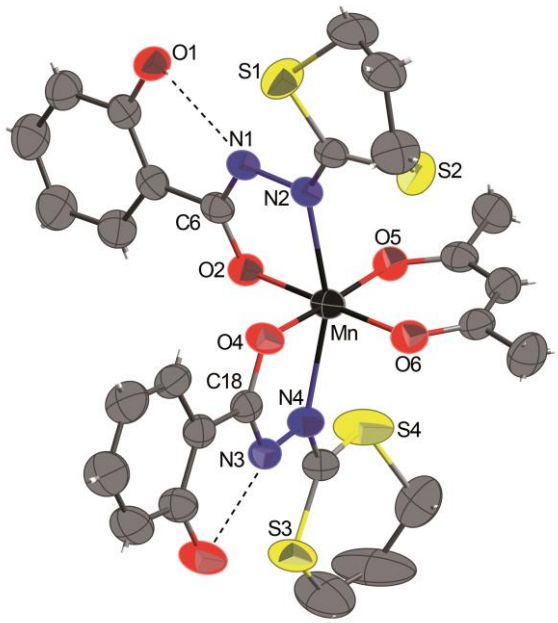

Figure 1: ORTEP view of the complex **1** with partial labelling scheme. The ellipsoids enclose 50% of the electronic density. Selected distances (Å) and angles (°): Mn–N2 2.261(2), Mn–N4 2.280(2), Mn–O2 1.922(2), Mn–O4 1.921(2), Mn–O5 1.912(3), Mn–O6 1.908(2); O5–Mn–O4 176.59(8), N2–Mn–N4 158.37(8), O6–Mn–O2 179.63(8). Dashed lines indicate intramolecular hydrogen bonds.

The Mn^{III} atom adopts a slightly distorted octahedral geometry with the O5–Mn–O4, N2–Mn–N4 and O6–Mn–O2 bond angles of 176.59(8)°, 158.37(8)° and 179.63(8)°, respectively, which are very similar to those observed in Fe^{III} complex supported by

2-salicyloylhydrazono-1,3-dithiolane ligand.[8] No specific intramolecular CH–π interaction has been detected, but two classical hydrogen bonds between the OH groups of the phenol rings and the hydrazine groups were detected as shown in figure 1 (dashed line). Only two examples of similar coordination mode for Mn^{III} acetylacetonate compounds containing binaphthyl Schiff base[14] and 1, 3-bis(salicy1ideneiminato)propane[15] ligands can be found in the Cambridge Data base.

The complex $Mn^{III}(H\mathbf{L})_3 \cdot CH_2Cl_2$ (**2**) was obtained in 31% yield by reacting three equivalents of $H_2\mathbf{L}$ with manganese acetate dihydrate in methanol (Scheme 2). Good quality crystals were obtained by slow diffusion of pentane to a solution of the complex in dichloromethane. In contrast to the case of 2-salicyloylhydrazono-1,3-dithiolane,[6] and in spite of addition of excess base (NaOAc, NEt_3 etc.) we were unable to generate the μ-methoxo dinuclear complex $Mn^{III}_2(\mu\text{-}OMe)_2(H\mathbf{L})_4$.

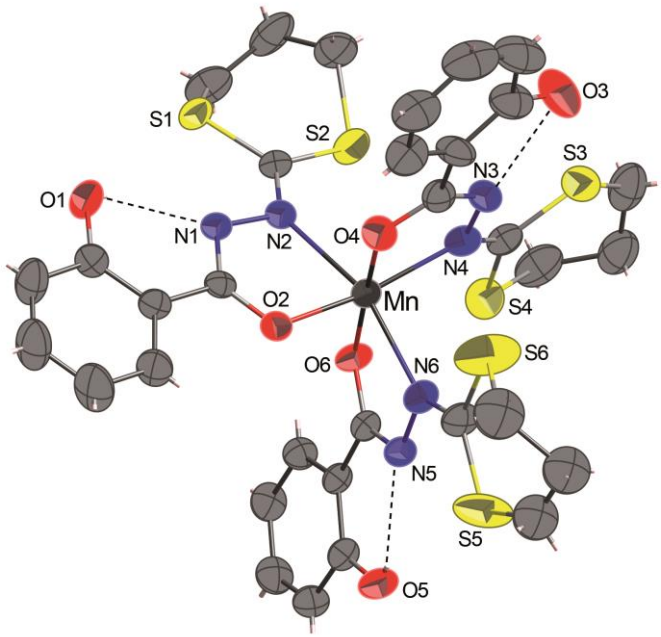

Figure 2: ORTEP view of the complex **2**·CH_2Cl_2 with partial labelling scheme. The ellipsoids enclose 50% of the electronic density. The solvent CH_2Cl_2 was omitted for clarity. Selected distances (Å) and angles (°): Mn–N2 2.294(3), Mn–N4 2.088(4), Mn–N6 2.259(3), Mn–O2 1.922(3), Mn–O4 1.892(3), Mn–O6 1.894(3); O4–Mn–O6 177.3(2), O2–Mn–N4 167.3(1), N2–Mn–N6 161.5(1).

The dark red complex **2**·CH_2Cl_2 crystallizes in the triclinic centrosymmetric space group *P*-1. The crystal structure shows that the Mn^{III} ion is surrounded by three anionic bidentate H**L**$^-$ ligands, forming a distorted octahedral geometry of the metal centre (see figure 2). All distances are in agreement and very similar, to those measured in complex **1** and with other manganese complexes containing 2-salicyloylhydrazono-1,3-dithiolane ligand.[13] As already observed in complex **1**, the intramolecular O–H···N hydrogen bonds are established between OH groups of the phenol rings and the hydrazine groups. Besides the previously reported manganese complex supported by three 2-salicyloylhydrazono-1,3-dithiolane ligands,[6] another very similar structure was observed in Mn^{III} complex bearing three *N'*-benzylidenesalicylhydrazide ligands.[16]

Attempts to synthesize $Mn^{III}_2(\mu\text{-}OMe)_2(HL)_4$.

Based on the observation that the μ-methoxo dinuclear complex[7, 8] is usually unstable in solution and probably dissociates into mononuclear entities, which in the solid state again tend to assemble into the well-organized μ-methoxo dinuclear structure, we initially focus our efforts on crystallization conditions which could promote the condensation of two mononuclear entities to form the dinuclear complex. The synthetic methods (as shown in Scheme 2) of the mononuclear entities are the same that those used in the case of ligand H_2**L**', where successful generation of the desired dinuclear μ-methoxo complex was observed.[6] However, in the current case with H_2**L** ligand, only single crystals of **2** were obtained by slow diffusion of pentane into a solution of CH_2Cl_2. Combinations of all solvents and non-solvents listed below (Table 1) have been tested on different proportions using slow liquid or vapour diffusion, but all failed to obtain a crystal of the desired dinuclear complex.

Table 1 Solvents and non-solvents tested for the crystallization of dinuclear μ-methoxo complex with ligand H_2**L**.

Solvents	Non solvents
$CHCl_3$	MeOH
CH_2Cl_2	EtOH
$ClCH_2CH_2Cl$	^{i}PrOH
DMF	Diethyl ether
THF	H_2O

The second attempt to synthesized the desired dinuclear complex was based on the assumption that there were little differences between the structures of the complex $Mn^{III}_2(\mu\text{-}OMe)_2(H\mathbf{L}')_4$ and the desired structure $Mn^{III}_2(\mu\text{-}OMe)_2(H\mathbf{L})_4$. Therefore, some tests have been set up to force the crystalline growth of $Mn^{III}_2(\mu\text{-}OMe)_2(H\mathbf{L})_4$ instead of the complex **2**. To do this, diverse proportions of powder from the reaction between two equivalents of H**L**' with manganese(III) acetate dihydrate were added to a chloroform solution of the powder obtained from the same reactions with H**L**, followed by slow diffusion of methanol into this mixed solution. However, unfortunately the nucleation of the complex $Mn^{III}_2(\mu\text{-}OMe)_2(H\mathbf{L}')_4$ did not seem to encourage the growth of $Mn^{III}_2(\mu\text{-}OMe)_2(H\mathbf{L})_4$.

1.3 Synthesis and characterization of iron complexes

Following a systematic procedure and taking in consideration some shared characteristics of iron and manganese, we synthesized in parallel, with the same ligand four iron complexes using commercial crystalline $FeCl_3$ and $Fe(acac)_3$ as metal sources.

The aim was to examine the possibility to obtain well-defined molecular complexes of Fe^{III} bearing $H_2\mathbf{L}$ ligand and to compare their respective reactivity towards the same ligand.

Synthesis of mononuclear complexes

The synthesis and crystallization methods of all the iron complexes are shown in Scheme 3. The direct reaction of three equivalents of the ligand $H_2\mathbf{L}$ with one equivalent of $FeCl_3$ in methanol in the absence of base affords a green powder. Recrystallization of the latter solid in $CHCl_3$ led to the formation of red rectangular crystals of the mononuclear Fe^{III} complex **3**·2$CHCl_3$ in a good yield (see scheme 3). The reaction of ligand $H_2\mathbf{L}$ (2 equivalents) with iron chloride (1 equivalent) in DMF as solvent affords a dark blue solution. A slow diffusion of MeOH in a sealed glass tube under a N_2 atmosphere led to a colour change from dark blue to yellow after one day and yellow single crystals of **4** (suitable for X-ray studies) were found

to be formed at the bottom of tube after 3 or 4 days. Similar to our previous observation with ligand H_2**L**',[7] it was assumed that this dark solution consists of a mononuclear Fe^{III} complex with two chelating H**L**$^-$ ligands, DMF and Cl^- in the coordination sphere of the iron (the analogue of III in scheme 1). Unfortunately, we did not succeed to crystallize this dark blue complex.

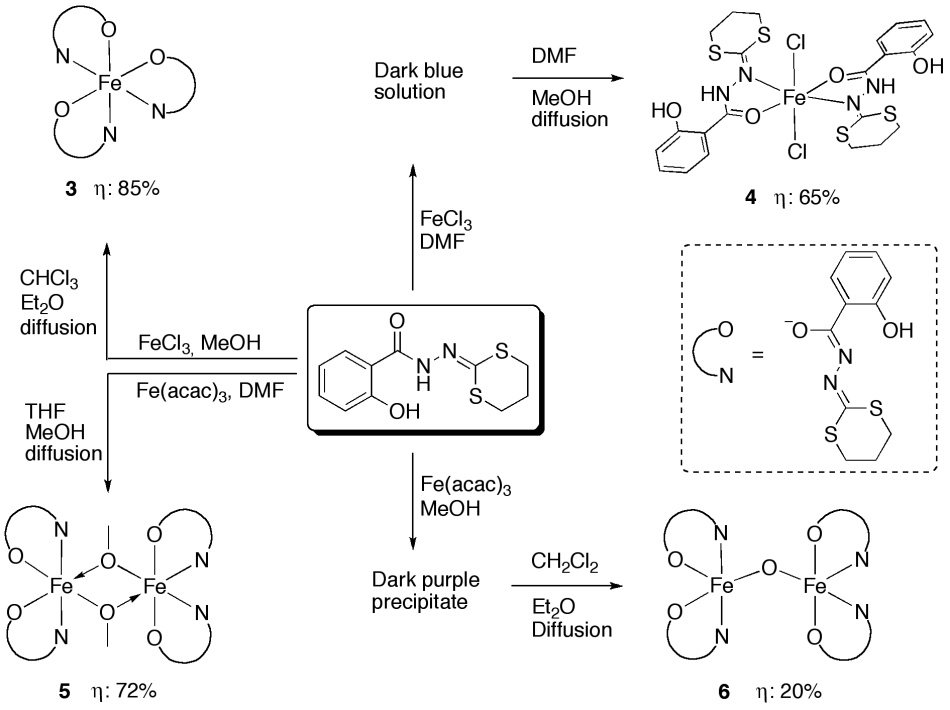

Scheme 3: Synthetic methods for the iron complexes **3**, **4**, **5** and **6**

Synthesis of dinuclear species

By using our previously reported procedure,[7] complex **5** (see scheme 3) was synthesized by the reaction of the ligand H_2**L** with $Fe(acac)_3$ in DMF, followed by slow diffusion of methanol into a THF solution of the product. Similarly, it was hypothesized that the formation of complex **5** occurs via a non isolated mononuclear specie $[Fe^{III}(\mathbf{L})_2\mathbf{L}_1\mathbf{L}_2]$, which possess two deprotonated 2-salicyloylhydrazono-1,3-dithiane ligands and two additional coordination moieties ($\mathbf{L}_1$ and $\mathbf{L}_2$). $\mathbf{L}_1$ and $\mathbf{L}_2$ are probably remaining acetylacetonate ligand from the metal precursor or the methoxy group and a molecule of solvent coordinated.[7] The reaction of 2 equivalents of the ligand with $Fe(acac)_3$ in methanol generated black precipitates, which can

be crystallized in the mixture of CH_2Cl_2/Et_2O to yield dark green crystals of **6** in a relatively low yield. Dinuclear iron complexes with oxo bridges have been extensively studied mainly due to their special physical properties and their relevance as intermediates in catalytic reactions, and a large number of μ-oxo-bridged diiron complexes have been structurally characterized. Similar structures to complex **6**, reported in literature, mainly bear ligands of salen,[17-21] salicylaldiminato[22] and N,N'-*o*-phenylenebis(oxamate)[23] type. In many cases, combining a less bulky ligand with Fe^{III} precursors and an excess of base in methanol as solvent, was reported to yield μ-oxo bridged diiron^{III} complexes where the O bridge is probably originated by the methanol solvent.[17-19,21,23,24] The oxidation of Fe^{II} to Fe^{III} by air dioxygen is an alternative method to synthesize μ-oxo bridged diiron^{III} complexes.[17,20,22,23] In addition to methanol, water also can act as source of the bridging O.[21,25-27] Based on the above analysis of the possible oxygen bridge origins reported in the literature, we assumed that the O bridge in complex **6** could probably come from some residual water present in the methanol solvent employed in the reaction.

Crystal structures description

The structures of the four iron complexes (**3**–**6**) have been completely characterized by single-crystal X-ray diffraction.

Complex **3**·2$CHCl_3$ crystallizes in the triclinic space group *P*-1. The Fe^{III} centre has a $[N_3O_3]$ coordination sphere with pseudo-octahedral geometry. The ligands H**L**$^-$ are coordinated to the iron as bidentate chelating agents via the azomethine nitrogen atoms (N2, N4, N6) and the iminolate oxygen atoms (O2, O4, O6) of the aroyl hydrazones in a propeller configuration fashion. The arrangement of the 2-salicyloylhydrazono-1,3-dithiane ligands in this iron complex is similar to the analogous manganese complex **2**. The Fe–N distances [2.123(3), 2.146(3) and 2.243(3) Å] and Fe–O distances [1.984(2), 1.957(2) and 1.952(2) Å] are similar to those found in the previously reported Fe^{III} complex supported by 2-salicyloylhydrazono-1,3-dithiolane ligand.[7] As shown in Fig. 3, the hydrogen bonding is

donated from phenol O–H to a neighbouring nitrogen atom of the hydrazine group in each ligand. Several Fe^{III} complexes containing an $[N_3O_3]$ coordination sphere and similar geometrical features have been reported in the literature with *o*-iminobenzosemiquinonato,[28] *o*-aminophenol[29] and 8-quinolinato.[30]

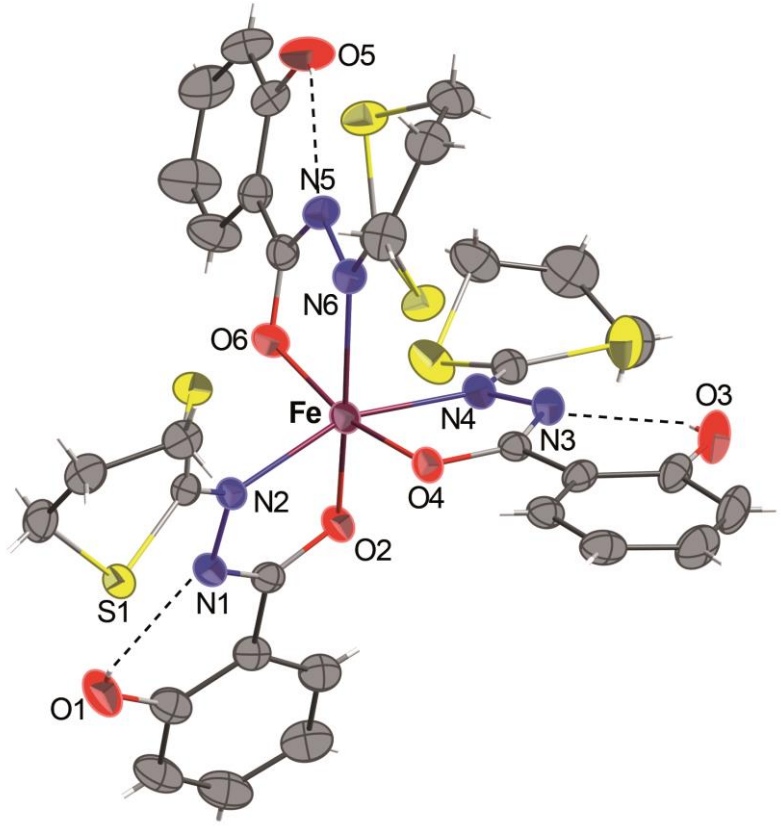

Figure 3: ORTEP view of the complex **3**·2$CHCl_3$ with partial labelling scheme. The ellipsoids enclose 50% of the electronic density. The solvent molecules ($CHCl_3$) were omitted for clarity. Selected distances (Å) and angles (°): Fe–N2 2.123(3), Fe–N4 2.146(3), Fe–N6 2.243(3), Fe–O2 1.984(2), Fe–O4 1.957(2), Fe–O6 1.952(2); O6–Fe–O4 165.7(1), N2–Fe–N4 158.5(2), O2–Fe–N6 165.3(1), O2–Fe–N2 76.7(1), O6–Fe–N6 74.7(1), O4–Fe–N4 76.6(1).

Complex **4**·2CH_3OH crystallizes in the monoclinic space group $P\ 2_1/c$. As shown in figure 4, the compound consists of a mononuclear complex of Fe^{II}. The presence of hydrogen atoms on the N1 and N1' nitrogen atoms (clearly visible by Fourier differences and by the special conformation of the hydroxyl groups) indicate that both bidentate ligands are neutral.

Considering both chloride atoms (-I) to complete the octahedral geometry, we consider that the iron cation, exhibit a +II oxidation state. In **4**, the two bidendate H_2**L** ligands are in a *trans* configuration, and the overall structure appears to be very similar to its analogues bearing benzoic hydrazide derivative ligands reported in chapter 2. In addition, the intramolecular H-bonds in each ligand (dashed lines in figure 4) were also detected and they are probably responsible for the quasi-planar orientation of the ligands. Complex **4** constitutes then a new example of iron(II) compound obtained via spontaneous reduction, which was already observed with the ligand H_2**L**' and related ligands as described in chapter 2.

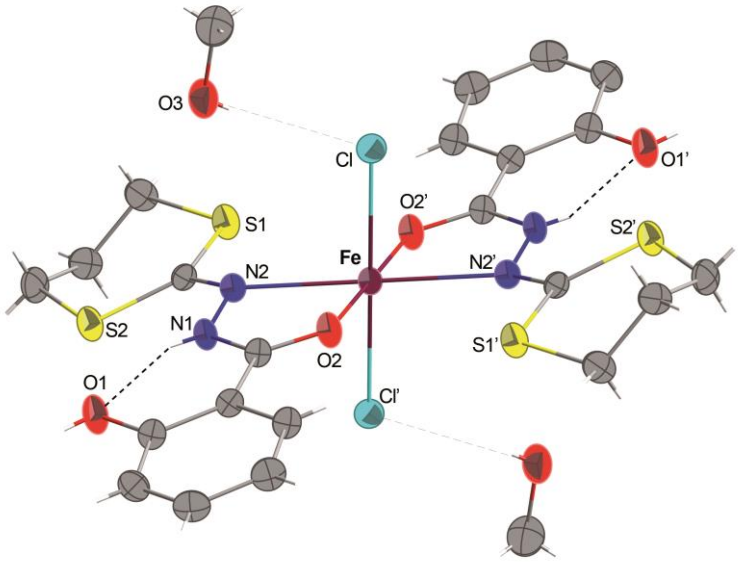

Figure 4: ORTEP view of the complex **4**·2CH_3OH with partial labelling scheme. The ellipsoids enclose 50% of the electronic density. Selected distances (Å) and angles (°): Fe–N2 2.292(2), Fe–O2 2.134(1), Fe–Cl 2.3995(5); O2–Fe–N2 73.15(4), Cl–Fe–Cl' 180, O2–Fe–O2' 180. Symmetry operator for equivalent positions: ' = –x+ 2, –y, –z + 2.

Single crystals of complex **5**·1/2CH_3OH suitable for X-ray diffraction analysis were obtained by slow diffusion of methanol into a THF solution of the solid. Complex **5**·1/2CH_3OH crystallize in the orthorhombic space group *A b a* 2. Exhibiting very similar structural features as its Fe^{III}, [7] Cr^{III}, [10] and Mn^{III} [6] analogues, complexes **5** crystallizes as a

neutral asymmetric dinuclear Fe^{III} complex in which each iron metal centre is chelated by two H**L**$^{-}$ bidentate ligands and connected to each other *via* two μ-OMe groups (figure 5). The two metal ions Fe1 and Fe2 are in slightly distorted octahedral geometries but with different environments. Around Fe1, the oxygen atoms O2–O2**'** are in a *trans* configuration and N2–N2**'** in a *cis* configuration, while around Fe2, the oxygen atoms O4–O4**'** are *cis* to one another and N4–N4**'** in a *trans* configuration. As previously pointed out, this situation is most likely related to two intramolecular CH–π interactions arising from one 1,3-dithiane CH moiety and the centroid of the neighbouring phenol group, as indicated in figure 5. Finally, considering our systematic research on such dinuclear μ-OMe metal complexes, a complete magnetic study of **5** was carried out, and the results are described below.

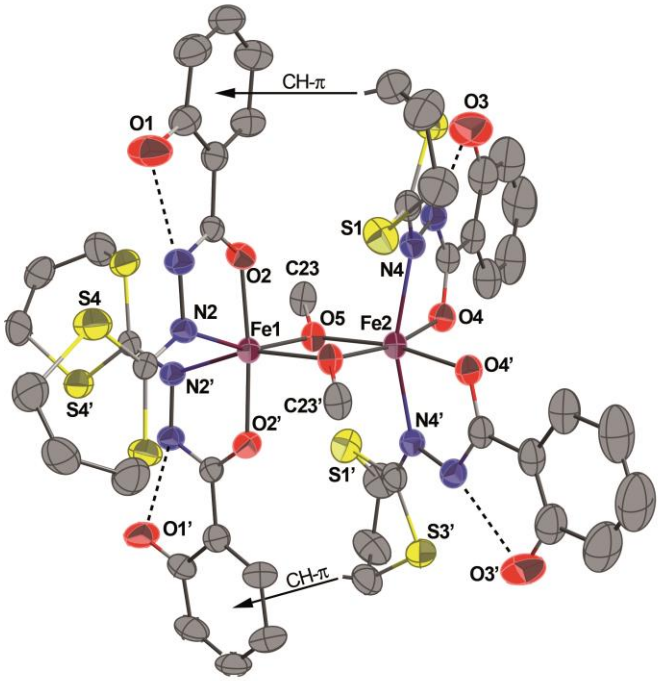

Figure 5: ORTEP view of the complex **5**·1/2CH_3OH with partial labelling scheme. H atoms and solvent molecules (CH_3OH) are omitted for clarity. The ellipsoids enclose 50% of the electronic density. The dashed lines show representative intramolecular hydrogen bonds and the arrows represent the CH–π interactions. Selected distances (Å) and angles (°): Fe1–N2 2.196(3), Fe1–O2 1.972(2), Fe1–O5 1.975(2), Fe2–O5 1.994(2), Fe2–O4 1.977(2), Fe2–N4 2.154(3); O2–Fe1–O2**'** 174.1(2), N2–Fe1–N2**'** 95.2(2), N4–Fe2–N4**'** 160.3(2), O4–Fe2–O4**'** 98.7(2), Fe1–O5–Fe2 102.44(9). Symmetry operator for equivalent positions: **'** = –x+ 1, –y, z.

Complex **6**·3CH_2Cl_2 crystallizes in the monoclinic space group *P* $2_1/c$. An ORTEP view is depicted in figure 6. The molecule contains a Fe–O–Fe core and the coordination geometry around each iron atom is described as distorted square pyramidal with the two hydrazine nitrogen atoms and the two carboxyl oxygen atoms of each ligand constituting the corners of the square plane and the μ-oxo oxygen atom occupying the axial position. No residual peak is detected in the Fourier difference map indicating unambiguously the absence of the hydrogen atom on the oxo oxygen atom. Also, the FeN_2O_2 coordination plane in each iron^{III} is oriented *trans* to the other relative to the oxo bridge, having a Fe–O–Fe bond angle of 167.1(2)°, which is in the normal range (135 ~ 180°) found in other closely related μ-oxo mono-bridged diiron complexes, where this angle is usually dominated by the steric parameters of the chelated ligands. [19,32-35] The Fe···Fe distance in **6** (3.475 Å) is in the same range as those already reported for complexes with Fe–O–Fe cores (3.39–3.56 Å).[17,24,33,36] The Fe–(μ-O) bond lengths observed [Fe1–O9 1.747(3), Fe2–O9 1.750(3) Å] are in the range found for other (μ-oxo)diiron^{III} complexes (1.75–1.80 Å)[17,20,33,37-39] but significantly shorter than that found in Fe–(μ-CH_3O) of complex **5** (1.975(2) Å). Similar to complex **5**, each iron atom is bound to two bidendate ligands in their basic forms and the geometry of the hydrazine chelating is comparable to those observed in either the mononuclear **3** or dinuclear μ-methoxo complex **5**. Both the Fe–$O_{iminolate}$ and Fe–$N_{azomethine}$ bond distances are shorter than their counterparts in complex **5**, probably due to the less steric pressures at the metal centres in complex **6** than those in **5**. No specific intramolecular CH–π interaction has been detected and only classical H-bonds occur between the OH groups of the phenol rings and the hydrazine groups.

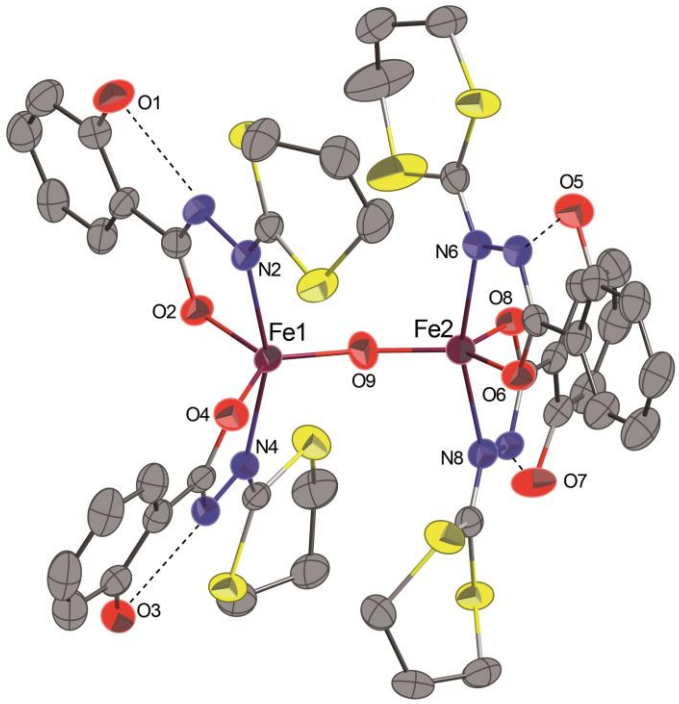

Figure 6: ORTEP view of the complex **6**·3CH_2Cl_2 with partial labelling scheme. H atoms and solvent molecules (CH_2Cl_2) were omitted for clarity. The ellipsoids enclose 50% of the electronic density. The dashed lines show representative intramolecular hydrogen bonds and the arrows represent the CH–π interactions. Selected distances (Å) and angles (°): Fe1–N2 2.135(3), Fe1–O2 1.948(3), Fe1–N4 2.131(3), Fe1–O4 1.946(3), Fe1–O9 1.747(3), Fe2–O9 1.750(3), Fe2–N6 2.126(3), Fe2–O6 1.960(3), Fe2–N8 2.120(3), Fe2–O8 1.954(3); N4–Fe1–N2 157.6(2), O4–Fe1–O2 119.2(1), Fe1–O9–Fe2 167.1(2), N8–Fe2–N6 161.0(2), O8–Fe2–O6 119.8(2).

Table 2: Crystal data and X-ray structure refinement parameters at 173 K for complexes **(1), (2)** and **(3)**

Compound reference	**1**	**2**•CH_2Cl_2	**3**•2($CHCl_3$)
Chemical formula	$C_{27}H_{29}MnN_4O_6S_4$	$C_{33}H_{33}MnN_6O_6S_6$•CH_2Cl_2	$C_{33}H_{33}FeN_6O_6S_6$•2($CHCl_3$)
Formula Mass	688.72	941.88	1096.60
Crystal system	Monoclinic	Triclinic	Triclinic
a/ [Å]	11.712(5)	10.429(2)	11.227(3)
b/ [Å]	12.670(5)	11.778(2)	13.922(7)
c/ [Å]	20.965(5)	17.263(3)	15.914(6)
α/ [°]	90.00	105.39(5)	69.021(2)
β/ [°]	98.49(1)	91.37(5)	89.488(2)
γ/ [°]	90.00	90.35(5)	77.920(2)
V [Å^3]	3076.9(19)	2043.6(6)	2265.1(15)
Space group	*P*21/*c*	*P*-1	*P*-1
Z	4	2	2
μ(Mo-K$_\alpha$) [mm^{-1}]	0.748	0.812	1.014
F(*000*)	1424	968	1118
Crystal size [mm]	0.13×0.11×0.10	0.20×0.14×0.12	0.15×0.12×0.10
θ_{min}–θ_{max}	1.76–30.03	1.22–30.04	1.69–27.51
Data set [*h*, *k*, *l*]	-15/16, -15/17, -23/29	-14/14, -16/16, -21/24	-14/14, -18/16, -20/20
Total, unique data, R_{int}	23981, 8992, 0.0503	24068, 11916, 0.0375	19566, 10304, 0.0420
Observed data [$I > 2\sigma(I)$]	5256	8810	7683
No. Reflections, No. Parameters	8992, 379	11916, 490	10304, 541
Final R_1 values ($I > 2\sigma(I)$)	0.0535	0.0847	0.0545
Final $wR(F^2)$ values ($I > 2\sigma(I)$)	0.1308	0.1906	0.1156
Final R_2 values (all data)	0.1079	0.1139	0.0817
Final $wR(F^2)$ values (all data)	0.1543	0.2064	0.1336
Goodness of fit on F^2	1.007	1.068	1.048
Max. and av. Shift/error	0.000/0.000	0.001/0.000	0.001/0.001
Min, Max residual density [eÅ^{-3}]	-0.711/0.603	-0.692/2.169	-1.611/1.787

Table 3: Crystal data and X-ray structure refinement parameters at 173 K for complexes (**4**),(**5**) and (**6**)

Compound reference	**4**•2(CH_{40})	**5**•1/2(CH_3O)	**6**•3(CH_2Cl_2)
Chemical formula	$C_{22}H_{24}Cl_2FeN_4O_4S_4$•2($CH_{40}$)	$C_{46}H_{50}Fe_2N_8O_{10}S_8$•1/2($CH_3O$)	$C_{44}H_{44}Fe_2N_8O_9S_8$•3($CH_2Cl_2$)
Formula Mass	727.53	1258.64	1451.83
Crystal system	Monoclinic	Orthorhombic	Monoclinic
a/ [Å]	10.394(4)	23.038(2)	12.8070(2)
b/ [Å]	9.405(4)	10.461(6)	32.3360(8)
c/ [Å]	17.332(3)	22.989(6)	15.2010(3)
α/ [°]	90.00	90.00	90.00
β/ [°]	114.676(19)	90.00	105.1750(11)
γ/ [°]	90.00	90.00	90.00
V [Å^3]	1539.58(95)	5540(4)	6075.6(2)
Space group	*P*21/*c*	*Aba*2	*P*21/*c*
Z	2	4	4
μ(Mo-K_α) [mm^{-1}]	0.980	0.888	1.075
F(*000*)	752	2602	2968
Crystal size [mm]	0.10×0.10×0.10	0.10×0.10×0.10	0.14×0.12×0.10
θ_{min}–θ_{max}	2.16–30.01	1.77–30.03	1.26–27.48
Data set [*h*, *k*, *l*]	-12/14, -13/11, -24/24	-32/31, -14/14, -29/32	-16/11, -38/41, -19/19
Total, unique data, R_{int}	14463, 4496, 0.0773	25825, 7431, 0.0592	37050, 13388, 0.0656
Observed data [$I > 2\sigma(I)$]	3713	5424	8532
No. Reflections, No. Parameters	4496, 191	7431, 350	13388, 721
Final R_1 values ($I > 2\sigma(I)$)	0.0395	0.0451	0.0576
Final $wR(F^2)$ values ($I > 2\sigma(I)$)	0.1004	0.1106	0.1645
Final R_2 values (all data)	0.0504	0.0736	0.1034
Final $wR(F^2)$ values (all data)	0.1070	0.1250	0.2001
Goodness of fit on F^2	1.070	1.007	1.082
Max. and av. Shift/error	0.002/0.000	0.001/0.000	0.003/0.000
Min, Max residual density [eÅ^{-3}]	-0.916/0.573	-0.532/0.588	-2.018/1.971

1.4 Magnetic measurements of the *μ*-methoxo dinuclear iron complex 5

The magnetic property of complex **5** was investigated in the solid state in the 1.8–300 K temperature range and an applied field of 5 kOe. The χT value at room temperature (6.62 emu·K·mol^{-1}) is smaller than the expected value for two high spin Fe^{III} (8.75 emu·K·mol^{-1} assuming g = 2). Upon cooling, the χT product increases to a maximum then decreases continuously to almost 0 (0.027 emu·K·mol^{-1} at 1.8 K). This indicates the occurrence of a relatively strong antiferromagnetic intramolecular interaction between the two Fe^{III} ions. There is a small contribution of an impurity that gives the sharp rise at the lowest end of temperatures. The data were fit using the following spin Hamiltonian where all parameters have their usual meaning and the spin operator **S** is defined as $\mathbf{S} = \mathbf{S}_{Fe1} + \mathbf{S}_{Fe2}$:

$$H = -J\, \mathbf{S}_{Fe1}\, \mathbf{S}_{Fe2} + g\, \beta\, H\, \mathbf{S}$$

To reproduce the data satisfactorily over the whole temperature region, including the small increase at the lowest temperatures, we consider a certain amount (ρ) of paramagnetic impurity ($\mathbf{S}_{impure}$ = 5/2). The fit leads the following values: J = -21.1(1) cm^{-1}, g = 2.06(1) and ρ = 1.38(5) % with a good agreement factor R = 3.15×10^{-5} where $R = (\chi_{exp}-\chi_{calc})^2 / \chi_{exp}^2$.

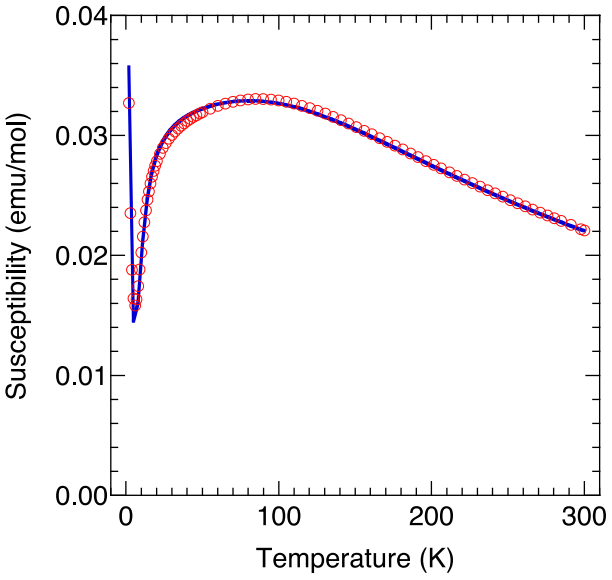

Figure 7: χ (circles) as a function of temperature for **5** and dark line corresponds to the fit of the χ = f(T) curve (see text).

1.5 Conclusions

In this work, we have demonstrated that the reactions of 2-salicyloylhydrazono-1,3-dithiane (H_2**L**) with different iron and manganese metal precursors under various conditions resulted in a series of new mononuclear or dinuclear complexes in good yields. All new complexes have been fully characterized by single crystal X-ray diffraction. The asymmetric dinuclear $Fe^{III}_2(\mu\text{-OMe})_2(H\mathbf{L})_4$ complex shows strong antiferromagnetic intramolecular coupling, which agrees with the previously proposed theoretical model for the related Mn^{III} complex.[6]

Following the previous findings that dinuclear μ-methoxo $Mn^{III}_2(\mu\text{-OMe})_2(H\mathbf{L}')_4$ presents one of the strongest intramolecular ferromagnetic interactions, our aim was the modulation of the magnetic interaction by small modifications of the peripheral ligand justifying the use of the 2-salicyloylhydrazono-1,3-dithiane ligand (H_2**L**). The similarity between the structures of H_2**L** and H_2**L**' would allow H_2**L** to be a suitable ligand to stabilize a dinuclear μ-methoxo Mn^{III} complex, which is expected to exhibit also a very strong intramolecular ferromagnetic interaction. However, we failed in the synthesis of such desired complex although many attempts have been made. We are a bit puzzled as we have successfully synthesized and characterized the dinuclear μ-methoxo Fe^{III}, Mn^{III} and Cr^{III} complexes chelated by $H\mathbf{L}'^{-}$ and in addition, dinuclear Fe^{III} and Cr^{III} complexes supported by $H\mathbf{L}^{-}$ were also successfully produced. Attempts are currently made in our laboratory, applying different synthetic methods and with the support of theoretical calculations, to achieve a better understanding of the different reactivity of the manganese when compared with other metals.

1.6 Experimental Section

General procedures: All manipulations were performed under aerobic conditions, using reagents and solvents as received. IR spectra were recorded in the region 4000-400 cm^{-1} on a Nicolet 6700 FT-IR spectrometer (ATR mode, diamond crystal). Elemental analysis was performed by the "Service de microanalyses", Université de Strasbourg. The ligand 2-salicyloylhydrazono-1,3-dithiane was prepared according to the reported procedure.[10]

Synthesis of $Mn^{III}(acac)(HL)_2$ (1). To a solution of 2-salicyloylhydrazono-1,3-dithiane (0.20 g, 0.74 mmol) in THF (20 mL) was added a solution of manganese acetylacetonate (0.13 g, 0.36 mmol) under stirring. The dark solution was further stirred at room temperature for 24 h, then the solvent was removed by vacuum and the resulting solid was washed with methanol and dried (yield: 0.17 g, 67%). Dark red single crystals suitable for X-ray analysis were obtained by slow diffusion of methanol in a chloroform solution of the complex. IR (pure, orbit diamond, cm^{-1}): 2361, 1517. Anal. Calcd. for $C_{27}H_{29}MnN_4O_6S_4$: C, 47.08; H, 4.24; N, 8.13. Found: C, 46.78; H, 4.17; N 7.79.

Synthesis of $Mn^{III}(HL)_3 \cdot CH_2Cl_2$ (2). To a solution of manganese acetate dihydrate (0.10 g, 0.36 mmol) in methanol (20 mL) was added 2-salicyloylhydrazono-1,3-dithiane (0.29 g, 1.08 mmol). The dark solution was further stirred at room temperature for 24 h before the solvent was removed under vacuum to afford a yellow solid (yield: 0.10 g, 31%). Red rectangular crystals suitable for X-ray analysis were obtained by slow diffusion of methanol through a CH_2Cl_2 solution of the complex. IR (pure, orbit diamond, cm^{-1}): 1588, 1515. Anal. Calcd. for $C_{33}H_{33}MnN_6O_6S_6 \cdot CH_2Cl_2$: C, 43.35; H, 3.75; N, 8.92. Found: C, 43.06; H, 3.68; N, 8.81.

Synthesis of $Fe^{III}(HL)_3 \cdot 2CHCl_3$ (3). $FeCl_3$ (0.013 g, 0.08 mmol) was added to the solution of H_2**L** (0.067 g, 0.25 mmol) dissolved in methanol (20 ml), and then the mixture was further stirred at room temperature for 24 h. After reaction the solvent was removed under vacuum to

obtain a green powder. Red rectangular crystals of **3**·2$CHCl_3$ were obtained by slow diffusion of diethyl ether into the $CHCl_3$ solution of the complex. (Yield: 0.075 g, 85%). IR (pure, orbit diamond, cm^{-1}): 1518, 1357, 1251, 754. Anal. Calc. for $C_{33}H_{33}FeN_6O_6S_6$·2$CHCl_3$: C, 38.33; H, 3.22; N, 7.66. Found: C, 38.51; H, 3.33; N 7.92.

Synthesis of $Fe^{II}(H_2L)_2Cl_2$·2CH_3OH (4). A yellow solution of $FeCl_3$ (0.019 g, 0.12 mmol) in DMF (1 mL) was added to a well-stirred colourless solution of the ligand (0.064 g, 0.24 mmol) in DMF (2 mL). The colour changes immediately from yellow to dark blue. The homogeneous mixture was left under stirring overnight at room temperature. A yellow crystalline powder of the complex was obtained after a slow diffusion (3 to 4 days) of MeOH into the crude reaction mixture in a sealed glass tube (Yield: 0.052 g, 65%). Anal. Calc. for $C_{22}H_{24}Cl_2FeN_4O_4S_4$·2$CH_3OH$: C, 39.62; H, 4.43; N, 7.70. Found: C, 39.71; H, 4,04; N 7.67.

Synthesis of $Fe^{III}_2(\mu$-OMe$)_2(HL)_4$·1/2CH_3OH (5). A solution of iron(III) acetylacetonate (0.035 g, 0.1 mmol) in DMF (2 mL) was added to a well-stirred solution of H_2**L** (0.054 g, 0.2 mmol) in DMF (2 mL), and the resulting mixture colour changed quickly from colourless to dark brown. The mixture was further stirred at room temperature for 24 h. DMF was removed under vacuum and the obtained product of this step (typically the mononuclear species) was dissolved in THF to yield a dark solution, into which slow diffusion of methanol (during 6 to 12h) affords well-formed orange crystals of **5**·1/2CH_3OH in good yield (0.045 g, 72 %). IR (pure, orbit diamond, cm^{-1}): 3513, 2814, 2921, 1619, 1588, 1520, 1487, 1364, 1252. Anal. Calc. for $C_{46}H_{50}Fe_2N_8O_{10}S_8$·1/2$CH_3OH$: C, 44.37; H, 4.12; N, 8.90. Found: C, 43.98; H, 3.94; N 8.71.

Synthesis of $Fe^{III}_2(\mu$-O$)(HL)_4$·3CH_2Cl_2 (6). A mixture of iron (III) acetylacetonate (0.035 g, 0.1 mmol) and H_2**L** (0.054 g, 0.2 mmol) in MeOH (20 mL) was stirred at room temperature in the dark and N_2 for 24 h. The black precipitate observed at the end of the reaction was filtered. The obtained black powder was washed with MeOH (2×5 mL) and dried under vacuum. Dark green crystals suitable for X-ray diffraction were obtained by slow diffusion of

diethyl ether into the CH_2Cl_2 solution of the black powder (yield: 0.015g, 20%). IR (pure, orbit diamond, cm^{-1}): 1482, 1359, 1303,1237, 979, 749. Anal. Calc. for $C_{44}H_{44}Fe_2N_8O_9S_8 \cdot 3CH_2Cl_2$: C, 38.88; H, 3.47; N, 7.72. Found: C, 38.69; H, 3.54; N, 7.49. After the initial synthesis above, we were unable to reproduce this reaction again for further characterization.

Magnetic measurements. Magnetic measurements were performed at the Institut de Physique et Chimie des matériaux de Strasbourg (UMR CNRS-ULP 7504) using a Quantum Design MPMS-XL SQUID magnetometer. The susceptibility measurement was performed in the 300-1.8 K temperature range and an applied field of 5 kOe. Isothermal field dependent magnetization measurement at room temperature confirms the absence of ferromagnetic impurities. Data were corrected for the sample holder and diamagnetism of the content estimated from Pascal constants.

Crystal structure determinations. Suitable crystals for the X-ray analyses of all compounds were obtained as described above. Single crystals of **1**–**6** were mounted on a Nonius Kappa-CCD area detector diffractometer (Mo Kα, λ = 0.71073 Å). The cell parameters were determined from reflections taken from one set of 10 frames (1.0° steps in phi angle), each at 20s exposure. The structures were solved using direct methods (*SHELXS97*) and refined against F^2 using the *SHELXL97* and *CRYSTALBUILDER* softwares.[41,42] The absorption was not corrected. All non-hydrogen atoms were refined anisotropically. Hydrogen atoms were generated according to stereochemistry and refined using a riding model in *SHELXL97*. Crystallographic data (excluding structure factors) have been deposited in the Cambridge Crystallographic Data Centre as Supplementary publication no. CCDC 844919 - 844924. Copies of the data can be obtained free of charge on application to CCDC, 12 Union Road, Cambridge CB2 1EZ, UK (fax: (+44)1223-336-033; e-mail: deposit@ccdc.cam.ac.uk)

1.7 References

1 O. Kahn, *Molecular Magnetism*, Wiley-VCH, New York, **1993**.

2 A. Cornia, A. C. Fabretti, L. Zobbi, A. Caneschi, D. Gatteschi, M. Mannini and R. Sessoli, in: R. Winpenny (Ed.), *Single-Molecule Magnets and Related Phenomena Structure and Bonding Book Series*, vol. 122, Springer, Berlin, Heidelberg, **2006**, p. 133.

3 R. Sessoli, *Mol. Cryst. Liq. Cryst.*, **1995**, 274, 145.

4 M. Ferbinteanu, H. Miyasaka, W. Wernsdorfer, K. Nakata, K. Sugiura, M. Yamashita, C. Coulon and R. Clérac, *J. Am. Chem. Soc.*, **2005**, 127, 3090–3099.

5 H. Hiraga, H. Miyasaka, K. Nakata, T. Kajiwara, S. Takaishi, Y. Oshima, H. Nojiri and M. Yamashita, *Inorg. Chem.*, **2007**, 46, 9661–9671.

6 C. Beghidja, G. Rogez, J. Kortus, M. Wesolek and R. Welter, *J. Am. Chem. Soc.*, **2006**, 128, 3140–3141.

7 N. Bouslimani, N. Clément, G. Rogez, P. Turek, M. Bernard, S. Dagorne, D. Martel, H. N. Cong and R. Welter, *Inorg. Chem.*, **2008**, 47, 7623–7630.

8 N. Bouslimani, N. Clément, G. Rogez, P. Turek, S. Choua, S. Dagorne and R. Welter, *Inorg. Chim. Acta*, **2010**, 363, 213–220.

9 C. Toussaint, C. Beghidja and R. Welter, *C. R. Chimie*, **2010**, 13, 343–352.

10 N. Clément, C. Toussaint, G. Rogez, C. Loose, J. Kortus, L. Brelot, S. Choua, S. Dagorne, P. Turek and R. Welter, *Dalton Trans.*, **2010**, 39, 4579–4585.

11 L. Bogani and W. Wernsdorfer, *Nature Mat.*, **2008**, 7, 179–186.

12 R. Welter, WO/**2009**/130562.

13 C. Beghidja, M. Wesolek and R. Welter, *Inorg. Chim. Acta*, **2005**, 358, 3881–3888.

14 M. Cheng, M. C. Chan, S. Peng, K. Cheung and C. Che, *J. Chem. Soc.*, *Dalton Trans.*, 1**997**, 3479–3482.

15 E. J. Larson and V. L. Pecoraro, *J. Am. Chem. Soc.*, **1991**, 113, 3810–3818.

17 R. Mayilmurugan, H. Stoeckli-Evans, E. Suresh and M. Palaniandavar, *Dalton Trans.*, **2009**, 5101–5114.

18 G. Ilyashenko, M. Motevalli and M. Watkinson, *Tetrahedron Asymm.*, **2006**, 17, 1625–1628.

19 J. Wu, S. Liu, T. D. Keene, A. Neels, V. Mereacre, A. K. Powell and S. Decurtins, *Inorg. Chem.*, 2008, **47**, 3452–3459.

20 C. J. Whiteoak, R. T. Martin de Rosales, A. J. P. White and G. J. P. Britovsek, *Inorg. Chem.*, **2010**, 49, 11106–11117.

21 K. Oyaizu, E. L. Dewi and E. Tsuchida, *Inorg. Chim. Acta*, **2001**, 321, 205–208.

22 J. M. Becker, J. Barker, G. J. Clarkson, R. van Gorkum, G. K. Johal, R. I. Walton and P. Scott, *Dalton Trans.*, **2010**, 39, 2309–2326.

23 E. Pardo, F. Lloret, R. Carrasco, M. C. Muñoz, T. Temporal-Sánchez and R. Ruiz-Garíc, *Inorg. Chim. Acta*, **2004**, 357, 2713–2720.

24 R. Shakya, D. R. Powell and R. P. Houser, *Eur. J. Inorg. Chem.*, **2009**, 5319–5327.

25 A. K. Boudalis, N. Lalioti, G. A. Spyroulias, C. P. Raptopoulou, A. Terzis, V. Tangoulis and S. P. Perlepes, *J. Chem. Soc., Dalton Trans.*, **2001**, 955–957.

26 A. K. Boudalis, C. P. Raptopoulou, A. Terzis and S. P. Perlepes, *Polyhedron*, **2004**, 23, 1271–1277.

27 A. Bacchi, I. Ivanovic-Burmazovic, G. Pelizzi and K. Andjelkovic, *Inorg. Chim. Acta*, **2001**, 313, 109–119.

28 H. Chun, C. N. Verani, P. Chaudhuri, E. Bothe, E. Bill, T. Weyhermüller and K. Wieghardt, *Inorg. Chem.*, **2001**, 40, 4157–4166.

29 S. Mukherjee, T. Weyhermüller, E. Bill, K. Wieghardt and P. Chaudhuri, *Inorg. Chem.*, **2005**, 44, 7099–7108.

30 B. Li, J. Zhang, X. Zhang, J. Tian and G. Huang, *Inorg. Chim. Acta*, **2011**, 366, 241–246.

31 N. Bouslimani, N. Clément, C. Toussaint, S. Hameury, P. Turek, S. Choua, S. Dagorne, D. Martel and R. Welter, *Eur. J. Inorg. Chem.*, **2009**, 3734–3741.

32 G. Ilyashenko, M. Motevalli and M. Watkinson, *Tetrahedron Asymm.*, **2006**, 17, 1625–1628.

33 D. M. Kurtz, Jr., *Chem. Rev.*, **1990**, 90, 585–606.

34 Q. Meng, L. Wang, Y. Liu and Y. Pang, *Acta Cryst.*, **2008**, E64, m63.

35 A. Ozarowski, B. R. McGarvey and J. E. Drake, *Inorg. Chem.*, **1995,** 34, 5558–5566.

36 G. L. Parrilha, C. Fernandes, A. J. Bortoluzzi, B. Szpoganicz, M. de S. Silva, C. T. Pich, H. Terenzi and A. Horn, Jr., *Inorg. Chem. Commun.*, **2008**, 11, 643–647.

37 T. Kojima, R. A. Leising, S. Yan and L. Que, Jr., *J. Am. Chem. Soc.*, **1993**, 115, 11328–11335.

38 R. M. Buchanan, S. Chen, J. F. Richardson, M. Bressan, L. Forti, A. Morvillo and R. H. Fish, *Inorg. Chem.*, **1994**, 33, 3208–3209.

39 J. Xu, J. Astner, O. Walter, F. W. Heinemann, S. Schindler, M. Merkel and B. Krebs, *Eur. J. Inorg. Chem.*, **2006**, 1601–1610.

40 B. V. Nonius, *Kappa CCD Operation Manual*, Delft, The Netherlands, **1997**.

41 G. M. Sheldrick, *SHELXL97: Program for the Refinement of Crystal Structures*; University of Göttingen, Göttingen, Germany, **1997**.

42 R. Welter, *Acta Cryst.*, **2006**, A62, s252.

Chapter 5:

Synthesis, Crystal Structures and Use in Ethylene Oligomerization Catalysis of Novel Mono- and Dinuclear Nickel Complexes Supported by (E)-*N'*-(1-(thiophen-2-yl)ethylidene)benzohydrazide Ligand.

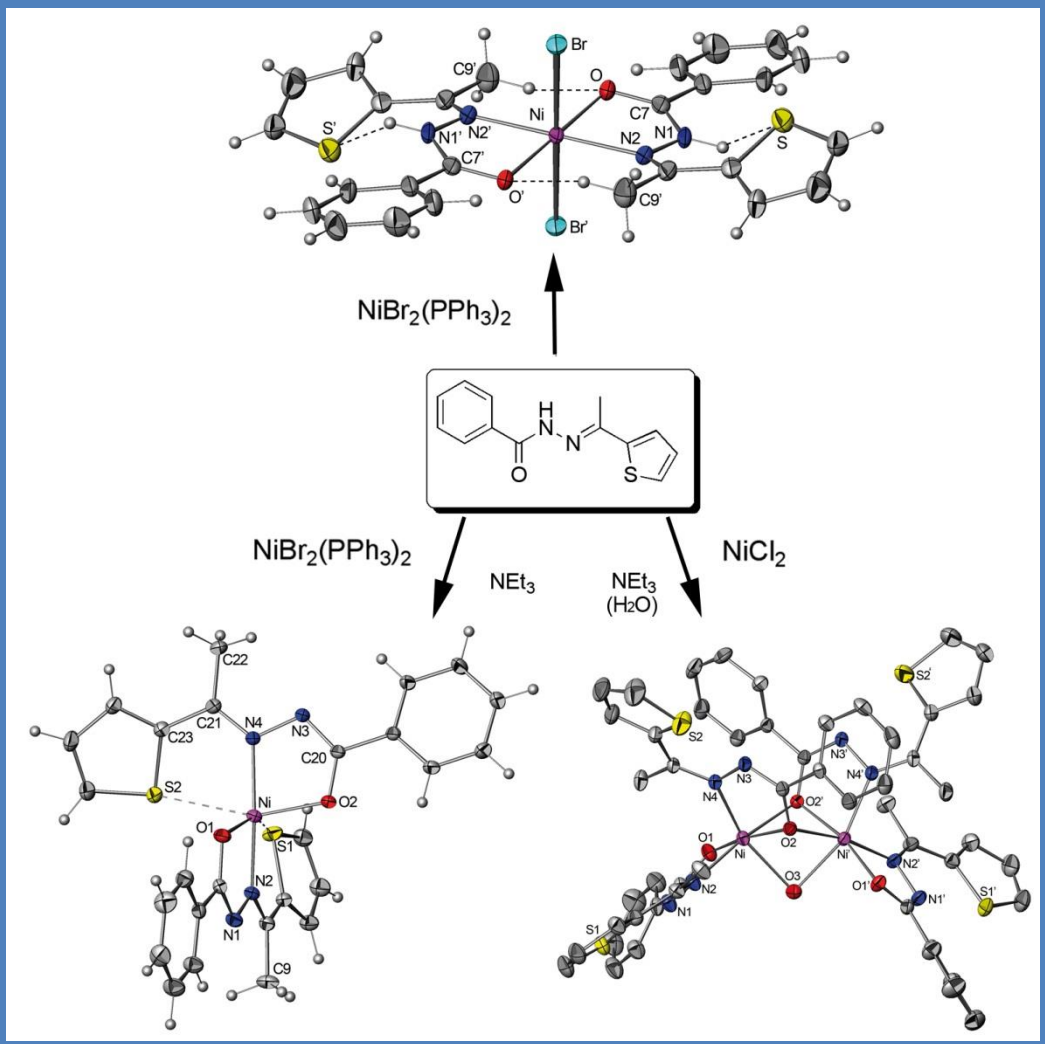

Chapter 5:

Synthesis, Crystal Structures and Use in Ethylene Oligomerization Catalysis of Novel Mono- and Dinuclear Nickel Complexes Supported by (E)-*N'*-(1-(thiophen-2-yl)ethylidene)benzohydrazide Ligand.

Synthesis, Crystal Structures and Use in Ethylene Oligomerization Catalysis of Novel Mono- and Dinuclear Nickel Complexes Supported by (E)-*N'*-(1-(thiophen-2-yl)ethylidene)benzohydrazide Ligand.

ABSTRACT: The coordination chemistry of Ni^{II} supported by (E)-*N'*-(1-(thiophen-2-yl) ethylidene)-benzoylhydrazone ligand (**HL**) is reported and discussed. The crystal structure of ligand **HL** has been determined as well as those of three new Ni^{II} complexes ($Ni(HL)_2Br_2$, NiL_2 and μ-aquo-Ni_2L_4). The pseudo-octahedral bis(chelate) Ni(II) complex **2** (NiL_2), in which unexpected and singular Ni···S interaction is observed, was evaluated as catalyst for the oligomerization of ethylene and found to provide ethylene dimers and trimers as primary products with a turnover frequency (TOF) of 312 00 mol of C_2H_4 per mol. of Ni and per hour.

Keywords: Coordination Chemistry, Nickel Complexes, Crystal Structure, Ethylene Oligomerization Catalysis.

1.1 Introduction

We earlier reported interesting magnetic properties of transition metal complexes supported by 2-salicyloylhydrazono-1,3-dithiolane (**H_2L^***) and its derivatives [1-7]. For instance, the dinuclear complex $Mn_2(\mathbf{HL}^*)_4(\mu\text{-}OCH_3)_2$ was found to exhibit the largest *J* value (J = +19.7 cm^{-1}) reported so far for a Mn^{III}-Mn^{III} ferromagnetic interaction [2]. On this basis, we have been working on slight modifications of the organic peripheral backbone as well as on using other metal centres, such as chromium [5], iron [3,7] and cobalt [6].

When exploring the iron chemistry with such aroyl hydrazone derivative ligands, we also observed an unusual spontaneous reduction from Fe^{III} to Fe^{II} of the mononuclear complexes [3]. This possible photo-induced redox reaction was subsequently fully investigated by electrochemistry, EPR studies, magnetic measurements, as well as solid-state molecular structure determinations. Such a phenomenon opens up new research opportunities, as recently pointed out by Wernsdorfer *et al* [8] and demonstrated by our patent [9].

With the purpose of acquiring more insight into the structural factors controlling and influencing the formation and stabilization of dinuclear complexes [2,7] in the crystalline state (with possible impact on their magnetic behaviour) and also due the spontaneous reduction of Fe^{III} to Fe^{II} observed in iron mononuclear species, the original ligand was modified at specific positions (see scheme 1). We have also become interested in studying the coordination chemistry of this type of aroyl hydrazone ligands with other transition metals, along with their possible applications as catalysts. In the present article, we report the synthesis and structural characterization of novel Ni^{II} complexes supported by the (E)-*N'*-(1-(thiophen-2-yl)ethylidene)-benzoyl-hydrazone ligand (H**L** Scheme 1) and their subsequent use in ethylene oligomerization catalysis.

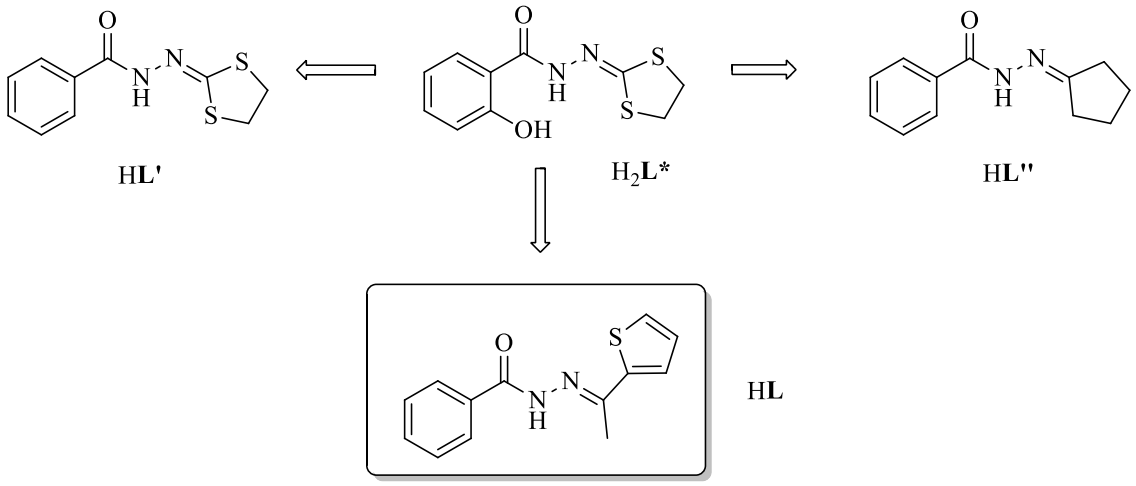

Scheme 1: Structural relationship between H**L** ((E)-*N'*-(1-(thiophen-2-yl)ethylidene)-benzoyl-hydrazone) and H_2**L*** (2-salicyloylhydrazono-1,3-dithiolane). The ligands H**L**', and H**L**'' have been previously described [4,7].

Results and discussion

1.2 Synthesis and structural characterization of (E)-N'-(1-(thiophen-2-yl)ethylidene)-benzoyl-hydrazone (H**L**)

The initial task of the present work dealt with the synthesis and characterization of (E)-*N'*-(1-(thiophen-2-yl)ethylidene)-benzoyl-hydrazone ligand. Following a literature procedure [13], H**L** was synthesized in 4.5 min, in high yield and on a five grams scale under microwave irradiation, starting from benzohydrazide and 2-acetylthiophene. Crystals suitable for single X-ray diffraction studies were extracted directly from this sample. The solid-state structure of H**L** is depicted in figure 1.

The ligand H**L** crystallizes in the orthorhombic space group Pbca with eight H**L** molecules in the unit cell. In the solid state, the H**L** molecules are not planar (52° between thiophene group and phenyl ring), which contrasts with our previous observations for related ligands (i.e. quite planar in the solid state); this is probably due to the absence of an OH group on the phenyl ring [1]. Three classical intermolecular hydrogen bonds (N–H···O and C–H···O) were detected [14]. The bond lengths and angles for these interactions are as follows: N1–H1···O1*: 0.879(3)Å/ 2.463(3)Å/ 3.323(3)Å/ 165.8°; C1–H1A···O1*: 0.949Å/ 2.387Å/ 3.234(4)Å/ 148.4°; C9–H9C···O1*: 0.980Å/ 2.380Å/ 3.241(4)Å/ 146.3°, (* = -1/2-x, -1/2+y, z). A selected packing diagram in the (a, c) sheet is provided in figure 1.

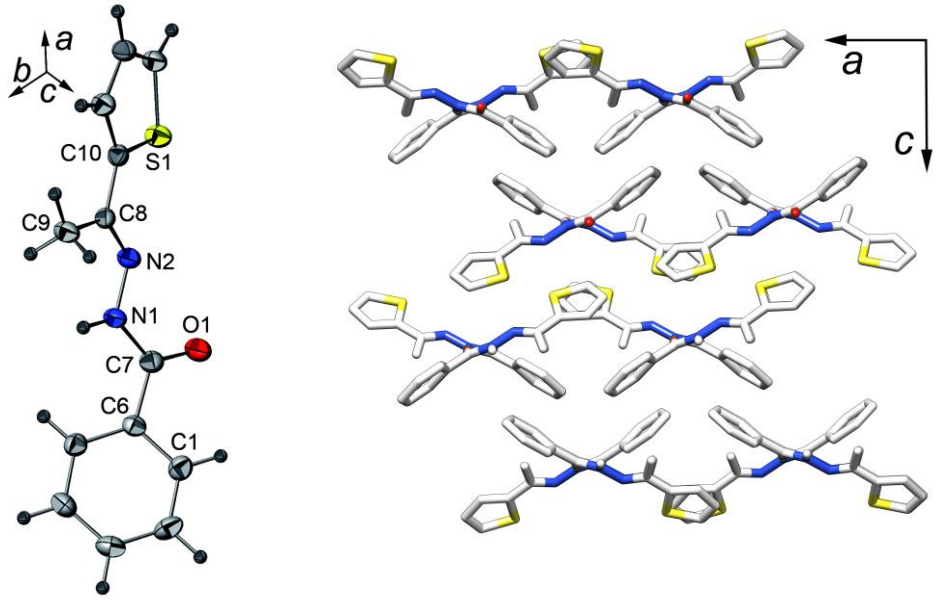

Figure 1: ORTEP view (left) and selected packing diagram (right) of the ligand H**L** with partial labelling scheme. The ellipsoids enclose 50% of the electronic density. On the packing diagram, the H atoms have been omitted for clarity.

Synthesis and structures of the derived Ni complexes (1-3)

1.3 Synthesis and crystal structure of $Ni(HL)_2(Br)_2$ (complex 1)

The reaction of $NiBr_2(PPh_3)_2$ with 2 equivalents of the ligand H**L** (THF, room temperature, 12 h) afforded complex **1** $[Ni(HL)_2(Br)_2]$ as a green powder with reasonable yield (Scheme 2). Green crystals of complex **1** suitable for single X-ray crystal structure determination were obtained by a slow Et_2O diffusion (at room temperature) into a CH_3CN solution of pure **1**. The molecular structure of complex **1** and a selected packing diagram is illustrated in figure 2 and 3 respectively.

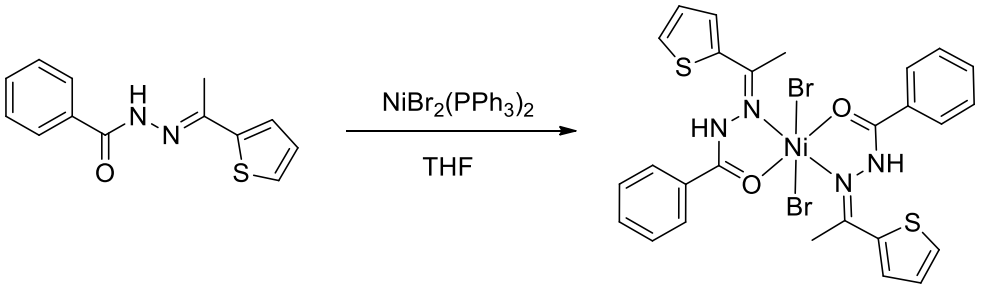

Scheme 2: Synthesis of $Ni(HL)_2(Br)_2$.

Complex **1** crystallizes in the monoclinic space group $P2_1/c$. Its solid-state molecular structure (figure 2) features a Ni^{2+} metal centre located on a crystallographic inversion centre -1. The Ni^{2+} ions are surrounded by two neutral H**L** ligands and two *trans*-located bromide ligands to complete the octahedral coordination geometry (Figure 2). The packing diagram shown in figure 3 also points out the position of the intermolecular N–H···Br hydrogen bonds. The parameters for intra- and inter-molecular hydrogen bonds for complex **1** are summarized in table 1.

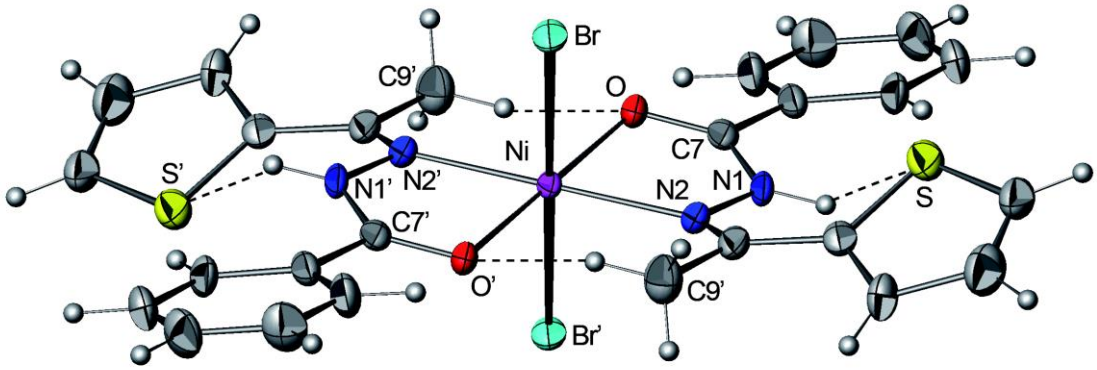

Figure 2: ORTEP view of complex **1** with a partial labelling scheme. Hydrogen bonds (intra molecular) are represented in dashed lines. The ellipsoids enclose 50% of the electronic density. Symmetry code for ' = -x, -y, -z. Selected distances (Å): Br–Ni 2.5502(5), Ni–O 2.036(4), Ni–N2 2.120(5), O–C7 1.233(6), N1–C7 1.352(7), N1–N2 1.404(7)

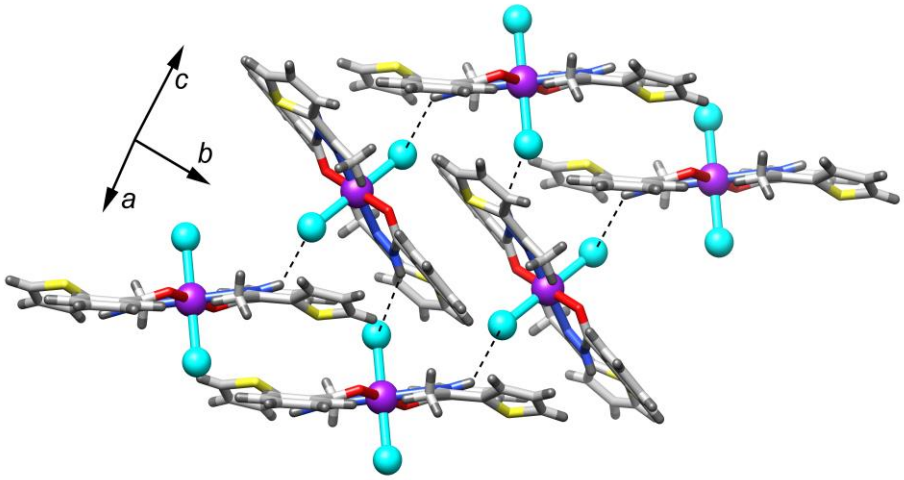

Figure 3: packing view showing N–H···Br hydrogen bonds (dashed lines).

Table 1 Bond lengths and angles of intramolecular and intermolecular hydrogen bonds in complex **1**.

Type	**Donor–H···Acceptor**	**d_{H-A} (Å)**	**d_{D-A} (Å)**	**D-H-A angle (°)**
Intramolecular	N(1)–H(1N)···S	2.328	2.879(5)	120.7
Intermolecular	N(1)–H(1N)···Br''	2.643	3.332(4)	135.9
Intramolecular	C(9)– H(9C)···O'	2.163	3.080(9)	155.1

(Symmetry codes: ' = -x, -y, -z; '' = -x, -1/2+y, 1/2-z)

Our group has recently reported similar coordination modes to that observed in complex **1** with Fe^{2+} ion coordinated by closely related ligands [3,4]. To the best of our knowledge, complex **1** is the first example of transition metal complex supported by the (E)-*N'*-(1-(thiophen-2-yl)ethylidene)-benzoyl-hydrazone ligand. Examples of complexes featuring similar coordination modes have been reported, where the metal centres are coordinated to two *trans*-located bromides and two N**,**O- chelating ligands [15-18].

1.4 Synthesis and crystal structure of $Ni(L)_2$ (complex 2)

When the reaction of $NiBr_2(PPh_3)_2$ with 2 equivalents of the ligand HL is carried out in the presence of an excess of Et_3N (20 equivalents to metal), the formation of complex **2**, in which the nickel centre is chelated by two anionic $\mathbf{L}^-$ ligands, is observed as deduced from X-ray crystallographic data (Scheme 3). The role of triethylamine is to capture the halide from the metal precursor, with the deposition of $Et_3N{\cdot}HBr$ (triethylamine hydrobromide) as a white solid. Dark crystals of complex **2** suitable for single crystal X-ray analysis were collected upon slow diffusion of Et_2O into a THF solution of species **2**. Figure 4 shows the ORTEP view of complex **2** along with selected bond lengths and angles.

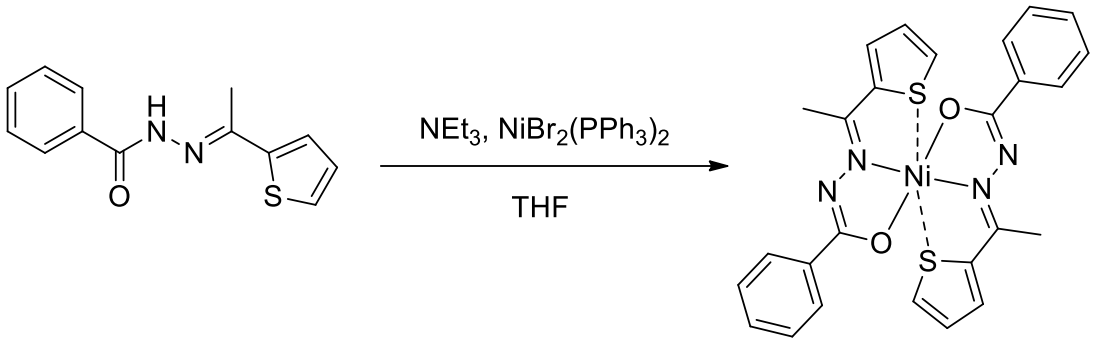

Scheme 3: Synthesis of Ni(**L**)$_2$

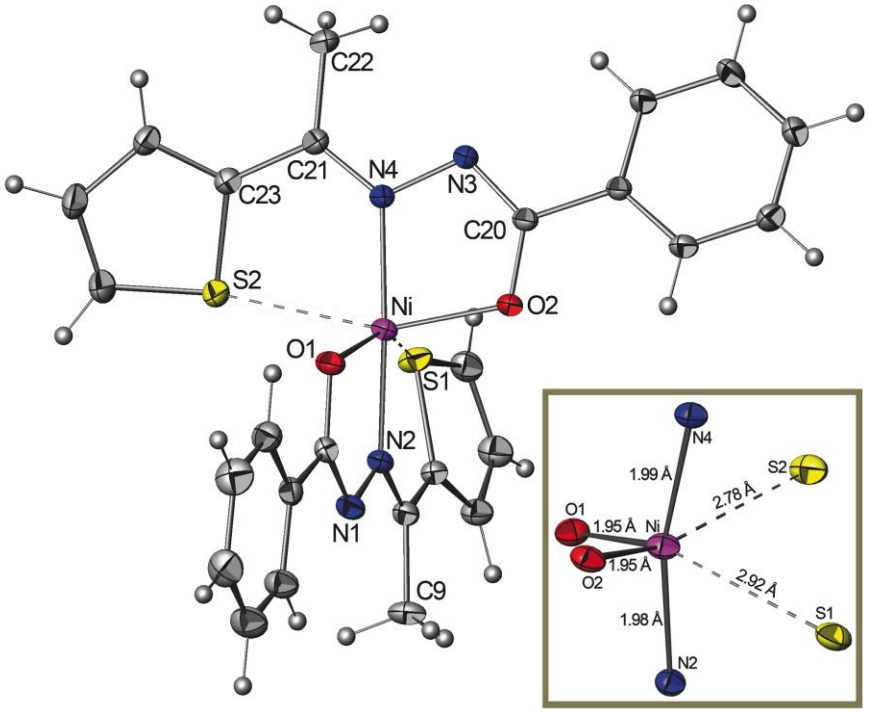

Figure 4: ORTEP view of compound **2** with partial labelling scheme. The ellipsoids enclose 50% of the electronic density. Selected distances (Å) and angles (°): Ni–O1 1.949(1), Ni–O2 1.949(1), Ni–N2 1.986(5), Ni–N4 1.990(1), Ni–S1 2.921(1), Ni–S2 2.781(1), O1–Ni–O2 107.85(5), N2–Ni–N4 165.58(6), O2–Ni–N4 81.27(5). Framed: selected view of the coordination sphere

Complex **2** crystallizes in a triclinic space group *P*-1 with two molecules in the unit cell. Its solid-state molecular structure exhibits a Ni^{2+} metal centre that may be seen as effectively chelated by two N,O,S-tridentate, L_2X-type anionic L^- ligands, both of which coordinating in a *mer*-fashion. This is rather an unusual coordination mode for this type of ligand, which classically behaves as a N,O-bidendate ligand. X-ray data contain no residual peak in the Fourier map differences, unambiguously indicating the absence of hydrogen on

the N1 and N3 atoms and establishing the mono-anionic nature of each chelating ligand (same conclusions have been made with close related ligands published by our group recently - see for examples refs 3 to 7). In contrast to the situation in complex **1**, where the sulphur external orientation is stabilized by the N-H···S hydrogen bonding and further stabilization derives from the two extra bromide ligands, complex **2** lacks both the NH moiety and bromides due to deprotonating of the ligand by the addition of Et_3N. The absence of the bromide ligands together with the rotation ability of the five-member ring about the exocyclic C-C bond may facilitate the coordination of the two sulphur atoms to the nickel centre.

The Ni-S interaction appears to be so weak, as deduced from the values of the Ni-S bond distances (2.92(1) and 2.78(1) Å for Ni–S1 and Ni–S2, respectively, in comparison with the average distance value of 2.39(2) Å founded for classical Ni-S bond – about 100 references into the CCDC data base). In a comparable example of nickel complex bearing two N,O,S-tridentate ligands[19], the analogue Ni-S distances were found to be about 0.3-0.4 Å shorter than those found in complex **2**.No classical hydrogen bonds were detected in the crystal structure of complex **2** but specific CH···π interactions were observed between one hydrogen atom of the methyl group and the thiophene ring (figure 5, on the right). To our knowledge, species **2** constitute the first example of a Ni complex in which the Ni^{2+} metals bears two N,O,S-tridentate ligands coordinated in *mer*-configuration. The use of complex **2** as a catalyst precursor for ethylene oligomerisation was also studied.

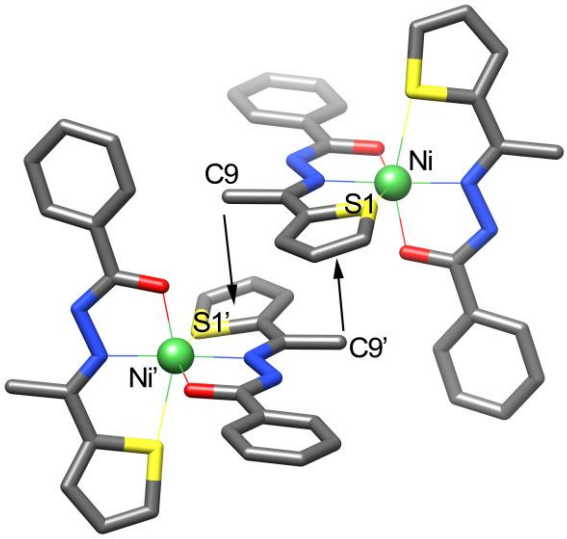

Figure 5: packing view. Arrows indicate CH···π bonds. Hydrogen atoms have been omitted for clarity. **'** is the symmetry code -x, 1-y, 1-z.

1.5 Synthesis and crystal structure of $Ni_2(\mu\text{-}H_2O)(\mu\text{-}L)_2(L)_2$ (complex 3)

Changing the nickel metal precursor from $NiBr_2(PPh_3)_2$ to $NiCl_2$ (under near identical reaction conditions to those used for the synthesis of species **2**) led to the formation of a new dinuclear complex **3**, whose identity and molecular structure was determined by X-ray crystallographic studies (scheme 4 and figure 6). The detailed reason for the formation of different complex structures by only changing the starting metal precursor is unknown at the moment. Green single crystals of complex **3** were obtained after slow diffusion of diethyl ether into a dichloromethane solution. Suitable single crystals can also be obtained by slow diffusion of THF into dichloromethane solution of the complex. Structure determination studies were conducted for both crystalline samples. The crystal structure obtained by THF diffusion is the one described here.

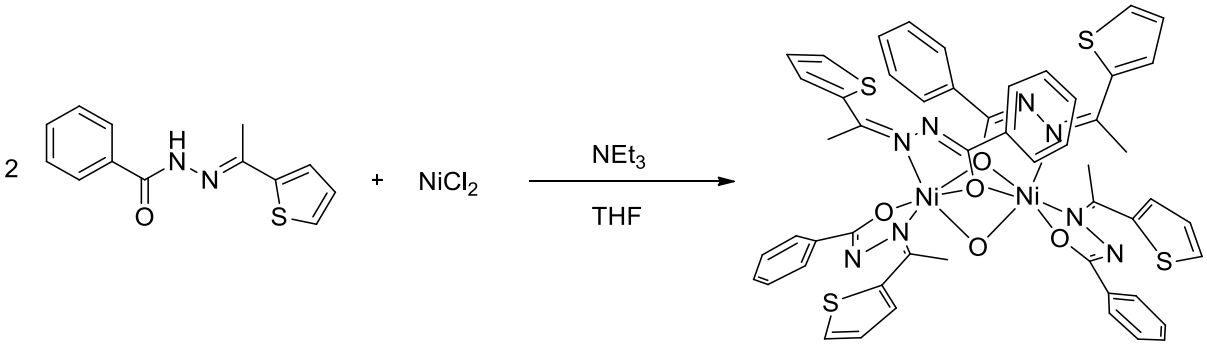

Scheme 4: Synthesis of $Ni_2(\mu\text{-}H_2O)(\mu\text{-}\mathbf{L})_2(\mathbf{L})_2$.

Complex **3** crystallizes in the monoclinic space group C 2/c with four molecules in the unit cell. Complex **3** is a Ni dinuclear specie, in which the Ni metal centres are linked to one another via two bridging $\mu:\eta^1,\eta^2$ anionic $\mathbf{L}^-$ ligands and a bridging μ-O water molecule. Thus, as shown in figure 6, each Ni^{2+} centre is surrounded by four anionic bidendate ligands $\mathbf{L}^-$: two being coordinated in a classical chelating η^2-N,O mode and two bridging $\mu:\eta^1,\eta^2$ anionic L^- moieties. Here again, the mono-anionic nature of the chelating data is supported by X-ray data: no residual peak is detected in the Fourier map differences, indicating the absence of the hydrogen atom on N1 (N1') and N3 (N3'). The hydrogen atoms of the water molecule are also clearly detected and form two classical hydrogen bonds with the oxygen atoms of the neighbouring THF solvent molecules in the crystal packing. All these observations confirm the +2 charge of Ni. Five examples of similar coordination for Ni^{2+} dinuclear compounds can

be found in the Cambridge Data base [20-24]. The Ni–Ni distance of 2.91 Å lies in the typical range for such dinuclear species. The presence of a bridging water molecule in this compound can be explained by the presence of water in the solvent used for these experiments.

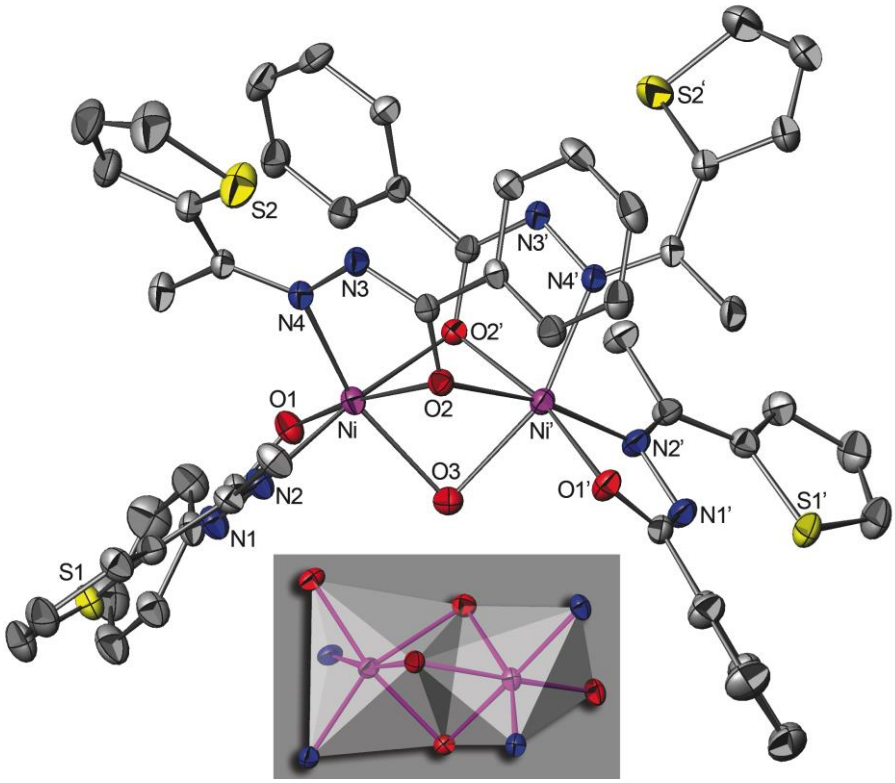

Figure 6: ORTEP view of the complex **3** with partial labelling scheme. The ellipsoids enclose 50% of the electronic density. Selected distances (Å) and angles (°): Ni–O1 1.949(1), Ni–O1 2.000(2), Ni–O2 2.039(2), Ni–N2 2.053(2), Ni–N4 2.053(2), Ni–O3 2.152(2), Ni–O2 2.1570(2), Ni–Ni 2.9101(6); Ni–O2–Ni 87.78(7), Ni–O3–Ni 85.09(10). Hydrogen atoms as well as THF solvent molecules have been omitted for clarity. Symmetry code for ' = -x+1, y, -z+1/2. Framed: view of the faces sharing of both deformed octahedral surrounded Ni^{2+} ions.

1.6 Ethylene oligomerization using complex 2 as catalyst precursor

We evaluated the bis(chelate) nickel complex **2** for ethylene oligomerization catalytic activity in the presence of 10 equivalent $AlEtCl_2$ as co-catalyst. Under an ethylene pressure of 10 bar, the complex **2**/$AlEtCl_2$ catalytic mixture was found to feature an activity comparable to that in related bis(chelate) Ni complexes [25,26]. Complex **2** exhibited a turnover frequency (TOF) of 31200 mol of C_2H_4 (mol of Ni h^{-1}) in the oligomerization of ethylene with dimers (64.8% in mass) and trimers (30.7%) as the major products. Traces of C8 (3.8%) and C10 (0.7%) olefins were also detected (figure 7). This product distribution is in contrast to the

results of the previously reported cobalt [27] and titanium [28] complexes, where the presence of thien-2-yl group in the ligand close to the metal centre usually led to the generation of olefins or polymers with longer carbon chains; this was ascribed to the coordination of the sulphur atom to the metal centre in the presumed transition state, likely to stabilize such an electron-deficient transition state for migratory insertion. The selectivity for α-olefins was relatively low (10% of 1-butene for ethylene dimers and 1.8% of α-C6 for trimers), which is probably due to the fast isomerization of the generated 1-butene and 1-hexene. Theoretical and experimental investigations reported in the literature indicate the real active site for olefin oligomerization or polymerization to be a cationic metal alkyl species that would then allow for the binding of the monomer and its subsequent insertion [29,30]. In our case, as reported for other N,O- bis(chelate) nickel(II) complexes with comparable ethylene oligomerization [26,31-33], it appears likely that the Lewis acid Al co-catalyst $AlEtCl_2$ abstracts one of the Ni-coordinated chelating ligand to form a reactive and electron-deficient alkyl Ni intermediate likely to be the catalytically active species [31,33].

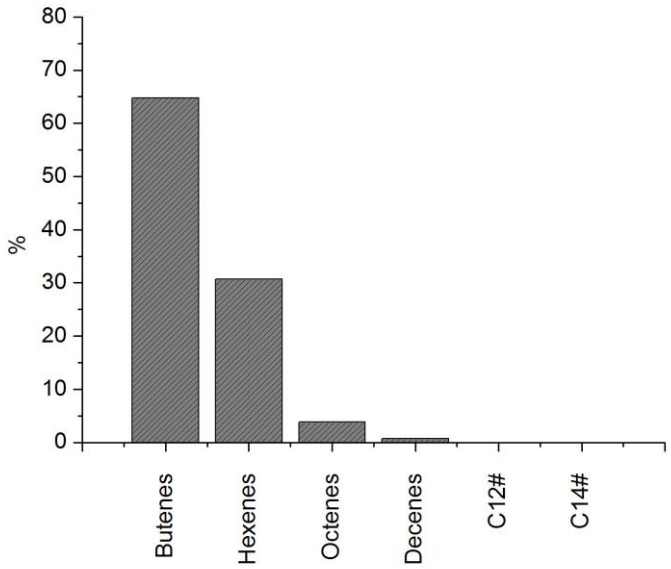

Figure 7: Product distribution in the oligomerization of ethylene using **2**/$AlEtCl_2$ catalytic mixture.

1.7 Concluding remarks – summary

(H**L**) readily synthesized in high yield and on 5 gram-scale within a few minutes under microwave irradiation, was found to be suitable for coordination to Ni(II) and afford structurally diverse H**L**$^-$ and **L**$^-$ supported Ni derivatives. Three types of nickel complexes, $Ni(HL)_2(Br)_2$, $Ni(L)_2$ and $Ni_2(\mu\text{-}H_2O)(\mu\text{-}L)_2(L)_2$ were prepared by reaction of H**L** with different nickel sources and/or under different reaction conditions. Thus, while the reaction of $NiBr_2(PPh_3)_2$ with H**L** in the absence of base, yielded the Ni complex $Ni(HL)_2(Br)_2$ (**1**), the addition of excess Et_3N in the reaction medium led to the formation of species **2**, $Ni(L)_2$ with two unexpected and original Ni···S interactions. The dinuclear complex **3** $[Ni_2(\mu\text{-}H_2O)(\mu\text{-}L)_2(L)_2]$, in which the two Ni(II) ions are connected through two bridging $\mu:\eta^1,\eta^2$ anionic L$^-$ ligands and a bridging μ-O water molecule, is accessible by the reaction of ligand HL with $NiCl_2$ in the presence of excess Et_3N. The solid-state structures of H**L** and of all three Ni complexes were all determined by single crystal X-ray diffraction studies. In the presence of 10 equivalent $AlEtCl_2$ as co-catalyst, complex $Ni(L)_2$ (**2**) was found to be active in ethylene oligomerization with a TOF value of 312 00 mol of C_2H_4 (mol. Ni. h.)$^{-1}$, which is similar to those obtained with bis(chelate) Ni(II) complexes coordinated by N,O chelates [25,31,32]. C4 and C6 olefins were the main products of the latter polymerization catalysis that occurs with low α-olefin selectivity.

1.8 Experimental section

General procedures

All manipulations were performed under aerobic conditions unless specified otherwise. Reagents and solvents were commercially purchased and used as received. NMR spectra were recorded at room temperature on a Bruker AVANCE 300 spectrometer (^{1}H, 300 MHz; ^{13}C, 75.47 MHz). IR spectra were recorded in the region 4000-100 cm^{-1} on a Nicolet 6700 FT-IR spectrometer (ATR mode, diamond crystal). Elemental analyses were performed by the "Service de microanalyses", Université de Strasbourg.

Synthesis of (E)-N'-(1-(thiophen-2-yl)ethylidene)-benzoyl-hydrazone (HL)

Benzhydrazide (5.00 g, 36.7 mmol) and 2-acetylthiophene (4.63g, 36.7 mmol) were placed in a quartz tube in a QV-50S reactor equipped with temperature and pressure probes, which was introduced in the microwave oven (Milestone Micro-SYNTH apparatus). The reaction proceeded under stirring for 4.5 min at 200W, with a final temperature of 247 °C and final pressure of 8.0 bar. The system was then allowed to cool down to room temperature, leading to crystallization of the hydrazone. Ethyl ether was added to the quartz tube to wash the product which was filtrated under reduced pressure and further washed with diethyl ether to afford 8.30 g (93%) of yellowish needles (m. p. 188-189 °C). ^{1}H NMR (d_6-DMSO): δ 2.39 (s, 3H, CH_3), 7.11 (s, 1H, Thio-H), 7.69-7.38 (m, 4H, 2 × Thio-H and 2 × Ar-H), 7.87 (s, 2H, Ar-H), 10.79 (br s, 1H, N-H). ^{13}C{^{1}H} NMR (d_6-DMSO): δ 14.9 (CH_3), 127.5 (C-Thio), 127.7 (C-Thio), 128.2 (C-Thio), 129.0 (C-Thio), 131.4 (C-Ar), 143.1(C-Ar), 152.6 (C=N), 163.4 (C=O). IR (pure, orbit diamond): 1652 (C=O), 1637 (N-H), 1541(C=N). Anal. Calcd. for $C_{13}H_{12}N_2OS$: C, 63.91; H, 4.95; N, 11.47. Found: C, 63.95; H, 4.94; N, 11.54.

Synthesis of complex 1 [Ni(HL)$_2$(Br)$_2$]

To a solution of $Ni(Br)_2(PPh_3)_2$ (0.15g, 0.20 mmol) in THF (20 mL), H**L**(0.1g, 0.41 mmol) was added. The green solution was left under stirring overnight at room temperature and then filtered. Green powder of the titled complex was obtained after solvent evaporation and then dried under vacuum. Green monocrystals suitable for X-ray crystal structure determination were obtained by slow diffusion of diethyl ether into an acetonitrile solution of the complex (yield: 0.15g, 52.5%). IR (pure, orbit diamond): 3310s, 2316m, 2289w, 1619m, 1571w. Anal. Calcd. for $C_{26}H_{24}Br_2N_4NiO_2S_2$: C, 44.16; H, 3.42; N, 7.92. Found: C, 44.27; H, 3.56; N 7.87.

Synthesis of complex 2 [Ni(L)$_2$]

Excess of Et_3N (0.56 mL, 4.0 mmol) was added to a solution of $Ni(Br)_2(PPh_3)_2$ (0.15g, 0.20 mmol) in THF (20 mL) until the formation of a white precipitate. (*E*)-*N'*-(1-(thiophen-2-yl)ethylidene)benzohydrazide (0.1g, 0.41 mmol) was added to the mixture and the solution was left under stirring overnight at room temperature. The white precipitate of $Et_3N{\cdot}HBr$ was filtered off and a yellow powder of the titled complex was obtained by solvent evaporation and then dried under vacuum. Dark monocrystals suitable for X-ray analysis were collected upon slow diffusion of diethyl ether into a THF solution of the titled complex (yield: 0.13g,

60%). IR (pure, orbit diamond): 1648m, 1577w, 1486m, 1438m, 1367w, 1309w, 1274w, 1189s, 1120s, 1024w, 720s, 696s. Anal. calcd for $C_{26}H_{22}N_4NiO_2S_2$: C, 57.27; H, 4.07; N, 10.27. Found: C, 57.25; H, 4.13; N, 10.44.

Synthesis of complex 3 [$Ni_2(\mu\text{-}H_2O)(\mu\text{-}L)_2(L)_2$]

To a well stirred solution of (*E*)-*N*'-(1-(thiophen-2-yl)ethylidene)benzohydrazide (0.1g, 0.41 mmol) in THF (12.5 mL), $NiCl_2$ (0.026 g, 0.2 mmol) was added. An excess of Et_3N (0.56 mL, 4.0 mmol) was added to the solution until the formation of a white precipitate. The solution was left under stirring overnight at room temperature and then the white precipitate (Et_3N·HBr) was filtered off. A green powder of the titled complex was obtained by solvent evaporation and then dried under vacuum. Green monocrystals suitable for X-ray crystal structure determination were collected by slow diffusion of diethyl ether into a dichloromethane solution of the titled complex (yield: 0.10 g, 25 %). IR (pure, orbit diamond): 2363m, 1645w, 1575w, 1509m, 1423w, 1270w. Anal. Calcd for $C_{60}H_{62}N_8Ni_2O_7S_4$ (3·2THF): C, 57.52; H, 4.99; N, 8.94. Found: C, 57.66; H, 4.76; N, 8.87.

Oligomerization of ethylene

4×10^{-5} mmol of Ni complex **2** was dissolved in 15 mL toluene and injected into the reactor under an ethylene flux. Then a 5 mL toluene solution of $AlEtCl_2$ (8×10^{-5} mol/L) was added to obtain a total volume of 20 mL. The reactor was pressurized to 10 bars and a rise in temperature was observed as a result of the reaction exothermicity. The 10 bar working pressure was maintained during the experiments through a continuous feed of ethylene from a reserve bottle placed on a balance to allow continuous monitoring of the ethylene uptake. At the end of the test (35 min), a dry ice bath was used to rapidly cool down the reactor, thus stopping the reaction. An ice bath was then used and when the inner temperature reached 0 ^oC, the ice bath was removed allowing the temperature to slowly rise to 10 ^oC. The gaseous phase was then transferred into a 10 L polyethylene tank filled with water. An aliquot of this gaseous phase was transferred into a Schlenk flask for GC analysis. The products in the reactor were alcoholyzed *in situ* by the addition of ethanol (10 mL), transferred into a Schlenk flask, and separated from the metal complexes by trap-to-trap evaporation (20^oC, 0.8 mbar) into a second Schlenk flask previously immersed in liquid nitrogen, in order to avoid any loss of product.

Crystal structure determinations

Suitable crystals for the X-ray analysis of all compounds were obtained as described above. Single crystals of the ligand and complexes **1** to **3** were mounted on a Nonius Kappa-CCD area detector diffractometer (Mo Kα λ = 0.71073 Å). The complete conditions of data collection (*Denzo* software [10]) and structure refinements are given in table I appendix chapter 5). The cell parameters were determined from reflections taken from one set of 10 frames (1.0° steps in phi angle), each at 20s exposure. The structures were solved using direct methods (*SHELXS97*) and refined against F^2 using the *SHELXL97* and *CRYSTALBUILDER* software [11,12]. The absorption was not corrected. All non-hydrogen atoms were refined anisotropically. Hydrogen atoms were generated according to stereochemistry and refined using a riding model in *SHELXL97*. Crystallographic data (excluding structure factors) have been deposited in the Cambridge Crystallographic Data Centre as Supplementary publication no. CCDC 835284 - 835288. Copies of the data can be obtained free of charge on application to CCDC, 12 Union Road, Cambridge CB2 1EZ, UK (fax: (+44)1223-336-033; e-mail: deposit@ccdc.cam.ac.uk)

1.9 References

1. C. Beghidja, M. Wesolek, R. Welter, Inorg. Chim. Acta 358 (**2005**) 3881-3888.
2. C. Beghidja, G. Rogez, J. Kortus, M. Wesolek, R. Welter, J. Am. Chem. Soc. 128 (**2006**) 3140-3141.
3. N. Bouslimani, N. Clément, G. Rogez, P. Turek, M. Bernard, S. Dagorne, D. Martel, H.N. Cong, R. Welter, Inorg. Chem. 47 (**2008**) 7623-7630.
4. N. Bouslimani, N. Clément, C. Toussaint, S. Hameury, P. Turek, S. Choua, S. Dagorne, D. Martel, R. Welter, Eur. J. Inorg. Chem. (**2009**) 3734-3741.
5. N. Clément, C. Toussaint, G. Rogez, C. Loose, J. Kortus, L. Brelot, S. Choua, S. Dagorne, P. Turek, R. Welter, Dalton Trans. 39 (**2010**) 4579-4585.
6. C. Toussaint, C. Beghidja, R. Welter, C. R. Chimie 13 (**2010**) 343-352.
7. N. Bouslimani, N. Clément, G. Rogez, P. Turek, S. Choua, S. Dagorne, R. Welter, Inorg. Chim. Acta 363 (**2010**) 213-220.
8. L. Bogani, W. Wernsdorfer, Nature Mat. 7 (**2008**) 179-186.
9. R. Welter, WO/**2009**/130562.
10. B.V. Nonius, *Kappa CCD Operation Manual*, Delft, The Netherlands, **1997**.
11. G.M. Sheldrick, *SHELXL97: Program for the Refinement of Crystal Structures*; University of Göttingen, Göttingen, Germany, **1997**.
12. R. Welter, Acta Cryst. A62 (**2006**) s252.
13. M.M. Andrade, M.T. Barros, J. Comb. Chem. 12 (**2010**) 245-247.
14. A.L. Spek, *PLATON software*, J. Appl. Cryst. 36 (**2003**) 7-13.
15. K.R. Adam, L.F. Lindoy, R.J. Smith, G. Anderegg, K. Henrick, M. McPartlin, P.A. Tasker, J. Chem. Soc., Chem. Commun. 18 (**1979**) 812-813.
16. H.J. Goodwin, K. Henrick, L.F. Lindoy, M. McPartlin, P.A. Tasker, Inorg. Chem. 21 (**1982**) 3261-3264.
17. D.J. Macchia, W.F. Furey Jnr, R.A. Lalancette, Acta Cryst. C49 (**1993**) 1706-1713.
18. L.K. Minacheva, N.B. Generalova, I.K. Kireeva, V.G. Sakharova, A.Y. Tsivadze, M.A. Porai-Koshits, Zh. Neorg. Khim. 38 (**1993**) 1666-1676.
19. S. Karmakar, S. B. Choudhury, D. Ray, A. Chakravorty, Polyhedron, 12 (**1993**) 2325-2329.
20. K.E. Vostrikova, V.I. Ovcharenko, G.V. Romanenko, V.N. Ikorskii, N.V. Podberezskaya, V.A. Reznikov, L.B. Volodarskii, Zh. Neorg. Khim. 37 (**1992**) 1755-1772.

21. E.D. McKenzie, F.S. Stephens, Inorg. Chim. Acta 32 (**1979**) 253-261.
22. W. Luo, X. Wang, G. Cheng, S. Gao, Z. Ji, Inorg. Chem. Commun. 11 (**2008**) 769-771.
23. L. Rodríguez, E. Labisbal, A. Sousa-Pedrares, J.A. García-Vázquez, J. Romero, M.L. Durán, J.A. Real, A. Sousa, Inorg. Chem. 45 (**2006**) 7903-7914.
24. A. Berkessel, K. Roland, M. Schröder, J.M. Neudörfl, J. Lex, J .Org. Chem. 71 (**2006**) 9312-9318.
25. E. Nelkenbaum, M. Kapon, M.S. Eisen, Organometallics 24 (**2005**) 2645-2659.
26. A. Kermagoret, P. Braunstein, Dalton Trans. (**2008**) 1564-1573.
27. C. Bianchini, D. Gatteschi, G. Giambastiani, I.G. Rios, A. Ienco, F. Laschi, C. Mealli, A. Meli, L. Sorace, A. Toti, F. Vizza, Organometallics 26 (**2007**) 726-739.
28. J. Huang, T. Wu, Y. Qian, Chem. Commun. (**2003**) 2816-2817.
29. D.J. Tempel, L.K. Johnson, R.L. Huff, P.S. White, M. Brookhart, J. Am. Chem. Soc. 122 (**2000**) 6686-6700.
30. L.H. Shultz, D.J. Tempel, M. Brookhart, J. Am. Chem. Soc. 123 (**2001**) 11539-11555.
31. L. Wang, C. Zhang, Z. Wang, Eur. J. Inorg. Chem. (**2007**) 2477-2487.
32. C. Carlini, M. Isola, V. Liuzzo, A.M.R. Galletti, G. Sbrana, Appl. Catal., A 231 (**2002**) 307-320.

Conclusion générale

Ce mémoire de thèse, structuré en cinq chapitres, résume trois années de recherche dans le cadre d'une chimie de coordination pluridisciplinaire, effectué au laboratoire DECOMET de l'université de Strasbourg, sous la direction du Professeur Richard WELTER.

Ce travail explore certains aspects de la chimie de coordination de complexes moléculaires à bases de métaux 3d supportés par des ligands de type aroyls hydrazones. Ces ligands organiques présentent une chimie proche de celle de la grande famille des 'bases de Schiff', molécules qui contiennent un groupement imine C=N. De nombreux travaux de recherche leur ont été et leur sont encore consacrés. Il y a plusieurs raisons à cela : une synthèse souvent aisée, et surtout une grande diversité de propriétés physico-chimiques de leurs complexes métalliques. Les hydrazones, de la famille des azométhines - dans laquelle l'azote de la fonction C=N est directement lié à un autre atome d'azote - à la place d'un carbone dans une simple base de Schiff - agissent comme des ligands prometteurs en photo chimie ou en catalyse homogène. Enfin, la fonctionnalisation de la partie hydrazone par un groupement -C=O conduit aux molécules nommées acyl- ou aroyl- hydrazone.

L'oxygène du groupement carbonyle et l'azote trigonal de la fonction imine sont les sites donneurs d'électrons, présents dans les composés aroyl hydrazone. Une de leurs autres propriétés est leur capacité à exister sous deux formes tautomères : la forme amide ou bien sous la forme iminol. Ils complexent typiquement les ions métalliques en formant des cycles chélates à cinq centres, via leur forme cétone neutre type L,L ou bien sous leur forme iminolate anionique type X,L.

Le laboratoire DECOMET explore la chimie de ces ligands depuis de nombreuses années. Le travail de cette thèse est plus particulièrement centré sur la photo chimie des complexes ferriques, afin d'élucider en particulier les mécanismes de la photo réduction. D'autres domaines sont également explorés, comme le magnétisme moléculaire ou encore la catalyse homogène (oligomérisation de l'éthylène) avec des complexes à base de Ni^{2+}.

En 2008, Le professeur Welter a mis en évidence un nouveau type de complexes moléculaires à base de Fer(III) qui se transforme photo chimiquement en complexe de Fe(II). Ceci s'est concrétisé par le dépôt d'un brevet international: Method and device for producing and storing energy, WO 2009/130562 A_1). Le retour Fe(+II) -->Fe(+III) est aisé. Il se fait soit électro

chimiquement soit chimiquement, avec l'oxygène contenu dans l'air par exemple. Le fait d'induire via l'absorption lumineuse un changement d'un degré d'oxydation stable vers un autre degré d'oxydation stable en solution peut être utilisé pour la circulation des électrons via un système approprié. Le Fer est le métal le plus abondant sur terre, et les produits de départ pour la synthèse des ligands sont bon marché. D'où l'intérêt évident de ce système dans la production d'énergie à partir de la lumière solaire.

Après avoir rappelé quelques généralités concernant les ligands utilisés et leur mode de coordination, le **chapitre 2** vient élucider le mécanisme de la photo réduction. Les complexes mis en jeu dans le processus ont été totalement caractérisés en solution et à l'état solide. Ce phénomène prend place en solution comme en solution gelée. La cinétique du processus photochimique a été suivie par UV-Visible comme par RPE. Cette photo réduction passe par un intermédiaire radicalaire et le solvant joue le rôle du donneur des électrons. Ce processus a été totalement étudié : l'effet du solvant, l'effet de la modification dans la sphère de coordination du complexe, l'effet de la modification de la périphérie des ligands et finalement l'effet des longueurs d'ondes.

D'autre part, dans le **troisième chapitre**, des travaux avec un ligand similaire de type hydrazine ont été réalisés. Le complexe $[[FeCl(DMF)_2]_2(L)]$, a été synthétisé et caractérisé par diffraction des rayons X, UV-Visible, infrarouge et électrochimie. L'étude magnétique réalisé sur ce complexe a révélé l'existence d'une interaction antiferromagnétique entre les ions ferriques avec une constante J = 5,98 cm^{-1}. Un phénomène très intéressant a été observé avec ce ligand bis-hydrazine, capable de complexer deux ions ferriques et, sous irradiation, ce complexe ferrique se photo réduit et il libère les deux ions métalliques (Fe^{2+}). Le ligand est alors disponible pour complexer deux nouveaux ions ferriques.

Les ligands des aroyl-hydrazone complexent de nombreux métaux de transition tels le fer et le manganèse à leurs degrés d'oxydation habituels, (+II) ou (+III). Les essais de complexation avec différents précurseurs de Mn^{2+}, Mn^{3+} et Fe^{3+} conduisent à de nouveaux complexes mono et binucléaires, de structures originales et présentant dans certains cas, des propriétés magnétiques remarquables. Le complexe binucléaire $Mn_2(HL^{(2)})_4(\mu\text{-}OMe)_2$ présente par exemple un couplage magnétique intramoléculaire exceptionnellement fort (J=+19.7 cm^{-1}). C'est à jour la plus forte valeur de couplage ferromagnétique rencontrée dans un complexe binucléaire de manganèse. En appuyant sur ce résultat important, dans le **chapitre 4**, on a

étudié les propriétés magnétiques d'une série des complexes de fer et du manganèse, mono et bi nucléaires avec le ligand H_2L^{8}, qui ont été synthétisés et caractérisés par radiocristallographie.

Dans le **chapitre 5**, on présente une diversité des complexes de nickel, parmi lequel un de ces composés présente une activité pour l'oligomérisation d'éthylène. La fonctionnalisation de la partie hydrazone par un hétérocycle dans une position appropriée, peut augmenter le nombre de sites de coordination et les ligands bidentates N,O- réagissent comme ligands tridentates N,S,O-. Le ligand tridentate H**L** possédant le groupement thiophène sur la partie hydrazone, a été synthétisé avec un très bon rendement, (en quelques minutes sous irradiations microondes), et offre une diversité de structure des complexes de nickel. La présence de la liaison C=N qui présente une caractéristique très attractive d'être une entité dynamique capable de subir une isomérisation cis-trans, peut induire un changement dans le mode de coordination du ligand, d'un tridentate N,S,O- à un bidentate NO. Trois différents types des complexes de nickel, $Ni(HL^{21})_2(Br)_2$, $Ni(L^{21})_2$ et $Ni_2(\mu\text{-}H_2O)(\mu\text{-}L^{21})_2(L^{21})_2$ ont été synthétisés, purifiés et caractérisés au laboratoire par les différentes méthodes spectroscopiques et caractérisés par diffraction des RX. En présence d'un co-catalyseur de $AlEtCl_2$, l'unique complexe de Ni supporté par deux ligands tridentates N,S,O- présente une forte activité pour l'oligomérisation d'éthylène. Cette activité est dûe à la décoordination de la faible liaison Ni-S qui en libérant un site de coordination sur le métal, permet la complexation de l'éthylène qui déclenche le cycle catalytique.

APPENDIX

Appendix chapter 2

- **C1** ($Fe(HL)_2(DMF)(Br)$):

Table I: Selected Experimental Bond Lengths (Å) and Angles (deg) for **C1**

Fe─O_2 (equatorial ligand)	1.9779(13)
Fe─O_4 (axial ligand)	1.9758(12)
Fe─O_5 (DMF)	2.0451(13)
Fe─N_2 (equatorial ligand)	2.1525(15)
Fe─N_4 (axial ligand)	2.2164(15)
Fe─Br_1	2.4160(3)
C═N (azomethine equatorial ligand)	1.298(2)
C═N (iminol equatorial ligand)	1.317(2)
C═N (azomethine axial ligand)	1.288(2)
C═N (iminol axial ligand)	1.309(2)
O4 Fe1 O2	160.01(5)
O4 Fe1 O5	98.80(5)
O2 Fe1 O5	91.08(5)
O4 Fe1 N2	92.39(6)
O2 Fe1 N2	75.83(6)
O5 Fe1 N2	166.11(6)
O4 Fe1 N4	74.24(5)
O2 Fe1 N4	88.72(5)
O5 Fe1 N4	88.87(6)
N2 Fe1 N4	86.27(6)
O4 Fe1 Br1	93.77(4)
O2 Fe1 Br1	102.95(4
O5 Fe1 Br1	93.69(4)
N2 Fe1 Br1	93.76(4)
N4 Fe1 Br1	167.99(4)

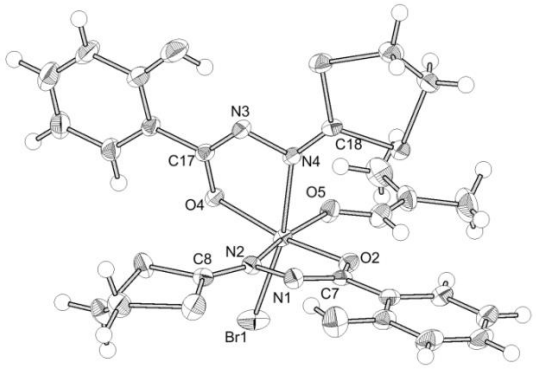

Figure A1: ORTEP view of **C1** ($Fe(HL)_2(DMF)(Br)$)

- **C2** ($Fe(H_2L)_2(Br)_2$):

Table II: Bond Lengths (Å) and Angles (deg) for **C2**

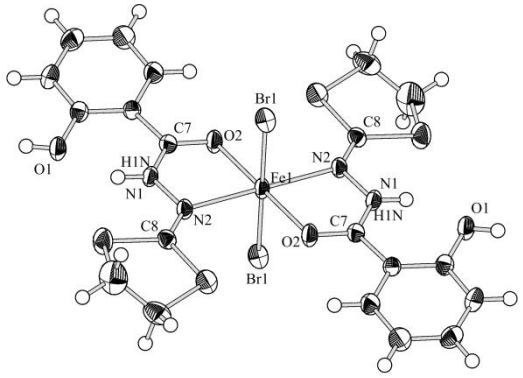

Figure A2: ORTEP view of **C2** ($Fe(H_2L)_2(Br)_2$)

Fe─O_2	2.077(2)
Fe─N_2	2.209(2)
Fe─Br_1	2.6547(12)
C_8─N_2 (C═N azomethine)	1.285(4)
C_7─N_1 (C─N amide)	1.334(4)
O2 Fe1 O2	180.0
O2 Fe1 N2	104.74(9
O2 Fe1 N2	75.26(9
N2 Fe1 N2	180.0
O2 Fe1 Br1	90.55(7)
O2 Fe1 Br1	89.45(7
N2 Fe1 Br1	90.99(7)
N2 Fe1 Br1	89.01(7)
N2 Fe1 Br1	90.99(7)
Br1 Fe1 Br1	180.0

- **C4** {[$(Fe(HL)_2(EtOH)(Br)]$.[$Fe(HL)_2(Br)$]} and **C3** {[$(Fe(HL)_2(EtOH)(Br)]$.[$Fe(HL)_2(Br)$]

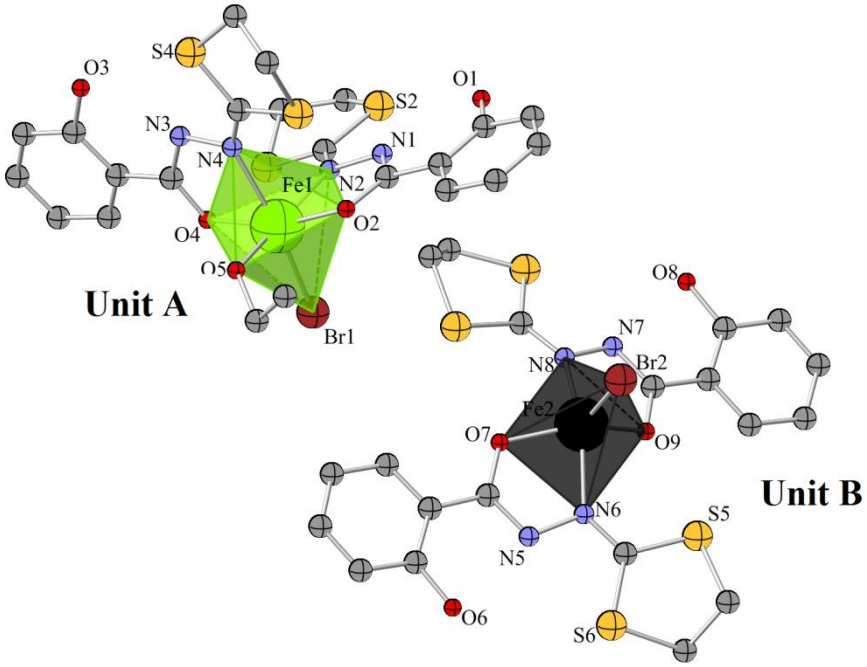

Figure A3: The two different units of **C4** (Fe^{III} in EtOH)

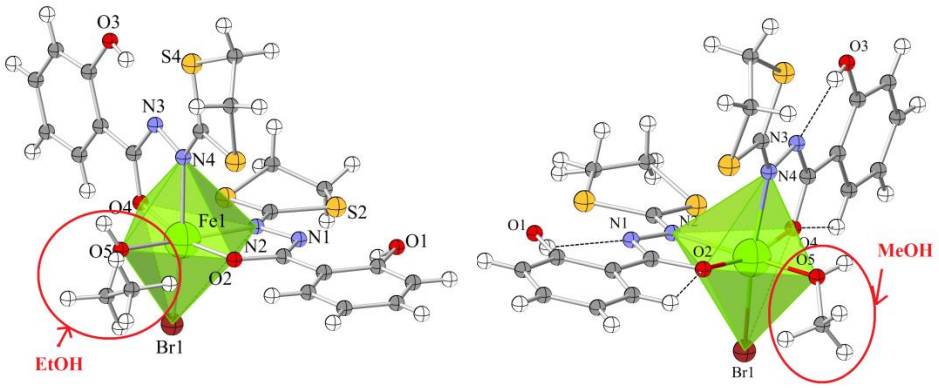

Figure A4: On the right unit A for **C4**. On the left Unit A for **C3**

Table III: Bond Lengths (Å) and Angles (deg) for unit A of **C3** and **C4**

	C4	C3
N2 Fe1	2.1525(15)	2.166(6)
N4 Fe1	2.2164(15)	2.218(6)
O2 Fe1	1.9779(13)	1.950(5)
O4 Fe1	1.9758(12)	1.918(5)
O5 Fe1	2.0451(13)	2.032(5)
Fe1 Br1	2.4160(3)	2.4545(15)
C_8—N_2	1.298(2)	1.297(9)
C_7—N1	1.317(2)	1.310(9)
C_{18}—N_4	1.288(2)	1.295(9)
C_{17}—N_3	1.309(2)	1.317(10)
O4 Fe1 O2	160.01(5)	165.9(2)
O4 Fe1 O5	98.80(5)	96.8(2)
O2 Fe1 O5	91.08(5)	89.3(2)
O4 Fe1 N2	92.39(6)	95.6(2)
O2 Fe1 N2	75.83(6)	76.9(2)
O5 Fe1 N2	166.11(6)	165.3(2)
O4 Fe1 N4	74.24(5)	75.7(2)
O2 Fe1 N4	88.72(5)	92.3(2)
O5 Fe1 N4	88.87(6)	85.3(2)
N2 Fe1 N4	86.27(6)	90.0(2)
O4 Fe1 Br1	93.77(4)	95.68(16)
O2 Fe1 Br1	102.95(4	96.64(16)
O5 Fe1 Br1	93.69(4)	93.23(18)
N2 Fe1 Br1	93.76(4)	93.47(17)
N4 Fe1 Br1	167.99(4)	170.97(16)

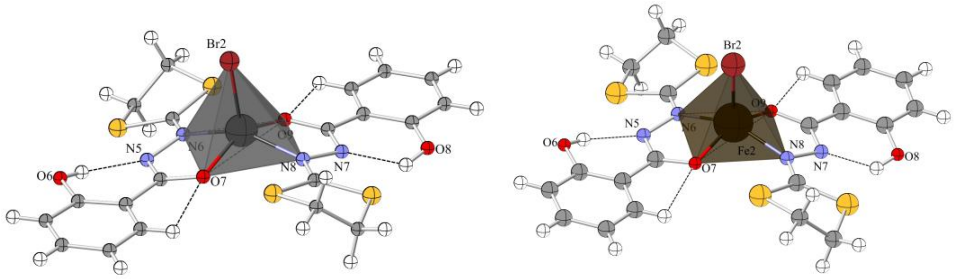

Figure A5: On the right unit B for **C4**. On the left Unit B for **C3**

Table IV: Bond Lengths (Å) and Angles (deg) for unit B of **C3** and **C4**

	C4	**C3**
N6 Fe2	2.091(9)	2.097(7)
N8 Fe2	2.092(9)	2.086(6)
O7 Fe2	1.945(8)	1.932(5)
O9 Fe2	1.930(8)	1.936(6)
Fe2 Br2	2.306(2)	2.3433(16)
O7 Fe2 O9	145.6(4)	145.4(3)
O7 Fe2 N8	92.0(4)	92.6(2
O9 Fe2 N8	77.8(3)	77.9(3
O7 Fe2 N6	77.8(3)	77.9(2
O9 Fe2 N6	94.2(3)	94.2(3
N8 Fe2 N6	149.1(4)	150.6(3
O7 Fe2 Br2	105.1(3)	105.14(18)
O9 Fe2 Br2	109.3(3)	109.5(2)
N8 Fe2 Br2	105.4(3)	105.64(19
N6 Fe2 Br2	105.4(3)	103.7(2)

- **Table V**: Crystal data and refinement details for **C1** and **C2**

Compound	**C1**	**C2**
Formula	$C_{23}H_{25}BrFeN_5O_5S_4$	$C_{20}H_{20}Br_2FeN_4O_4S_4$
Color	Blue dark	yellow
Formula weight ($g.mol^{-1}$)	715.48	724.31
Crystal system	Monoclinic	Monoclinic
Space group	P 21/c	P 21/c
a [Å]	19.1871(7)	9.247(5)
b [Å]	9.8892(3)	10.538(5)
c [Å]	16.1429(6)	16.051(5)
α [°]	90.00	90.00
β [°]	97.9110(10)	106.541(5)
γ [°]	90.00	90.00
V [$Å^3$]	3033.89(18)	1499.4(12)
Z	4	2
Density (calc) [$g.cm^{-3}$]	1.566	1.604
μ(MoKα) [mm^{-1}]	2.130	3.477
F(000)	1536	720
Crystal Size [mm]	0.35 × 0.22 × 0.18	0.30 × 0.25 × 0.20
Data Collection		
θ Min-Max [°]	2.14 - 30.99	2.30- 27.48
Dataset [h, k, l]	-26/27, -14/11, -23/14	-12/11, -13/13, -20/20
Tot., Uniq. Data, R(int)	28023, 9669, 0.0270	20418, 3430, 0.0726
Observed data [I > 2σ(I)]	7033	2822
Refinement		
N*reflections*, N*parameters*	9669, 356	3430, 161
R2, R1,	0.0578, 0.0358	0.0496 , 0.0395,
wR_2, wR_1		
GooF		
Max. and Av. Shift/Error	0.001, 0.000	0.001,0.000
Min,Max. Resd. Dens. [$e/Å^3$]	-0.691, 0.884	-0.777,0.896

- Table **VI**: Crystal data and refinement details for **C3** and **C4**

Compound	**C3.Et_2O EtOH**	**C4.Et_2O MeOH**
Formula	$C_{46}H_{52}Br_2Fe_2N_8O_{10}S_8$	C45 H50 Br2 Fe2 N8 O10 S8
Color	Black	Black
Formula weight ($g.mol^{-1}$)	1404.96	1390.93
Crystal system	Monoclinic	Monoclinic
Space group	P 21/c	P 21/c
a [Å]	9.545(5)	9.4569(2)
b [Å]	21.509(5)	21.4942(7)
c [Å]	28.379(5)	28.3397(7)
α [°]	90.00	90.00
β [°]	104.206(11)	103.079(2)
γ [°]	90.00	90.00
V [$Å^3$]	3033.89(18)	5611.1(3)
Z	4	4
Density (calc) [$g.cm^{-3}$]	1.652	1.647
μ(MoKα) [mm^{-1}]	2.286	2.300
F(000)	2856	2824
Crystal Size [mm]	0.25 × 0.22 × 0.10	0.35 × 0.22 × 0.10
Data Collection		
θ Min-Max [°]	1.20- 27.48	1.20- 27.44
Dataset [h, k, l]	-12/11, -26/27, -36/29	-12/11, -26/27, -28/36
Tot., Uniq. Data, R(int)	34746, 12886, 0.1177	41278, 12710, 0.0856
Observed data [I > 2σ(I)]	7067	7572
Refinement		
Reflections, parameters	12886, 680	12710, 681
R_2, R_1	0.2222, 0.1288	0.1571, 0.0882
wR_2, wR_1	0.3325, 0.2792	0.2656, 0.2282
GooF	1.136	1.076
Max. and Av. Shift/Error	0.000, 0.000	0.001,0.000
Min,Max. Resd. Dens. [$e/Å^3$]	1.848, 0.930	-2.037, 2.299

Figure A6: designed cuvette for freeze pump procedure.

- EPR spectrum of **C8** and **C10**

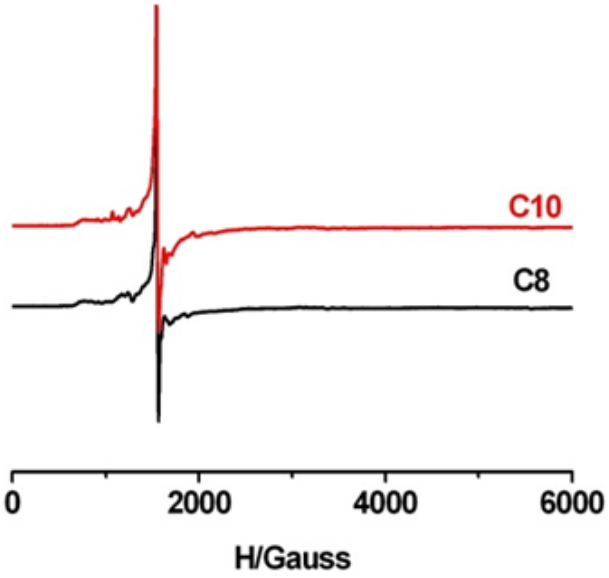

Figure A7 : EPR spectra of **C8** and **C10** complexes recorded at 20K in frozen DMF solution at 10^{-2} M.

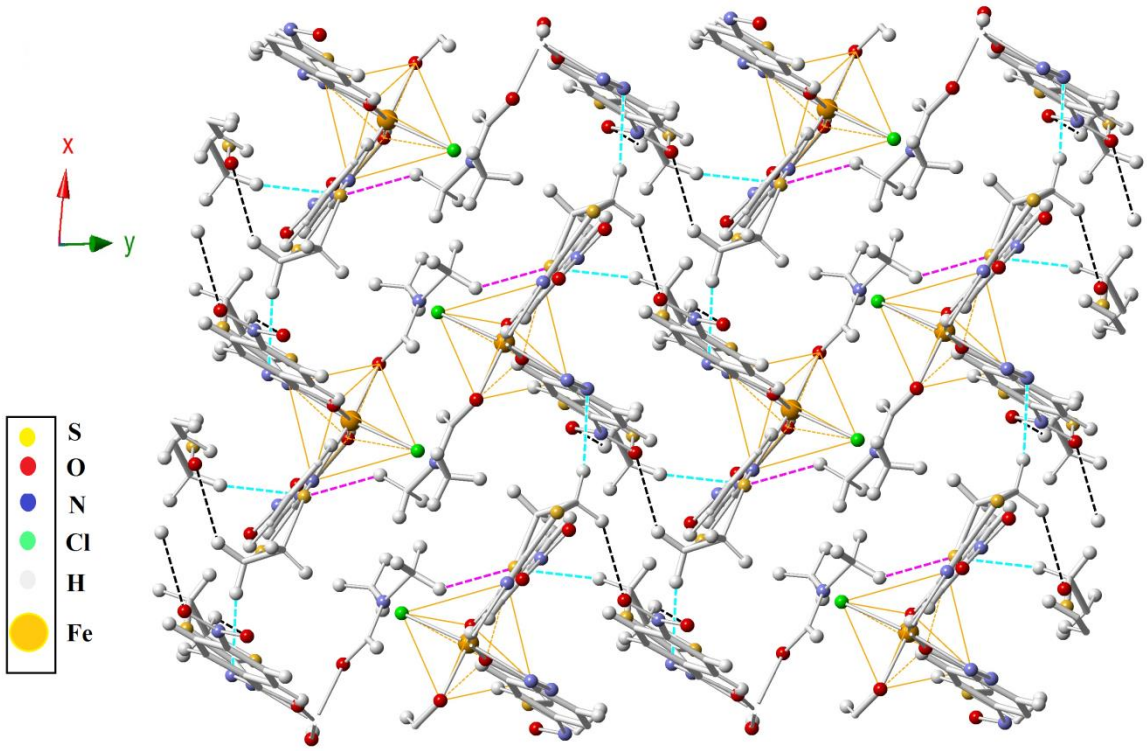

Figure A8: Packing view of **C10**. Black dashed line: intermolecular hydrogen bonds between O4 and C9**'** via H9B**'** (**'** symmetry code 1-x, 1 -y, 1-z). Magenta dashed line: intermolecular hydrogen bonds between S2 and C22**"** via H22**"** (**''** symmetry code 1-x, -y, 1-z). Cyan dashed line: intermolecular hydrogen bonds between N5 and C9**"'** **via** H9A**"'** (**'''** symmetry code 1+x, +y, +z); between N2 and C19**""'** via H19B**""'** (**""'** symmetry code 1-x, 1-y, -z).

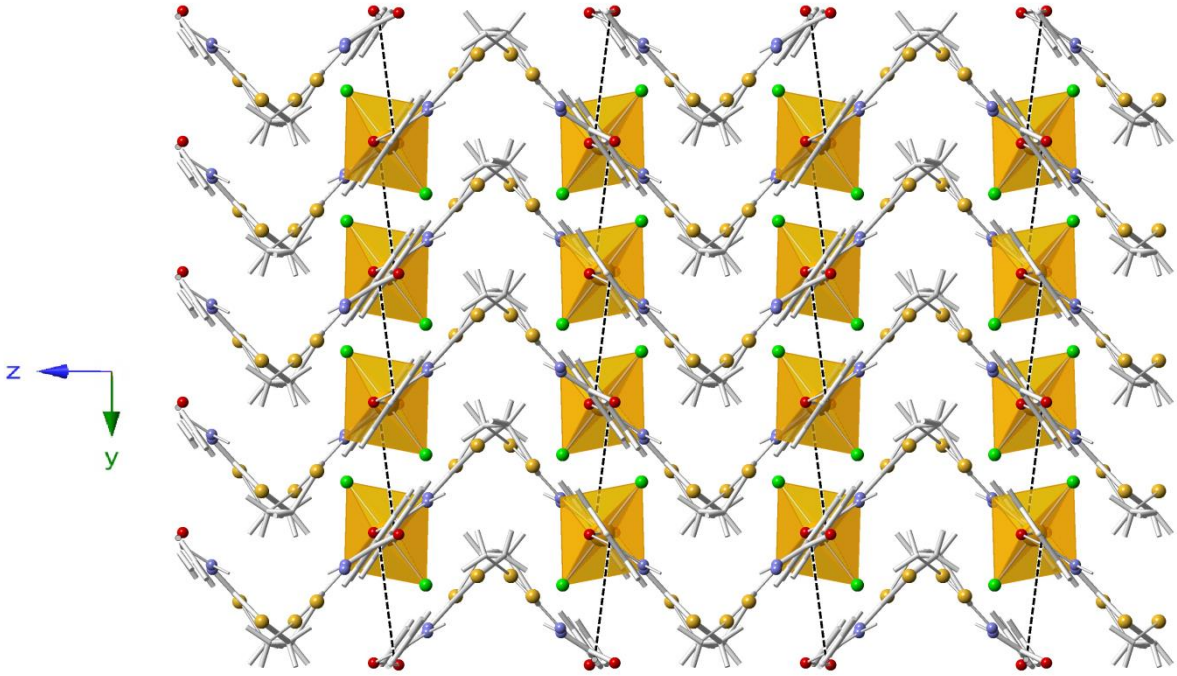

Figure A9: packing view of **C9** in the lattice plane (0, Y, Z). Dashed black line interaction between the Centre of the phenyl ring (C5-C10) and (C5-C10)' (' is the symmetry code 1-x, 1-y, 1-z)

Table VII: Crystal data and refinement details for **HL"**, **C8** and **C10**

Compound	**HL"**	**C10**	**C9**
Formula	$C_{10}H_9N_3O_3S_2$	$C_{26}H_{30}ClFeN_8O_8S_4$	$C_{20}H_{20}Cl_2FeN_4O_2S_4$
Color	Blue dark	Black	603.39
Formula weight (g.mol^{-1})	283.32	802.12	603.39
Crystal system	Monoclinic	triclinic	Monoclinic
Space group	P 21/c	P-1	C 2/c
a [Å]	7.9030(4)	9.1410(3)	18.8973(7)
b [Å]	6.1470(2)	14.6030(5)	9.5606(4)
c [Å]	24.4490(13)	14.6750(4)	16.5638(6)
α [°]	90.00	65.0990(15)	90.00
β [°]	98.480(2)	86.8310(18)	107.043(2)
γ [°]	90.00	81.1420(18)	90.00
V [Å^3]	1174.74(9)	1755.51(10)	2861.15(19)
Z	4	2	4
Density (calc) [g.cm^{-3}]	1.602	1.517	1.401
μ(MoKα) [mm^{-1}]	0.457	0.801	1.029
F(000)	584	826	1232
Crystal Size [mm]	0.10 × 0.10 × 0.10	0.10 × 0.10 × 0.10	0.35 × 0.25 × 0.20
Data Collection			
θ Min-Max [°]	3.31 - 30.06	1.53 - 30.03	2.25- 27.48
Dataset [h, k, l]	-11/11, 8/7, -34/34	-12/12, -20/20, -16/20	-19/24, -11/12, -21/21
Tot., Uniq. Data, R(int)	4602, 3150, 0.0169	19957, 10214, 0.1147	8645, 3289, 0.0364
Observed data [I > 2σ(I)]	2562	7832	2772
Refinement			
Reflections, parameters	3150, 163	10214, 433	3289, 151
R2, R1	0.0534, 0.0392	0.0855, 0.0632	0.0457, 0.0379
wR_2, wR_1	0.1045, 0.0955	0.1933, 0.1667	0.1040, 0.1003
GooF	1.047	1.064	1.100
Max. and Av. Shift/Error	0.001, 0.000	0.001, 0.000	0.001, 0.000
Min,Max. Resd. Dens.	-0.493, 0.427	-1.786, 0.786	-0.491, 1.046

Appendix chapter 3

Experimental

Synthesis

H_2L' and **H_2L'''** were prepared using previously published procedures [1]. **H_4L''** was obtained commercially (Acros Organics) and was used as received.

The studied molecules are depicted scheme AA1.

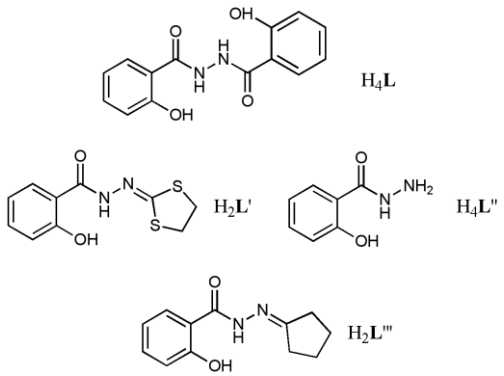

AA1: Molecules investigated in this work

UV-Visible measurements

Similar behaviour as H_4L is observed in the case of the compound H_2L' for the evolution vs. the concentration (Figure A1), the addition of base (Figure A2) and acid (figure A3). Although the components of the measured absorption band are less well resolved (see later discussion).

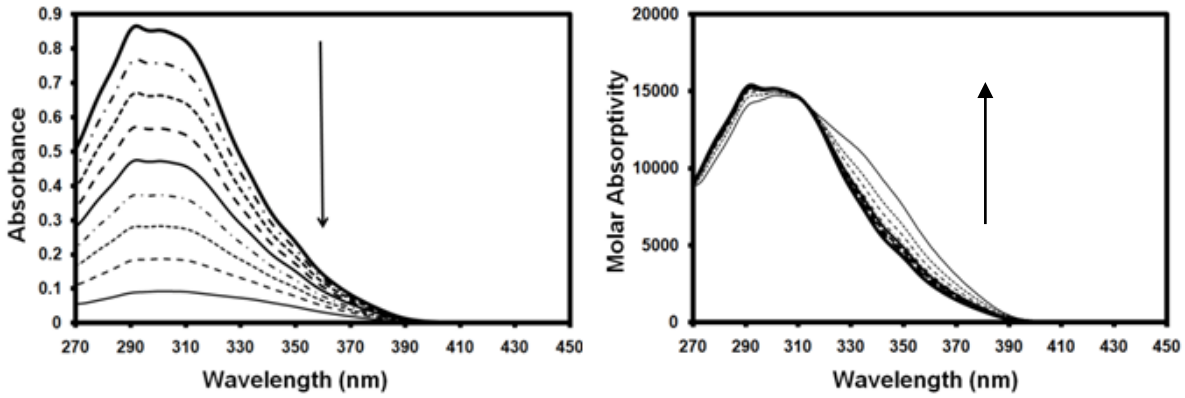

A1: *Absorption spectra (left) and molar absorptivity (right) of H_2L' for different concentrations: 5.6 10^{-5} M, 5.0 10^{-5} M, 4.4 10^{-5} M, 3.7 10^{-5} M, 3.1 10^{-5} M, 2.5 10^{-5} M, 1.9 10^{-5} M, 1.3 10^{-5} M and 6.3 10^{-6} M*

(The arrow indicates the sense of the absorbance changes with decrease of the concentration)

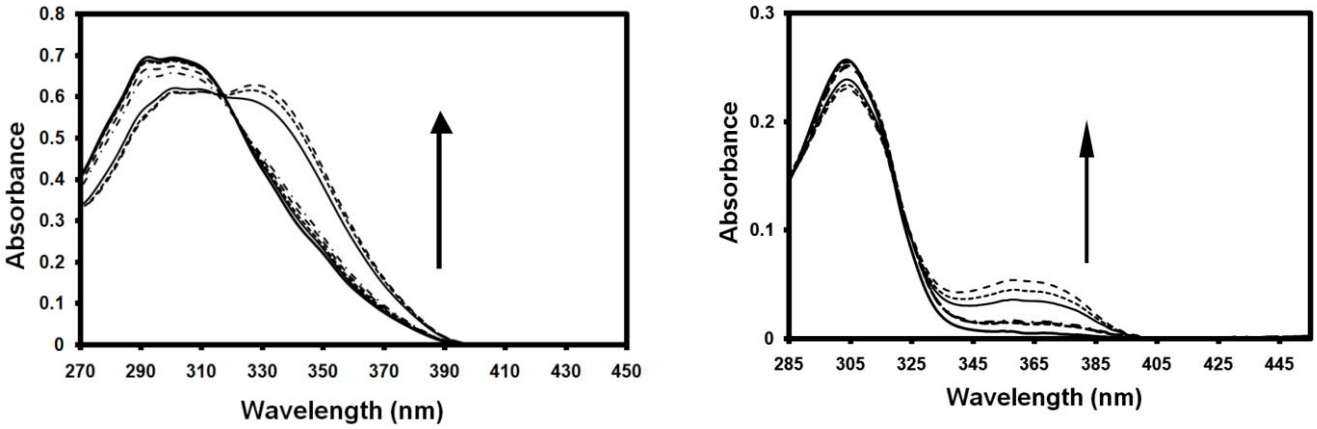

A2: *Absorbance changes resulting from the addition of triethylamine*

Left: H_2L' (5 10^{-5} M) with triethylamine concentrations equal to 0 M, 5 10^{-5} M, 1 10^{-4} M, 2 10^{-4} M, 3 10^{-4} M, 5 10^{-3} M, 1 10^{-2} M and 1.5 10^{-2} M

Right: H_4L'' (5 10^{-5} M) with triethylamine concentrations equal to 0 M, 5 10^{-5} M, 1 10^{-4} M, 1.5 10^{-4} M, 6 10^{-3} M, 1.8 10^{-2} M and 3.7 10^{-2} M

(The arrows indicate the sense of the absorbance changes due to addition of triethylamine)

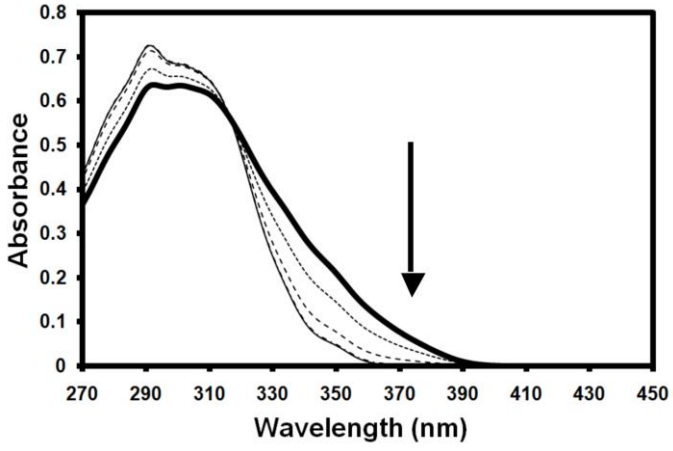

A3: *Absorbance changes due to the addition of HCl*

H_2L' (5 10^{-5} M) with HCl concentrations of 0 M, 5 10^{-5} M, 1 10^{-4} M, 1.5 10^{-4} M, 2 10^{-4} M

(The arrows indicate the sense of the absorbance changes due to addition of HCl)

These results indicate that the spectroscopic changes reflect the protonation states of the molecules. Each molecule possesses a phenol and hydrazide or hydrazone functions which can play the role of acid groups [2-4]. In the case of H_4L, aggregation phenomenon is excluded considering DOSY NMR measurement depicted on Figure A4 (see the text of the article for the hydrodynamic volume data).

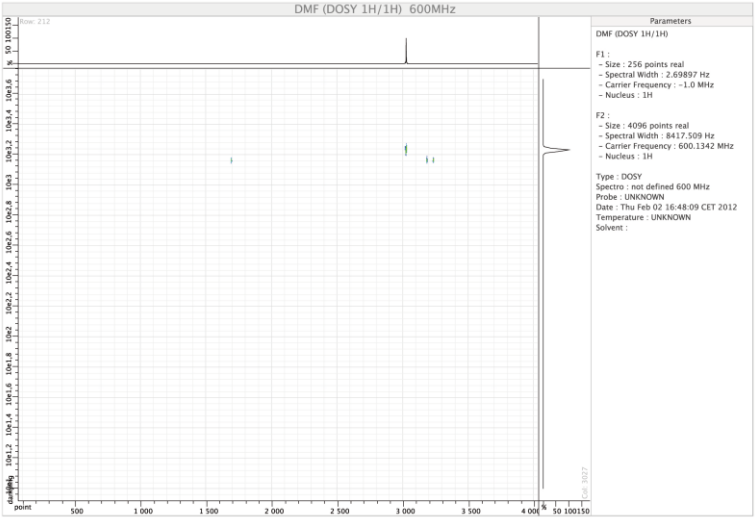

A4: *DOSY-NMR of 1 mM H_4L in DMF*

Thus, for both the present and previously studied systems [2,3], a basic understanding can be gained of their spectroscopic characteristics. In the selected wavelength range, electronic absorption spectra are a convolution of several transitions involving the functions Ph-OH, Ph-CO-NH-N=R and Ph-CO-NH-.

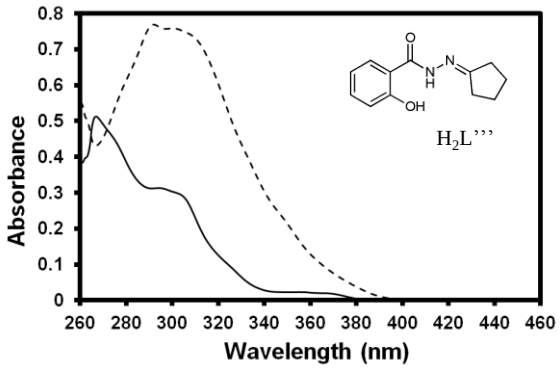

A5: *Absorbance spectra of H_2L' (dotted line) and H_2L''' (thin line), both at 5 10^{-5} M*

The nature (electron donor or not) of R has a strong influence on their absorbance properties within the molecule and on the overlapping of signals. An example of spectral changes can be seen when the electron donor group of $H_2L^{'}$ is exchange by a group with lower electron donor character (Figure A5). Two bands are observed which can correspond to a splitting of the broad signal of $H_2L^{'}$ and can be assigned to transition involving the overall function R'-CO-NH-N=R [2, 3].

Other transitions are present under the two broad bands. Indeed, the overall signal corresponds to the convolution involving the acid-base equilibria of the CO-N**H**-N=R ↔ CO-N^--N=R and Ph-OH↔ Ph-O^-. For these reactions, intramolecular hydrogen bonding, which could influence the absorbance properties, have to be taken into account. From different studies [2,3], several types of hydrogen bonds could be considered as depicted on scheme SS2.

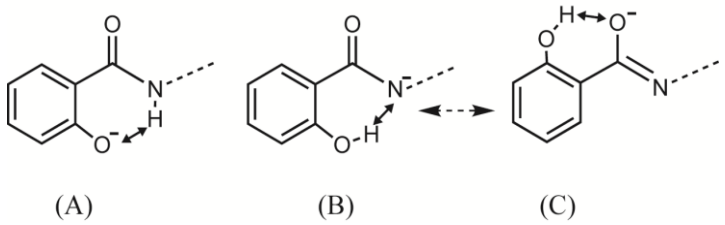

AA 2: *Potential intramolecular hydrogen bonds occurring in studied (salicyl)hydrazine derivatives.*

Focusing on these collected data, it is possible to underline two points: Firstly, for the same concentration, the second band occurring into H_4L spectrum is more prominent compared to the first one, than what in observed in the case of $H_2L^{'}$. Secondly, with two equivalents of triethylamine, this second band develops more for H_4L compared to $H_2L^{'}$ or $H_4L^{''}$. The origin of this behaviour could simply be attributed to the two equivalent acid functions present in the H_4L molecule. Thus, higher signal can be expected. But, a second hypothesis, based on the difference of the acidity power of the molecules, could also be pointed out. All the investigations performed in this study would be in agreement with the second approach (see discussion below and electrochemical section). In the case of $H_2L^{'}$, the combination of the hydrazone and hydrazide function would confer a greater acidity to the N-H proton than this of H_4L (scheme AA3). This effect can be supported considering the electronic delocalizations effect which stabilize the N^- state [2,3]. In these conditions, this proton would be more acid in the case of $H_2L^{'}$.

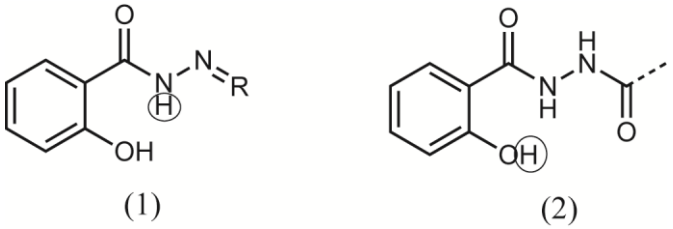

(1) (2)

AA 3: *The circle indicates the more acid proton in the case of:*

(1) H_2L' or H_4L'' and (2) H_4L

This last hypothesis would allow us to explain the observed results. In the case of $H_2L^{'}$, some electronic transitions are related to the acid-base reaction involving the hydrazide/hydrazone part which are often overlap with the Ph-OH/PhO^- group [2,3]. If the N**H** proton are acid and more than in the case of Ph-O**H**, then the molecule could be mainly in the case B and C of the scheme 2. In this context, the proportion of $PH-O^-$ is small. For H_4L, the opposite behaviour would be the origin of the observed property because of the lack of hydrazide/hydrazone part. The NH proton, which is less acid, leads the stabilisation of the $Ph-O^-$ group and even increases the acidity of the phenol function. Then, the case A of the scheme 2 can exist and the proportion of $Ph-O^-$ would be more important. One can notice that the enol equilibrium is not involved in the reasoning. Because it is common to all molecules, one can assume that it brings equivalent effect, therefore it is not a pertinent parameter.

When a base is added to a solution of $H_2L^{'}$, the predominant reaction would be the exchange of the proton from NH function. More this process evolves and more Ph-OH would be involves via equilibrium and hydrogen bond. Then, only after removing a significant part of NH protons, the Ph-OH protons would be affected. In the case of H_4L, less quantity of base will be necessary because the main protons source is the Ph-OH function. Regarding the addition of HCl acid, the difference between H_4L and $H_2L^{'}$ are lower than in the precedent case. In the case of addition of HCl acid, all the basic functions can react. $H_2L^{'}$ has three basic sites which are the $N^- \leftrightarrow C-O^-$, $Ph-O^-$ and a third which corresponds to the protonation of N=C. The electronic transition should again overlap with the other processes to form the broad band at short wavelengths. The molecule H_4L has both $Ph-O^-$ and N- functions then the necessary amount of acid should be higher for $H_2L^{'}$ than for H_4L.

Electrochemical measurements

Cyclic voltammograms for the compounds H_4L, $H_2L^{'}$ and $H_4L^{''}$ are given in Figure A6. All show a quasi reversible reduction step but only $H_2L^{'}$ and $H_4L^{''}$ show oxidation processes (irreversible).

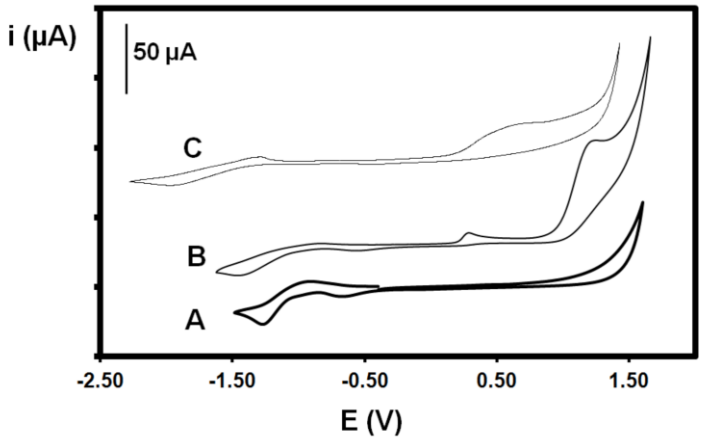

A 6: *Cyclic voltammograms of A) H_4L, B) $H_2L^{'}$ and C) $H_4L^{''}$: C = 5mM, Pt working electrode, Pt pseudo reference electrode, $TBAPF_6$ = 150 mM, v = 0.1 $V.s^{-1}$*

This behaviour is consistent with the electronic distribution on the hydrazone function which only occurs on molecules $H_2L^{'}$ and $H_4L^{''}$. The reduction step corresponds to proton reduction as it can be deduced from a comparison involving carbon and platinum electrodes [5] (Figure A7).

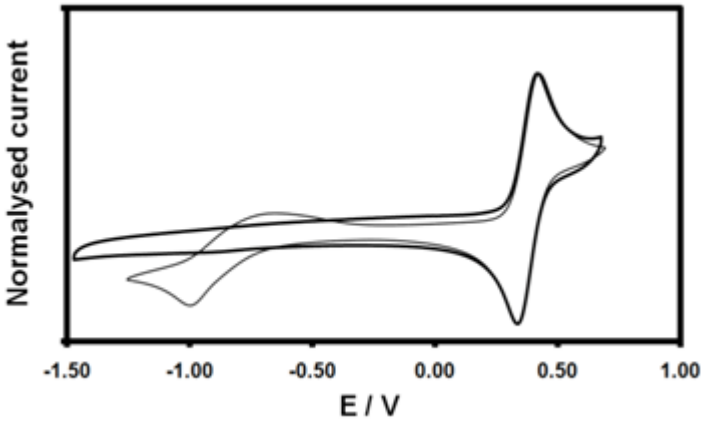

A 7: *Cyclic voltammograms of H_4L (5 mM) recorded with carbon (thick line) and platinum (thin line) electrodes. DMF, $TBAPF_6$ = 150 mM, v = 0.1 $V.s^{-1}$.*

Cyclic voltammetry as a function of concentration provided a satisfyingly linear current-concentration relation (Figure A8) for both H_4L and $H_2L^{'}$.

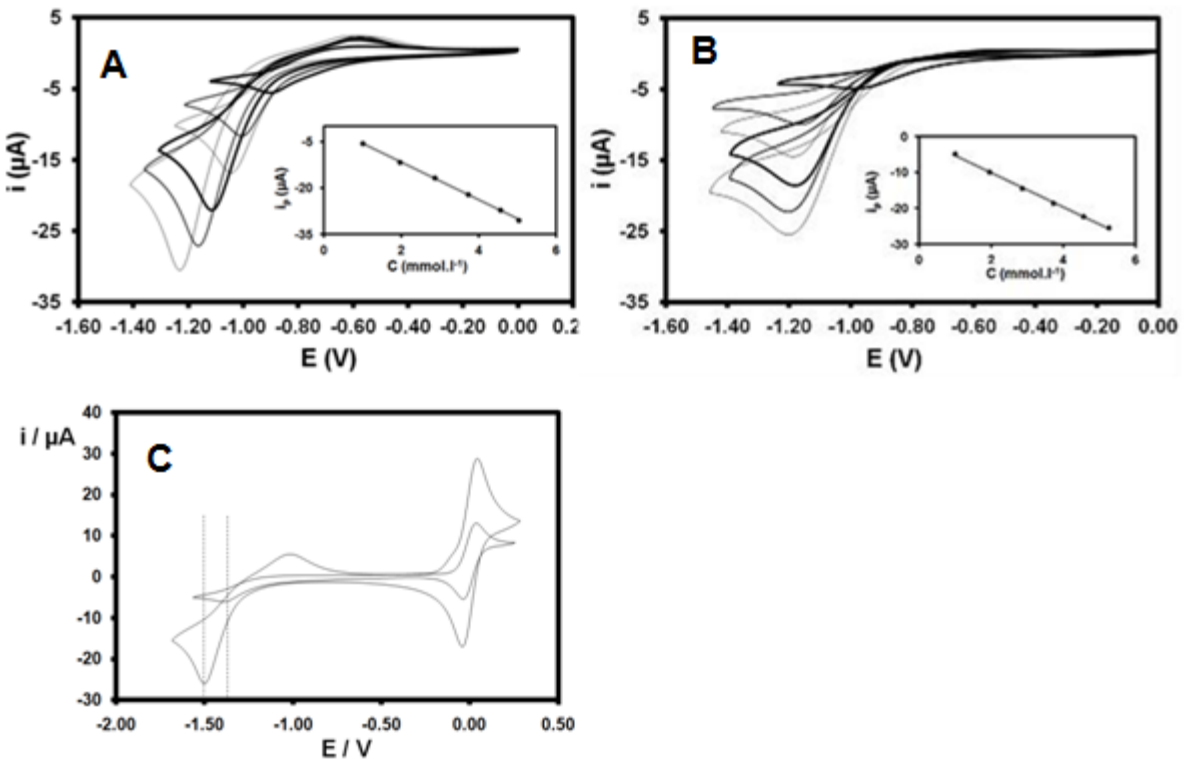

A 8: *Cyclic voltammograms of A) H_4L and B) H_2L' for different concentrations: 1, 1.95, 2.85, 3.72, 4.54 and 5 mM. C) Cyclic voltammogram of H_4L for 1 mM and 5 mM with ferrocene to calibrate the potentials. DMF, Pt working electrode, Pt pseudo reference electrode, $TBAPF_6$ = 150 mM, v = 0.1V.s-1, (insert: Ip vs. C)*

Further studies involving changing the scan rate (Figure A9) provided a good linear plot of I_p vs. $v^{1/2}$, again consistent with H_4L displaying no abnormal properties.

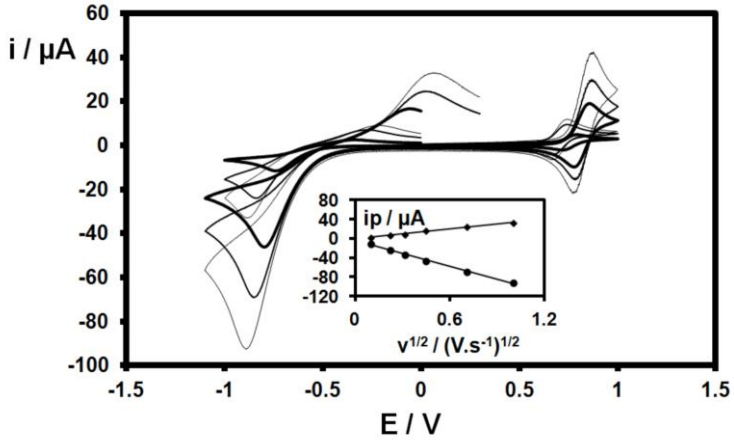

A 9: *Cyclic voltammograms of H_4L (5 mM) for different scan rates :0.01, 0.05, 0.1, 0.2, 0.5 and 1 $V.s^{-1}$. Pt working electrode, $TBAPF_6$ = 150 mM (Insert: Ip vs. $v^{1/2}$)*

Hence, some interesting information can be reached considering Figures A8 and A10.

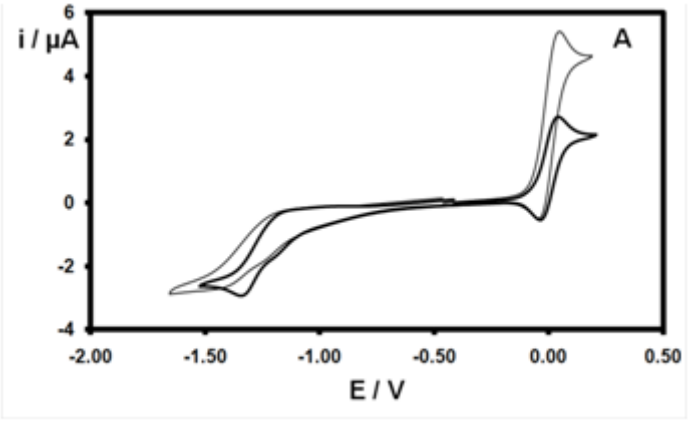

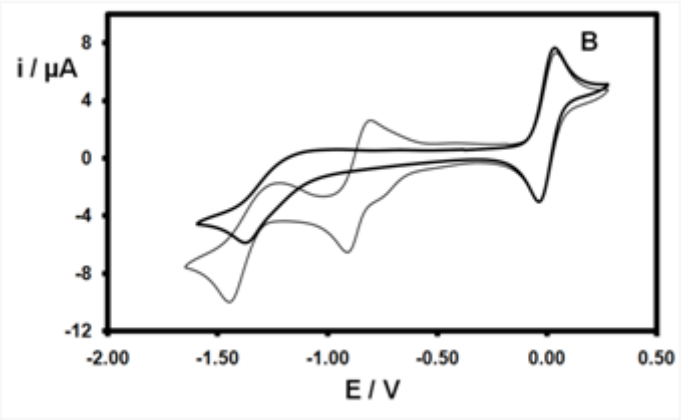

A 10: *A) H_4L (thick line) and H_2L' (thin line) 1 mM, v = 0.02 $V.s^{-1}$.*
B) H_4L 1 mM (thick line) and H_4L 1 mM with HCl 1 mM (thin line), v = 0.1 $V.s^{-1}$
Pt working electrode, $TBAPF_6$ = 150 mM, the potential of ferrocene is arbitrary fixed to 0 V.

The current intensity peaks related to H_4L and H_2L' are similar and in comparison with an equivalent of HCl, it becomes possible to indicate that this signal would correspond to only one proton. From this result, it is possible to assume that, despite of the presence of two equivalents phenol functions on H_4L molecule, statically only one is engaged. This point allows us to rule out the hypothesis (assumed previously) related to the number of active acid functions.

However, H_4L does not seem present expected evolution when the potential parameter is considered (Figures A8C and A9). This kinetic behaviour is confirmed plotting E_p vs. Log(v). The result is presented Figure A12 and indicates that kinetic limitation has influence on the proton potential reduction in a scan rate range of 0.002 $V.s^{-1}$ – 100 $V.s^{-1}$. Hence, there is not range of scan rate wherein the potential is independent of the scan rate. In the case of compounds H_2L' and H_2L'', cyclic voltammograms (Figure A10A) and successive records show shape evolution consistent with kinetic limitations. Adsorption of ligands onto platinum electrode is probably the origin of the protons reduction kinetic limitation.

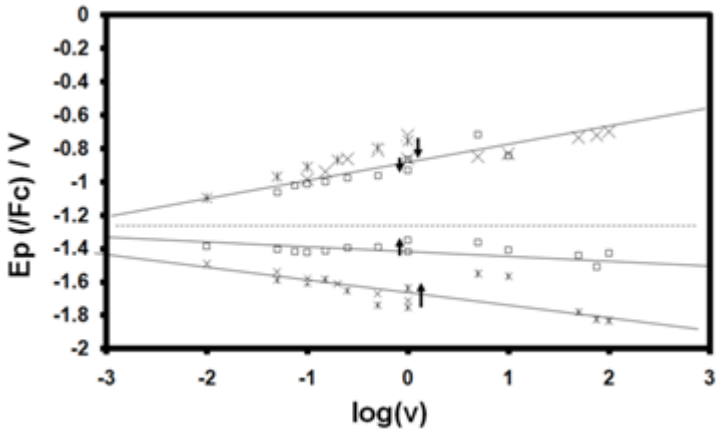

A 12: *Plot of E_p vs. Log(v) for H_4L : 1 mM (square) and 5 mM (cross) . Arrows show measurements performed with both Pt electrode and Pt microelectrode at 1 $V.s^{-1}$ to indicate that resistance effect is not the only limitation.*

EPR

EPR measurement: EPR spectra were recorded on EMX Bruker spectrometer (operating at 10 GHz) equipped with an Oxford Instruments ESR 900 continuous-flow helium cryostat. The static field was controlled with a Hall probe, whereas the microwave frequency was simultaneously recorded with a frequency counter (HP-5350 B). Samples were illuminated with an Argon-Krypton laser (model stability 2018-RM from Spectra Physic) using the multiline mode (superposition of visible lines from the blue (457 nm) up to the green (574 nm)) directly *in situ* in the EPR cavity.

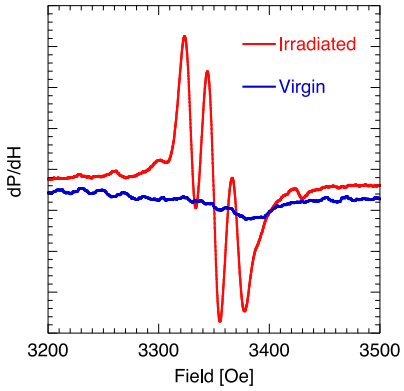

Fig A13: EPR spectra of the iron complex in DMF at 6 K: blue line before irradiation, red line after 3 hours of irradiation.

In this study, chemical physics properties comparisons have been performed between N,N'-bis(salicyl)hydrazine and related mono salicylic hydrazide derivatives. UV-Vis spectroscopy and electrochemistry studies allow us to point out acid-base differences despite apparent close chemical similarities. Although for each type of molecule, only one proton is involved in the acid-base equilibrium, the proton exchange site is different between N,N'-bis(salicyl)hydrazine and related mono salicylic hydrazide derivatives. In the first case, the Ph-OH group provides protons whereas in the second case, the NH group is engaged in the acid-base equilibrium. This observation can be understood assuming that acidic power of identical acid functions are affected because of the presence or not of the hydrazide /hydrazone combination within the molecules. Hence, a relative positioning acidic power can be proposed:

$$PhOH_{(H4L)} \geq NH_{(H4L)} \text{ and } NH_{(H2L')} > PhOH_{(H2L')}$$

References

[1] N. Bouslimani, N. Clément, G. Rogez, P. Turek, S. Choua, S. Dagorne, R. Welter, *Inorganica Chimica Acta* 2010, **363**, 213–220.

[2] R. M. Issa, Y. M. Temerk, M. M. Ghoneim, J. Y. Maghrabi, *Bull. Fac. Sci. K.A.U. Jeddah* 1978, **2**, 167-178.

[3] H. F. F. El-Baradie, M. A. Khattab, R. M. Issa, J. Y. Maghrabi, *J. Chem. Tech. Biotechnol.* 1983, **33A**, 123-129.

[4] E. Anxolabéhère-Mallart, C. Costentin, C. Policar, M. Robert, J.-M. Savéant, A.-L. Teillout, *Faraday Discuss.* 2011, **148**, 83-95.

[5] S. S. Kurek, B.J. Laskowka, A. Stoklosa, Electrochim. Acta, 2006, **51**, 2606-2414.

Appendix chapter 5

- Ligand HL

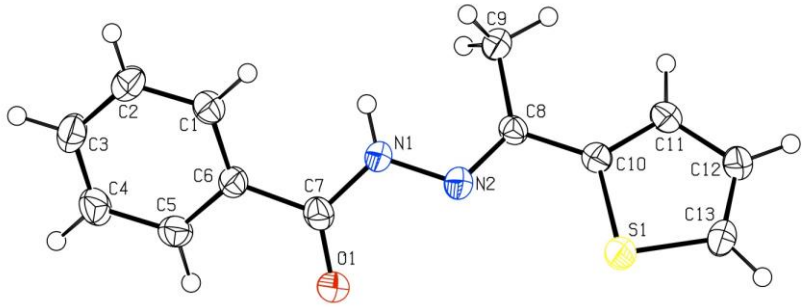

Figure A1: Full labeled ORTEP views with ellipsoids enclosing 50% of the electronic density

- Complex_1

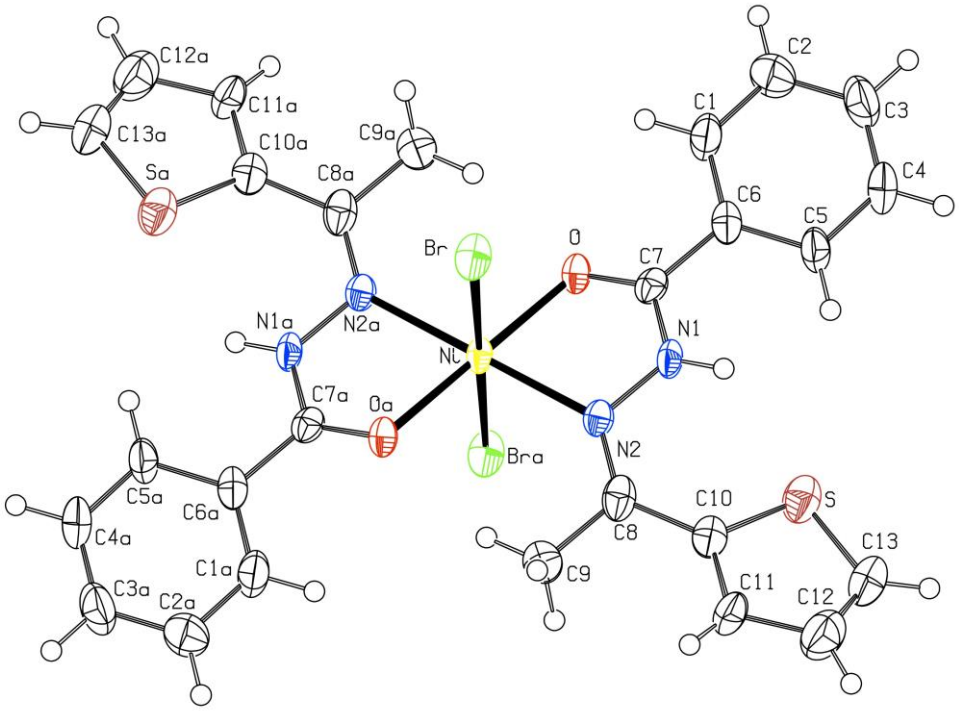

Figure A2: Full labeled ORTEP views with ellipsoids enclosing 50% of the electronic density

- Complex_2

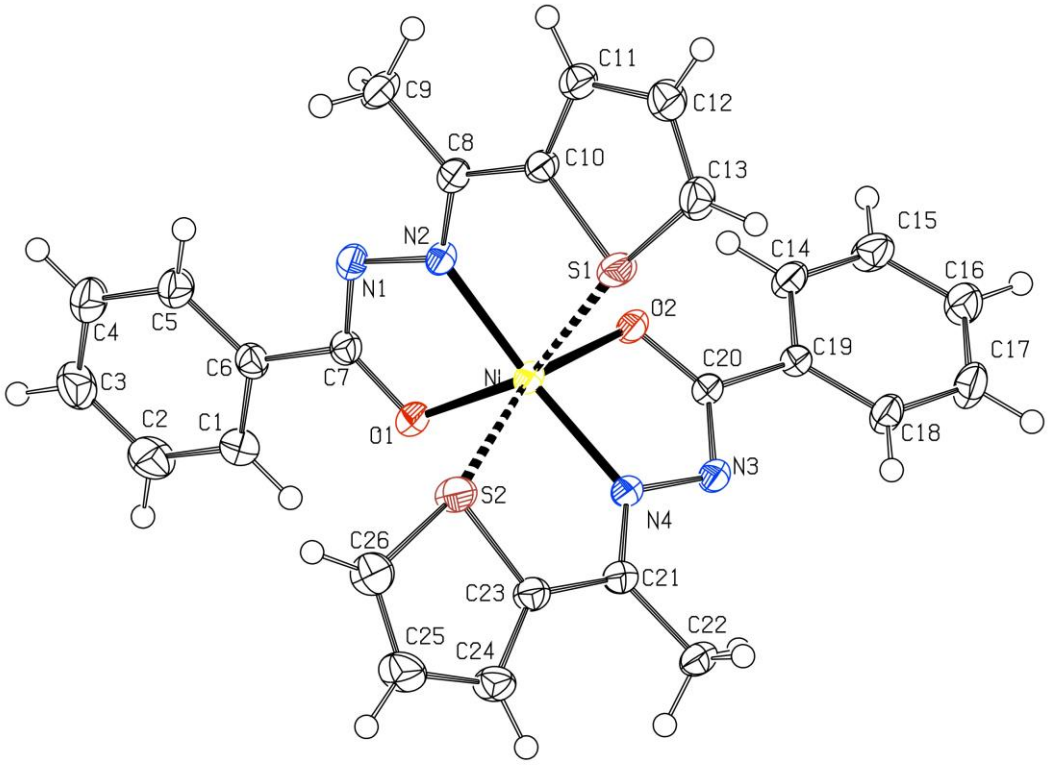

Figure A3: Full labeled ORTEP views with ellipsoids enclosing 50% of the electronic density

- Complex_3

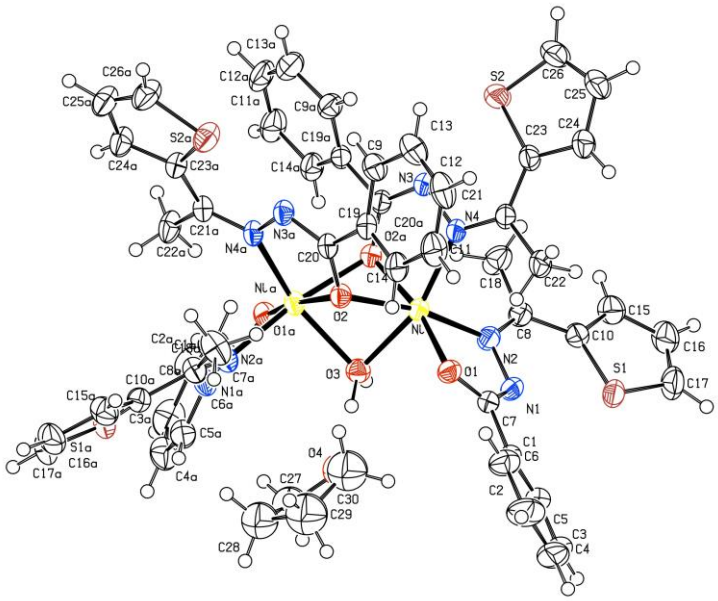

Figure A4: Full labeled ORTEP views with ellipsoids enclosing 50% of the electronic density

Table I: Crystal data and X-ray structure refinement parameters at 173 K for complexes 1; 2; 3.ether; 3.THF and HL

Compound reference	complex_1	complex_2	complex_3_ether	complex_3_THF	ligand_HL
Formula	$C_{26}H_{24}Br_2N_4NiO_2S_2$	$C_{26}H_{22}N_4NiO_2S_2$	$C_{52}H_{46}N_8Ni_2O_5S_4 \bullet C_8H_{20}O_2$	$C_{52}H_{46}N_8Ni_2O_5S_4 \bullet 2(C_4H_8O)$	$C_{13}H_{12}N_2OS$
Formula Mass	707.14	545.31	1256.87	1252.84	244.31
Crystal system	Monoclinic	Triclinic	Monoclinic	Monoclinic	Orthorhombic
a [Å]	11.4240(7)	7.8040(3)	25.7700(8)	25.9210(8)	9.894(1)
b [Å]	8.8690(9)	12.2810(6)	11.6390(5)	11.7640(4)	10.531(1)
c [Å]	13.9170(6)	14.5590(7)	23.5110(7)	23.4510(5)	22.474(1)
α [°]	90.000(4)	71.942(2)	90.00	90.00	90.00
β [°]	102.314(4)	81.824(2)	121.6561(16)	123.0900(15)	90.00
γ [°]	90.000(3)	82.121(2)	90.00	90.00	90.00
V [Å^3]	1377.62(17)	1306.71(10)	6002.6(4)	5991.2(3)	2341.6(3)
Space group	*P*21/*c*	*P*-1	*C*2/*c*	*C*2/*c*	*Pbca*
Z	2	2	4	4	8
μ(Mo-K$_\alpha$) [mm^{-1}]	3.788	0.932	0.825	0.827	0.260
F(*000*)	708	564	2632	2616	1024
Crystal size [mm]	0.10×0.10×0.10	0.20×0.15×0.10	0.10×0.09×0.08	0.12×0.10×0.08	0.20×0.12×0.08
θ_{min}–θ_{max}	0.998–27.485	1.48–30.09	0.998–30.034	0.998–30.034	1.81–27.84
Data set [*h*, *k*, *l*]	-14/14,-9/11, -18/17	-10/11, -16/17, 0/20	-35/36, -14/16, -33/33	-32/36, -14/16, -32/32	-12/12, -13/13, -29/29
Total, unique data, R_{int}	8590, 3150, 0.0526	7533, 7533, 0.0000	14380, 8741, 0.0316	29786, 8763, 0.0824	5181, 2777, 0.0677
Observed data [$I > 2\sigma(I)$]	2416	6393	5919	6429	1689
No. reflections, No. parameters	3150, 169	7533, 316	8741, 366	8763, 341	2777, 154
Final R_1 values ($I > 2\sigma(I)$)	0.0609	0.0374	0.0584	0.0563	0.0499
Final $wR(F^2)$ values ($I > 2\sigma(I)$)	0.1492	0.1176	0.1603	0.1606	0.1169
Final R_1 values (all data)	0.0937	0.0449	0.1010	0.0846	0.1074
Final $wR(F^2)$ values (all data)	0.1692	0.1226	0.1967	0.1877	0.1595
Goodness of fit on F^2	1.115	1.106	1.150	1.074	1.067
Max. and av. Shift/error	0.000/0.000	0.001/0.000	0.001/0.000	0.003/0.000	0.007/0.001
Min, Max residual density [eÅ^{-3}]	-1.188, 1.513	-0.763, 0.403	-1.377, 2.735	-1.212, 1.206	-0.355, 0.292

Khaled CHEAIB

Synthèse, caractérisation et propriétés photochimiques de complexes de métaux de transition 3d supportés par des ligands de type aroyle-hydrazone

Résumé

Ce travail de thèse explorait certains aspects de la chimie de coordination de complexes moléculaires à bases de métaux 3d (Fe, Cu, Mn et Ni) supportés par des ligands azotés de type aroyle-hydrazone. Le travail de cette thèse était plus particulièrement centré sur le développement des nouveaux ligands et la photo chimie des complexes ferriques, afin d'élucider en particulier les mécanismes de la photo réduction qui valorise un brevet du laboratoire sur la production et le stockage d'énergie solaire via la photo réduction d'ions ferriques. Les complexes mis en jeu dans le processus ont été totalement caractérisés en solution et à l'état solide. Ce phénomène prend place en solution comme en solution gelée. La cinétique du processus photochimique a été suivie par UV-Visible comme par RPE. Cette photo réduction passe par un intermédiaire radicalaire et le solvant joue le rôle du donneur des électrons. Ce processus a été totalement étudié : l'effet du solvant, l'effet de la modification dans la sphère de coordination du complexe, l'effet de la modification de la périphérie des ligands et finalement l'effet des longueurs d'ondes. D'autres domaines sont également explorés, comme le magnétisme moléculaire ou encore la catalyse homogène (oligomérisation de l'éthylène) avec des complexes à base de Ni^{2+}.

Mots-clés : Chimie de coordination, aroyl-hydrazone, photo-réduction et magnétisme moléculaire

Résumé en anglais

This PhD thesis explored some aspects of the coordination chemistry of molecular complexes based on 3d transition metal ions (Fe, Cu, Mn and Ni) coordinated by multidentate aroyl-hydrazone ligands. The work of this thesis was particularly focused on the development of new ligands, their coordination chemistry and the photochemistry of ferric complexes. The central objective of this work was to elucidate the mechanism of the photo reduction process, in order to valorize an already accepted laboratory patent on the production and storage of solar energy. The complexes involved in the process have been fully characterized in solution and in the solid state. This phenomenon takes place in solution as in frozen solution. The kinetics of the photochemical process was followed by UV-Visible as by RPE. This photo reduction passes through a radical intermediate and the solvent plays the role of the electron donor. This process has been fully studied: the effect of the solvent, the effect of the modification in the coordination sphere of the complex, the effect of the modification of the periphery of the ligands and finally the effect of the light and different wavelengths. Other fields are also explored, such as molecular magnetism for different mono and dinuclear iron and manganese complexes or even homogeneous catalysis (oligomerization of ethylene) with complexes based on Ni(II).

Key-words: Coordination chemistry, aroyl-hydrazone, photo-reduction and molecular magnetism